



Norwegian University of Life Sciences
Faculty of Chemistry, Biotechnology
and Food Science

Philosophiae Doctor (PhD)
Thesis 2021:91

Functional insights into novel factors affecting cell division in Gram-positive bacteria

Funksjonell innsikt i nye celledelingsfaktorer hos Gram-positive bakterier

Ine Storaker Myrbråten

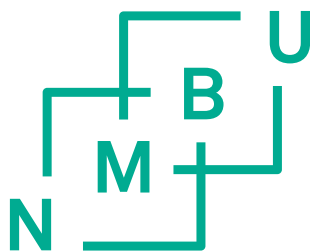
Functional insights into novel factors affecting cell division in Gram- positive bacteria

Funksjonell innsikt i nye celledelingsfaktorer
hos Gram-positive bakterier

Philosophiae Doctor (PhD) Thesis
Ine Storaker Myrbråten

Norwegian University of Life Sciences
Faculty of Chemistry, Biotechnology and Food Science

Ås (2021)



Thesis number 2021:91

ISSN 1894-6402

ISBN 978-82-575-1868-4

Table of Contents

Acknowledgements	III
Summary	V
Sammendrag	VII
List of papers	IX
1. Introduction	1
1.1. <i>Staphylococcus aureus</i> – an antibiotic resistant opportunistic pathogen	2
1.2. Surrounding the staphylococcal cell	2
1.2.1. Structure of staphylococcal peptidoglycan.....	4
1.2.2. Teichoic acids.....	4
1.2.2.1. Structure of wall teichoic acids (WTA)	5
1.2.2.2. Structure of lipoteichoic acids (LTA)	5
1.3. The cell cycle of <i>S. aureus</i>	6
1.3.1. Chromosome replication and segregation	7
1.3.2. Selection of division plane, assembly of the Z ring and the divisome.	8
1.3.3. Synthesis of new cell wall.....	10
1.3.3.1. The biosynthetic pathway of peptidoglycan production	10
1.3.3.2. Biosynthesis of wall teichoic acids.....	13
1.3.3.3. Biosynthesis of lipoteichoic acids.....	15
1.3.4. Cell splitting and hydrolases	17
1.3.5. Other processes affecting cell cycle and cell morphology of <i>S. aureus</i> ..	19
1.4. Cell biology and novel cell cycle factors of non-spherical Firmicutes	20
1.4.1. The rod-shaped <i>Lactobacillus plantarum</i>	21
1.4.2. The oval-shaped <i>Streptococcus pneumoniae</i>	22
2. Aims of the study	24
3. Summary of papers	25

Paper I	25
Paper II.....	26
Paper III	27
Paper IV	28
4. Main results and discussion.....	29
4.1. Methodological considerations.....	29
4.1.1. Why and how study essential genes – the CRISPRi approach.....	29
4.1.2. Selection of staphylococcal strains for study of cell division genes..	31
4.2. The CozE proteins.....	32
4.2.1. The essentiality and roles of CozE proteins vary between species...	32
4.2.2. The functionality of staphylococcal CozE proteins	33
4.3. SmdA – identified from a dual screening approach.....	37
4.3.1. Subcellular localization- and gene knockdown screens.....	37
4.3.2. Phenotyping of strains with altered levels of SmdA reveals a novel staphylococcal morphology determinant.....	37
5. Concluding remarks and future perspectives.....	41
References.....	43
Paper I-IV	

Acknowledgements

The work presented here was carried out in the Molecular Microbiology group, Department of Chemistry, Biotechnology and Food Science at The Norwegian University of Life Sciences with support from the university and the Research Council of Norway.

First of all, I would like to thank my amazing supervisor, Associate Professor Morten Kjos, for excellent guidance and help throughout the work with this thesis. Your knowledge, ideas and skills are truly inspiring, and I am very grateful for you always making time for my questions. I will also thank my co-supervisor Professor Leiv Sigve Håvarstein for all your contributions and ideas.

Dr. Daniel Straume, thank you for all your ideas, troubleshooting and guidance in the lab. Dr. Gro Anita Stamsås, I am very grateful I got to work with you. In addition to your scientific skills, you always spread joy and laughter. Zhian, your assistance and help in the lab has been so valuable! You are definitely the most efficient person I have ever met.

I also want to direct a special thanks to my (former) fellow PhD-student(s) that I have shared office with: Dr. Anja Ruud Winther, Katarzyna Wiaroslawa Piechowiak and Marita Torrissen Mårli. Thank you for the complaining-sessions, pep-talks, supportive words, true-crime stories, and glasses of wine and laughter's we have shared. Also, fellow PhD-students, Maria and Maria, and the rest of the MolMik group; thank you for making the lab such a great place to work, I have really appreciated my time here!

To all the co-authors: thank you for your contributions and good cooperation during the work with the papers!

Lastly, my family and friends also deserves a big thanks! You are always supportive and have faith in me. My dear husband Runar, who has really made an effort to make it easier for me to finish this work. I really appreciate having you and our sweet girls to come home to after work.

Ås, October 2021

Ine Storaker Myrbråten

Summary

The opportunistic pathogen *Staphylococcus aureus* is a major contributor to a range of different infections in human and animals that have become difficult to treat because of the rise of antibiotic resistant strains. New antibacterial strategies are therefore needed. Processes related to bacterial multiplication and cell integrity are attractive therapeutic targets since these involves proteins and mechanisms that are essential for the bacterium. Detailed understanding of such processes, as well as genetic tools to study them, is therefore needed to facilitate development of new combat strategies. The work in this thesis contributed (i) to identify and elucidate the role and importance of novel cell division factors in spherical-shaped *S. aureus* (ii) to understanding the functional conservation of these cell division factors in bacterial species with other cell shapes (oval-shaped *Streptococcus pneumoniae* and rod-shaped *Lactobacillus plantarum*) and (iii) to develop CRISPR interference (CRISPRi) systems for controlled knockdown of essential genes in *S. aureus* and *Lactobacillus plantarum*.

In Paper I and II, the membrane proteins CozEa and CozEb in *S. aureus* were studied. CozEa and CozEb were identified as putative cell division factors in Paper I due to their homology to the *S. pneumoniae* elongation factor CozE (coordinator of zonal elongation). Staphylococcal cells do not elongate in the same manner, so we were encouraged to investigate their function in spherical *S. aureus*. Since a double deletion mutant of the CozE proteins was lethal, we developed and utilized a CRISPRi tool to show that the CozE proteins mediate cell division control, possibly through interactions with the early cell division protein EzrA. We also showed that the CozE-EzrA interaction was conserved in *S. pneumoniae* and that the staphylococcal CozE proteins could complement the *cozE* deletion phenotype of *S. pneumoniae*. By further investigating the functions of these proteins in Paper II, we found that the CozE proteins have a functional link to the biosynthesis of staphylococcal lipoteichoic acids (LTA), and that CozEb is involved in control of LTA polymer length. Defects in the LTA biosynthesis pathway and altered LTA length have previously been shown to produce enlarged cells and septum formation abnormalities in *S. aureus*. Together, the results in Paper I and II, demonstrate that the CozE proteins affect this interplay between LTA biosynthesis and cell division.

In Paper III, we performed a subcellular localization- and gene knockdown screen of essential staphylococcal proteins with unknown function in an attempt to identify

novel factors affecting the cell cycle of *S. aureus*. A gene with locus tag SAOUHSC_01908 was selected for further studies based on its observed subcellular localization and cell division defects upon depletion. This protein, named staphylococcal morphology determinant A (SmdA), was shown to be essential for proper cell morphology maintenance during cell division, by affecting several stages of the cell division process. Notably, the knockdown of the protein also increased the sensitivity of resistant *S. aureus* to cell wall targeting antibiotics, and in particular β -lactams.

Finally, in Paper IV, *L. plantarum* was developed as a model to study cell division factors in rod-shaped, Gram-positive bacteria. *L. plantarum* has been extensively studied for its potential as a probiotic, and as a delivery vehicle of antigens and other therapeutic molecules, but increased knowledge about essential processes in this bacterium is needed for further strain improvements. A CRISPRi system was constructed as a new genetic tool for studies of essential genes. By using this CRISPRi system, phenotypes resulting from knockdown of established cell cycle factors (*dnaA*, *ezrA*, *acm2*) were reported and used to demonstrate the functionality of the system. We show that the CozE homologs in *L. plantarum* are non-essential and not involved in cell elongation or -division in this species. On the other hand, the recently discovered pneumococcal EloR and KhpA proteins are important for cell elongation in this bacterium.

Sammendrag

Den opportunistiske patogene bakterien *Staphylococcus aureus* forårsaker en rekke ulike infeksjoner i mennesker og dyr som har blitt vanskelige å behandle på grunn av spredningen av antibiotikaresistente stammer. Det er derfor et behov for nye antibakterielle strategier. Proteiner og mekanismer som påvirker celledeling og celleintegritet er essensielle for at bakterien skal overleve, og er derfor attraktive angrepspunkter for antibiotika. Detaljert forståelse av slike prosesser, så vel som genetiske verktøy for å studere dem, er derfor nødvendig for å tilrettelegge for utviklingen av nye strategier. Arbeidet i denne oppgaven har bidratt med (i) å identifisere og belyse funksjonen til nye celledelingsfaktorer i den kokkformede bakterien *S. aureus*, (ii) å forstå hvordan funksjonen til disse celledelingsfaktorene er konservert i bakteriearter med andre fasonger (den ovalformede *Streptococcus pneumoniae* og den stavformede *Lactobacillus plantarum*), og (iii) å utvikle CRISPR interferens (CRISPRi)-systemer for kontrollert nedregulering av essensielle gener i *S. aureus* og *L. plantarum*.

I Artikkel I og II ble membranproteinene CozEa og CozEb studert i *S. aureus*. CozEa og CozEb ble identifisert som antatte celledelingsfaktorer i Artikkel I på grunn av deres homologi til *S. pneumoniae* sin elongeringsfaktor CozE («coordinator of zonal elongation», koordinator av lateral forlengelse av cellen). Siden stafylokokkceller er runde, forlenger de seg ikke på samme måte som ovalformede streptokokkceller, så vi ønsket derfor å undersøke hvilken funksjon CozE har i *S. aureus*. Det var ikke mulig å fjerne begge *cozE* genene samtidig i *S. aureus*. Derfor utviklet vi et CRISPRi-verktøy og brukte dette til å vise at CozE-proteinene er involvert i kontroll av celledelingen i *S. aureus*. Dette skjer muligens via interaksjoner med det tidlige celledelingsproteinet EzrA. Vi viser også at denne CozE-EzrA interaksjonen er konservert i *S. pneumoniae*, og at CozE-proteinene fra stafylokokker kan komplementere *cozE* delesjonsfenotypen i *S. pneumoniae*. Ved å videre undersøke funksjonene av disse proteinene i Artikkel II, fant vi ut at CozE-proteinene har en funksjonell kobling til biosyntesen av stafylokokker sin lipoteikoinisyre («lipoteichoic acids», LTA, anionisk overflatepolymer som er festet i membranen). Spesifikt ble det vist at CozEb er involvert i lengdekontroll av LTA-polymerene. Defekter i biosyntesen av LTA, samt forandringer i lengden av LTA, har tidligere blitt vist å føre til forstørrede celler og unormale septumdannelser i *S. aureus*. Til sammen viser resultatene i Artikkel I og II at CozE-proteinene påvirker dette samspillet mellom biosyntesen av LTA og celledeling.

I Artikkel III utførte vi en subcellulær lokaliserings- og nedreguleringsscreen av essensielle stafylokokkproteiner med ukjent funksjon, i et forsøk på å identifisere nye faktorer som påvirker cellesyklusen til *S. aureus*. Et gen, med lokusnavn SAOUHSC_01908, ble valgt ut til videre studier fordi dette proteinet lokaliserte til septum av cellen, og klare celledelingsdefekter ble observert ved nedregulering av genuttrykket. Dette proteinet, som vi her kaller SmdA («staphylococcal morphology determinant A»), ble vist å være essensielt for riktig cellemorfologi gjennom påvirkning av flere steg i celledelingsprosessen. Særlig interessant var det at nedregulering av dette proteinet medførte økt sensitivitet mot antibiotika som angriper celleveggen i *S. aureus*. Spesielt ble methicillinresistente stafylokokker vist å bli mer sensitive for betalaktamer.

Til slutt, i Artikkel IV, ble *L. plantarum* utviklet som en modell for å studere celledelingsfaktorer i stavformede, Gram-positive bakterier. *L. plantarum* har blitt forsket mye på for dens potensial som probiotikum og som leveringsvektor for antigener og andre terapeutiske molekyler. Likevel vil økt kunnskap om essensielle prosesser i denne bakterien være viktig for videre forbedring av aktuelle bakteriestammer. Et CRISPRi-system ble konstruert som et nytt genetisk verktøy for studier av essensielle gener i denne bakterien. Ved å bruke dette systemet viste vi fenotyper fra nedregulering av kjente cellesyklusfaktorer (*dnaA*, *ezrA*, *acm2*), for å demonstrere funksjonaliteten av nedreguleringsystemet. Vi viste også at CozE-homologene i *L. plantarum* ikke er essensielle eller involvert i celleforlengelse eller -deling i denne bakteriearten. Derimot ble to andre nylig karakteriserte elongeringsfaktorer hos *S. pneumoniae*, EloR og KhpA, vist å være viktige for celleforlengelse i denne bakterien også.

List of papers

- Paper I** Stamsås, G. A.*, **Myrbråten, I. S.***, Straume, D., Salehian, Z., Veening, J. W., Håvarstein, L. S. & Kjos, M. (2018). CozEa and CozEb play overlapping and essential roles in controlling cell division in *Staphylococcus aureus*. *Molecular Microbiology*, 109(5): 615-632. doi: 10.1111/mmi.13999.
*These authors contributed equally.
- Paper II** Barbuti, M. D., **Myrbråten, I. S.**, Stamsås, G. A., Heggenhougen, M. V., Straume, D. & Kjos, M. The function of CozE proteins is linked to lipoteichoic acid biosynthesis in *Staphylococcus aureus* (Manuscript).
- Paper III** **Myrbråten, I. S.**, Stamsås, G. A., Chan, H., Morales Angeles, D., Knutsen, T. M., Salehian, Z., Shapaval, V., Straume, D. & Kjos, M. SmdA is a novel cell morphology determinant in *Staphylococcus aureus* (Manuscript).
- Paper IV** **Myrbråten, I. S.**, Wiull, K., Salehian, Z., Håvarstein, L. S., Straume, D., Mathiesen, G. & Kjos, M. (2019). CRISPR interference for rapid knockdown of essential cell cycle genes in *Lactobacillus plantarum*. *mSphere*, 4(2): e00007-19. doi: 10.1128/mSphere.00007-19.

Paper by author not included in this thesis

Kuczkowska, K., **Myrbråten, I.**, Øverland, L., Eijsink, V. G., Follmann, F., Mathiesen, G. & Dietrich, J. (2017). *Lactobacillus plantarum* producing a *Chlamydia trachomatis* antigen induces a specific IgA response after mucosal booster immunization. *PLoS One*, 12(5): e0176401. doi: 10.1371/journal.pone.0176401.

1. Introduction

Antibiotics target essential processes and structures in bacteria to kill the cells or stop their multiplication. Most pathogenic bacteria multiply by binary fission, although the exact mechanisms of division vary due to differences in cell morphologies between species. Some of the conserved cell cycle processes, such as DNA replication and synthesis of peptidoglycan in the bacterial cell wall, are well established targets for commonly used antibiotics. For example, fluoroquinolones inhibit DNA synthesis, while β -lactams, such as penicillin, stops synthesis of peptidoglycan. However, with the development and spread of antibiotic resistance, there is an urgent need to explore novel therapeutic targets in antibiotic resistant pathogens. In this context, there are still processes critical for bacterial cell division, morphology maintenance and cell integrity, which are potentially excellent, but yet underexploited antibiotic targets. This include for example proteins involved in the early stages of cell division (Sass & Brötz-Oesterhelt, 2013) and teichoic acid biosynthesis (Pasquina et al., 2013). In order to fully appreciate the repertoire of potential antibiotic targets in the bacterial cell cycle, it is of critical importance to understand how the proteins involved work and how different processes are functionally linked. By studying such essential processes, new possible targets for future therapeutics can appear, as well as new knowledge that represent unknown values in the future.

In the work of this thesis, essential, yet unstudied proteins and processes important for maintaining cell morphology and integrity during cell division in the priority pathogen *Staphylococcus aureus* (Tacconelli et al., 2018) have been identified and investigated. In addition, some of the same proteins have also been studied in bacteria with other shapes and modes of division to understand their functional conservation across different bacteria. In the following sections, a general background on important structures and processes involved in the cell cycle of the spherical bacterium *S. aureus* are given, as well as some details on cell division factors in oval-shaped *Streptococcus pneumoniae* and rod-shaped *Lactobacillus plantarum*.

1.1. *Staphylococcus aureus* – an antibiotic resistant opportunistic pathogen

Staphylococcus aureus is a Gram-positive, spherical bacterium belonging to the Firmicutes. It is an opportunistic pathogen in human and animals, and 20-30 % of the human population is persistent nasal carriers (Kluytmans et al., 1997; Sakr et al., 2018). Infections can manifest in different ways, ranging from superficial skin infections to invasive, life-threatening infections like sepsis, endocarditis, or meningitis. *S. aureus* infections are commonly treated with antibiotics from the β -lactam class, such as oxacillin or cephalosporins, or with the glycopeptide vancomycin, depending on the antibiotic susceptibility profile of the infectious strain (David & Daum, 2017). However, the emergence of antimicrobial resistant strains has made staphylococcal infections more difficult to treat. As mentioned above, a common feature of antibiotics is that they target essential processes that the bacterial cells rely on to be able to divide and survive. These targeted processes can be the synthesis of the cell wall, the integrity of the cell membrane, DNA transcription or protein translation (Etebu & Ariekpar, 2016). Bacteria have, however, an incredible ability to adapt to external changes, such as antibiotic exposure, and *S. aureus* is no exception. For instance, while β -lactams target cell wall synthesis by binding to the so-called penicillin binding proteins (PBP), the problematic methicillin-resistant *S. aureus* (MRSA) acquired a gene, *mecA*, encoding an additional PBP (PBP2A) that has lower affinity for β -lactams. PBPs are essential in the synthesis of peptidoglycan, the major constituent of the cell wall, and by expressing PBP2A, MRSA can continue this vital process even in the presence of β -lactam antibiotics (Hartman & Tomasz, 1984; Rossi et al., 1985; Ubukata et al., 1985). Similarly, the equally problematic vancomycin-resistant *S. aureus* (VRSA) has acquired vancomycin resistance genes from enterococci to alter the target for this class of antibiotics (McGuinness et al., 2017).

1.2. Surrounding the staphylococcal cell

A bacterial cell is surrounded by several layers of polymeric structures. These are critical for cell integrity and shape, as well as for protection and communication with the external environment. A simplified overview of the cell envelope layers of *S. aureus* is given in **Fig. 1**. In the outermost layer, facing the environment, is a polysaccharide capsule. The capsule, which helps *S. aureus* avoid the immune system

and phagocytic engulfment, can vary greatly both in thickness and composition. Eleven different serotypes of capsular polysaccharides have so far been identified, and the level of expression is highly variable and dependent on environmental conditions (O’Riordan & Lee, 2004; Sompolinsky et al., 1985). Under this capsule, the staphylococcal cell wall is located. This structure encloses the cell membrane and provides structural support against the high internal turgor pressure and maintenance of cell shape. The main component of the cell wall is peptidoglycan, a macromolecule that serves as an anchor for polysaccharides, proteins, and wall teichoic acids (**Section 1.2.1. and 1.2.2.**). Finally, the cytoplasmic membrane, consisting of a bilayer of phospholipids as well as conjugated lipids, glycolipids and lipoteichoic acids (**Section 1.2.2**), represents a selective permeability barrier between the inside and outside of the cell. It also consists of integrated membrane proteins and building blocks for the extracytoplasmic cell wall structures, that needs to be translocated across the membrane at some point during cell wall synthesis.

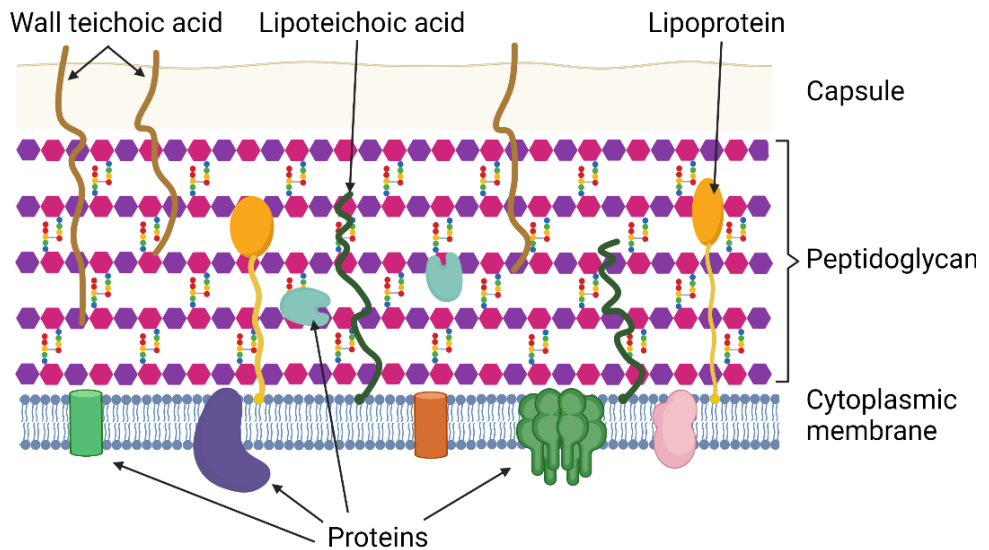


Fig. 1. Schematic overview of the surrounding layers of a staphylococcal cell. The layers consist of the cytoplasmic membrane, peptidoglycan, and a capsule. Proteins, lipoproteins, lipoteichoic acids and wall teichoic acids attached to the cell wall or membrane are indicated. Figure created with BioRender.com.

1.2.1. Structure of staphylococcal peptidoglycan

The cell wall of *S. aureus* is about 20 nm (Pasquina-Lemonche et al., 2020) where the main component is a mesh of peptidoglycan (PG). The core unit of PG is a β -1 \rightarrow 4 linked *N*-acetylglucosamine (GlcNAc)-*N*-acetylmuramic acid (MurNAc) disaccharide, where a stem peptide is attached to MurNAc (Ghuysen, 1968; Giesbrecht et al., 1998). The PG mesh is composed of glycan chains of alternating GlcNAc and MurNAc residues, with an average length of approximately 10 disaccharides (Sidow et al., 1990), linked together by peptide bridges between the stem peptides (Fig. 2). The stem peptides, consisting of L-alanine, D-glutamine, L-lysine, and two D-alanine residues, are connected between the L-lysine of one stem peptide to the fourth D-alanine of another stem peptide by a pentaglycine cross-bridge (a process which result in loss of the terminal D-alanine; Fig. 2). It is estimated that about 90 % of the stem peptides form such bridges to connect the glycan chains (Labischinski, 1992). This results in a high degree of crosslinking, a characteristic trait of *S. aureus*.

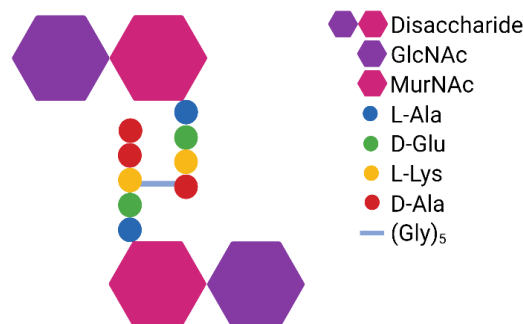


Fig. 2. Crosslinking of glycan chains. A stem peptide, attached to MurNAc of the disaccharide backbone, forms a pentaglycine bridge through its L-lysine with D-alanine of another stem peptide. Figure created with BioRender.com.

1.2.2. Teichoic acids

Teichoic acids are anionic glycopolymers usually made of glycerol-phosphate (GroP) or ribitol-phosphate (RboP). It is believed that teichoic acids compensate for the outer membrane found in Gram-negative bacteria which are absent in Gram-positives. Collectively, the PG and teichoic acids are responsible for, among other things, molecule trafficking, regulation of hydrolases, cation homeostasis and protection against environmental stress factors. Additionally, they represent an anchor site for extracellular proteins and function as important virulence factors (Neuhaus &

Baddiley, 2003; Swoboda et al., 2010; Xia et al., 2010a). Teichoic acids are either covalently linked to the PG and called wall teichoic acid (WTA), or linked to the membrane and hence called lipoteichoic acid (LTA). In wild-type cells, it is possible to knock out WTA production, but not simultaneously as LTA synthesis is compromised (Oku et al., 2009). On the other hand, LTA synthase mutants usually obtain suppressor mutations, and LTA is thus more essential for staphylococcal viability than WTA (Hesser et al., 2020a).

1.2.2.1. Structure of wall teichoic acids (WTA)

The structure of WTA can vary between bacterial species, but WTA of *S. aureus* mainly consist of polyribitol phosphate (poly-RboP) (**Fig. 3**). WTA is linked to MurNAc in the PG via a linkage unit consisting of a GlcNAc-1-P and *N*-acetylmannosamine (ManNAc) disaccharide with two GroP units linked to ManNAc. The main chain consists of 11-40 RboP units (Neuhaus & Baddiley, 2003; Swoboda et al., 2010; Xia et al., 2010a) (**Fig. 3**). The phosphate groups are negatively charged, but WTA are usually decorated with D-alanine residues that have a positive charge through the free amino group (Baddiley et al., 1962; Xia et al., 2010a). Additionally, WTA are glycosylated by addition of GlcNAc to the RboP units through α - or β -O-linkages (Sanderson et al., 1962; Winstel et al., 2014). The substitution patterns (addition of D-alanine and α - and/or β -O linked GlcNAc) are different among *S. aureus* strains and have been shown to vary in response to environmental conditions. Furthermore, these modifications are important for the bacterial physiology, for instance regarding resistance to harmful molecules, as well as nasal colonization and pathogenesis (Mistretta et al., 2019; Swoboda et al., 2010; Winstel et al., 2015). A recent study by Du et al. (2021), for example, demonstrated that *Staphylococcus epidermidis* changed from WTA consisting of GroP to RboP (*S. aureus* type) when switching from a commensal to pathogenic lifestyle. This emphasize the role of WTA in the physiology and pathogenesis of *S. aureus*. A further description of WTA biosynthesis is given in **Section 1.3.3.2**.

1.2.2.2. Structure of lipoteichoic acids (LTA)

The structure of staphylococcal LTA is less diverse between strains than that of WTA. LTA consists of chains of poly-GroP attached to the plasma membrane through a diglycosyl-diacylglycerol (Glc₂DAG) lipid anchor (**Fig. 3**). LTA and Glc₂DAG constitute approximately 5 % and 7 % of the lipids in the *S. aureus* membrane, respectively, while the remaining constituents are non-glycosylated DAG (20 %) and phospholipids (primarily phosphatidylglycerol) (Koch et al., 1984). LTA is believed to

not extend through the whole PG and thus not be surface exposed (**Fig. 1**) (Reichmann et al., 2014). As WTA, LTA is also decorated with D-alanyl esters at the GroP units, modulating their charge and properties (Reichmann & Gründling, 2011; Xia et al., 2010a), and can be glycosylated with GlcNAc (Rismondo et al., 2021). A further description of the LTA synthesis pathway is given in **Section 1.3.3.3**.

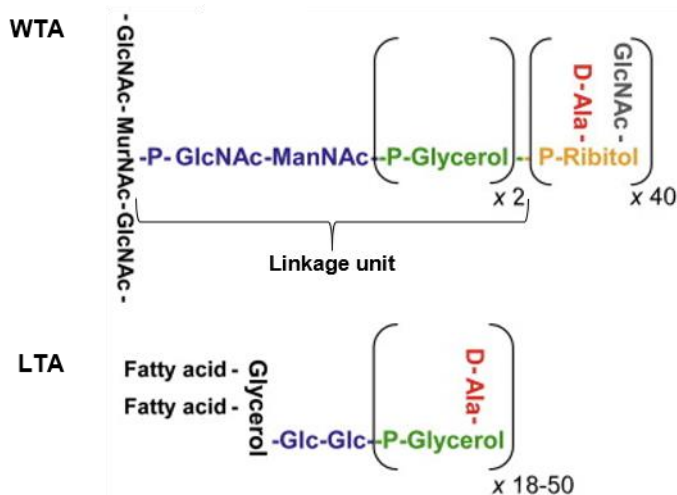


Fig. 3. Schematic representation of the structures of staphylococcal teichoic acids. Structure of wall teichoic acid (WTA) is shown at the top, and the structure of lipoteichoic acid (LTA) is shown at the bottom. The figure is reprinted from Xia et al. (2010a) with permission from Elsevier.

1.3. The cell cycle of *S. aureus*

Division of a bacterial cell into two daughter cells is a vital process for survival and growth. The time between each division is defined as a cell cycle. During such a cycle, the bacterial cell needs to replicate the DNA and segregate the chromosomes, synthesize new cell wall, and eventually divide and split. Proteins and protein complexes involved in these processes have to exert their functions in a timely and spatially coordinated manner to ensure that one cell in the end splits into two equal daughter cells, each consisting of a fully segregated nucleoid protected by the surrounding layers (**Fig. 1**). Malfunctions in one of the cell cycle processes will be detrimental to the integrity, morphology and eventually survival of the cells. Such malfunctions may be due to incorrect levels or activities of enzymes involved, or inaccurate timing and/or -subcellular localization of the processes.

1.3.1. Chromosome replication and segregation

Replication of the circular chromosomal DNA is initiated by binding of the replication initiation factor DnaA to AT-rich sequences within the single origin of replication, *oriC*. DNA is unwinded and the replication machinery, also known as the replisome, assembles. The replisomes synthesize new DNA bi-directionally from *oriC* until they meet the replication terminus, *ter*. Here, the replisome dissolves and the cell now holds two sets of sister chromosomes (Hajduk et al., 2016; Katayama et al., 2010).

Next, the two sister chromosomes need to be segregated into two sister cell compartments within the cell. Several processes, primarily studied in other bacteria, have also been shown to be important to ensure proper chromosome segregation in *S. aureus*. The structural maintenance of chromosomes (SMC) complex and ParB/SpoOJ (Chan et al., 2020; Yu et al., 2010) are two proteins with connected functions. ParB/SpoOJ is a DNA-binding protein which binds to specific *parS* sequences in the *oriC*-proximal region (Chan et al., 2020; Gruber & Errington, 2009). The SMC protein is a condensin that has an important role in packing and organization of the chromosome (Britton et al., 1998). SMC has been shown to interact with ParB/SpoOJ (Sullivan et al., 2009) and Chan et al. (2020) demonstrated that SpoOJ and SMC work together for maintaining proper chromosome segregation in *S. aureus*: correct localization of SMC was dependent on SpoOJ, and deletion of *spoOJ* and *smc* simultaneously increased the number of cells with segregation defects, although the viability of *S. aureus* was not severely affected.

Furthermore, DNA translocases, which act as DNA pumps, that move the chromosomes into the two daughter cells at the very end of septum formation, are important in the last steps of chromosome segregation. It has been shown that *S. aureus* requires either the DNA translocase SpoIIIE or FtsK to obtain normal chromosome segregation (Veiga & G Pinho, 2016). By examining cells with almost completed septum, Veiga and G Pinho (2016) observed that SpoIIIE concentrated in foci inside the septum opening in 50 % of the cells, where SpoIIIE is thought to actively pump DNA away from being bisected by the septum.

Neither the SMC/SpoOJ system nor SpoIIIE/FtsK translocases are essential, although deletion of both SMC and SpoOJ simultaneously, or SpoIIIE and FtsK simultaneously, results in an increase of chromosome management defects (Chan et al., 2020; Veiga & G Pinho, 2016). To my knowledge, it is not investigated if deletion of SMC/SpoOJ and SpoIIIE/FtsK is lethal or if cells still would be viable. Nonetheless, it seems likely

that *S. aureus* has several systems, partially overlapping, to ensure efficient chromosome segregation. Furthermore, the lack of essentiality of these proteins have been proposed to be a result of the involvement of additional passive processes affecting the nucleoid in chromosome segregation, such as DNA replication, DNA transcription and entropy, as concluded from studies in other bacteria and by computer modeling (Dworkin & Losick, 2002; Jun & Mulder, 2006; Lemon & Grossman, 2001; Pinho et al., 2013). While the studies so far render the abovementioned proteins as important for proper chromosome segregation in *S. aureus*, they also support the existence of additional systems contributing to this essential process.

1.3.2. Selection of division plane, assembly of the Z ring and the divisome

To coordinate cell division and cell wall synthesis with chromosome segregation, correct selection of division plane is crucial. Up until recently, staphylococcal cells were thought to be fully spherical with an intricate geometry of division site selection in which cell division occurred in three consecutive, perpendicular planes. Recent research have, however, shed new light on details underlying staphylococcal division. Monteiro et al. (2015) utilized super-resolution microscopy to demonstrate that *S. aureus* in fact does elongate slightly during growth, and Reichmann et al. (2019) showed that *S. aureus* harbour both septal and lateral PG synthesis machineries (**Section 1.3.3.1.**). Saraiva et al. (2020) finally demonstrated that division in fact does not necessarily happen in three consecutive, perpendicular planes, as previously thought, although the division plane is always perpendicular to the previous.

In bacteria, division site selection is controlled at the level of division ring (also known as Z ring) assembly, where the initial cell division protein FtsZ polymerizes and forms a scaffold for other proteins involved. Two well-established systems for division site selection exist; the Min- and nucleoid occlusion (Noc) system, but only the latter is present in *S. aureus*. The Noc protein binds DNA, presumably all over the chromosome but with concentrated levels near *oriC*, and inhibits polymerization of FtsZ and hence formation of the Z ring. As segregation of the chromosomes progresses, less Noc will be present at midcell. Consequently, the Z ring assembly can start at this Noc-free location and the division plane is determined (Veiga et al., 2011). Noc is, additionally, shown to be a regulator of DNA replication initiation, and thus

represent the tight relationship and interplay between the processes of chromosome biology and cell division (Pang et al., 2017). Another protein linking these processes is CcrZ, a recently discovered conserved cell cycle regulator in Firmicutes, which couples Z ring formation to initiation of DNA replication by DnaA (Gallay et al., 2021).

As mentioned, cell division initiates by polymerization of FtsZ into the Z ring (Begg & Donachie, 1985; Bi & Lutkenhaus, 1991). FtsZ is a cytoplasmic tubulin homologue, that assembles into dynamic filaments in a GTP-dependent manner (De Boer et al., 1992). Attachment of FtsZ to the inner surface of the cytoplasmic membrane is achieved by FtsA. FtsZ is a highly conserved protein among bacteria, and the Z ring act as a scaffold for the recruitment of the other conserved cell division proteins, which together establish a large complex of proteins called the divisome (Adams & Errington, 2009). Proteins that have been identified as regulators of Z ring formation and part of the divisome include EzrA, SepF and GpsB. EzrA was first identified in *Bacillus subtilis* as a negative regulator of Z ring assembly (Levin et al., 1999), and has been shown in *S. aureus* to be important for cell size homeostasis and for linking late cell wall synthesis proteins (extracellular processes) with the intracellular division ring (Jorge et al., 2011; Steele et al., 2011). EzrA interacts with many cell division proteins, and both GpsBs and PBP2s septal localization is dependent on EzrA (Steele et al., 2011). Using super-resolution microscopy, Lund et al. (2018) showed that inhibition of division ring assembly (targeting FtsZ) caused both FtsZ, EzrA and PG synthesis to delocalize (leading to morphogenic shape-changes and thick cell wall), and that PG synthesis (see **Section 1.3.3.1.**) followed the localization of FtsZ and EzrA.

When the Z ring is assembled, recruitment of the other proteins which constitutes the divisome starts. The main early division proteins (after FtsZ) are already mentioned, FtsA and EzrA, while SepF, GpsB, FtsL, DivIB and DivIC are proteins commonly referred to as late division proteins. Additionally, the PG synthesizing proteins PBP1, PBP2, PBP3, PBP4, RodA and FtsW are also members of the divisome. All the proteins constituting the divisome either have an active role in synthesis of new PG or in coordination of these processes related to cell division (Booth & Lewis, 2019; Pinho et al., 2013). Recent developments have shown that the Z ring and the divisome do not constitute a fixed ring-structure, but rather moves dynamically around as patches in the division plane due to polymerization and depolymerization of FtsZ (Bisson-Filho et al., 2017). This dynamic movement, called treadmilling, is particularly

important for the early phase of cell division (Monteiro et al., 2018; Whitley et al., 2021).

1.3.3. Synthesis of new cell wall

In order to maintain cell morphology and integrity during cell growth and division, new cell wall needs to be synthesized for incorporation into the existing PG mesh and for making the septal cross wall. In **Section 1.2.1. and 1.2.2.**, the structures of the main parts constituting the cell wall were explained.

1.3.3.1. The biosynthetic pathway of peptidoglycan production

The synthesis of PG (see structure in **Section 1.2.1.**) is a multistep process which starts in the cytoplasm, continues at the inner membrane leaflet before the final polymerization steps occur at the outside of the cell membrane (overview in **Fig. 4**). Initially, the uridine diphosphate (UDP)-linked sugar precursors are made in the cytoplasm. UDP-*N*-acetylglucosamine (UDP-GlcNAc) is synthesized first from fructose-6-phosphate, catalyzed by the enzymes GlmSMU (Barreteau et al., 2008). The enzymes MurA and MurB uses UDP-GlcNAc to produce UDP-MurNAc, before the amino acids, constituting the stem peptide, are attached consecutively by the enzymes MurCDEF, to make UDP-MurNAc-pentapeptide (Barreteau et al., 2008). Next, the membrane protein MraY catalyzes the linking of the MurNAc-pentapeptide to the transport lipid undecaprenyl phosphate (C₅₅-P, also known as bactoprenol), making lipid I. Lipid II is then formed by MurG, which adds GlcNAc to lipid I (Bouhss et al., 2007). Still at the inner surface of the plasma membrane, the pentaglycine chain (Gly₅) is added to the third amino acid in the stem peptide, L-lysine, by a process catalyzed by FemABX (Rohrer & Berger-Bächi, 2003). At this point, Lipid II-Gly₅ is flipped to the outer side of the plasma membrane by MurJ (Sham et al., 2014). Importantly, MurJ seems to be the protein responsible for directing peptidoglycan synthesis to the septum (Monteiro et al., 2018), and the last steps of PG synthesis takes place by transglycosylation (polymerization of subunits from lipid II to form the glycan chain) and transpeptidation (crosslinking of stem peptides).

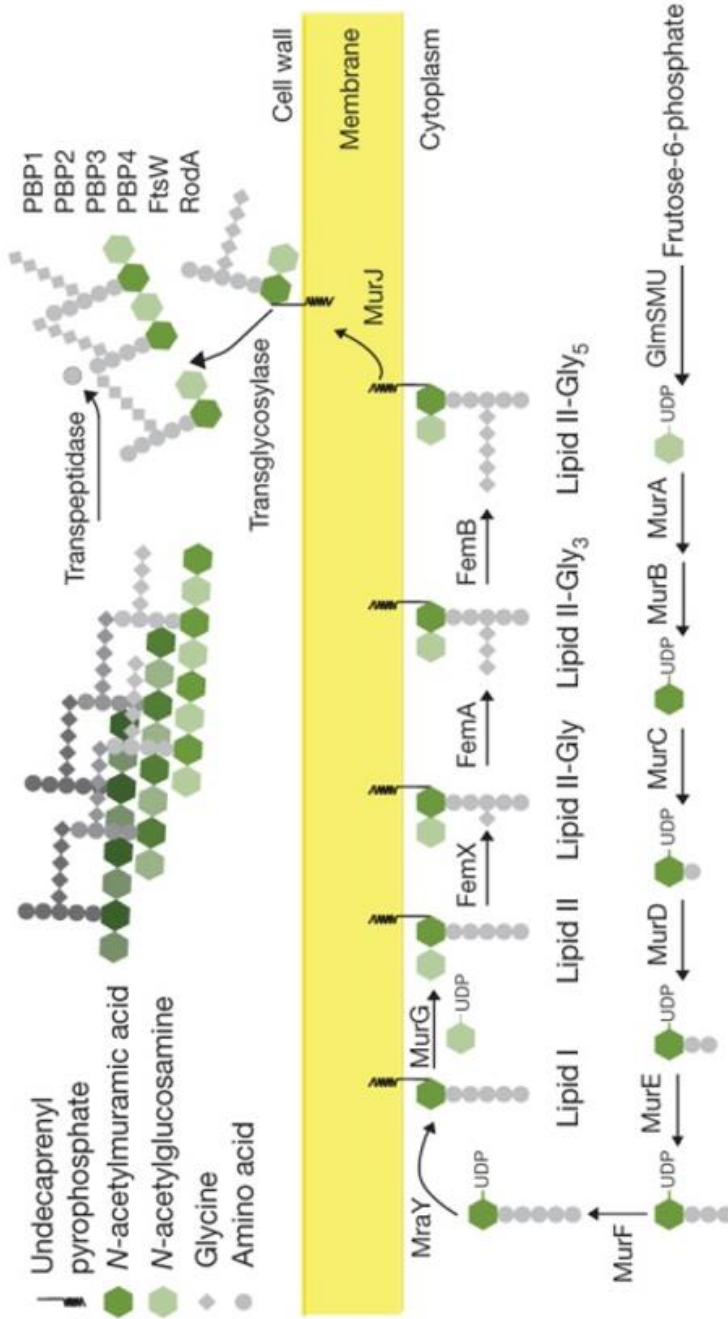


Fig. 4. Schematic presentation of peptidoglycan synthesis in *S. aureus*. Synthesis of the precursor Lipid II-Gly₅ starts in the cytoplasm (by GlmSMU, MurABCDE) and is finalized at the intracellular face of the membrane (by MurY, MurG, FemABX). MurJ flips Lipid II-Gly₅ across the membrane, and the peptidoglycan mesh is synthesized by the transglycosylation- and transpeptidation processes exerted by PBP1, PBP2, PBP3, PBP4, FtsW and RodA. The figure is reprinted from Monteiro et al. (2018) with permission from Nature.

Penicillin binding proteins (PBPs) are the main proteins involved in this final stage of peptidoglycan synthesis. These proteins are grouped into low molecular mass (LMM) PBPs and high molecular mass (HMM) PBPs, and the group of HMM PBPs is further divided into class A PBPs (aPBPs), which are bifunctional with both transglycosylase and transpeptidase activity, and class B PBPs (bPBPs), which only have transpeptidase activity (Goffin & Ghuysen, 1998). *S. aureus* encodes four penicillin binding proteins (PBP1-4) with variable essentiality; the essential PBP2 belongs to class A, the essential PBP1 and non-essential PBP3 belongs to class B, while PBP4 is a non-essential LMM PBP. PBPs are the target for the β -lactam antibiotics such as penicillin. The MRSA strains encode a fifth PBP, namely the transpeptidase PBP2A, with low affinity to β -lactams, thus being responsible for the β -lactam resistant phenotype of these bacteria (**Section 1.1**).

Exciting findings recent years have assigned specific functions to several staphylococcal PBPs. It started when the functionality of RodA, a protein belonging to the family of shape, elongation, division and sporulation (SEDS) proteins, was elucidated in the rod-shaped *B. subtilis* (Meeske et al., 2016). SEDS proteins were identified as a new family of PG polymerases, harboring transglycosylase activity. They were shown to work together with bPBPs and thus act as transglycosylase and transpeptidase pairs, where RodA and FtsW together with their cognate bPBP polymerizes lateral and septal PG, respectively, in these cells (Cho et al., 2016; Emami et al., 2017; Taguchi et al., 2019). Rods and ovococci, like *B. subtilis*, *E. coli* and *S. pneumoniae*, contains between 6 and 16 PBPs (Sauvage et al., 2008). These elongating species hold two cell division machineries, namely the divisome and the elongasome, where the latter is responsible for the lateral PG synthesis and elongation of the cells (Den Blaauwen et al., 2008; Stamsås et al., 2017). Coccus-shaped *S. aureus*, on the other hand, has been recognized as a simple model organism because it contains only four PBPs which mainly synthesize PG in one machinery at septum (Pinho & Errington, 2003; Reed et al., 2015). On this basis, the presence of the SEDS members RodA and FtsW in *S. aureus* raised the question on what role they exhibited in this round-shaped bacterium. However, as it was shown that *S. aureus* elongate slightly (Monteiro et al., 2015), these cells in fact also have an elongation-specific complex. Specifically, RodA works in pair with PBP3 and FtsW works in pair with PBP1 to perform the transglycosylation and transpeptidation reactions needed for elongation and septal PG synthesis, respectively. The coordinated activity of these machineries is therefore responsible for obtaining the coccoid cell morphology (Reichmann et al., 2019).

The only bifunctional PBP in *S. aureus* is PBP2. This protein has a septum-enriched localization (Monteiro et al., 2018; Pinho & Errington, 2005), and while being essential, the exact function is not known. It has been suggested that aPBPs in bacteria are not involved in the primary PG synthesis, but instead being important for repair and maintenance of the PG mesh (Straume et al., 2021). Whether this is true for *S. aureus* awaits further studies. Finally, the LMM PBP4 of *S. aureus* function as a secondary transpeptidase, responsible for the high degree of cross-linking found in *S. aureus* (Atilano et al., 2010; Wyke et al., 1981). PBP4 is additionally proven to be an important contributor for β -lactam resistance (Da Costa et al., 2018; Hamilton et al., 2017; Henze & Berger-Bächi, 1995; Hill et al., 2019; Memmi et al., 2008).

1.3.3.2. Biosynthesis of wall teichoic acids

WTA of *S. aureus* primarily consists of RboP (**Section 1.2.2.1. and Fig. 3**), and the genes involved in WTA biosynthesis in *S. aureus* are named *tar* for teichoic acid ribitol (Sewell & Brown, 2014). A schematic presentation of WTA biosynthesis is found in **Fig. 5**. The synthesis starts in the cytoplasm, where the linkage unit (GroP₁₋₂-ManNAc-GlcNAc-P, **Fig. 3**) is initially attached to the lipid carrier C₅₅-P (bactoprenol) (Kojima et al., 1983), which is the same lipid carrier used for the biosynthesis of PG (**Section 1.3.3.1.**). The first two enzymes, TarO and TarA, moves GlcNAc-1-P from UDP-GlcNAc to C₅₅-P (Soldo et al., 2002) and attaches ManNAc, respectively, to make ManNAc-GlcNAc-C₅₅-P. The linkage unit is finalized by addition of two GroP units, attached consecutively by TarB and TarF (Ginsberg et al., 2006; Sewell & Brown, 2014). Subsequently, TarL catalyze the polymerization of RboP to produce WTA consisting of poly-RboP (Brown et al., 2008). TarD and TarIJ are the enzymes producing the WTA precursors cytidine diphosphate (CDP)-Gro and CDP-Rbo, respectively (Badurina et al., 2003; Pereira & Brown, 2004). While still intracellular, TarM and TarS are responsible for, respectively, adding α - or β -O linked GlcNAc modifications (Brown et al., 2012; Xia et al., 2010b), before the TarGH ABC transport system exports the poly-RboP across the membrane (Lazarevic & Karamata, 1995). Here, the DltABCD proteins can further modify the molecules by decorating the poly-RboP by D-alanylation (Neuhaus & Baddiley, 2003). The LytR-CpsA-Psr (LCP) proteins MsrR (LcpA) and SA0908 (LcpB) are suggested to be responsible for the anchoring of poly-RboP to the PG, as a deletion mutant (Δ *lcp*) was demonstrated to release WTA to the culture medium (Chan et al., 2013; Dengler et al., 2012; Stefanović et al., 2021).

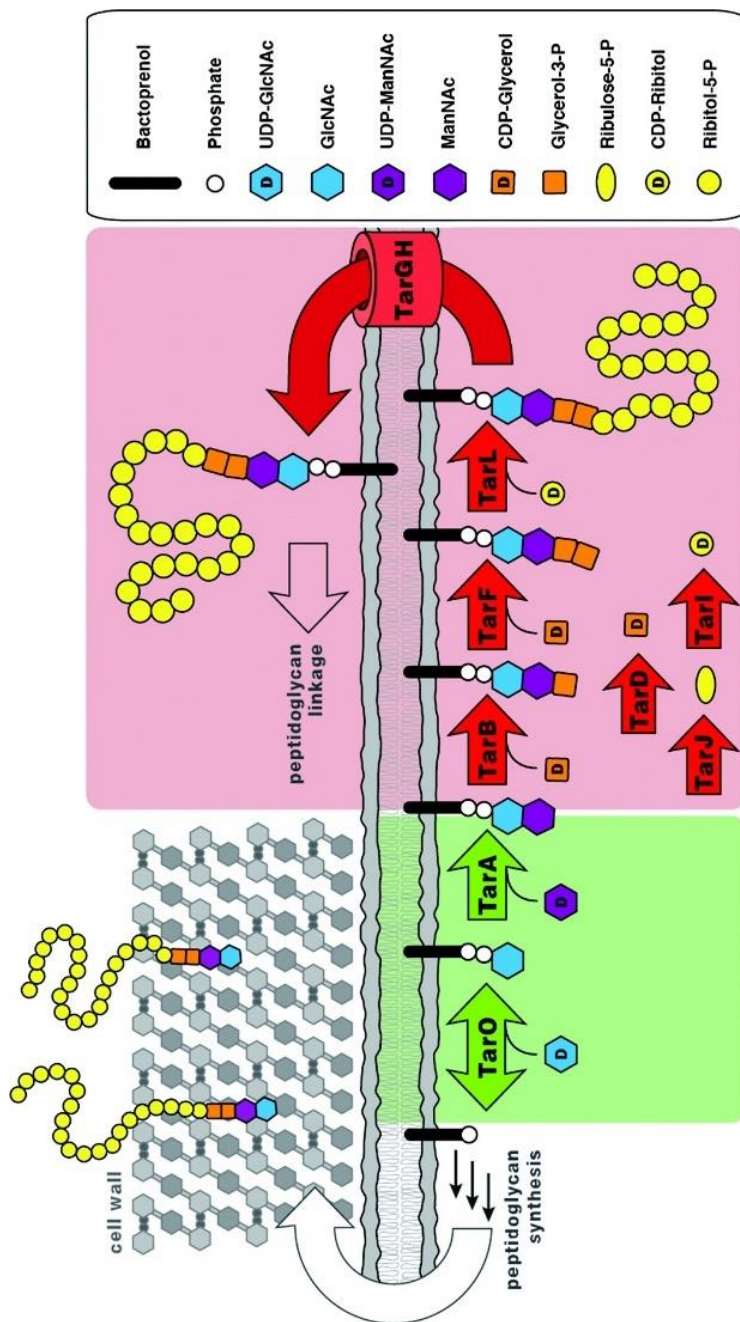


Fig. 5. Schematic illustration of the biosynthesis of wall teichoic acids in *S. aureus*. TarO and TarA catalyze the first steps, resulting in attachment of GlcNAc and MannNAc to the lipid carrier. TarB and TarF attach the two GroP units, and TarL is responsible for polymerizing the RboP-chain. TarGH translocate the polymer to the external face of the cytoplasmic membrane, followed by anchoring of WTA to the peptidoglycan. TarD is responsible for making the CDP-Gro precursor, and TarJ and TarI for making CDP-Rbo precursor. The figure is reproduced from Swoboda et al. (2009), with permission from Wiley.

Interestingly, it has been shown that the early biosynthetic genes *tarO* and *tarA* are not essential, while the genes whose product functions later in the biosynthetic pathway, like *tarB*, *tarD*, *tarF*, *tarL*, *tarI* and *tarG*, are essential. The essentiality of these genes is however lost if *tarO* or *tarA* is deleted simultaneously, which indicates that accumulation of intermediate products are toxic for the cells (D'Elia et al., 2006; D'Elia et al., 2009; Meredith et al., 2008).

1.3.3.3. Biosynthesis of lipoteichoic acids

LTA is linked to the cytoplasmic membrane via the Glc₂DAG anchor, with a chain consisting of D-alanylated poly-GroP (**Section 1.2.2.2.** and **Fig. 3.**). The biosynthesis of LTA (**Fig. 6**) also starts in the cytoplasm with the glycosyltransferase UgtP (also called YpfP), producing the Glc₂DAG anchor. Specifically, UgtP catalyzes the transfer of two glucose units, derived from UDP-Glc, to DAG (Jorasch et al., 2000; Kiriukhin et al., 2001). LtaA is then responsible for transporting the Glc₂DAG anchor across the membrane (Gründling & Schneewind, 2007a), and on the extracellular side of the cytoplasmic membrane, LtaS polymerize the GroP chain by utilizing phosphatidylglycerol (Ptd-Gro) as source for the GroP units (Emdur & Chiu, 1975; Glaser & Lindsay, 1974; Gründling & Schneewind, 2007b). DAG on the extracellular side is a byproduct from this reaction and is probably recycled back into Ptd-Gro (Jerga et al., 2007). The DltABCD is, as mentioned, responsible for D-alanylation of TA. Intracellularly, DltA charges DltC with a D-alanine, which then will bind to the membrane-bound channel protein DltB. It is not fully established how the next steps continues, but it is believed to involve either a direct transfer of the D-alanine from DltB to DltD, and subsequently to LTA, or with an intermediate step where DltB transfers the D-alanine to a lipid carrier, before it moves to DltD and finally LTA (Ma et al., 2018; Rismondo et al., 2021; Wood et al., 2018). Additionally, LTA can also be glycosylated, and the glycosyltransferase CsbB, the flippase GtcA and the glycosyltransferase YfhO are together responsible for attachment of GlcNAc onto LTA (Kho & Meredith, 2018; Rismondo et al., 2021).

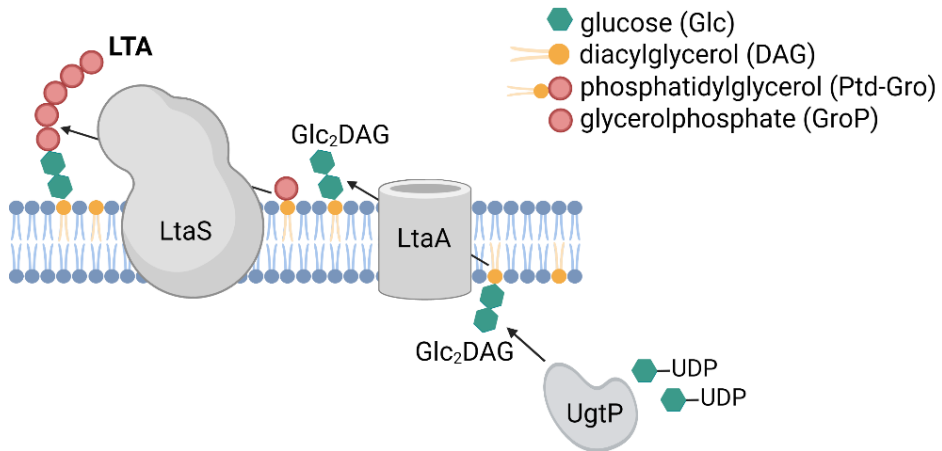


Fig. 6. LTA biosynthesis in *S. aureus*. UgtP attaches two glucose (Glc) units (from uridine diphosphate (UDP)-Glc) to diacylglycerol (DAG), creating Glc₂DAG. LtaA translocate the anchor to the extracellular side, and LtaS subsequently synthesize LTA by moving glycerolphosphate (GroP) from phosphatidylglycerol (Ptd-Gro) to the growing chain. Figure created with BioRender.com.

Deletion mutants of *ugtP* still produces LTA, but instead of being anchored via Glc₂DAG, LTA is polymerized directly on Ptd-Gro (Kiriukhin et al., 2001). Similarly, deletion mutants of *ltaA* also have LTA, but exhibit reduced amounts of Glc₂DAG-anchored LTA compared to wild-type, and have a mixture of Glc₂DAG- and Ptd-Gro-anchored LTA (Gründling & Schneewind, 2007a). This implies that a fraction of the UgtP-produced Glc₂DAG is still translocated over the membrane to some extent in the absence of LtaA, by a yet unknown mechanism. Additionally, the length of LTA polymers has proven to vary in relation to which anchor unit that is used, where the Glc₂DAG-anchored polymers are shorter than Ptd-Gro-anchored ones (Gründling & Schneewind, 2007a; Hesser et al., 2020a). Importantly, LTA length influences both fitness and stress responses, where the shorter Glc₂DAG-anchored LTA is preferable (Hesser et al., 2020a). Hesser et al. (2020b) demonstrated that LtaS has an inherent capacity of controlling the LTA length based on the identity and concentration of the starter units – the lipid anchors Glc₂DAG or Ptd-Gro, and that Δ *ugtP* strains acquired suppressor mutations in *ltaS* which rescued the abnormal long LTA phenotype. *S. aureus* with deletion of either *ugtP* or *ltaA* is, as explained, still viable, but their absence cause morphogenic changes in form of enlarged cells with both misplaced and multiple septa (Hesser et al., 2020a; Kiriukhin et al., 2001). Deletion of the

synthase *ltaS* results in cells without LTA that are only able to grow at high sucrose- or sodium chloride concentrations and exhibit highly aberrant cell morphologies (Corrigan et al., 2011; Gründling & Schneewind, 2007b; Oku et al., 2009). These deletion phenotypes, and results from protein-protein interaction studies between LTA biosynthesis proteins and divisome proteins (Reichmann et al., 2014), strongly suggest a tight link between LTA biosynthesis and coordination of cell division.

1.3.4. Cell splitting and hydrolases

After new PG is fully synthesized by the divisome, so that a septal wall physically separates the two daughter cell compartments, splitting of the mother cell is needed. The actual splitting process happens fast and is over within milliseconds (Monteiro et al., 2015; Zhou et al., 2015). Hydrolases play an important role in cell splitting, though, they are not believed to degrade the whole septal wall. Instead, these enzymes initiate the splitting process by hydrolyzing the peripheral wall bridge that connects the daughter cells (**Fig. 7**), and this, together with mechanical factors, results in a sudden crack that separate the cells (Matias & Beveridge, 2007; Zhou et al., 2015).

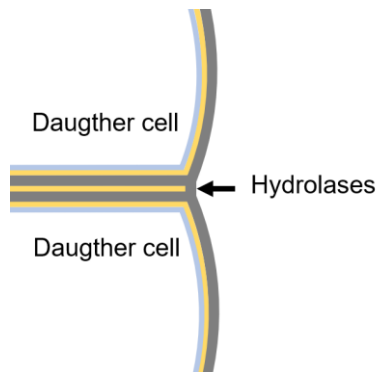


Fig. 7. Cell splitting. A simple, schematic illustration of where hydrolases act during splitting of a cell. The enzymes do not hydrolyze the entire septal wall, but rather the peripheral wall bridge that connects the two daughter cells. Grey; peptidoglycan, blue; cytoplasmic membrane, yellow; low density zones, which both separates each daughter cells new cell wall and corresponds to the periplasmic space between the membrane and the cell wall.

Bacterial hydrolases have different roles regarding what kind of bond in the peptidoglycan they hydrolyze (**Fig. 8**). Glucosaminidases and muramidases cut bonds within the glycan chain, amidases cut the bond connecting the stem peptide to the

glycan chain, endopeptidases cut within the stem peptide, and carboxypeptidases cut off the terminal amino acid of the stem peptide (Vollmer et al., 2008).

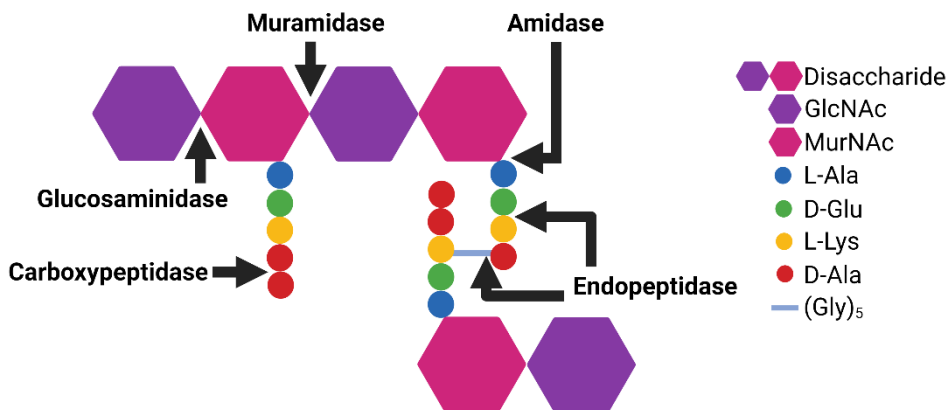


Fig. 8. Target point of different hydrolases. The figure illustrates which bonds in the peptidoglycan that are cleaved by the different groups of hydrolases. Glucosaminidases and muramidases cleaves the glycosidic bonds in the glycan chain, while amidases cleaves off the entire stem peptide, endopeptidases cut within the stem peptide, and carboxypeptidases cut off the terminal amino acid of a stem peptide. Figure created with BioRender.com.

S. aureus holds many different hydrolases, whose roles are important for both remodeling of PG and for cell splitting. The major hydrolase of *S. aureus*, and the best characterized one, is Atl. This is a bi-functional hydrolase that contains two functional domains; an amidase (AmiA) and a glucosaminidase (GlcA) that are released upon proteolytic processing of Atl (Oshida et al., 1995). AmiA cleaves off the stem peptide, the linkage between MurNAc and L-alanine (Biswas et al., 2006), while GlcA cleaves in the glycan chain (**Fig. 8**). Recent research by Nega et al. (2020) demonstrated that GlcA was dependent on AmiA's activity to first strip off the stem peptides, and that GlcA acted on naked glycan chains only, where it worked as an exoenzyme to release MurNAc-GlcNAc disaccharides (**Fig. 2**). Two other important hydrolases involved in cell splitting of *S. aureus* are Sle1 (Kajimura et al., 2005) and LytN (Frankel et al., 2011), which both contains a catalytic CHAP domain and PG-binding LysM domain(s). Sle1 is an amidase, while LytN both functions as an amidase and an endopeptidase cutting the D-Ala-glycine bond (**Fig. 8**) (Frankel et al., 2011; Kajimura et al., 2005).

To allow insertion of new PG during growth and to achieve correct separation of daughter cells, but at the same time avoid uncontrolled lytic activity, it is important that the activity of hydrolases are properly regulated at different levels. The essential two-component regulatory system, WalK/WalR (previously called YycG/YycF), has been demonstrated to be an important regulator of autolytic activity in *S. aureus* (Dubrac & Msadek, 2004; Dubrac et al., 2007), as well as other bacteria (Dobihal et al., 2019; Dubrac et al., 2008). WalKR is a two-component regulatory system where a transmembrane histidine kinase, WalK, senses an extracellular signal, and activates the response regulator, WalR, which in turn acts as a transcriptional regulator of hydrolase genes and thus controls cell wall homeostasis (Fabret & Hoch, 1998; Fabret et al., 1999). The signal sensed by WalK is not known, but recent evidence from *B. subtilis* suggest that they may sense cleaved products from different hydrolases as proxy for the maturity of the cell wall (Dobihal et al., 2019). Several other mechanisms are also described as regulators of hydrolases in different bacteria, including proteolysis (**Section 1.3.5.**), direct inhibitors and activators, and localization control (Do et al., 2020). The enzymes involved in cell splitting need to localize to the septum. Teichoic acids have, for example, been shown to be critical for recruitment of Atl and other hydrolases to septum. The abundance of matured WTA is probably lower in septum compared to the old cell wall surrounding the cell, and has been suggested to repel Atl-derived enzymes, and thereby direct this activity to the septum (Schlag et al., 2010). The septal localization of Sle1 and LytN is also dependent on WTA, as a *tarO* deletion strain or tunicamycin-treated (inhibiting TarO) cells failed to achieve the septal localization of the LysM-containing cell splitting hydrolases (Frankel & Schneewind, 2012). Additionally, Zoll et al. (2012) found that Atl binds to LTA, and that it failed to localize at the septal region in an LTA depleted strain.

1.3.5. Other processes affecting cell cycle and cell morphology of *S. aureus*

As mentioned above, cell cycle processes are highly intertwined and need to be regulated and coordinated by different mechanisms to allow proper cell integrity. Proteins involved need to be maintained at proper levels and at the correct subcellular localization during the cell cycle. Control mechanisms thus include, but is not limited to, transcriptional regulation, for example by WalKR, and localization control via a myriad of dynamic protein-protein interactions, as well as interaction with other structures. Several examples of this are given above. Additionally, more

general processes such as secretion and translocation of proteins and molecules across the membrane play important roles. Molecules need to move across the membrane leaflets and proteins involved in the latter steps of cell wall synthesis execute their function on the cell surface. For example, the secretion-associated proteins SecDF have been shown to be important for virulence and antibiotic resistance and, notably, for performing normal cell division, thus highly affecting the cell morphology (Quiblier et al., 2011).

Another level of regulation is controlled protein folding and degradation by chaperones and proteolytic enzymes with different targets. For example, PBP2A, the β -lactam resistance determinant in MRSA, has been shown to require the chaperones PrsA and HtrA1 for proper folding extracellularly (Roch et al., 2019). Another example is the ClpP protease that can associate with the chaperone ClpX to create a proteolytic complex (Frees et al., 2003). ClpX has been assigned a regulative function in the cell cycle, especially during cold-stress, by controlling cell splitting of daughter cells. Jensen et al. (2019) suggested a model where $\Delta clpX$ cause Sle1 to conduct premature cell splitting, and that inhibitors of PG- and WTA biosynthesis (β -lactams or TarO inhibitors) indirectly affect the activity of Sle1 (presumably due to the role of WTA in localization of Sle1, **Section 1.3.4.**).

1.4. Cell biology and novel cell cycle factors of non-spherical Firmicutes

Although most pathogens divide by binary fission, genus-related differences in cell cycle mechanisms occur. These differences can often be attributed different shapes. To investigate the functional conservation and genus-related differences for some of the cell division factors across bacteria with different cellular shapes, this thesis also includes results from both the rod-shaped beneficial bacterium *L. plantarum* and the oval-shaped pathogen *S. pneumoniae*. Understanding essential processes, such as the cell cycle, in these bacteria is needed to exploit the full potential of the beneficial bacterial strains and for finding new antimicrobial targets in pathogens.

1.4.1. The rod-shaped *Lactobacillus plantarum*

Lactobacillus plantarum is an important bacterium within aspects related to food and health. It has been utilized for food preservation due to its production of bacteriocins (Cleveland et al., 2001), implicated as a probiotic (Alander et al., 1999; de Vries et al., 2006; Niedzielin et al., 2001; Qin et al., 2021; Zago et al., 2011) and exploited for its potential as a delivery vector of therapeutic molecules (Bermudez-Humaran et al., 2011; Kuczkowska et al., 2016; Kuczkowska et al., 2017; Wells & Mercenier, 2008). Knowledge about bacterial cell cycle processes is thus important to allow further improvement of strains for utilization in health aspects; by enhancing protein secretion (therapeutic purpose) or improve properties involved in host cell interactions (as probiotics).

However, the cell cycle processes of *L. plantarum* have been very little studied, both due to research regarding this bacterium has generally had a different focus (food and health), and that molecular tools for exploring such processes have been scarce. In this work we used (and developed) *L. plantarum* as another model for cell cycle studies in rod-shaped Firmicutes bacteria. While many of the cell cycle factors described above for *S. aureus* are also conserved in *L. plantarum*, the knowledge about cell division in *L. plantarum* may generally be inferred from similarities to the rod-shaped, Gram-positive model organism *B. subtilis*, as both are members of the class Bacilli in the phylum Firmicutes. Many of the details found about the cell cycle in *B. subtilis* (Errington & Wu, 2017) most likely also applies for *L. plantarum*. For example, *L. plantarum* has an MreB cytoskeletal protein which directs cell wall synthesis along the lateral axis, in addition to FtsZ, which dictates septal axis also in these bacteria. However, there are also major differences in the cell biology of these two species. For instance, *B. subtilis* has, in contrast to lactobacilli, the ability to make endospores as part of their life cycle. Furthermore, the PG composition is different between the two, since *L. plantarum* synthesize PG precursors resulting in terminal D-alanine-D-lactate instead of D-alanine-D-alanine in the stem peptides – which provides natural resistance to vancomycin (Ferain et al., 1996). It is therefore important to study these processes specifically in *L. plantarum*. Some research groups have contributed with information regarding *L. plantarum*-specific cell cycle factors and morphology determinants. For example, the Hols' lab investigates the functional role of the 12 hydrolases in *L. plantarum*. They showed that the glucosaminidase Acm2 is crucial for cell separation, that the endopeptidase LytA was important for morphogenesis (Rolain et al., 2012) and that LytB is involved in correct placement of the division plane (Duchêne et al., 2019).

1.4.2. The oval-shaped *Streptococcus pneumoniae*

S. pneumoniae is another important human pathogen which is responsible for a range of different infections. In contrast to *S. aureus* and *L. plantarum*, *S. pneumoniae* cells have an oval shape. Many of the proteins involved in cell division and PG synthesis discussed above are conserved also in this species, including FtsZ, FtsA, FtsW, EzrA and GpsB (**Section 1.3.2.**) (Ducret & Grangeasse, 2021; Pinho et al., 2013; Xiang et al., 2019). Although these cells clearly elongate, they lack the rod-shape determining factor MreB present in *B. subtilis* and *L. plantarum*. Somewhat similar to *S. aureus*, cell wall synthesis occurs in the midcell area of these cells, where a divisome and elongasome complex consisting of dedicated PG synthesis proteins are responsible for septal and peripheral synthesis, respectively.

Exactly how the coordination of elongation and septal synthesis in these ovococcal cells is accomplished, is not fully understood. However, several cell division factors have been identified in *S. pneumoniae* recently which have shed light on the questions which comprises regulation of streptococcal elongation. Among these, a protein called MapZ is shown to arrive to midcell prior to FtsZ, thus defining the division site. Additionally, MapZ leaves early from this location, creating two ring structures that moves laterally in different directions towards the future division site of the daughter cells (Fleurie et al., 2014; Holečková et al., 2014). This protein is mainly conserved among the *Streptococcaceae*, and is thus an example of a key cell division factor which is not conserved across different bacterial phyla.

Furthermore, another factor involved in elongation, called CozE (for coordinator of zonal elongation), was identified in this bacterium by Fenton et al. (2016). CozE proteins are conserved across different bacterial phyla. As a member of the MreCD complex, it was shown to control the midcell localization of the bifunctional class A PBP1a and thereby promote elongation and streptococcal morphology. Interaction studies confirmed association to both MreC and PBP1a, it was showed that CozE localization was dependent on MreC and that deletion of *cozE* resulted in PG synthesis defects (Ducret & Grangeasse, 2017; Fenton et al., 2016). A CozE homolog was very recently identified in the same species, namely CozEb (Stamsås et al., 2020). This protein is less important for viability and has an opposite effect on cell size homeostasis compared to CozE, as $\Delta cozEb$ mutant cells were smaller than wild-type cells. CozEb is part of the same protein complex as CozE and PBP1a, but CozEb was not required for PBP1a localization. A double deletion mutant of both *cozE* genes resulted in severe effects on morphology and hampered growth. CozEb was

additionally shown to be able to partially compensate for the loss of CozE – demonstrating an overlapping function and that, together, both CozE proteins are important for shape and size (Stamsås et al., 2020).

Finally, the RNA-binding proteins EloR (Stamsås et al., 2017) and KhpA (Zheng et al., 2017) are two other recently identified elongation factors in *S. pneumoniae*. These two proteins form a heterocomplex, that is likely recruited to midcell by MltG, a lytic transglycosylase important for lateral PG synthesis (Tsui et al., 2016; Winther et al., 2021). The absence of either EloR or KhpA leads to both smaller and shorter cells (Stamsås et al., 2017; Zheng et al., 2017). EloR and KhpA are conserved in different oval- and rod-shaped bacteria (including *L. plantarum*), but homologs are not found in *S. aureus*.

2. Aims of the study

Understanding the molecular details underlying essential cell cycle processes in bacteria can contribute with valuable knowledge for development of new antibacterial strategies to overcome the growing problem of antibiotic resistant pathogens, as well as for optimization of bacterial strains for beneficial food- and health related bacteria.

In this light, the main aim of this thesis was to identify and get functional insights into hitherto unknown, essential cell division factors in *S. aureus*, and study whether their functions were conserved in other bacterial species with different cell shapes. To achieve this, three sub-goals were set up.

1. With the currently available genetic tools in *S. aureus* and *L. plantarum*, studies of essential genes are time-consuming and methodologically challenging. The aim here was to establish CRISPR interference systems to allow for functional studies of essential cell cycle genes in these bacteria (Paper I and IV).
2. A CozE protein was identified as a coordinator of zonal elongation in *S. pneumoniae* (Fenton et al., 2016). This proposed elongation factor is present in bacteria with both spherical and elongated shapes. The aim here was to understand the function and importance of CozE-homologs in spherical *S. aureus* and perform comparative studies of the function of these in the ovococcal *S. pneumoniae*, as well as in the rod-shaped *L. plantarum* (Paper I, II, IV).
3. It is still not fully established how the different processes are coordinated during the staphylococcal cell cycle, and yet unidentified cell cycle factors are likely to exist. By starting from a phenotypic screen of essential proteins with unknown functions, we here aimed to identify and functionally characterize novel factors contributing to cell cycle regulation in *S. aureus* (Paper III).

3. Summary of papers

Paper I

CozEa and CozEb play overlapping and essential roles in controlling cell division in *Staphylococcus aureus*

Stamsås, G. A. *, **Myrbråten, I. S. ***, Straume, D., Salehian, Z., Veening, J. W., Håvarstein, L. S. & Kjos, M. (2018). *Molecular Microbiology*, 109(5): 615-632.

*These authors contributed equally.

A protein called coordinator of zonal elongation, CozE, was identified in *S. pneumoniae* as an important elongation regulator (Fenton et al., 2016). In contrast to the oval-shaped *S. pneumoniae*, round-shaped *S. aureus* synthesize new cell wall only in the septal area. Nevertheless, two homologs of the pneumococcal *cozE* were found in the staphylococcal genome: SAOUHSC_00948 and SAOUHSC_01358. We therefore investigated the role of these proteins in *S. aureus* SH1000. The two membrane proteins were named CozEa and CozEb, respectively, and showed 31 % and 30 % identity to the pneumococcal CozE. It was possible to delete one of the staphylococcal *cozE* genes at a time, but a double knockout was lethal. We developed a CRISPRi system to enable phenotyping of a double CozE-deprived strain (e.g., depletion of CozEa in a $\Delta cozEb$ strain). Absence of both CozE proteins highly affected the morphology of *S. aureus*, as demonstrated by cells displaying both thicker septa and problems with initiation of septum formation, and disturbances in the chromosome biology observed by abnormal staining patterns of the nucleoids. We showed that CozEa and CozEb interacted with the early cell division protein EzrA, and that lack of the CozE proteins seemed to affect the localization pattern of EzrA. This interaction and its impact on localization pattern were conserved in *S. pneumoniae*. Additionally, we demonstrated that the staphylococcal *cozEa* and *cozEb* could complement a *cozE* deletion in *S. pneumoniae*: it was possible to delete the essential streptococcal *cozE* when the staphylococcal *cozEa* and *cozEb* were expressed, and that the phenotype of *S. pneumoniae* CozE-deprivation was partially rescued with expression of the staphylococcal CozE proteins. Thus, CozEa and CozEb together perform an essential function in controlling cell division in *S. aureus*, possibly by interacting with EzrA, and this function seem to be conserved also in *S. pneumoniae*.

Paper II

The function of CozE proteins in linked to lipoteichoic acid biosynthesis in *Staphylococcus aureus*

Barbuti, M. D., **Myrbråten, I. S.**, Stamsås, G. A., Heggenhougen, M. V., Straume, D. & Kjos, M. Manuscript.

By further investigation of the CozEa and CozEb functionality in *S. aureus*, we initially demonstrated that the synthetic lethal and overlapping functions were conserved among different strains, including methicillin-sensitive *S. aureus* (MSSA) and MRSA. By examining the cell cycle phases in CozE-deprived cells, it became evident that an overrepresentation of the population had delayed initiation of septum formation, fully in line with the results from a different MSSA strain in Paper I. Based on phenotype-similarity between CozE-depleted cells and cells lacking lipoteichoic acids (LTA) (Hesser et al., 2020a), and that deletion of *ltaS* (essential LTA synthase) resulted in suppressor mutations in *cozEb* (Corrigan et al., 2011), we looked for and identified links between LTA biosynthesis and the CozE proteins. By utilizing the CRISPRi system, we found that removal of *cozEb* rescued the growth reduction observed in *LtaS* depleted cells. Intriguingly, the opposite was observed in $\Delta cozEa$; here *LtaS* depletion resulted in increased growth reduction compared to a strain depleted of *LtaS* alone. Furthermore, we show that UgtP (glycosyltransferase making the Glc₂DAG-anchor) and *LtaA* (LTA flippase) were modulating the essentiality of the CozE proteins in opposite directions: the significant growth reduction observed in cells depleted of both CozEa and CozEb were alleviated in a $\Delta ltaA$ genetic background, but aggravated in a $\Delta ugtP$ background. Lastly, a unique role of CozEb in controlling the length of LTA was discovered. This study clearly demonstrates a link between CozE proteins and LTA biosynthesis in *S. aureus*, but the exact mechanism explaining this relationship needs further investigation.

Paper III

SmdA is a novel cell morphology determinant in *Staphylococcus aureus*

Myrbråten, I. S., Stamsås, G. A., Chan, H., Morales Angeles, D., Knutsen, T. M., Salehian, Z., Shapaval, V., Straume, D. & Kjos, M. Manuscript.

From an initial subcellular localization- and gene knockdown screen of essential, hypothetical genes in *S. aureus*, we identified a membrane protein with septal-enriched localization. The established CRISPRi system was used to knock down gene expression, and the observed phenotype with irregular morphology, recognized by abnormal septum formation and cell splitting problems, implied a role in cell division. The protein, with locus tag SAOUHSC_01908 and here named staphylococcal morphology determinant A (SmdA), was by sequence alignments shown to be fully conserved in the *Staphylococcaceae* family. It has a predicted N-terminal membrane-spanning helix, with a large intracellularly part harboring partial homology to an uncharacterized, nuclease-related domain (NERD). By overexpression and mutagenesis, we identified residues that are critical for the function of SmdA, located near the C-terminus and within the NERD. Pulldown experiments and bacterial two-hybrid assays revealed that SmdA interacts with many proteins, including cell division factors such as EzrA, PBPs and Atl. We show that *S. aureus* require balanced amounts of membrane-attached SmdA to coordinate cell division and cell splitting to maintain the staphylococcal morphology, as both its depletion, overexpression and overexpression without the transmembrane helix results in major morphology defects. Notably, knockdown of SmdA results in increased sensitivity to cell wall targeting antibiotics, including re-sensitization to β -lactams in MRSA, which makes SmdA a potential candidate as a future antimicrobial target.

Paper IV

CRISPR interference for rapid knockdown of essential cell cycle genes in *Lactobacillus plantarum*

Myrbråten, I. S., Wiull, K., Salehian, Z., Håvarstein, L. S., Straume, D., Mathiesen, G. & Kjos, M. (2019). *mSphere*, 4(2): e00007-19.

Cell cycle processes in the important food- and health related bacterium *L. plantarum*, represents a scarce research field. Yet, detailed information about the involved processes represents valuable potential for strain improvements. We established a CRISPRi system as a genetic tool in this bacterium, allowing for easy and rapid gene knockdown studies of almost any gene of interest, including essential genes. We demonstrated that the depletion system was functional by knocking down the glucosaminidase Acm2, the DNA replication initiator DnaA and the early cell division protein EzrA, leading to, respectively, pronounced cell chaining, anucleate and abnormal nucleoid morphology, and elongated cells (probably due to delayed cell division). We further investigated the role of cell division proteins characterized in round-shaped *S. aureus* and the ovococci *S. pneumoniae*, which had not yet been studied in rod-shaped bacteria. The two CozE homologs found in *L. plantarum* did not seem to be important for elongation, as in *S. pneumoniae* (Fenton et al., 2016; Straume et al., 2017) or for coordination of cell division, as in *S. aureus* (Paper I and II). Two RNA-binding proteins, EloR and KhpA, that were recently shown to be involved in regulation of cell elongation in *S. pneumoniae* (Stamsås et al., 2017; Winther et al., 2019; Zheng et al., 2017) were shown to be important for proper cell elongation in rod-shaped *L. plantarum* as well.

4. Main results and discussion

The results from this thesis have both contributed with new genetic tools in *S. aureus* and *L. plantarum* (Paper I and IV), and with new insights into novel cell division factors, mainly in *S. aureus* (Paper I, II and III), but also in *S. pneumoniae* (Paper I) and *L. plantarum* (Paper IV). Two different approaches were used for identification of novel morphology- and cell division factors in *S. aureus*: a homology-based approach where the candidate proteins showed homology to a newly identified cell division factor in another bacterium (Paper I and II), and a “starting-from-scratch” approach with an initial screen to select a candidate protein to be subjected for further functional studies (Paper III).

4.1. Methodological considerations

4.1.1. Why and how study essential genes – the CRISPRi approach

As emphasized earlier, essential genes, including those involved in the bacterial cell cycle, are common targets by antibiotics, as bacteria depends on these genes for survival and growth. Bacteria are surpassing us in the evolutionary perspective. With their minimal generation time of about 20-30 minutes and great ability of adapting to external changes, they will most likely develop resistance to most current and new antibiotics as well. To keep up with their evolutionary traits and avoid being put 100 years back in time – medically speaking, it is important to learn more about the essential processes to allow development of new combat strategies. In that light, essential genes represent a pool for new, potential antimicrobial targets. Additionally, learning such details about beneficial bacterial species, like *L. plantarum*, can provide a basis for new strain improvements and further utilization in different applications.

Hence, functional studies of essential processes in bacteria can provide great benefits, however, such studies encounter methodological hurdles. A normal approach for investigating the function of unknown genes is by construction, and phenotyping, of inactivation- or deletion mutants. This approach is, however, solely applicable with non-essential genes, as deleting essential genes by definition render a bacterium non-viable. To circumvent this issue, systems to knock down gene expression can be used.

In this work, CRISPR interference (CRISPRi) systems for knockdown in *S. aureus* and *L. plantarum* (Paper I and IV) were successfully developed and implemented. This allowed for investigation of many essential genes and processes in these species where construction of mutants is otherwise rather laborious (Paper I-IV).

Great strides have been made in the field of molecular tools for genome editing and gene silencing since the functional description of Type II CRISPR-Cas systems by Jinek et al. (2012), a discovery that led Jennifer Doudna and Emmanuelle Charpentier to be awarded the Nobel Prize in Chemistry of 2020. This has revolutionized the molecular toolbox within genome editing and gene depletion systems in bacteria (Bikard et al., 2013; Jiang et al., 2013; Jinek et al., 2012; Larson et al., 2013; Liu et al., 2017; Qi et al., 2013) (Paper I and Paper IV). The CRISPR-Cas Type II system is simple and consists of the endonuclease Cas9 (from *Streptococcus pyogenes*) and a chimeric single guide RNA, which is required for guiding Cas9 to a specific DNA target sequence (by homology and recognition of a so-called protospacer-adjacent motif, PAM, 5'-NGG-3' for the Cas9 used here). CRISPRi utilize a catalytical inactive, "dead" Cas9 (dCas9), which still binds DNA but has lost its endonuclease activity. Expression of both dCas9 and sgRNA simultaneously results in transcriptional blockage of the target gene by dCas9, guided to the target sequence (protospacer) by sgRNA (Bikard et al., 2013; Qi et al., 2013). The specificity and relative simplicity of this CRISPR/(d)Cas9 system allows for easy target exchange and clear rules for design of new sgRNAs. CRISPRi systems are thus increasingly established in different bacterial species and represents a powerful tool for efficient and specific knockdown of gene expression, as demonstrated for the *S. aureus* and *L. plantarum* CRISPRi systems developed in this thesis (Paper I-IV). CRISPRi can be said to have exceeded the potential ever harbored by alternative approaches, such as antisense RNA techniques, and this is attributed higher stability and predictability of the CRISPRi system (Song et al., 2015; Tian et al., 2017).

Our work also demonstrated some of the inherent limitations of CRISPRi. Most importantly, since CRISPRi functions as a transcriptional roadblock, it results in polar effects on transcription of genes on the same transcriptional unit. One interesting example of this is the knockdown of the bicistronic *ugtP-ltaA* in *S. aureus* (Paper II). When knocking down this operon in wild-type and in a strain lacking CozE-proteins, we initially observed that the CozE-mediated growth defect was partially rescued, suggesting a functional link between UgtP/LtaA and CozE-proteins. Interestingly, further experiments in fact demonstrated that the two encoded proteins, UgtP and

LtaA, had completely opposite effects on growth in the genetic background lacking CozE (for details, see Paper II and discussion in **Section 4.2.2.**). Such a result would not have been possible to obtain using CRISPRi alone, and polar effects must thus always be taken into consideration when interpreting results from these experiments.

Furthermore, one should also be aware of potential off-targets and toxic effects of the CRISPRi system itself, as previously demonstrated in *E. coli* (Cui et al., 2018). To avoid off-target effects and sgRNA toxicity, the sgRNAs used here were carefully designed to bind close to the first PAM-proximal downstream of the start codon of the gene of interest (thus inside the target gene, but as close to the 5' end of the gene as possible), without any potential binding sites other places in the genome. RNA-seq data with strains carrying the *S. aureus* CRISPRi system (data not shown) has verified the specificity of this system. Related to this, the CRISPRi systems implemented here are carried on plasmids, which may potentially impact the strains. We did not see any such effect for the *S. aureus* system (Paper I-III), however, in *L. plantarum*, the strain carrying both CRISPRi-plasmids displayed somewhat reduced growth compared to the wild-type control. Furthermore, overexpression of dCas9 also had impact on the growth rate in this case. It is therefore possible that the CRISPRi system alone affect cellular processes in *L. plantarum*, and it is of critical importance to include proper controls when working with this strain.

4.1.2. Selection of staphylococcal strains for study of cell division genes

Although one should think that the mechanisms of cell division should be fully conserved between different strains within the same species, previous studies in *S. aureus*, as well as other species have illustrated that even minor strain specific variations between typically used model strains can have impact on the results and importance of different proteins. The choice of model strain may therefore impact the results. In this thesis, different frequently used model strains for staphylococcal research were utilized in the various papers. In Paper I, *S. aureus* SH1000 was used exclusively, while in Paper II and III we expanded this to include NCTC8325-4, HG001, JE2 and COL. From these, JE2 and COL are MRSA strains, in which the former has the advantage of an available transposon mutant library (Fey et al., 2013). The MSSA strains used are all closely related to the sepsis isolate NCTC8325; NCTC8325-4 is a

phage cured version of NCTC835, while SH1000 is a derivative of NCTC8325-4, in which a deletion in the alternative sigma factor (SigB encoded by *rsbU*) has been repaired. Additional SNP between the strains also exists (Bæk et al., 2013; O'Neill, 2010). Finally, in HG001, mutations in two regulators of NCTC8325 (the already mentioned *rsbU*, as well as *tcaR*) have been repaired (Herbert et al., 2010). While these differences are mostly thought to influence virulence of *S. aureus* under different conditions (Bæk et al., 2013), changes in the SigB-mediated stress response may also affect pathways related to the cell wall and drug resistance. Since several different strains were used in this thesis, it was possible to get an insight into the functional conservation of the studied mechanisms (i.e., related to CozE and SmdA) across various MRSA and MSSA strains. In general, there were very little strain variations in the results obtained, showing that the mechanisms are conserved. One exception to this was in relation to SmdA (Paper III), where HG001 displayed a more severe phenotypic change upon SmdA depletion compared to the other strains (see **Section 4.3.2.** for discussion). It will potentially be possible to use this difference to get further insights into the mechanism of SmdA in future studies.

4.2. The CozE proteins

4.2.1. The essentiality and roles of CozE proteins vary between species

As mentioned in **Section 1.4.2.**, the CozE protein was first identified in the ovococcus *S. pneumoniae* as an important contributor to cell elongation and morphology (Fenton et al., 2016). Interestingly, genes encoding CozE homologs are widely distributed among bacterial phyla (Fenton et al., 2016), mostly with at least two paralogs per genome, and in species with various cell shapes, including both cocci such as *S. aureus* and rods such as *L. plantarum*. In Paper I and II, we studied the two encoded CozE homologs in *S. aureus*. While single deletions of *cozEa* and *cozEb* could readily be made, they constitute a synthetic lethal pair in both MSSA and MRSA strains, and depletion of both CozEa and CozEb at the same time resulted in severe growth- and morphological defects. In Paper II, it was also demonstrated that CozEa and CozEb in fact have unique, non-essential functions related to LTA biosynthesis. Together, results from Paper I and II thus show that in *S. aureus*, the individual roles of CozEa and CozEb are not essential, but their overlapping functionality is.

The situation appears to be different in the rod-shaped *L. plantarum*. In Paper IV, we show that the two CozE homologs, neither alone or in combination, seem to be important for growth or cell size in this species. The current results thus suggest no major role for CozE proteins in viability, cell size homeostasis or morphology in this bacterium. It may be that the function of CozE proteins are fully non-essential in *L. plantarum*, but we cannot rule out that these genes become more important under different environmental- or nutritional settings, or genetic backgrounds. It is for example possible that *L. plantarum* encode non-homologous proteins which functionally complement the role of the CozE proteins.

A second CozE protein was also recently described in *S. pneumoniae* (named CozEb) (Stamsås et al., 2020). In this bacterium, the individual *cozE* and *cozEb* deletions behaved somewhat different compared to what we observed in *S. aureus* and *L. plantarum*; deletion of *cozE* alone results in severe growth- and morphological defects, and CozE seems to be more important than CozEb. A deletion strain of the latter displayed a less dramatic phenotype, although growth and cell size control were affected here as well (Fenton et al., 2016; Stamsås et al., 2020). However, similar to *S. aureus*, overlapping functionality between the two CozE-proteins was observed, as a double deletion strain had further reduced growth and increased morphological defects compared to single deletions. In addition to that, CozEb could partially compensate for the loss of CozE (Stamsås et al., 2020). Adding to this, we also found that overexpression of the staphylococcal CozEa and CozEb in the *S. pneumoniae* Δ *cozE* mutant, rescued the growth- and morphology defect in this strain (Paper I). Together, this shows that while the dependence of CozE proteins vary between species, their functions seem to be conserved (at least between *S. aureus* and *S. pneumoniae*).

4.2.2. The functionality of staphylococcal CozE proteins

But what is the actual function of the conserved CozE proteins? The initial proposed role of the CozE membrane protein is to localize the class A PBP1a of *S. pneumoniae* (an important contributor to cell elongation and morphology) to midcell, via protein-protein interactions and complex formation with PBP1a, MreC, MreD and DivIVA (Fenton et al., 2016; Straume et al., 2017). This may indeed be the case, but results presented in this thesis, suggest that the picture may be more complex (Paper I and II). For example, the staphylococcal CozE proteins were not found to interact with any of the PBPs by using bacterial two-hybrid assays. The only interaction conserved

between *S. aureus* and *S. pneumoniae* in this assay was between CozEa and MreC. Among the candidates tested, the early cell division EzrA was the only protein found to interact with both CozEa and CozEb, and the CozE proteins also affected the subcellular localization of EzrA. Based on EzrA's role in cell division (**Section 1.3.2.**), its delocalization explains the delocalized cell wall synthesis and septum formation in CozE-deprived *S. aureus* strains (Paper I and II). The CozE-EzrA relationship was conserved in *S. pneumoniae*, as the proteins were shown to interact and depletion of CozE also resulted in delocalized EzrA in this species (Paper I). These results thus show that the coordination of cell division and septum formation is influenced by the combined action of both CozE proteins in *S. aureus*.

In Paper II we uncovered several synthetic genetic links between *cozEa*, *cozEb* and the biosynthetic genes of LTA; *ugtP*, *ltaA* and *ltaS*, strongly indicating a functional relationship. The genetic links turned out to be quite complex (partial overview in **Fig. 9**). Most interesting; (i) the growth reduction present when *LtaS* was depleted in wild-type background, could partially be rescued if *cozEb* was deleted, while the growth reduction was more severe in $\Delta\textit{cozEa}$. (ii) Simultaneous depletion of *CozEa* and *CozEb* results in severe fitness- and cell division defects in wild-type background, which are alleviated in a $\Delta\textit{ltaA}$ background, but aggravated in the $\Delta\textit{ugtP}$ background (**Fig. 9**). Translated into functionality; *CozEa* and *CozEb* are more essential when no Glc₂DAG LTA-anchor is produced by *UgtP*. On the other hand, when this anchor is produced but the flipping of the anchor is inhibited by deletion of *LtaA*, the combined role of *CozEa* and *CozEb* are not essential anymore (see **Fig. 6** for schematic overview of LTA biosynthesis).

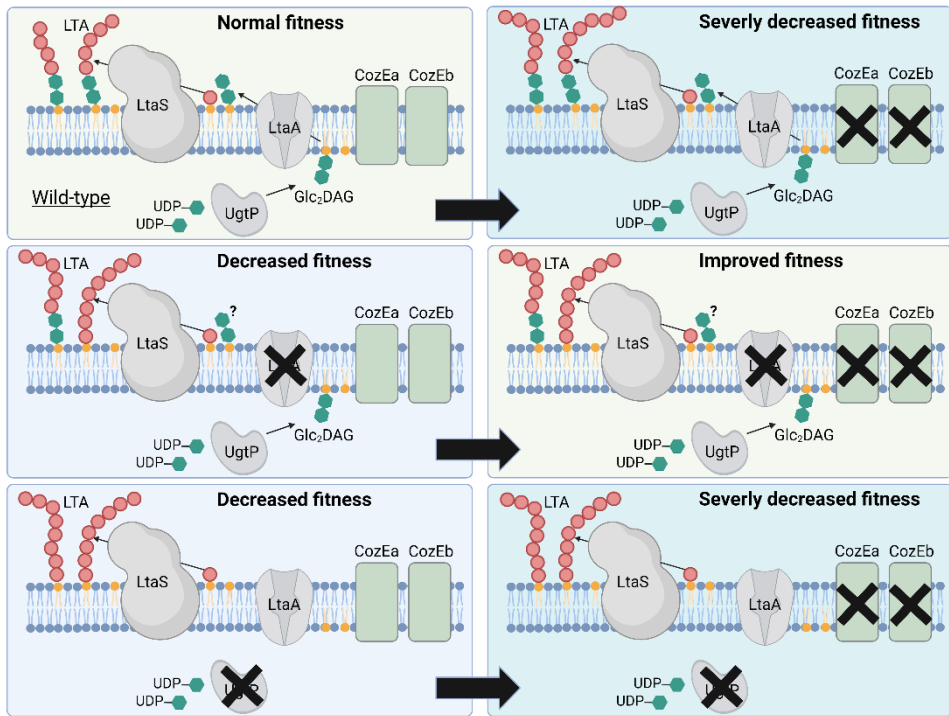


Fig. 9. Synthetic genetic link between the *cozE* genes and LTA biosynthesis. An overview showing how absence of different genes and gene combinations affect *S. aureus* fitness. Figure created with BioRender.com.

Based on the opposite genetic interactions observed for UgtP and LtaA, and that $\Delta cozEb$, similar to $\Delta ugtP$ and $\Delta ltaA$, mutants produce longer LTA polymers than wild-type (Gründling & Schneewind, 2007a; Hesser et al., 2020a), it is tempting to speculate that the actual role of the CozE proteins is related to the functionality of UgtP or LtaA, or the products/substrates from the pathways they are part of (Fig. 6). Since the intracellular UgtP localize to the membrane by an unknown mechanism in *S. aureus* (Reichmann et al., 2014), our first thought was that CozEb might be responsible for UgtP localization. Although UgtP still displayed a membrane-localization in a $\Delta cozEb$ mutant in our microscopy setup, the fraction of cells with this localization was somewhat reduced compared to wild-type background (Paper II). This potential localization defect should be investigated more thoroughly, for example by using super-resolution microscopy techniques. In this context, it is relevant to note that in *B. subtilis*, the localization of the UgtP homolog has been shown to depend on its substrate UDP-Glc, as well as nutrient conditions (Weart et

al., 2007). Although this does not seem to be the case for *S. aureus* (Reichmann et al., 2014), CozEb may influence the synthesis, or membrane localization, of some other molecule that govern UgtP recruitment to the membrane.

Some other aspects of UgtP in *B. subtilis* are also interesting to note. This protein has been suggested to act as a metabolic sensor which controls cell size in this bacterium (Weart et al., 2007). Specifically, UgtP can inhibit Z ring formation by binding and sequestering FtsZ. This inhibition of FtsZ is dependent on the levels of UDP-Glc, which again is reflected by the accessibility to nutrients (nutrient rich conditions gives high levels of UDP-Glc and promotes binding of UgtP to FtsZ) (Chien et al., 2012). This provides a direct link between UgtP and cell division regulation in *B. subtilis*, which may also be present in *S. aureus*. Although highly speculative at this point; if CozE somehow alter synthesis or flipping of Glc₂DAG or other membrane lipids, this would alter the balance between lipids in the membrane and potentially mediate changes in LTA (due to different accessibility to starter units) and affect cell division, cell size homeostasis and septum formation (via UgtP or other protein-protein interactions). The fact that all the LTA biosynthetic genes have been shown to interact with several cell division proteins (early and late), including EzrA (Reichmann et al., 2014), illustrates that there are tight links between these processes which should be explored further. Therefore, it could be interesting to further investigate if alterations in LTA synthesis – including the substrates and products of UgtP – affect EzrA localization, as observed for CozE-deprived cells (Paper I), to see if this possibly could reveal a cooperative function between CozE proteins and LTA synthesis proteins in controlling localization of the Z ring and cell wall synthesis.

LTA and WTA play somewhat redundant roles in staphylococcal cell division; although LTA appears to be the most important, the two pathways cannot be deleted simultaneously and are inversely regulated (Hesser et al., 2020a; Oku et al., 2009). Another tempting hypothesis related to the overlapping essentiality of CozEa and CozEb, is that they are somehow connected to the fact that presence of either WTA or LTA is essential (Oku et al., 2009), and that CozEa may influence WTA synthesis since CozEb affects LTA (Paper II). This hypothesis needs experimental backup, and for future experiments, the levels of WTA and LTA should be measured in the different CozE mutants.

4.3. SmdA – identified from a dual screening approach

4.3.1. Subcellular localization- and gene knockdown screens

We hypothesized that it should be possible to identify novel cell cycle factors among the conserved, essential genes with unknown function present on *S. aureus* genomes. The revelation of the novel, staphylococcal morphology determinant, SmdA (Paper III), was derived from a “starting-from-scratch” study, where a subcellular localization- and knockdown screen was performed on 27 essential proteins with unknown function to identify potential novel cell cycle factors. The selection of genes to be included in the screen was based on their conservation across *S. aureus* genomes, gene essentiality information (Chaudhuri et al., 2009; Santiago et al., 2015; Valentino et al., 2014) and annotation status in the Uniprot- and Patric database. However, as mentioned in Paper III, several of the genes included in the screen have by this time been annotated and studied by other research groups. SmdA was chosen for further studies because it had a septum-enriched localization and showed morphological defects upon depletion, which are attributed to proteins with a potential role in cell division. Still, other genes from the screen exhibited interesting subcellular localizations and knockdown phenotypes, and their functional roles should be subjected for further studies.

4.3.2. Phenotyping of strains with altered levels of SmdA reveals a novel staphylococcal morphology determinant

As being annotated as an essential gene, we expected depletion of SmdA to result in growth reduction. Indeed, clearly reduced viability was observed upon SmdA depletion on agar plates. Surprisingly, however, no observable growth defect was detected in liquid medium, except in strain HG001. A possible explanation to this discrepancy could be that SmdA depleted cells becomes bigger and form clusters, and that this possibly influences the optical density measurements, thus masking the difference in population size. Similar effects have been described before as Campbell et al. (2012) noticed an increased biomass of a targocil-treated culture, which was not reflected in viable colonies. The somewhat variable essentiality of SmdA between different *S. aureus* strains (HG001 seem to be more affected by depletion of SmdA) could either be due to differences in genetic background, in protein stability or even efficiency of the CRISPRi depletions between strains. The transcriptional silencing by

CRISPRi was however confirmed in *S. aureus* SH1000. After multiple unsuccessful attempts of making knockout mutants (in different *S. aureus* strains), we concluded that the gene indeed was essential for viability under our experimental conditions.

We were not able to pinpoint the exact function of SmdA in this work. The results obtained in Paper III support a functional role of SmdA, directly or indirectly, affecting several steps of the cell cycle. Based on both the observed phenotypes in absence of SmdA (increased sensitivity to cell wall targeting antibiotics, misplaced septum synthesis and increased resistance to autolysis, overview in **Fig. 10**) and protein interactions (SmdA interacts with PBPs, EzrA, Atl among others), a link to placement of the division ring and PG synthesis, as well as compromised cell splitting, can be assigned. Additionally, overexpression of full length SmdA and of the intracellular part only (SmdA Δ TMH), led to similar morphological defects (with a more severe phenotype for SmdA Δ TMH, in which the membrane localization is lost). Thus, balanced amounts of membrane-bound SmdA seem to be a requirement of *S. aureus* for properly conducting a normal cell cycle and for obtaining its coccoid morphology (**Fig. 10**).

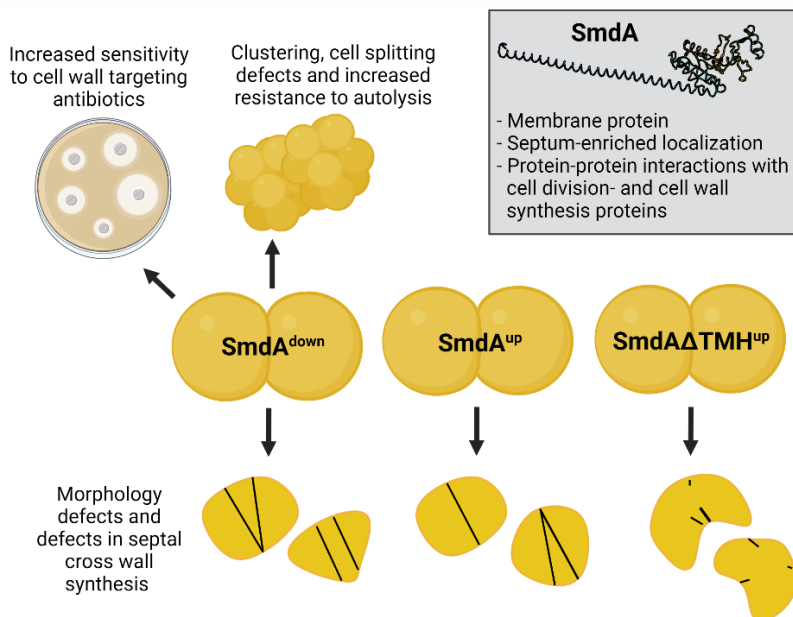


Fig. 10. Overview of the resulting effects of different expression levels and -variants of SmdA. A balanced amount of membrane-attached SmdA is important for division ring placement, peptidoglycan synthesis, autolytic splitting and susceptibility to cell wall targeting antibiotics. Superscript “down”/“up” indicates depletion and overexpression, respectively. Grey box; AlphaFold2-predicted structure of SmdA (Jumper et al., 2021), and other characteristics with this protein. Figure created with BioRender.com.

SmdA is fully conserved in the family *Staphylococcaceae*. It is predicted that the major part of the protein is located intracellularly, while being attached to the membrane through an N-terminal membrane helix. This topology, has however, not been experimentally confirmed yet. Additionally, SmdA was predicted to harbor a so-called nuclease-related domain (NERD). To our knowledge, research regarding the functionality of this domain is scarce, and it is given the name due to distant similarity to endonucleases, although no nuclease- or nucleic acid-related function has yet been demonstrated (Grynberg & Godzik, 2004). Our study brings novel insight regarding such domains, as we identified residues within NERD that was proven to be important for maintaining protein function (H145, R150 and T151). The AlphaFold2-predicted (Jumper et al., 2021) structure of SmdA suggests that it harbors a long N-terminal helix and a C-terminal structured region (containing the NERD domain) (Paper III). If the C-terminal structured domain in fact is a nucleic acid (DNA) interacting domain, SmdA would then represent a link between DNA and the membrane – and possibly the nucleoid and cell division. However, this remains highly speculative at this point.

We showed, by pulldowns and bacterial two-hybrid assays, that SmdA interacted with the cell division proteins PBP1, PBP2, PBP3 and EzrA. Furthermore, proteins known to be involved in folding, degradation, and export processes were also pulled down with SmdA, including PrsA and HtrA1 (extracellular chaperones/protease), ClpB, ClpC and FtsH (ATP-dependent proteolysis complexes), and SpsB and SecD (signal peptidase and secretion protein). The relevance of these interactions needs to be investigated further, but it is interesting to note that several characteristics of these proteins resembles the observed phenotypes of SmdA knockdowns. (i) PrsA and HtrA1 are extracellular chaperones whose deletion have been shown to re-sensitized MRSA to β -lactams because they are required for PBP2A folding (Roch et al., 2019). (ii) FtsH is a metalloprotease important for virulence and stress resistance (Lithgow et al., 2004), and has been shown to sensitize MRSA to β -lactams by degrading UgtP (Yeo et al., 2021). (iii) A SecDF mutant is shown to have increased sensitivity to β -lactams and have cell separation defects (Quiblier et al., 2011). Proteins involved in different parts of the cell cycle need to be properly folded and present in the cell in proper amounts at the correct localization (i.e., proteins need to be secreted if they exhibit their functions extracellularly). With the obvious effects on morphology, and with its large number of associated proteins, it is tempting to suspect a functional role of SmdA as a scaffold protein, for example, by facilitating interactions between cell cycle proteins or between proteins involved in folding/turnover, or even as a component important for coordination of these

processes. Disturbance in such processes could possibly explain the pleiotropic effects observed with unbalanced amounts of SmdA and expression of a mislocalized SmdA Δ TMH.

As mentioned, *S. aureus* strains depleted of SmdA become more susceptible to antibiotics targeting the cell wall, and most notably, the absence of SmdA sensitizes the MRSA strain COL to β -lactams. This characteristic of SmdA is rather typical for proteins involved in different stages of cell division (Roemer et al., 2013). It also suggests that SmdA could be a potential future, narrow spectrum therapeutic target, since inhibitors of SmdA (if identified) could act synergistically with β -lactams against MRSA.

5. Concluding remarks and future perspectives

In this work, CRISPRi gene depletion systems were established in *S. aureus* and *L. plantarum* (Paper I and IV). This tool offers a platform for functional studies of essential genes and possibilities for rapid screening of gene-phenotype relationships in these bacteria. Further development and improvement of the CRISPRi systems, for example by chromosomal integration, could further expand their potential for different purposes.

This work also discloses and provides functional insights into hitherto unknown factors affecting the cell cycle in *S. aureus* (Paper I, II and III), namely the CozE proteins and SmdA. The work also reveals that the CozE proteins vary in their importance between *S. aureus*, *S. pneumoniae* and *L. plantarum*. The *cozE* genes encoded by *S. aureus* have overlapping and essential roles, but also individual, non-essential unique functions. The proteins are critical for proper coordination of cell division and septum formation in this species and links to cell division as well as LTA biosynthesis are demonstrated. Future research will be needed to fully explain the relationship between CozE proteins and the biosynthesis of LTA, as well as how this relates to the already known effects LTA have on cell division and localization of septum synthesis.

By the work presented in Paper III, we show that the hitherto unstudied protein SmdA is important in the cell division processes and for maintenance of morphology in *S. aureus*. Future studies are needed to further investigate the exact role(s) possessed by SmdA. Furthermore, the ability of SmdA to modulate antibiotic susceptibility, especially in MRSA, render this protein as an exciting candidate as target for future narrow spectrum antimicrobial development. The work in Paper III also highlights the up- and downsides of a “starting-from-scratch” screen-approach as the one used here (subcellular localization and knockdown phenotype). We were able to identify candidates and characterized SmdA as a novel factor affecting cell division in *S. aureus*, however, as the background knowledge about the potential function of this protein is almost non-existing, it was challenging to pinpoint any exact functional role of this protein. Nevertheless, this work forms a basis for further studies to improve

Concluding remarks and future perspectives

our knowledge about molecular details responsible for the involvement of SmdA in the *S. aureus* cell cycle.

The most significant contribution from the work presented in Paper IV, is the establishment of a new genetic tool in *L. plantarum*. Also, initial insights into putative cell division genes were revealed. In contrast to results for *S. aureus* and *S. pneumoniae* from Paper I and II, the CozE homologs in *L. plantarum* did not seem to play a major role for controlling cell elongation and division. On the other hand, the newly identified streptococcal elongation factors EloR and KhpA, were demonstrated to be important for elongation also in this rod-shaped bacterium.

References

- Adams, D. W. & Errington, J. (2009). Bacterial cell division: assembly, maintenance and disassembly of the Z ring. *Nature reviews microbiology*, 7 (9): 642-653. doi: 10.1038/nrmicro2198. PMID: 19680248.
- Alander, M., De Smet, I., Nollet, L., Verstraete, W., Von Wright, A. & Mattila-Sandholm, T. (1999). The effect of probiotic strains on the microbiota of the Simulator of the Human Intestinal Microbial Ecosystem (SHIME). *International journal of food microbiology*, 46 (1): 71-79. doi: 10.1016/s0168-1605(98)00182-2.
- Atilano, M. L., Pereira, P. M., Yates, J., Reed, P., Veiga, H., Pinho, M. G. & Filipe, S. R. (2010). Teichoic acids are temporal and spatial regulators of peptidoglycan cross-linking in *Staphylococcus aureus*. *Proceedings of the national academy of sciences*, 107 (44): 18991-18996. doi: 10.1073/pnas.1004304107.
- Baddiley, J., Buchanan, J., Martin, R. & Rajbhandary, U. (1962). Teichoic acid from the walls of *Staphylococcus aureus* H. 2. Location of phosphate and alanine residues. *Biochemical journal*, 85 (1): 49-56. doi: 10.1042/bj0850049.
- Badurina, D. S., Zolli-Juran, M. & Brown, E. D. (2003). CTP: glycerol 3-phosphate cytidylyltransferase (TarD) from *Staphylococcus aureus* catalyzes the cytidylyl transfer via an ordered Bi-Bi reaction mechanism with micromolar Km values. *Biochimica et biophysica acta*, 1646 (1-2): 196-206. doi: 10.1016/s1570-9639(03)00019-0.
- Barreteau, H., Kovač, A., Boniface, A., Sova, M., Gobec, S. & Blanot, D. (2008). Cytoplasmic steps of peptidoglycan biosynthesis. *FEMS microbiology reviews*, 32 (2): 168-207. doi: 10.1111/j.1574-6976.2008.00104.x.
- Begg, K. J. & Donachie, W. D. (1985). Cell shape and division in *Escherichia coli*: experiments with shape and division mutants. *Journal of bacteriology*, 163 (2): 615-622. doi: 10.1128/jb.163.2.615-622.1985.
- Bermudez-Humaran, L. G., Kharrat, P., Chatel, J. M. & Langella, P. (2011). Lactococci and lactobacilli as mucosal delivery vectors for therapeutic proteins and DNA vaccines. *Microbial cell factories*, 10 (Suppl 1): S4. doi: 10.1186/1475-2859-10-s1-s4.
- Bi, E. & Lutkenhaus, J. (1991). FtsZ ring structure associated with division in *Escherichia coli*. *Nature*, 354 (6349): 161-164. doi: 10.1038/354161a0.
- Bikard, D., Jiang, W., Samai, P., Hochschild, A., Zhang, F. & Marraffini, L. A. (2013). Programmable repression and activation of bacterial gene expression using an engineered CRISPR-Cas system. *Nucleic acids research*, 41 (15): 7429-7437. doi: 10.1093/nar/gkt520.
- Bisson-Filho, A. W., Hsu, Y. P., Squyres, G. R., Kuru, E., Wu, F., Jukes, C., Sun, Y., Dekker, C., Holden, S., VanNieuwenhze, M. S., et al. (2017). Treadmilling by FtsZ filaments drives peptidoglycan synthesis and bacterial cell division. *Science*, 355 (6326): 739-743. doi: 10.1126/science.aak9973.
- Biswas, R., Voggu, L., Simon, U. K., Hentschel, P., Thumm, G. & Götz, F. (2006). Activity of the major staphylococcal autolysin Atl. *FEMS microbiology letters*, 259 (2): 260-268. doi: 10.1111/j.1574-6968.2006.00281.x.

References

- Booth, S. & Lewis, R. J. (2019). Structural basis for the coordination of cell division with the synthesis of the bacterial cell envelope. *Protein science*, 28 (12): 2042-2054. doi: 10.1002/pro.3722.
- Bouhss, A., Trunkfield, A. E., Bugg, T. D. & Mengin-Lecreulx, D. (2007). The biosynthesis of peptidoglycan lipid-linked intermediates. *FEMS microbiology reviews*, 32 (2): 208-233. doi: 10.1111/j.1574-6976.2007.00089.x.
- Britton, R. A., Lin, D. C.-H. & Grossman, A. D. (1998). Characterization of a prokaryotic SMC protein involved in chromosome partitioning. *Genes & development*, 12 (9): 1254-1259. doi: 10.1101/gad.12.9.1254.
- Brown, S., Zhang, Y.-H. & Walker, S. (2008). A revised pathway proposed for *Staphylococcus aureus* wall teichoic acid biosynthesis based on *in vitro* reconstitution of the intracellular steps. *Chemistry & biology*, 15 (1): 12-21. doi: 10.1016/j.chembiol.2007.11.011.
- Brown, S., Xia, G., Luhachack, L. G., Campbell, J., Meredith, T. C., Chen, C., Winstel, V., Gekeler, C., Irazoqui, J. E. & Peschel, A. (2012). Methicillin resistance in *Staphylococcus aureus* requires glycosylated wall teichoic acids. *Proceedings of the national academy of sciences*, 109 (46): 18909-18914. doi: 10.1073/pnas.1209126109.
- Bæk, K. T., Frees, D., Renzoni, A., Barras, C., Rodriguez, N., Manzano, C. & Kelley, W. L. (2013). Genetic variation in the *Staphylococcus aureus* 8325 strain lineage revealed by whole-genome sequencing. *PLoS One*, 8 (9): e77122. doi: 10.1371/journal.pone.0077122.
- Campbell, J., Singh, A. K., Swoboda, J. G., Gilmore, M. S., Wilkinson, B. J. & Walker, S. (2012). An antibiotic that inhibits a late step in wall teichoic acid biosynthesis induces the cell wall stress stimulon in *Staphylococcus aureus*. *Antimicrobial agents and chemotherapy*, 56 (4): 1810-20. doi: 10.1128/aac.05938-11.
- Chan, H., Söderström, B. & Skoglund, U. (2020). Spo0J and SMC are required for normal chromosome segregation in *Staphylococcus aureus*. *MicrobiologyOpen*, 9 (4): e999. doi: 10.1002/mbo3.999.
- Chan, Y. G., Frankel, M. B., Dengler, V., Schneewind, O. & Missiakas, D. (2013). *Staphylococcus aureus* mutants lacking the LytR-CpsA-Psr family of enzymes release cell wall teichoic acids into the extracellular medium. *Journal of bacteriology*, 195 (20): 4650-4659. doi: 10.1128/JB.00544-13.
- Chaudhuri, R. R., Allen, A. G., Owen, P. J., Shalom, G., Stone, K., Harrison, M., Burgis, T. A., Lockyer, M., Garcia-Lara, J., Foster, S. J., et al. (2009). Comprehensive identification of essential *Staphylococcus aureus* genes using Transposon-Mediated Differential Hybridisation (TMDH). *BMC genomics*, 10 (1): 291. doi: 10.1186/1471-2164-10-291.
- Chien, A. C., Zareh, S. K., Wang, Y. M. & Levin, P. A. (2012). Changes in the oligomerization potential of the division inhibitor UgtP co-ordinate *Bacillus subtilis* cell size with nutrient availability. *Molecular microbiology*, 86 (3): 594-610. doi: 10.1111/mmi.12007.
- Cho, H., Wivagg, C. N., Kapoor, M., Barry, Z., Rohs, P. D., Suh, H., Marto, J. A., Garner, E. C. & Bernhardt, T. G. (2016). Bacterial cell wall biogenesis is mediated by SEDS and PBP polymerase families functioning semi-autonomously. *Nature microbiology*, 1 (10): 1-8. doi: 10.1038/nmicrobiol.2016.172.

- Cleveland, J., Montville, T. J., Nes, I. F. & Chikindas, M. L. (2001). Bacteriocins: safe, natural antimicrobials for food preservation. *International journal of food microbiology*, 71 (1): 1-20. doi: 10.1016/s0168-1605(01)00560-8.
- Corrigan, R. M., Abbott, J. C., Burhenne, H., Kaefer, V. & Gründling, A. (2011). c-di-AMP is a new second messenger in *Staphylococcus aureus* with a role in controlling cell size and envelope stress. *PLoS pathogens*, 7 (9): e1002217. doi: 10.1371/journal.ppat.1002217.
- Cui, L., Vigouroux, A., Rousset, F., Varet, H., Khanna, V. & Bikard, D. (2018). A CRISPRi screen in *E. coli* reveals sequence-specific toxicity of dCas9. *Nature communications*, 9 (1): 1912. doi: 10.1038/s41467-018-04209-5.
- D'Elia, M. A., Pereira, M. P., Chung, Y. S., Zhao, W., Chau, A., Kenney, T. J., Sulavik, M. C., Black, T. A. & Brown, E. D. (2006). Lesions in teichoic acid biosynthesis in *Staphylococcus aureus* lead to a lethal gain of function in the otherwise dispensable pathway. *Journal of bacteriology*, 188 (12): 4183-4189. doi: 10.1128/JB.00197-06.
- D'Elia, M. A., Henderson, J. A., Beveridge, T. J., Heinrichs, D. E. & Brown, E. D. (2009). The N-acetylmannosamine transferase catalyzes the first committed step of teichoic acid assembly in *Bacillus subtilis* and *Staphylococcus aureus*. *Journal of bacteriology*, 191 (12): 4030-4034. doi: 10.1128/JB.00611-08.
- Da Costa, T. M., De Oliveira, C. R., Chambers, H. F. & Chatterjee, S. S. (2018). PBP4: a new perspective on *Staphylococcus aureus* β -lactam resistance. *Microorganisms*, 6 (3): 57. doi: 10.3390/microorganisms6030057.
- David, M. Z. & Daum, R. S. (2017). Treatment of *Staphylococcus aureus* infections. *Current topics in microbiology and immunology*, 409: 325-383. doi: 10.1007/82_2017_42.
- De Boer, P., Crossley, R. & Rothfield, L. (1992). The essential bacterial cell-division protein FtsZ is a GTPase. *Nature*, 359 (6392): 254-256. doi: 10.1038/359254a0.
- de Vries, M. C., Vaughan, E. E., Kleerebezem, M. & de Vos, W. M. (2006). *Lactobacillus plantarum*—survival, functional and potential probiotic properties in the human intestinal tract. *International dairy journal*, 16 (9): 1018-1028. doi: 10.1016/j.idairyj.2005.09.003.
- Den Blaauwen, T., De Pedro, M. A., Nguyen-Disteche, M. & Ayala, J. A. (2008). Morphogenesis of rod-shaped sacculi. *FEMS microbiology reviews*, 32 (2): 321-344. doi: 10.1111/j.1574-6976.2007.00090.x.
- Dengler, V., Meier, P. S., Heusser, R., Kupferschmied, P., Fazekas, J., Friebe, S., Staufer, S. B., Majcherczyk, P. A., Moreillon, P., Berger-Bächi, B., et al. (2012). Deletion of hypothetical wall teichoic acid ligases in *Staphylococcus aureus* activates the cell wall stress response. *FEMS microbiology letters*, 333 (2): 109-120. doi: 10.1111/j.1574-6968.2012.02603.x.
- Do, T., Page, J. E. & Walker, S. (2020). Uncovering the activities, biological roles, and regulation of bacterial cell wall hydrolases and tailoring enzymes. *Journal of biological chemistry*, 295 (10): 3347-3361. doi: 10.1074/jbc.REV119.010155.
- Dobihal, G. S., Brunet, Y. R., Flores-Kim, J. & Rudner, D. Z. (2019). Homeostatic control of cell wall hydrolysis by the WalRK two-component signaling pathway in *Bacillus subtilis*. *Elife*, 8: e52088. doi: 10.7554/eLife.52088.

References

- Du, X., Larsen, J., Li, M., Walter, A., Slavetinsky, C., Both, A., Carballo, P. M. S., Stegger, M., Lehmann, E. & Liu, Y. (2021). *Staphylococcus epidermidis* clones express *Staphylococcus aureus*-type wall teichoic acid to shift from a commensal to pathogen lifestyle. *Nature microbiology*, 6 (6): 757-768. doi: 10.1038/s41564-021-00913-z.
- Dubrac, S. & Msadek, T. (2004). Identification of genes controlled by the essential YycG/YycF two-component system of *Staphylococcus aureus*. *Journal of bacteriology*, 186 (4): 1175-1181. doi: 10.1128/JB.186.4.1175-1181.2004.
- Dubrac, S., Boneca, I. G., Poupel, O. & Msadek, T. (2007). New insights into the WalK/WalR (YycG/YycF) essential signal transduction pathway reveal a major role in controlling cell wall metabolism and biofilm formation in *Staphylococcus aureus*. *Journal of bacteriology*, 189 (22): 8257-69. doi: 10.1128/jb.00645-07.
- Dubrac, S., Bisicchia, P., Devine, K. M. & Msadek, T. (2008). A matter of life and death: cell wall homeostasis and the WalKR (YycGF) essential signal transduction pathway. *Molecular microbiology*, 70 (6): 1307-1322. doi: 10.1111/j.1365-2958.2008.06483.x.
- Duchêne, M. C., Rolain, T., Knoops, A., Courtin, P., Chapot-Chartier, M. P., Dufrêne, Y. F., Hallet, B. F. & Hols, P. (2019). Distinct and specific role of NlpC/P60 endopeptidases LytA and LytB in cell elongation and division of *Lactobacillus plantarum*. *Frontiers in microbiology*, 10: 713. doi: 10.3389/fmicb.2019.00713.
- Ducret, A. & Grangeasse, C. (2017). Bacterial physiology: wrapping the cell in a CozE shell. *Nature microbiology*, 2 (3): 1-2. doi: 10.1038/nmicrobiol.2016.262.
- Ducret, A. & Grangeasse, C. (2021). Recent progress in our understanding of peptidoglycan assembly in Firmicutes. *Current opinion in microbiology*, 60: 44-50. doi: 10.1016/j.mib.2021.01.011.
- Dworkin, J. & Losick, R. (2002). Does RNA polymerase help drive chromosome segregation in bacteria? *Proceedings of the national academy of sciences*, 99 (22): 14089-14094. doi: 10.1073/pnas.182539899.
- Emami, K., Guyet, A., Kawai, Y., Devi, J., Wu, L. J., Allenby, N., Daniel, R. A. & Errington, J. (2017). RodA as the missing glycosyltransferase in *Bacillus subtilis* and antibiotic discovery for the peptidoglycan polymerase pathway. *Nature microbiology*, 2: 16253. doi: 10.1038/nmicrobiol.2016.253.
- Emdur, L. & Chiu, T.-h. (1975). The role of phosphatidylglycerol in the *in vitro* biosynthesis of teichoic acid and lipoteichoic acid. *FEBS letters*, 55 (1): 216-219. doi: 10.1016/0014-5793(75)80995-1.
- Errington, J. & Wu, L. J. (2017). Cell cycle machinery in *Bacillus subtilis*. *Subcellular biochemistry*, 84: 67-101. doi: 10.1007/978-3-319-53047-5_3.
- Etebu, E. & Ariekpar, I. (2016). Antibiotics: Classification and mechanisms of action with emphasis on molecular perspectives. *International journal of applied microbiology and biotechnology research*, 4: 90-101.
- Fabret, C. & Hoch, J. A. (1998). A two-component signal transduction system essential for growth of *Bacillus subtilis*: implications for anti-infective therapy. *Journal of bacteriology*, 180 (23): 6375-6383. doi: 10.1128/JB.180.23.6375-6383.1998.

- Fabret, C., Feher, V. A. & Hoch, J. A. (1999). Two-component signal transduction in *Bacillus subtilis*: how one organism sees its world. *Journal of bacteriology*, 181 (7): 1975-1983. doi: 10.1128/JB.181.7.1975-1983.1999.
- Fenton, A. K., El Mortaji, L., Lau, D. T., Rudner, D. Z. & Bernhardt, T. G. (2016). CozE is a member of the MreCD complex that directs cell elongation in *Streptococcus pneumoniae*. *Nature microbiology*, 2: 16237. doi: 10.1038/nmicrobiol.2016.237.
- Ferain, T., Hobbs, J. N., Jr., Richardson, J., Bernard, N., Garmyn, D., Hols, P., Allen, N. E. & Delcour, J. (1996). Knockout of the two *ldh* genes has a major impact on peptidoglycan precursor synthesis in *Lactobacillus plantarum*. *Journal of bacteriology*, 178 (18): 5431-5437. doi: 10.1128/jb.178.18.5431-5437.1996.
- Fey, P. D., Endres, J. L., Yajjala, V. K., Widhelm, T. J., Boissy, R. J., Bose, J. L. & Bayles, K. W. (2013). A genetic resource for rapid and comprehensive phenotype screening of nonessential *Staphylococcus aureus* genes. *mBio*, 4 (1): e00537-12. doi: 10.1128/mBio.00537-12.
- Fleurie, A., Lesterlin, C., Manuse, S., Zhao, C., Cluzel, C., Lavergne, J. P., Franz-Wachtel, M., Macek, B., Combet, C., Kuru, E., et al. (2014). MapZ marks the division sites and positions FtsZ rings in *Streptococcus pneumoniae*. *Nature*, 516 (7530): 259-262. doi: 10.1038/nature13966.
- Frankel, M. B., Hendrickx, A. P., Missiakas, D. M. & Schneewind, O. (2011). LytN, a murein hydrolase in the cross-wall compartment of *Staphylococcus aureus*, is involved in proper bacterial growth and envelope assembly. *Journal of biological chemistry*, 286 (37): 32593-32605. doi: 10.1074/jbc.M111.258863.
- Frankel, M. B. & Schneewind, O. (2012). Determinants of murein hydrolase targeting to cross-wall of *Staphylococcus aureus* peptidoglycan. *Journal of biological chemistry*, 287 (13): 10460-10471. doi: 10.1074/jbc.M111.336404.
- Frees, D., Qazi, S. N., Hill, P. J. & Ingmer, H. (2003). Alternative roles of ClpX and ClpP in *Staphylococcus aureus* stress tolerance and virulence. *Molecular microbiology*, 48 (6): 1565-1578. doi: 10.1046/j.1365-2958.2003.03524.x.
- Gallay, C., Sanselicio, S., Anderson, M. E., Soh, Y. M., Liu, X., Stamsås, G. A., Pellicciari, S., van Raaphorst, R., Dénéréaz, J., Kjos, M., et al. (2021). CcrZ is a pneumococcal spatiotemporal cell cycle regulator that interacts with FtsZ and controls DNA replication by modulating the activity of DnaA. *Nature microbiology*, 6 (9): 1175-1187. doi: 10.1038/s41564-021-00949-1.
- Ghuysen, J.-M. (1968). Use of bacteriolytic enzymes in determination of wall structure and their role in cell metabolism. *Bacteriological reviews*, 32 (4 Pt 2): 425-464.
- Giesbrecht, P., Kersten, T., Maidhof, H. & Wecke, J. (1998). Staphylococcal cell wall: morphogenesis and fatal variations in the presence of penicillin. *Microbiology and molecular biology reviews*, 62 (4): 1371-1414. doi: 10.1128/MMBR.62.4.1371-1414.1998.
- Ginsberg, C., Zhang, Y.-H., Yuan, Y. & Walker, S. (2006). *In vitro* reconstitution of two essential steps in wall teichoic acid biosynthesis. *ACS chemical biology*, 1 (1): 25-28. doi: 10.1021/cb0500041.
- Glaser, L. & Lindsay, B. (1974). The synthesis of lipoteichoic acid carrier. *Biochemical and biophysical research communications*, 59 (3): 1131-1136. doi: 10.1016/s0006-291x(74)80096-3.

References

- Goffin, C. & Ghuysen, J.-M. (1998). Multimodular penicillin-binding proteins: an enigmatic family of orthologs and paralogs. *Microbiology and molecular biology reviews*, 62 (4): 1079-1093. doi: 10.1128/MMBR.62.4.1079-1093.1998.
- Gruber, S. & Errington, J. (2009). Recruitment of condensin to replication origin regions by ParB/SpoOJ promotes chromosome segregation in *B. subtilis*. *Cell*, 137 (4): 685-696. doi: 10.1016/j.cell.2009.02.035.
- Grynberg, M. & Godzik, A. (2004). NERD: a DNA processing-related domain present in the anthrax virulence plasmid, pXO1. *Trends in biochemical sciences*, 29 (3): 106-110. doi: 10.1016/j.tibs.2004.01.002.
- Gründling, A. & Schneewind, O. (2007a). Genes required for glycolipid synthesis and lipoteichoic acid anchoring in *Staphylococcus aureus*. *Journal of bacteriology*, 189 (6): 2521-2530. doi: 10.1128/JB.01683-06.
- Gründling, A. & Schneewind, O. (2007b). Synthesis of glycerol phosphate lipoteichoic acid in *Staphylococcus aureus*. *Proceedings of the national academy of sciences*, 104 (20): 8478-8483. doi: 10.1073/pnas.0701821104.
- Hajduk, I. V., Rodrigues, C. D. & Harry, E. J. (2016). Connecting the dots of the bacterial cell cycle: Coordinating chromosome replication and segregation with cell division. *Seminars in cell and developmental biology*, 53: 2-9. doi: 10.1016/j.semcdb.2015.11.012.
- Hamilton, S. M., Alexander, J. A. N., Choo, E. J., Basuino, L., da Costa, T. M., Severin, A., Chung, M., Aedo, S., Strynadka, N. C. J., Tomasz, A., et al. (2017). High-level resistance of *Staphylococcus aureus* to β -lactam antibiotics mediated by penicillin-binding protein 4 (PBP4). *Antimicrobial agents and chemotherapy*, 61 (6): e02727-16. doi: 10.1128/AAC.02727-16.
- Hartman, B. J. & Tomasz, A. (1984). Low-affinity penicillin-binding protein associated with beta-lactam resistance in *Staphylococcus aureus*. *Journal of bacteriology*, 158 (2): 513-516. doi: 10.1128/jb.158.2.513-516.1984.
- Henze, U. U. & Berger-Bächi, B. (1995). *Staphylococcus aureus* penicillin-binding protein 4 and intrinsic beta-lactam resistance. *Antimicrobial agents and chemotherapy*, 39 (11): 2415-2422. doi: 10.1128/AAC.39.11.2415.
- Herbert, S., Ziebandt, A.-K., Ohlsen, K., Schäfer, T., Hecker, M., Albrecht, D., Novick, R. & Götz, F. (2010). Repair of global regulators in *Staphylococcus aureus* 8325 and comparative analysis with other clinical isolates. *Infection and immunity*, 78 (6): 2877-2889. doi: 10.1128/IAI.00088-10.
- Hesser, A. R., Matano, L. M., Vickery, C. R., Wood, B. M., Santiago, A. G., Morris, H. G., Do, T., Losick, R. & Walker, S. (2020a). The length of lipoteichoic acid polymers controls *Staphylococcus aureus* cell size and envelope integrity. *Journal of bacteriology*, 202 (16): e00149-20. doi: 10.1128/JB.00149-20.
- Hesser, A. R., Schaefer, K., Lee, W. & Walker, S. (2020b). Lipoteichoic acid polymer length is determined by competition between free starter units. *Proceedings of the national academy of sciences*, 117 (47): 29669-29676. doi: 10.1073/pnas.2008929117.
- Hill, M. A., Lam, A. K., Reed, P., Harney, M. C., Wilson, B. A., Moen, E. L., Wright, S. N., Pinho, M. G. & Rice, C. V. (2019). BPEI-Induced Delocalization of PBP4 Potentiates β -Lactams against MRSA. *Biochemistry*, 58 (36): 3813-3822. doi: 10.1021/acs.biochem.9b00523.

- Holečková, N., Doubravová, L., Massidda, O., Molle, V., Buriánková, K., Benada, O., Kofroňová, O., Ulrych, A. & Branny, P. (2014). LocZ is a new cell division protein involved in proper septum placement in *Streptococcus pneumoniae*. *mBio*, 6 (1): e01700-14. doi: 10.1128/mBio.01700-14.
- Jensen, C., Bæk, K. T., Gallay, C., Thalsø-Madsen, I., Xu, L., Jousselin, A., Torrubia, F. R., Paulander, W., Pereira, A. R. & Veening, J.-W. (2019). The ClpX chaperone controls autolytic splitting of *Staphylococcus aureus* daughter cells, but is bypassed by β -lactam antibiotics or inhibitors of WTA biosynthesis. *PLoS pathogens*, 15 (9): e1008044. doi: 10.1371/journal.ppat.1008044.
- Jerga, A., Lu, Y. J., Schujman, G. E., de Mendoza, D. & Rock, C. O. (2007). Identification of a soluble diacylglycerol kinase required for lipoteichoic acid production in *Bacillus subtilis*. *Journal of biological chemistry*, 282 (30): 21738-21745. doi: 10.1074/jbc.M703536200.
- Jiang, W., Bikard, D., Cox, D., Zhang, F. & Marraffini, L. A. (2013). RNA-guided editing of bacterial genomes using CRISPR-Cas systems. *Nature biotechnology*, 31 (3): 233-239. doi: 10.1038/nbt.2508.
- Jinek, M., Chylinski, K., Fonfara, I., Hauer, M., Doudna, J. A. & Charpentier, E. (2012). A programmable dual-RNA-guided DNA endonuclease in adaptive bacterial immunity. *Science*, 337 (6096): 816-821. doi: 10.1126/science.1225829.
- Jorasch, P., Warnecke, D. C., Lindner, B., Zähringer, U. & Heinz, E. (2000). Novel processive and nonprocessive glycosyltransferases from *Staphylococcus aureus* and *Arabidopsis thaliana* synthesize glycolipids, glycosphingolipids, glycosphingolipids and glycosylsterols. *European journal of biochemistry*, 267 (12): 3770-3783. doi: 10.1046/j.1432-1327.2000.01414.x.
- Jorge, A. M., Hoiczky, E., Gomes, J. P. & Pinho, M. G. (2011). EzrA contributes to the regulation of cell size in *Staphylococcus aureus*. *PLoS One*, 6 (11): e27542. doi: 10.1371/journal.pone.0027542.
- Jumper, J., Evans, R., Pritzel, A., Green, T., Figurnov, M., Ronneberger, O., Tunyasuvunakool, K., Bates, R., Žídek, A., Potapenko, A., et al. (2021). Highly accurate protein structure prediction with AlphaFold. *Nature*, 596 (7873): 583-589. doi: 10.1038/s41586-021-03819-2.
- Jun, S. & Mulder, B. (2006). Entropy-driven spatial organization of highly confined polymers: lessons for the bacterial chromosome. *Proceedings of the national academy of sciences*, 103 (33): 12388-12393. doi: 10.1073/pnas.0605305103.
- Kajimura, J., Fujiwara, T., Yamada, S., Suzawa, Y., Nishida, T., Oyamada, Y., Hayashi, I., Yamagishi, J., Komatsuzawa, H. & Sugai, M. (2005). Identification and molecular characterization of an N-acetylmuramyl-L-alanine amidase Sle1 involved in cell separation of *Staphylococcus aureus*. *Molecular microbiology*, 58 (4): 1087-1101. doi: 10.1111/j.1365-2958.2005.04881.x.
- Katayama, T., Ozaki, S., Keyamura, K. & Fujimitsu, K. (2010). Regulation of the replication cycle: conserved and diverse regulatory systems for DnaA and oriC. *Nature reviews microbiology*, 8 (3): 163-170. doi: 10.1038/nrmicro2314.
- Kho, K. & Meredith, T. C. (2018). Salt-induced stress stimulates a lipoteichoic acid-specific three-component glycosylation system in *Staphylococcus aureus*. *Journal of bacteriology*, 200 (12): e00017-18. doi: 10.1128/JB.00017-18.

References

- Kiriukhin, M. Y., Debabov, D. V., Shinabarger, D. L. & Neuhaus, F. C. (2001). Biosynthesis of the glycolipid anchor in lipoteichoic acid of *Staphylococcus aureus* RN4220: role of YpfP, the diglucoacyldiacylglycerol synthase. *Journal of bacteriology*, 183 (11): 3506-3514. doi: 10.1128/JB.183.11.3506-3514.2001.
- Kluytmans, J., Van Belkum, A. & Verbrugh, H. (1997). Nasal carriage of *Staphylococcus aureus*: epidemiology, underlying mechanisms, and associated risks. *Clinical microbiology reviews*, 10 (3): 505-520. doi: 10.1128/CMR.10.3.505.
- Koch, H. U., Haas, R. & Fischer, W. (1984). The role of lipoteichoic acid biosynthesis in membrane lipid metabolism of growing *Staphylococcus aureus*. *European journal of biochemistry*, 138 (2): 357-363. doi: 10.1111/j.1432-1033.1984.tb07923.x.
- Kojima, N., Araki, Y. & Ito, E. (1983). Structure of linkage region between ribitol teichoic acid and peptidoglycan in cell walls of *Staphylococcus aureus* H. *Journal of biological chemistry*, 258 (15): 9043-9045.
- Kuczkowska, K., Kleiveland, C. R., Minic, R., Moen, L. F., Øverland, L., Tjåland, R., Carlsen, H., Lea, T., Mathiesen, G. & Eijsink, V. G. (2016). Immunogenic properties of *Lactobacillus plantarum* producing surface-displayed *Mycobacterium tuberculosis* antigens. *Applied and environmental microbiology*, 83 (2): e02782-16. doi: 10.1128/AEM.02782-16.
- Kuczkowska, K., Myrbråten, I., Øverland, L., Eijsink, V. G., Follmann, F., Mathiesen, G. & Dietrich, J. (2017). *Lactobacillus plantarum* producing a *Chlamydia trachomatis* antigen induces a specific IgA response after mucosal booster immunization. *PloS one*, 12 (5): e0176401. doi: 10.1371/journal.pone.0176401.
- Labischinski, H. (1992). Consequences of the interaction of β -lactam antibiotics with penicillin binding proteins from sensitive and resistant *Staphylococcus aureus* strains. *Medical microbiology and immunology*, 181 (5): 241-265. doi: 10.1007/BF00198846.
- Larson, M. H., Gilbert, L. A., Wang, X., Lim, W. A., Weissman, J. S. & Qi, L. S. (2013). CRISPR interference (CRISPRi) for sequence-specific control of gene expression. *Nature protocols*, 8 (11): 2180-2196. doi: 10.1038/nprot.2013.132.
- Lazarevic, V. & Karamata, D. (1995). The *tagGH* operon of *Bacillus subtilis* 168 encodes a two-component ABC transporter involved in the metabolism of two wall teichoic acids. *Molecular microbiology*, 16 (2): 345-355. doi: 10.1111/j.1365-2958.1995.tb02306.x.
- Lemon, K. P. & Grossman, A. D. (2001). The extrusion-capture model for chromosome partitioning in bacteria. *Genes & development*, 15 (16): 2031-2041. doi: 10.1101/gad.913301.
- Levin, P. A., Kurtser, I. G. & Grossman, A. D. (1999). Identification and characterization of a negative regulator of FtsZ ring formation in *Bacillus subtilis*. *Proceedings of the national academy of sciences*, 96 (17): 9642-9647. doi: 10.1073/pnas.96.17.9642.
- Lithgow, J. K., Ingham, E. & Foster, S. J. (2004). Role of the *hprT-ftsH* locus in *Staphylococcus aureus*. *Microbiology*, 150 (2): 373-381. doi: 10.1099/mic.0.26674-0.

- Liu, X., Gallay, C., Kjos, M., Domenech, A., Slager, J., van Kessel, S. P., Knoops, K., Sorg, R. A., Zhang, J. R. & Veening, J. W. (2017). High-throughput CRISPRi phenotyping identifies new essential genes in *Streptococcus pneumoniae*. *Molecular systems biology*, 13 (5): 931. doi: 10.15252/msb.20167449.
- Lund, V. A., Wacnik, K., Turner, R. D., Cotterell, B. E., Walther, C. G., Fenn, S. J., Grein, F., Wollman, A. J., Leake, M. C., Olivier, N., et al. (2018). Molecular coordination of *Staphylococcus aureus* cell division. *eLife*, 7: e32057. doi: 10.7554/eLife.32057.
- Ma, D., Wang, Z., Merrikh, C. N., Lang, K. S., Lu, P., Li, X., Merrikh, H., Rao, Z. & Xu, W. (2018). Crystal structure of a membrane-bound O-acyltransferase. *Nature*, 562 (7726): 286-290. doi: 10.1038/s41586-018-0568-2.
- Matias, V. R. & Beveridge, T. J. (2007). Cryo-electron microscopy of cell division in *Staphylococcus aureus* reveals a mid-zone between nascent cross walls. *Molecular microbiology*, 64 (1): 195-206. doi: 10.1111/j.1365-2958.2007.05634.x.
- McGuinness, W. A., Malachowa, N. & DeLeo, F. R. (2017). Vancomycin resistance in *Staphylococcus aureus*. *Yale journal of biology and medicine*, 90 (2): 269-281.
- Meeske, A. J., Riley, E. P., Robins, W. P., Uehara, T., Mekalanos, J. J., Kahne, D., Walker, S., Kruse, A. C., Bernhardt, T. G. & Rudner, D. Z. (2016). SEDS proteins are a widespread family of bacterial cell wall polymerases. *Nature*, 537 (7622): 634-638. doi: 10.1038/nature19331.
- Memmi, G., Filipe, S. R., Pinho, M. G., Fu, Z. & Cheung, A. (2008). *Staphylococcus aureus* PBP4 is essential for β -lactam resistance in community-acquired methicillin-resistant strains. *Antimicrobial agents and chemotherapy*, 52 (11): 3955-3966. doi: 10.1128/AAC.00049-08.
- Meredith, T. C., Swoboda, J. G. & Walker, S. (2008). Late-stage polyribitol phosphate wall teichoic acid biosynthesis in *Staphylococcus aureus*. *Journal of bacteriology*, 190 (8): 3046-3056. doi: 10.1128/jb.01880-07.
- Mistretta, N., Brossaud, M., Telles, F., Sanchez, V., Talaga, P. & Rokbi, B. (2019). Glycosylation of *Staphylococcus aureus* cell wall teichoic acid is influenced by environmental conditions. *Scientific reports*, 9 (1): 3212. doi: 10.1038/s41598-019-39929-1.
- Monteiro, J. M., Fernandes, P. B., Vaz, F., Pereira, A. R., Tavares, A. C., Ferreira, M. T., Pereira, P. M., Veiga, H., Kuru, E. & VanNieuwenhze, M. S. (2015). Cell shape dynamics during the staphylococcal cell cycle. *Nature communications*, 6 (1): 1-12. doi: 10.1038/ncomms9055.
- Monteiro, J. M., Pereira, A. R., Reichmann, N. T., Saraiva, B. M., Fernandes, P. B., Veiga, H., Tavares, A. C., Santos, M., Ferreira, M. T., Macario, V., et al. (2018). Peptidoglycan synthesis drives an FtsZ-treadmilling-independent step of cytokinesis. *Nature*, 554 (7693): 528-532. doi: 10.1038/nature25506.
- Nega, M., Tribelli, P. M., Hipp, K., Stahl, M. & Götz, F. (2020). New insights in the coordinated amidase and glucosaminidase activity of the major autolysin (Atl) in *Staphylococcus aureus*. *Communications biology*, 3 (1): 1-10. doi: 10.1038/s42003-020-01405-2.
- Neuhaus, F. C. & Baddiley, J. (2003). A continuum of anionic charge: structures and functions of D-alanyl-teichoic acids in Gram-positive bacteria. *Microbiology and molecular biology reviews*, 67 (4): 686-723. doi: 10.1128/mubr.67.4.686-723.2003.

References

- Niedzielin, K., Kordecki, H. & Birkenfeld, B. (2001). A controlled, double-blind, randomized study on the efficacy of *Lactobacillus plantarum* 299V in patients with irritable bowel syndrome. *European journal of gastroenterology and hepatology*, 13 (10): 1143-1147. doi: 10.1097/00042737-200110000-00004.
- O'Neill, A. J. (2010). *Staphylococcus aureus* SH1000 and 8325-4: comparative genome sequences of key laboratory strains in staphylococcal research. *Letters in applied microbiology*, 51 (3): 358-61. doi: 10.1111/j.1472-765X.2010.02885.x.
- O'Riordan, K. & Lee, J. C. (2004). *Staphylococcus aureus* capsular polysaccharides. *Clinical microbiology reviews*, 17 (1): 218-234. doi: 10.1128/CMR.17.1.218-234.2004.
- Oku, Y., Kurokawa, K., Matsuo, M., Yamada, S., Lee, B.-L. & Sekimizu, K. (2009). Pleiotropic roles of polyglycerolphosphate synthase of lipoteichoic acid in growth of *Staphylococcus aureus* cells. *Journal of bacteriology*, 191 (1): 141-151. doi: 10.1128/JB.01221-08.
- Oshida, T., Sugai, M., Komatsuzawa, H., Hong, Y.-M., Suginaka, H. & Tomasz, A. (1995). A *Staphylococcus aureus* autolysin that has an N-acetylmuramoyl-L-alanine amidase domain and an endo-beta-N-acetylglucosaminidase domain: cloning, sequence analysis, and characterization. *Proceedings of the national academy of sciences*, 92 (1): 285-289. doi: 10.1073/pnas.92.1.285.
- Pang, T., Wang, X., Lim, H. C., Bernhardt, T. G. & Rudner, D. Z. (2017). The nucleoid occlusion factor Noc controls DNA replication initiation in *Staphylococcus aureus*. *PLoS genetics*, 13 (7): e1006908. doi: 10.1371/journal.pgen.1006908.
- Pasquina-Lemonche, L., Burns, J., Turner, R., Kumar, S., Tank, R., Mullin, N., Wilson, J., Chakrabarti, B., Bullough, P. & Foster, S. (2020). The architecture of the Gram-positive bacterial cell wall. *Nature*: 1-4. doi: 10.1038/s41586-020-2236-6.
- Pasquina, L. W., Santa Maria, J. P. & Walker, S. (2013). Teichoic acid biosynthesis as an antibiotic target. *Current opinion in microbiology*, 16 (5): 531-537. doi: 10.1016/j.mib.2013.06.014.
- Pereira, M. P. & Brown, E. D. (2004). Bifunctional catalysis by CDP-ribitol synthase: convergent recruitment of reductase and cytidyltransferase activities in *Haemophilus influenzae* and *Staphylococcus aureus*. *Biochemistry*, 43 (37): 11802-11812. doi: 10.1021/bi048866v.
- Pinho, M. G. & Errington, J. (2003). Dispersed mode of *Staphylococcus aureus* cell wall synthesis in the absence of the division machinery. *Molecular microbiology*, 50 (3): 871-881. doi: 10.1046/j.1365-2958.2003.03719.x.
- Pinho, M. G. & Errington, J. (2005). Recruitment of penicillin-binding protein PBP2 to the division site of *Staphylococcus aureus* is dependent on its transpeptidation substrates. *Molecular microbiology*, 55 (3): 799-807. doi: 10.1111/j.1365-2958.2004.04420.x.
- Pinho, M. G., Kjos, M. & Veening, J.-W. (2013). How to get (a) round: mechanisms controlling growth and division of coccoid bacteria. *Nature reviews microbiology*, 11 (9): 601-614. doi: 10.1038/nrmicro3088.
- Qi, L. S., Larson, M. H., Gilbert, L. A., Doudna, J. A., Weissman, J. S., Arkin, A. P. & Lim, W. A. (2013). Repurposing CRISPR as an RNA-guided platform for sequence-

- specific control of gene expression. *Cell*, 152 (5): 1173-1183. doi: 10.1016/j.cell.2013.02.022.
- Qin, S., Huang, Z., Wang, Y., Pei, L. & Shen, Y. (2021). Probiotic potential of *Lactobacillus* isolated from horses and its therapeutic effect on DSS-induced colitis in mice. *Microbial pathogenesis*: 105216. doi: 10.1016/j.micpath.2021.105216.
- Quiblier, C., Zinkernagel, A. S., Schuepbach, R. A., Berger-Bächi, B. & Senn, M. M. (2011). Contribution of SecDF to *Staphylococcus aureus* resistance and expression of virulence factors. *BMC microbiology*, 11: 72. doi: 10.1186/1471-2180-11-72.
- Reed, P., Atilano, M. L., Alves, R., Hoiczuk, E., Sher, X., Reichmann, N. T., Pereira, P. M., Roemer, T., Filipe, S. R., Pereira-Leal, J. B., et al. (2015). *Staphylococcus aureus* survives with a minimal peptidoglycan synthesis machine but sacrifices virulence and antibiotic resistance. *PLoS pathogens*, 11 (5): e1004891. doi: 10.1371/journal.ppat.1004891.
- Reichmann, N. T. & Gründling, A. (2011). Location, synthesis and function of glycolipids and polyglycerolphosphate lipoteichoic acid in Gram-positive bacteria of the phylum Firmicutes. *FEMS microbiology letters*, 319 (2): 97-105. doi: 10.1111/j.1574-6968.2011.02260.x.
- Reichmann, N. T., Piçarra Cassona, C., Monteiro, J. M., Bottomley, A. L., Corrigan, R. M., Foster, S. J., Pinho, M. G. & Gründling, A. (2014). Differential localization of LTA synthesis proteins and their interaction with the cell division machinery in *Staphylococcus aureus*. *Molecular microbiology*, 92 (2): 273-286. doi: 10.1111/mmi.12551.
- Reichmann, N. T., Tavares, A. C., Saraiva, B. M., Jousselin, A., Reed, P., Pereira, A. R., Monteiro, J. M., VanNieuwenhze, M. S., Fernandes, F. & Pinho, M. G. (2019). SEDS-bPBP pairs direct lateral and septal peptidoglycan synthesis in *Staphylococcus aureus*. *Nature microbiology*, 4: 1368-1377. doi: 10.1038/s41564-019-0437-2.
- Rismondo, J., Gillis, A. & Gründling, A. (2021). Modifications of cell wall polymers in Gram-positive bacteria by multi-component transmembrane glycosylation systems. *Current opinion in microbiology*, 60: 24-33. doi: 10.1016/j.mib.2021.01.007.
- Roch, M., Lelong, E., Panasencko, O. O., Sierra, R., Renzoni, A. & Kelley, W. L. (2019). Thermosensitive PBP2a requires extracellular folding factors PrsA and HtrA1 for *Staphylococcus aureus* MRSA β -lactam resistance. *Communications biology*, 2: 417. doi: 10.1038/s42003-019-0667-0.
- Roemer, T., Schneider, T. & Pinho, M. G. (2013). Auxiliary factors: a chink in the armor of MRSA resistance to β -lactam antibiotics. *Current opinion in microbiology*, 16 (5): 538-548. doi: 10.1016/j.mib.2013.06.012.
- Rohrer, S. & Berger-Bächi, B. (2003). FemABX peptidyl transferases: a link between branched-chain cell wall peptide formation and β -lactam resistance in Gram-positive cocci. *Antimicrobial agents and chemotherapy*, 47 (3): 837-846. doi: 10.1128/AAC.47.3.837-846.2003.
- Rolain, T., Bernard, E., Courtin, P., Bron, P. A., Kleerebezem, M., Chapot-Chartier, M. P. & Hols, P. (2012). Identification of key peptidoglycan hydrolases for morphogenesis, autolysis, and peptidoglycan composition of *Lactobacillus*

References

- plantarum* WCFS1. *Microbial cell factories*, 11: 137. doi: 10.1186/1475-2859-11-137.
- Rossi, L., Tonin, E., Cheng, Y. R. & Fontana, R. (1985). Regulation of penicillin-binding protein activity: description of a methicillin-inducible penicillin-binding protein in *Staphylococcus aureus*. *Antimicrobial agents and chemotherapy*, 27 (5): 828-831. doi: 10.1128/AAC.27.5.828.
- Sakr, A., Brégeon, F., Mège, J.-L., Rolain, J.-M. & Blin, O. (2018). *Staphylococcus aureus* nasal colonization: an update on mechanisms, epidemiology, risk factors, and subsequent infections. *Frontiers in microbiology*, 9: 2419. doi: 10.3389/fmicb.2018.02419.
- Sanderson, A. R., Strominger, J. L. & Nathenson, S. G. (1962). Chemical structure of teichoic acid from *Staphylococcus aureus*, strain Copenhagen. *Journal of biological chemistry*, 237 (12): 3603-3613.
- Santiago, M., Matano, L. M., Moussa, S. H., Gilmore, M. S., Walker, S. & Meredith, T. C. (2015). A new platform for ultra-high density *Staphylococcus aureus* transposon libraries. *BMC genomics*, 16 (1): 1-18. doi: 10.1186/s12864-015-1361-3.
- Saraiva, B. M., Sorg, M., Pereira, A. R., Ferreira, M. J., Caulat, L. C., Reichmann, N. T. & Pinho, M. G. (2020). Reassessment of the distinctive geometry of *Staphylococcus aureus* cell division. *Nature communications*, 11 (1): 1-7. doi: 10.1038/s41467-020-17940-9.
- Sass, P. & Brötz-Oesterhelt, H. (2013). Bacterial cell division as a target for new antibiotics. *Current opinion in microbiology*, 16 (5): 522-530. doi: 10.1016/j.mib.2013.07.006.
- Sauvage, E., Kerff, F., Terrak, M., Ayala, J. A. & Charlier, P. (2008). The penicillin-binding proteins: structure and role in peptidoglycan biosynthesis. *FEMS microbiology reviews*, 32 (2): 234-258. doi: 10.1111/j.1574-6976.2008.00105.x.
- Schlag, M., Biswas, R., Krismer, B., Kohler, T., Zoll, S., Yu, W., Schwarz, H., Peschel, A. & Götz, F. (2010). Role of staphylococcal wall teichoic acid in targeting the major autolysin Atl. *Molecular microbiology*, 75 (4): 864-873. doi: 10.1111/j.1365-2958.2009.07007.x.
- Sewell, E. W. & Brown, E. D. (2014). Taking aim at wall teichoic acid synthesis: new biology and new leads for antibiotics. *The journal of antibiotics*, 67 (1): 43-51. doi: 10.1038/ja.2013.100.
- Sham, L.-T., Butler, E. K., Lebar, M. D., Kahne, D., Bernhardt, T. G. & Ruiz, N. (2014). Bacterial cell wall. MurJ is the flippase of lipid-linked precursors for peptidoglycan biogenesis. *Science*, 345 (6193): 220-222. doi: 10.1126/science.1254522.
- Sidow, T., Johannsen, L. & Labischinski, H. (1990). Penicillin-induced changes in the cell wall composition of *Staphylococcus aureus* before the onset of bacteriolysis. *Archives of microbiology*, 154 (1): 73-81. doi: 10.1007/BF00249181.
- Soldo, B., Lazarevic, V. & Karamata, D. (2002). *tagO* is involved in the synthesis of all anionic cell-wall polymers in *Bacillus subtilis* *Microbiology*, 148 (7): 2079-2087. doi: 10.1099/00221287-148-7-2079.
- Sompolinsky, D., Samra, Z., Karakawa, W., Vann, W., Schneerson, R. & Malik, Z. (1985). Encapsulation and capsular types in isolates of *Staphylococcus aureus* from

- different sources and relationship to phage types. *Journal of clinical microbiology*, 22 (5): 828-834. doi: 10.1128/jcm.22.5.828-834.1985.
- Song, C. W., Lee, J. & Lee, S. Y. (2015). Genome engineering and gene expression control for bacterial strain development. *Biotechnology journal*, 10 (1): 56-68. doi: 10.1002/biot.201400057.
- Stamsås, G. A., Straume, D., Ruud Winther, A., Kjos, M., Frantzen, C. A. & Håvarstein, L. S. (2017). Identification of EloR (Spr1851) as a regulator of cell elongation in *Streptococcus pneumoniae*. *Molecular microbiology*, 105 (6): 954-967. doi: 10.1111/mmi.13748.
- Stamsås, G. A., Restelli, M., Ducret, A., Freton, C., Garcia, P. S., Håvarstein, L. S., Straume, D., Grangeasse, C. & Kjos, M. (2020). A CozE homolog contributes to cell size homeostasis of *Streptococcus pneumoniae*. *mBio*, 11 (5): e02461-20. doi: 10.1128/mBio.02461-20.
- Steele, V. R., Bottomley, A. L., Garcia-Lara, J., Kasturiarachchi, J. & Foster, S. J. (2011). Multiple essential roles for EzrA in cell division of *Staphylococcus aureus*. *Molecular microbiology*, 80 (2): 542-555. doi: 10.1111/j.1365-2958.2011.07591.x.
- Stefanović, C., Hager, F. F. & Schäffer, C. (2021). LytR-CpsA-Psr glycopolymer transferases: Essential bricks in Gram-positive bacterial cell wall assembly. *International journal of molecular sciences*, 22 (2): 908. doi: 10.3390/ijms22020908.
- Straume, D., Stamsås, G. A., Berg, K. H., Salehian, Z. & Håvarstein, L. S. (2017). Identification of pneumococcal proteins that are functionally linked to penicillin-binding protein 2b (PBP2b). *Molecular microbiology*, 103 (1): 99-116. doi: 10.1111/mmi.13543.
- Straume, D., Piechowiak, K. W., Kjos, M. & Håvarstein, L. S. (2021). Class A PBPs: It is time to rethink traditional paradigms. *Molecular microbiology*, 116 (1): 41-52. doi: 10.1111/mmi.14714.
- Sullivan, N. L., Marquis, K. A. & Rudner, D. Z. (2009). Recruitment of SMC by ParB-*parS* organizes the origin region and promotes efficient chromosome segregation. *Cell*, 137 (4): 697-707. doi: 10.1016/j.cell.2009.04.044.
- Swoboda, J. G., Meredith, T. C., Campbell, J., Brown, S., Suzuki, T., Bollenbach, T., Malhowski, A. J., Kishony, R., Gilmore, M. S. & Walker, S. (2009). Discovery of a small molecule that blocks wall teichoic acid biosynthesis in *Staphylococcus aureus*. *ACS chemical biology*, 4 (10): 875-883. doi: 10.1021/cb900151k.
- Swoboda, J. G., Campbell, J., Meredith, T. C. & Walker, S. (2010). Wall teichoic acid function, biosynthesis, and inhibition. *ChemBioChem*, 11 (1): 35-45. doi: 10.1002/cbic.200900557.
- Tacconelli, E., Carrara, E., Savoldi, A., Harbarth, S., Mendelson, M., Monnet, D. L., Pulcini, C., Kahlmeter, G., Kluytmans, J., Carmeli, Y., et al. (2018). Discovery, research, and development of new antibiotics: the WHO priority list of antibiotic-resistant bacteria and tuberculosis. *The Lancet infectious diseases*, 18 (3): 318-327. doi: 10.1016/s1473-3099(17)30753-3.
- Taguchi, A., Welsh, M. A., Marmont, L. S., Lee, W., Sjodt, M., Kruse, A. C., Kahne, D., Bernhardt, T. G. & Walker, S. (2019). FtsW is a peptidoglycan polymerase that is functional only in complex with its cognate penicillin-binding protein. *Nature microbiology*, 4 (4): 587-594. doi: 10.1038/s41564-018-0345-x.

References

- Tian, P., Wang, J., Shen, X., Rey, J. F., Yuan, Q. & Yan, Y. (2017). Fundamental CRISPR-Cas9 tools and current applications in microbial systems. *Synthetic and systems biotechnology*, 2 (3): 219-225. doi: 10.1016/j.synbio.2017.08.006.
- Tsui, H. C. T., Zheng, J. J., Magallon, A. N., Ryan, J. D., Yunck, R., Rued, B. E., Bernhardt, T. G. & Winkler, M. E. (2016). Suppression of a deletion mutation in the gene encoding essential PBP2b reveals a new lytic transglycosylase involved in peripheral peptidoglycan synthesis in *Streptococcus pneumoniae* D39. *Molecular microbiology*, 100 (6): 1039-1065. doi: 10.1111/mmi.13366.
- Ubukata, K., Yamashita, N. & Konno, M. (1985). Occurrence of a beta-lactam-inducible penicillin-binding protein in methicillin-resistant staphylococci. *Antimicrobial agents and chemotherapy*, 27 (5): 851-857. doi: 10.1128/AAC.27.5.851.
- Valentino, M. D., Foulston, L., Sadaka, A., Kos, V. N., Villet, R. A., Santa Maria, J., Lazinski, D. W., Camilli, A., Walker, S. & Hooper, D. C. (2014). Genes contributing to *Staphylococcus aureus* fitness in abscess-and infection-related ecologies. *mBio*, 5 (5): e01729-14. doi: 10.1128/mBio.01729-14.
- Veiga, H., Jorge, A. M. & Pinho, M. G. (2011). Absence of nucleoid occlusion effector Noc impairs formation of orthogonal FtsZ rings during *Staphylococcus aureus* cell division. *Molecular microbiology*, 80 (5): 1366-1380. doi: 10.1111/j.1365-2958.2011.07651.x.
- Veiga, H. & G Pinho, M. (2016). *Staphylococcus aureus* requires at least one FtsK/SpoIIIE protein for correct chromosome segregation. *Molecular microbiology*, 103 (3): 504-517. doi: 10.1111/mmi.13572.
- Vollmer, W., Joris, B., Charlier, P. & Foster, S. (2008). Bacterial peptidoglycan (murein) hydrolases. *FEMS microbiology reviews*, 32 (2): 259-86. doi: 10.1111/j.1574-6976.2007.00099.x.
- Weart, R. B., Lee, A. H., Chien, A.-C., Haeusser, D. P., Hill, N. S. & Levin, P. A. (2007). A metabolic sensor governing cell size in bacteria. *Cell*, 130 (2): 335-347. doi: 10.1016/j.cell.2007.05.043.
- Wells, J. M. & Mercenier, A. (2008). Mucosal delivery of therapeutic and prophylactic molecules using lactic acid bacteria. *Nature reviews microbiology*, 6 (5): 349-362. doi: 10.1038/nrmicro1840.
- Whitley, K. D., Jukes, C., Tregidgo, N., Karinou, E., Almada, P., Cesbron, Y., Henriques, R., Dekker, C. & Holden, S. (2021). FtsZ treadmilling is essential for Z-ring condensation and septal constriction initiation in *Bacillus subtilis* cell division. *Nature communications*, 12 (1): 2448. doi: 10.1038/s41467-021-22526-0.
- Winstel, V., Xia, G. & Peschel, A. (2014). Pathways and roles of wall teichoic acid glycosylation in *Staphylococcus aureus*. *International journal of medical microbiology*, 304 (3-4): 215-221. doi: 10.1016/j.ijmm.2013.10.009.
- Winstel, V., Kühner, P., Salomon, F., Larsen, J., Skov, R., Hoffmann, W., Peschel, A. & Weidenmaier, C. (2015). Wall teichoic acid glycosylation governs *Staphylococcus aureus* nasal colonization. *mBio*, 6 (4): e00632-15. doi: 10.1128/mBio.00632-15.
- Winther, A. R., Kjos, M., Stamsås, G. A., Håvarstein, L. S. & Straume, D. (2019). Prevention of EloR/KhpA heterodimerization by introduction of site-specific amino acid substitutions renders the essential elongasome protein PBP2b

- redundant in *Streptococcus pneumoniae*. *Scientific reports*, 9 (1): 1-13. doi: 10.1038/s41598-018-38386-6.
- Winther, A. R., Kjos, M., Herigstad, M. L., Håvarstein, L. S. & Straume, D. (2021). EloR interacts with the lytic transglycosylase MltG at midcell in *Streptococcus pneumoniae* R6. *Journal of bacteriology*, 203 (9): e00691-20. doi: 10.1128/JB.00691-20.
- Wood, B. M., Santa Maria, J. P., Matano, L. M., Vickery, C. R. & Walker, S. (2018). A partial reconstitution implicates DltD in catalyzing lipoteichoic acid D-alanylation. *Journal of biological chemistry*, 293 (46): 17985-17996. doi: 10.1074/jbc.RA118.004561.
- Wyke, A. W., Ward, J. B., Hayes, M. V. & Curtis, N. A. (1981). A role *in vivo* for penicillin-binding protein-4 of *Staphylococcus aureus*. *European journal of biochemistry*, 119 (2): 389-393. doi: 10.1111/j.1432-1033.1981.tb05620.x.
- Xia, G., Kohler, T. & Peschel, A. (2010a). The wall teichoic acid and lipoteichoic acid polymers of *Staphylococcus aureus*. *International journal of medical microbiology*, 300 (2-3): 148-154. doi: 10.1016/j.ijmm.2009.10.001.
- Xia, G., Maier, L., Sanchez-Carballo, P., Li, M., Otto, M., Holst, O. & Peschel, A. (2010b). Glycosylation of wall teichoic acid in *Staphylococcus aureus* by TarM. *Journal of biological chemistry*, 285 (18): 13405-13415. doi: 10.1074/jbc.M109.096172.
- Xiang, Z., Li, Z., Zeng, J., Li, Y. & Li, J. (2019). Regulation of cell division in Streptococci: Comparing with the model rods. *Current issues in molecular biology*, 32: 259-326. doi: 10.21775/cimb.032.259.
- Yeo, W.-S., Jeong, B., Ullah, N., Shah, M. A., Ali, A., Kim, K. K. & Bae, T. (2021). FtsH sensitizes methicillin-resistant *Staphylococcus aureus* to β -Lactam antibiotics by degrading YpfP, a lipoteichoic acid synthesis enzyme. *Antibiotics*, 10 (10): 1198. doi: 10.3390/antibiotics10101198.
- Yu, W., Herbert, S., Graumann, P. L. & Götz, F. (2010). Contribution of SMC (structural maintenance of chromosomes) and SpoIIIE to chromosome segregation in Staphylococci. *Journal of bacteriology*, 192 (15): 4067-4073. doi: 10.1128/jb.00010-10.
- Zago, M., Fornasari, M. E., Carminati, D., Burns, P., Suárez, V., Vinderola, G., Reinheimer, J. & Giraffa, G. (2011). Characterization and probiotic potential of *Lactobacillus plantarum* strains isolated from cheeses. *Food microbiology*, 28 (5): 1033-1040. doi: 10.1016/j.fm.2011.02.009.
- Zheng, J. J., Perez, A. J., Tsui, H. C. T., Massidda, O. & Winkler, M. E. (2017). Absence of the KhpA and KhpB (JAG/EloR) RNA-binding proteins suppresses the requirement for PBP2b by overproduction of FtsA in *Streptococcus pneumoniae* D39. *Molecular microbiology*, 106 (5): 793-814. doi: 10.1111/mmi.13847.
- Zhou, X., Halladin, D. K., Rojas, E. R., Koslover, E. F., Lee, T. K., Huang, K. C. & Theriot, J. A. (2015). Bacterial division. Mechanical crack propagation drives millisecond daughter cell separation in *Staphylococcus aureus*. *Science*, 348 (6234): 574-8. doi: 10.1126/science.aaa1511.
- Zoll, S., Schlag, M., Shkumatov, A. V., Rautenberg, M., Svergun, D. I., Götz, F. & Stehle, T. (2012). Ligand-binding properties and conformational dynamics of autolysin repeat domains in staphylococcal cell wall recognition. *Journal of bacteriology*, 194 (15): 3789-3802. doi: 10.1128/JB.00331-12.

PAPER I

CozEa and CozEb play overlapping and essential roles in controlling cell division in *Staphylococcus aureus*

Gro Anita Stamsås,^{1†} Ine Storaker Myrbråten,^{1†}
Daniel Straume,¹ Zhian Salehian,¹
Jan-Willem Veening,² Leiv Sigve Håvarstein¹
and Morten Kjos^{1*}

¹Faculty of Chemistry, Biotechnology and Food Science, Norwegian University of Life Sciences, Ås, Norway.

²Department of Fundamental Microbiology, Faculty of Biology and Medicine, University of Lausanne, Lausanne, Switzerland.

Summary

Staphylococcus aureus needs to control the position and timing of cell division and cell wall synthesis to maintain its spherical shape. We identified two membrane proteins, named CozEa and CozEb, which together are important for proper cell division in *S. aureus*. CozEa and CozEb are homologs of the cell elongation regulator CozE^{Spn} of *Streptococcus pneumoniae*. While *cozEa* and *cozEb* were not essential individually, the $\Delta\text{cozEa}\Delta\text{cozEb}$ double mutant was lethal. To study the functions of *cozEa* and *cozEb*, we constructed a CRISPR interference (CRISPRi) system for *S. aureus*, allowing transcriptional knockdown of essential genes. CRISPRi knockdown of *cozEa* in the ΔcozEb strain (and vice versa) causes cell morphological defects and aberrant nucleoid staining, showing that *cozEa* and *cozEb* have overlapping functions and are important for normal cell division. We found that CozEa and CozEb interact with and possibly influence localization of the cell division protein EzrA. Furthermore, the CozE–EzrA interaction is conserved in *S. pneumoniae*, and cell division is mislocalized in *cozE*^{Spn}-depleted *S. pneumoniae* cells. Together, our results show that CozE proteins mediate control of cell division in *S. aureus* and *S. pneumoniae*, likely via interactions with key cell division proteins such as EzrA.

Accepted 30 May, 2018. *For correspondence. E-mail morten.kjos@nmbu.no; Tel. +47 67232951; Fax +47 64965901.

[†]These authors contributed equally to this work.

Introduction

Bacterial cell division initiates when the tubulin-like protein FtsZ polymerizes into a ring structure (Z-ring) located at the future division site. The Z-ring then serves as a scaffold for recruitment of cell division and cell wall synthesis proteins, forming the multiprotein complex known as the divisome. Several of the proteins constituting the divisome are widely conserved in most bacteria, while others are specific for bacterial subgroups or have diverged significantly (Pinho *et al.*, 2013). Positioning and timing of Z-ring assembly and cell wall synthesis are dependent on the shape of the bacterium; and there are large variations between coccal, ovococcal and rod-shaped bacteria.

Staphylococcus aureus often serves as the model organism for cell division studies in spherical bacteria. *S. aureus* is an opportunistic pathogen, which persistently colonizes around 20% of the human population (Grice and Segre, 2011), causing both superficial infections on the skin and invasive, life-threatening sepsis as well as endocarditis in humans (Foster *et al.*, 2014; Rasigade and Vandenesch, 2014). Furthermore, *S. aureus* is an important pathogen among livestock (causing mastitis and other infections) and is a problematic food pathogen. Treatment of *S. aureus* infections with antibiotics is increasingly challenging due to the rise of antibiotic resistant strains, including MRSA (methicillin-resistant *S. aureus* which are resistant to β -lactam antibiotics) and VRSA (vancomycin-resistant *S. aureus*).

Cell division in spherical *S. aureus* occurs in three consecutive planes, where every new round of division is orthogonal to the previous division plane (Pinho *et al.*, 2013). Many key cell division proteins known from other model bacteria are conserved in *S. aureus*, including FtsZ, FtsA, EzrA, GpsB, DivIB, DivIC, FtsL, MurJ, DivIVA, MreC and MreD (Pinho and Errington, 2003; Pinho and Errington, 2004; Steele *et al.*, 2011; Pinho *et al.*, 2013; Bottomley *et al.*, 2014; Monteiro *et al.*, 2018). These proteins are in different ways involved in formation of the division ring and for ensuring proper cell wall synthesis and cell division. For example, EzrA is a key early cell division protein linking division ring formation and the cell wall synthesis machinery (Jorge *et al.*, 2011; Steele *et al.*, 2011). Synthesis of new cell wall in staphylococci mainly occurs at midcell. The recruitment of cell wall synthesis

proteins (i.e. transpeptidases PBP1, PBP3 and PBP4 and the bi-functional transpeptidase/transglycosylase PBP2 responsible for synthesizing the peptidoglycan sacculus) to midcell was recently shown to be driven by the putative lipid II flippase MurJ (Monteiro *et al.*, 2018). The current models of the *S. aureus* cell cycle suggest an initial, gradual increase in cell volume by slight elongation, followed by recruitment of MurJ and PBPs to the septum, which drives cross-wall synthesis and cell constriction. To split the daughter cells, hydrolases perforate the cell wall before the actual splitting/popping of daughter cells occurs on a timescale of milliseconds (Monteiro *et al.*, 2015; Zhou *et al.*, 2015; Lund *et al.*, 2018; Monteiro *et al.*, 2018).

During each cell cycle, peptidoglycan synthesis and cell division need to be coordinated with DNA replication and chromosome segregation. This is to ensure correct cell size homeostasis and that the two daughter cells each get one copy of the chromosome in time before the cell splits. Misregulation would result in daughter cells of variable sizes without DNA or guillotining of the chromosome by the septal cross-wall. How the timing and localization of Z-ring assembly and cell wall synthesis are regulated in *S. aureus*, given the geometry of cell division in three consecutive perpendicular planes, is still an unanswered question. One protein involved in this coordination is probably Noc (nucleoid occlusion protein) which both controls DNA replication (Pang *et al.*, 2017) and inhibits Z-ring formation across the nucleoid (Veiga *et al.*, 2011). Recent results also predict the protein DivIVA to have an important role in linking chromosome segregation with cell division (Bottomley *et al.*, 2017).

The important human pathogen *S. pneumoniae* is an ovococcal bacterium, in which both septal (division) and peripheral (elongation) cell wall synthesis occur in the mid-cell area (Ducret and Grangeasse, 2017). In these cells, positioning of the Z-ring at mid-cell has been shown to depend on several factors, including the chromosomal origin of replication (van Raaphorst *et al.*, 2017) and the peptidoglycan binding protein MapZ (Fleurie *et al.*, 2014; Holeckova *et al.*, 2014). Most likely, the septal and peripheral cell wall growth in pneumococcal cells are mediated by separate protein machineries, whose actions are tuned by different regulatory proteins such as StkP, MreCD, GpsB, DivIVA and EloR (Beilharz *et al.*, 2012; Fleurie *et al.*, 2014; Ducret and Grangeasse, 2017; Rued *et al.*, 2017; Stamsås *et al.*, 2017; Straume *et al.*, 2017; Zheng *et al.*, 2017). Another protein involved in regulation of cell wall synthesis in pneumococci, named CozE (for coordinator of zonal elongation, SPD_0768 in strain D39 and Spr0777 in strain R6), was recently identified (Fenton *et al.*, 2016; Straume *et al.*, 2017). CozE, a multi-transmembrane spanning protein, was found to be essential for normal growth, however, its essentiality was abolished

in the absence of the bifunctional penicillin-binding protein PBP1a or the cell wall elongation proteins MreC and MreD (Fenton *et al.*, 2016). In protein-protein interaction assays, CozE was found to be associated with the same proteins (PBP1a, MreC, MreD) as well as DivIVA and PBP2b (Fenton *et al.*, 2016; Straume *et al.*, 2017). CozE was thus proposed to be a key regulator of cell elongation in *S. pneumoniae* by positioning PBP1a via interactions with MreC and MreD (Fenton *et al.*, 2016; Ducret and Grangeasse, 2017). CozE proteins are widespread among different bacteria (Fenton *et al.*, 2016). Here we studied the two homologs of CozE in spherical *S. aureus* cells. We show that the CozE proteins are involved in coordinating cell division in *S. aureus* and that this function is conserved also in *S. pneumoniae*.

As a means to study the functionality of essential genes, we also develop a CRISPR interference (CRISPRi) system for *S. aureus*. With CRISPRi, the CRISPR/Cas9-system is harnessed to knock down gene expression of any gene of interest (Bikard *et al.*, 2013; Qi *et al.*, 2013). Transcriptional knockdown is achieved by two components: a catalytically inactive Cas9 protein (dCas9) and a single guide RNA (sgRNA). Unlike the Cas9 nuclease, dCas9 does not cleave DNA, but the DNA-binding capability is still intact. A single guide RNA (sgRNA), containing a gene-specific base-pairing region and a structured region for interaction with dCas9, is designed to target the gene of interest. Upon co-expression, the dCas9-sgRNA complex will bind DNA and serve as a transcriptional roadblock for the RNA polymerase, thereby downregulating transcription.

Results

The two CozE homologs of S. aureus

The protein CozE (for coordinator of zonal elongation) was recently identified as an essential cell division protein in oval shaped pneumococcal cells, where it has been shown to be involved in regulation of proper cell elongation (Fenton *et al.*, 2016; Straume *et al.*, 2017). Spherical *S. aureus* does not elongate to the same extent as *S. pneumoniae* and other rod- or oval-shaped bacteria, although a short elongation phase has been observed during the cell cycle (Pinho *et al.*, 2013; Monteiro *et al.*, 2015). Nevertheless, homology searches showed that *S. aureus* encodes two proteins homologous to CozE, and we therefore set out to unravel the function of CozE in these spherical cells. Sequence comparison of the pneumococcal CozE (hereafter CozE^{Spn}) with the two CozE-homologs of *S. aureus* SH1000, SAOUHSC_00948 (hereafter CozEa) and SAOUHSC_01358 (hereafter CozEb), shows that they are 31% and 30% identical to CozE^{Spn} respectively (Fig. S1). When compared

with each other, CozEa and CozEb are 30% identical. Topology predictions suggest that these proteins have 8 or 9 transmembrane segments (Fig. S1). The *cozEa* gene is predicted to be monocistronic, while *cozEb* is located as the last open reading frame on a three-gene operon which also encodes a transcription antiterminator (*glcT*) and a small, putative membrane spanning protein (SAOUHSC_01357) (Fig. 1A).

Using the temperature sensitive vector pMAD (Arnaud *et al.*, 2004), *cozEa* and *cozEb* were deleted individually in *S. aureus* SH1000 by allelic exchange with a spectinomycin resistance cassette. The deletion mutants SAMK24 ($\Delta\textit{cozEa}::\textit{spc}$) and SAMK21 ($\Delta\textit{cozEb}::\textit{spc}$) did not exhibit any growth defect compared to wild-type (Fig.

1B). Analysis of cell sizes showed that the cell diameter of both mutants, on average, are slightly smaller compared to the wild-type (Fig. 1C and D). No obvious differences in cell wall labelling (using fluorescent vancomycin, VanFL) or nucleoid staining patterns (using DAPI) were observed between the mutants and wild-type (Fig. 1C).

In order to see whether the two mutant strains, SAMK21 and SAMK24, had acquired any suppressor mutations elsewhere in the genome, we resequenced their genomes and compared it to the SH1000 wild-type genome. SAMK24 did not contain any additional mutations. In SAMK21, a single conservative SNP was found in the gene *thil* (SAOUHSC_01824) encoding a probable tRNA sulphurtransferase. This SNP (A970T) resulted in

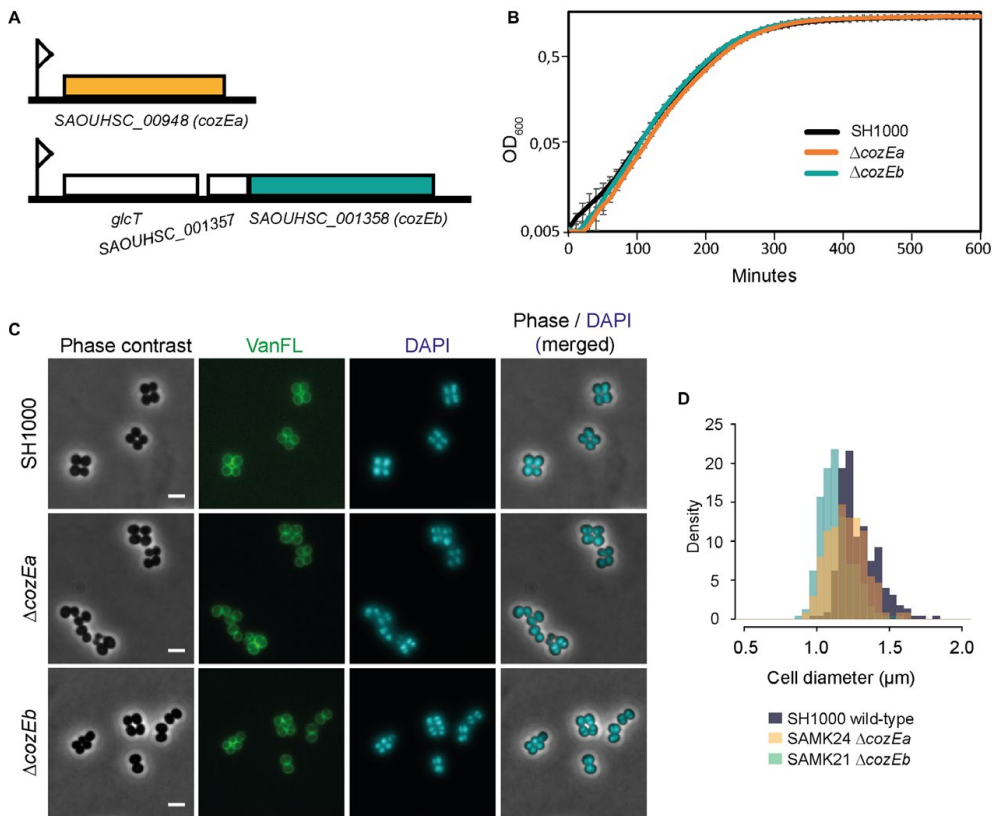


Fig. 1. *cozEa* and *cozEb* of *S. aureus*.

A. Genetic organization of the *cozEa* (SAOUHSC_00948) and *cozEb* (SAOUHSC_01358) genetic loci.

B. Growth curves SH1000 wild-type, SAMK24 ($\Delta\textit{cozEa}$) and SAMK21 ($\Delta\textit{cozEb}$) in BHI medium at 37°C.

C. Micrographs of SH1000, SAMK21 and SAMK24. Phase contrast (PC) images and staining with fluorescent vancomycin (VanFL) and DAPI are shown as well as an overlay of the two latter. The scale bars are 2 μm .

D. Histogram of the cell diameters of SH1000, SAMK24 and SAMK21 (>250 cells analyzed per sample) as measured using MicrobeJ (Ducret *et al.*, 2016). Both SAMK21 and SAMK24 were significantly smaller than SH1000 ($P < 0.05$, Kolmogorov-Smirnov test).

a conservative substitution of isoleucine with a phenylalanine (I324F). Our later experiments (see below) show that this mutation is not important for the functionality of *cozEb* (or *cozEa*) and we therefore conclude that neither *CozEa* nor *CozEb* are essential for normal growth and cell division in *S. aureus* SH1000.

Single deletions of *cozEa* or *cozEb* both cause a small reduction in cell size. To investigate the effects of a double deletion, another pMAD deletion vector (pMAD-*cozEa::sac*) was constructed to delete *cozEa* in the Δ *cozEb::spc* background. However, despite multiple attempts, we were unable to obtain the double deletion strain. This suggests that *cozEa* and *cozEb* may have complementary and essential functions.

Construction of a two-plasmid CRISPR interference system for *S. aureus*

Since double deletions of *cozEa* and *cozEb* could not be obtained, we instead wanted to study the phenotypes of the cells when *cozEa* or *cozEb* gene expression was knocked down in Δ *cozEb* or Δ *cozEa* background, respectively. We therefore constructed a CRISPR/dCas9 knockdown system to allow inducible depletion of essential genes. The CRISPR interference systems developed for *S. pneumoniae* and *Bacillus subtilis* (Peters *et al.*, 2016; Liu *et al.*, 2017) were used as models. A *dcas9* gene, encoding a catalytically inactive Cas9, was cloned downstream of an IPTG-inducible promoter in the low-copy number plasmid pLOW (pSK41 minireplicon, Fig. 2A) (Liew *et al.*, 2011). A single guide RNA (sgRNA) construct, consisting of a 20 nt base-pairing region and a Cas9-handle region, was inserted downstream of a synthetic, constitutive promoter in the plasmid pCG248 (replicon T181, Fig. 2A) (Helle *et al.*, 2011). Targeting of the gene of interest is accomplished by replacing the 20 nt sequence using inverse PCR as described in the Methods section. Notably, multi-sgRNA plasmids can be constructed using the BglII and BamHI restriction sites located up- and downstream of the sgRNA construct, as outlined in Fig. S2. A schematic view of the resulting two-plasmid CRISPRi system is shown in Fig. 2A.

To quantify the efficiency of our CRISPRi system, we created an RN4220-derivative strain with constitutive expression of a monomeric superfolder GFP (*m(sf)GFP*), SAMK56, and designed an sgRNA targeting the *m(sf)gfp* gene. As shown in Fig. 2B, GFP expression could be titrated by increasing the IPTG concentrations. Maximum depletion was obtained with ≥ 100 μ M IPTG. To investigate how quick GFP expression was switched off after IPTG induction, SAMK56 was induced with 100 μ M IPTG and samples were taken every 30th min for 3 h. The GFP fluorescence levels (Fig. 2C) decreased rapidly (signal reduced by ca. 90% within 60 min), suggesting that

expression was switched off almost immediately. Specific transcriptional knockdown was also demonstrated using qPCR (Fig. S3, see below for details). Note that for some of our later experiments, we observed a faster depletion of cell division proteins when increasing the IPTG concentration to 400 μ M. Furthermore, as a proof of the functionality of the CRISPRi system in targeting essential cell cycle genes, we created sgRNAs targeting the DNA replication initiator *dnaA* (encoded on an operon with *dnaN*) and *pbp1* (monocistronic) encoding a penicillin-binding protein. The CRISPRi strains were analyzed by growth assays and microscopy (Fig. 2D–F), and the observed phenotypes were as expected, confirming the suitability of the CRISPRi system to study the function of essential genes; compared to the control strain (Fig. 2D), the *pbp1* depletion resulted in clustered, larger cells with aberrant morphologies (Fig. 2E) (Pereira *et al.*, 2007; Pereira *et al.*, 2009) while *dnaA* depletion resulted in anucleate cells with variable sizes and nucleoid morphologies (Fig. 2F).

CozEa and *CozEb* have overlapping functions and are important for proper cell cycle progression in *S. aureus*

We made sgRNA constructs targeting *cozEa* and *cozEb*, and depleted expression of *cozEa* in the Δ *cozEb* background and vice versa. Note that *cozEa* is monocistronic, while *cozEb* is located as the last gene in the operon, and the knockdown will therefore have minimal polar effects (Peters *et al.*, 2016; Liu *et al.*, 2017). No growth reduction was observed upon knockdown of the individual genes in wild-type background (as expected from the deletion mutants) (Fig. 3A and B). We performed RT-qPCR on these CRISPRi-strains and verified that transcription of *cozEa* and *cozEb* was specifically knocked down (Fig. S3). After diluting the cells to OD₆₀₀ of 0.05 with and without 150 μ M IPTG and culturing for 2 h, the expression of *cozEa* and *cozEb* was reduced 23-fold and 13-fold in the respective strains when comparing induced and non-induced conditions.

While no effect on growth was observed by depleting *cozEa* or *cozEb* expression in wild-type background, knockdown of the other gene in the respective deletion backgrounds caused dramatic reduction in growth (Fig. 3A and B). The initial doubling time after CRISPRi-induction is more affected in GS1167 (Δ *cozEa*, sgRNA(*cozEb*), $t_d^{\text{induced}} = 52$ min and $t_d^{\text{non-induced}} = 34$ min) than in GS1163 (Δ *cozEb*, sgRNA(*cozEa*), $t_d^{\text{induced}} = 38$ min and $t_d^{\text{non-induced}} = 35$ min). However, after approximately 300 min of dCas9-induction, the growth is dramatically reduced for both GS1167 and GS1163 (Fig. 3). From this we conclude that *cozEa* and *cozEb* have overlapping functions in *S. aureus*.

The phenotypes of the GS1167 (Δ *cozEa::spc*, depleted *cozEb*) and GS1163 (Δ *cozEb::spc*, depleted *cozEa*)

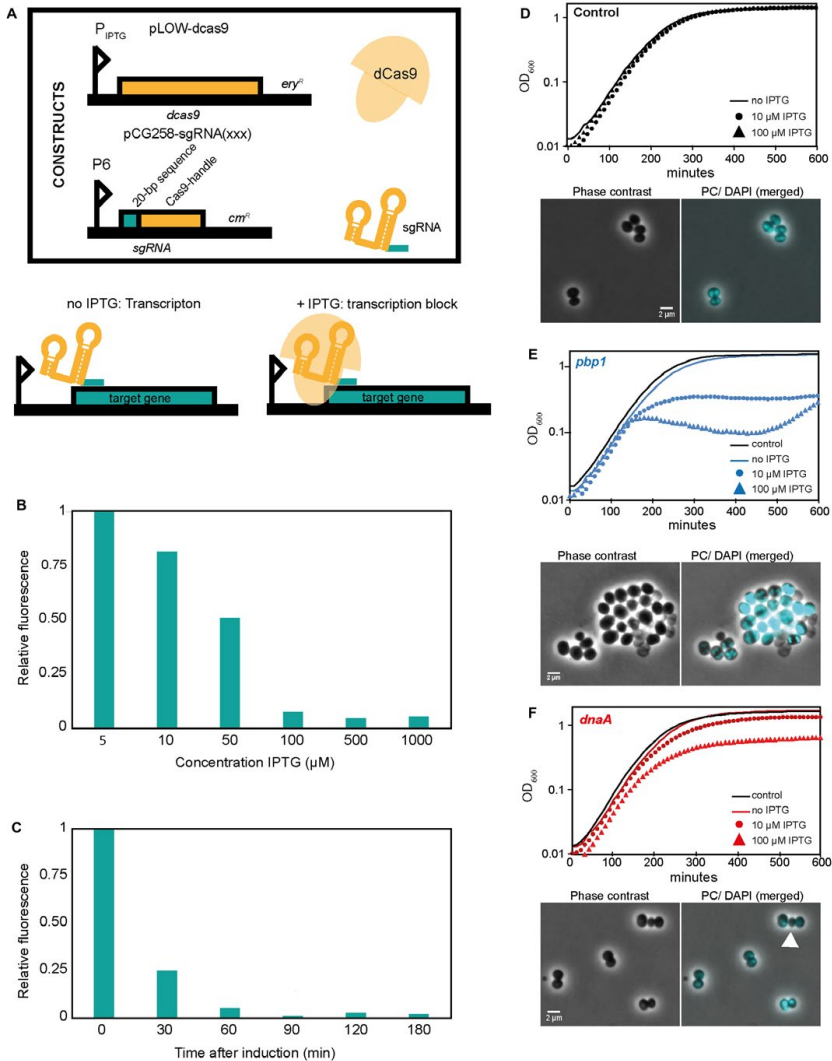


Fig. 2. Two-plasmid CRISPR interference system for *S. aureus*.

A. Schematic representation of the plasmids carrying dCas9 and sgRNA. The sgRNA is constitutively expressed, while the level of dCas9 is controlled by the inducible P_{lac} promoter. Upon addition of IPTG, dCas9 will be expressed and the dCas9-sgRNA-DNA complex formation will lead to transcription block and knockdown of the target gene.

B-C. Knockdown of GFP expression in a strain constitutively expressing *m(sfgfp)* (SAMK56).

B. Fluorescence after induction with various IPTG concentrations. The fluorescence values are given relative to the fluorescence of a non-depleted strain. The experiment was repeated twice with similar results.

C. The temporal dynamics of GFP depletion after addition of 100 μ M IPTG. The fluorescence at the time of IPTG addition was set to 1, and measured at different time points. The experiment was repeated twice with similar results.

D-F. Growth and phenotypic characterization of cells with depletion using CRISPRi. Growth curves in BHI medium at 37°C and micrographs are shown. The cultures were diluted to OD₆₀₀ \approx 0.01 prior to growth analysis. The scale bars are 2 μ m.

D. Control cells carrying non-targeting sgRNA. E. Depletion of *pbp1*. *pbp1* depleted cells were significantly larger than wild-type cells ($1.78 \pm 0.38 \mu$ m, $n = 126$ for the *pbp1* depletion versus $1.41 \pm 0.34 \mu$ m, $n = 250$ for the control, $P < 0.05$, Kolmogorov-Smirnov test).

F. Depletion of *dnaA*, resulted in formation of anucleate cells (10.2%, $n = 234$). The arrowhead points to an example of an anucleate cell.

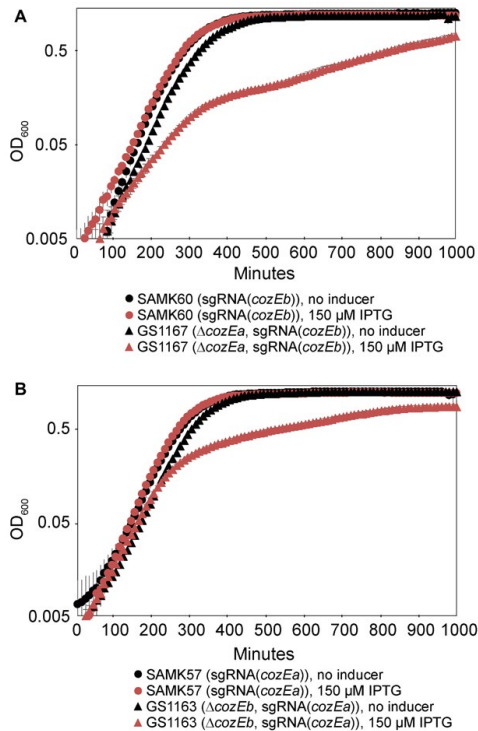


Fig. 3. Functional redundancy of *cozEa* and *cozEb*. A. Strains carrying sgRNA targeting *cozEb* in wild-type background (circles, strain SAMK57) compared to the Δ *cozEa* background (triangles, strain GS1167). Growth curves with (red) or without (black) induction of dCas9 expression with 150 μ M IPTG are shown. B. Strains carrying sgRNA targeting *cozEa* in wild-type background (circles, strain SAMK60) compared to the Δ *cozEb* strain (triangles, strain GS1163). Growth curves with (red) or without (black) induction of dCas9 expression with 150 μ M IPTG are shown.

strains were then further investigated by microscopy. Phase contrast micrographs revealed severely perturbed cell morphologies when the CRISPRi system is induced, displaying both variable cell shapes and sizes as well as increased clustering of cells (Fig. 4A). Measurements of the cell diameter of CRISPRi-induced GS1167 and GS1163 cells show that they have a very wide distribution compared to the wild type (Fig. 4B). We also made a double sgRNA strain allowing knockdown of both *cozEa* and *cozEb* simultaneously with the CRISPRi system (strain SAMK75), and as expected this strain displayed similar phenotype as the GS1167 and GS1163 strains (Fig. S4).

Perturbed morphologies in cells depleted of both *cozEa* and *cozEb* prompted us to further analyze cell division

placement by transmission electron microscopy (TEM) (Fig. 4C and D and S4 Fig.). In GS1167 cells (Δ *cozEa::spc* with depleted *cozEb*) depleted for 4 h, cells could initiate septum formation in only one of the daughter cells prior to cell splitting (Fig. 4D, lower panels) and non-perpendicular septum formation resulting in misshaped cells was also observed (Fig. 4D, top right panel). Spatial and temporal coordination of cell division thus seem compromised in cells lacking *CozEa* and *CozEb*. Empty, lysed cells were also observed (Fig. 4D). Furthermore, the cell wall also appeared to be thicker in the mutant cells, and comparison of septum thickness based on the TEM images shows that the GS1167 on average has thicker septal cross-wall compared to wild-type cells (Fig. S6). In mildly depleted cells (depletion for 1 hour), the phenotype is less severe, however, uncoordinated initiation of septum formation and aberrant septa were also observed here (Fig. S5). Electron micrographs of the individual deletions showed that Δ *cozEa* mutants display both lysed cells (Fig. S5) and have thicker septa than wild-type (Fig. S6). These phenotypes were not observed in Δ *cozEb* cells (Fig. S1 and S6).

Notably, nucleoid staining of the cells depleted of both *cozEa* and *cozEb* using DAPI was also abnormal, displaying non-homogeneous staining patterns. A large fraction of the cells appeared to have high intensity or highly condensed DAPI signals (47.1 % for GS1167, 22.9 % for GS1163, $n > 250$) compared to the wild type, and some cells were also anucleate under these conditions (4.1 % for GS1167 and 2.0 % for GS1163, $n > 250$) (Fig. 4A and zoomed images in Fig. 4E). The chromosome biology of the cells thus also seems to be perturbed when *CozEa* and *CozEb* are lacking.

CozEa and *CozEb* do not affect cell wall composition, but interact with key cell division proteins

TEM images showed that the septal cell wall appeared different between wild-type and the *cozE*-deficient cells; coordination of cell wall synthesis seems to be compromised (Fig. 4) and the septal cell wall is thicker in cells lacking *cozEa* (Fig. S5). In *S. pneumoniae*, *CozE^{Spn}* has been shown to interact with the bi-functional penicillin binding protein PBP1a (Fenton *et al.*, 2016). To get insight into whether *CozEa* and *CozEb* could influence cell wall synthesis, we first investigated whether these proteins could interact with any of the four PBPs of *S. aureus* (PBP1, PBP2, PBP3 and PBP4) using bacterial two-hybrid assays (see Material and Methods for detailed description) (Karimova *et al.*, 2005). While *CozEa* and *CozEb* both self-interacted and interacted with each other, no interaction was found with any of the PBPs of *S. aureus* (Fig. 5A, Fig. S7). We also tested the methicillin-resistant

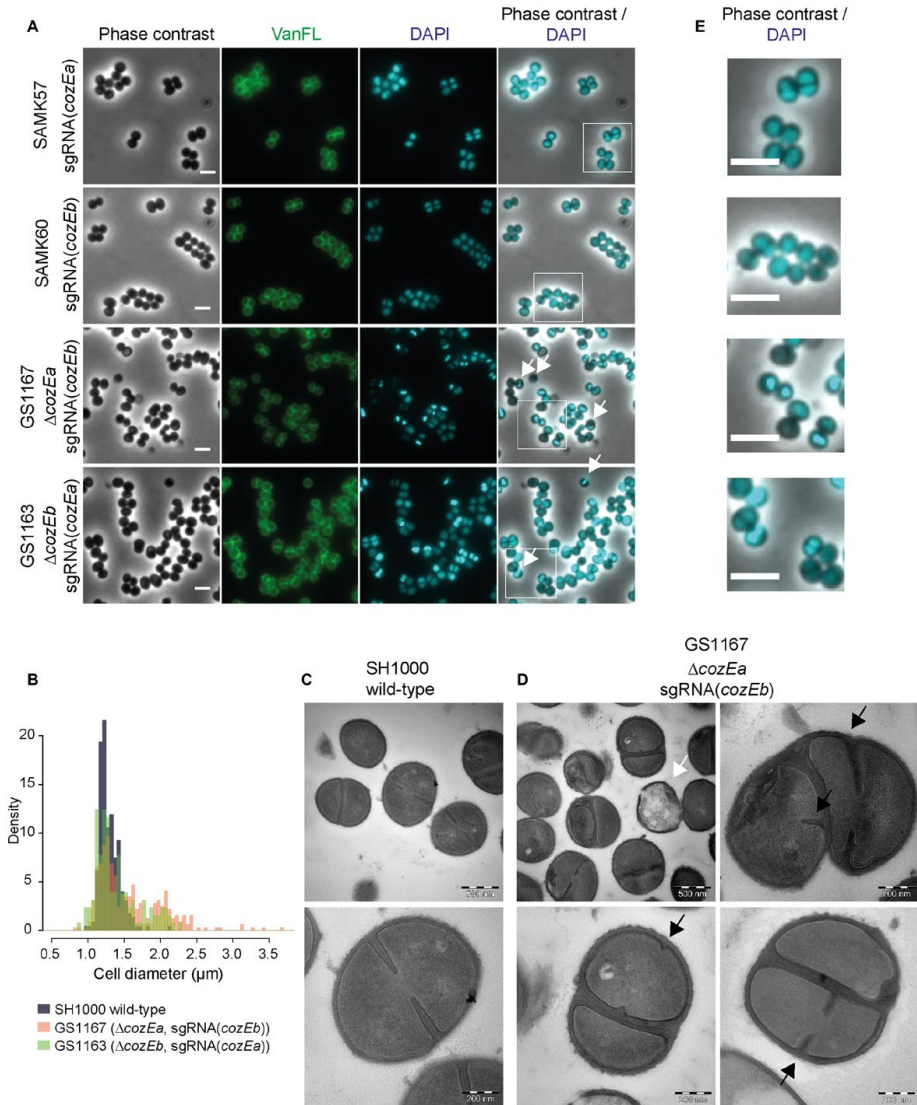


Fig. 4. *CozEa/CozEb* phenotypes in *S. aureus* SH1000.

A. Phase contrast micrographs are shown to the left. The cells were also stained with fluorescent vancomycin and DAPI to visualize cell wall and the nucleoid respectively. Overlay of DAPI and phase contrast images are shown. White arrows point to cells with aberrant nucleoids. The scale bars are 2 μ m. The white squares indicate the area magnified in Fig. 4E.

B. Histogram of cell diameter distribution for wild-type cells (grey) and Δ *cozEa::spc* with depleted *cozEb* (GS1167, orange) cells and Δ *cozEb::spc* with depleted *cozEa* (GS1163, green) induced with 150 μ M IPTG. Both GS1167 and GS1163 are different from wild-type ($P < 0.05$, Kolmogorov-Smirnov test), with high proportion of the cells with diameters larger than 1.5 μ m (7.9% for wild-type compared to 44.2% for GS1167 and 27.9% for GS1163, $n > 150$ for all strains).

C–D. Transmission electron micrographs of wild-type cells (**C**, SH1000) and Δ *cozEa::spc* with depleted *cozEb* (**D**, GS1167) cells. The white arrow points to a lysed cell. Black arrows point to septum initiation in GS1167 cells. Two different magnifications are shown, as indicated by the scale bars.

E. Magnified insets from Fig. 4A with overlays of DAPI and phase contrast images, demonstrating the variation in nucleoid staining between the strains.

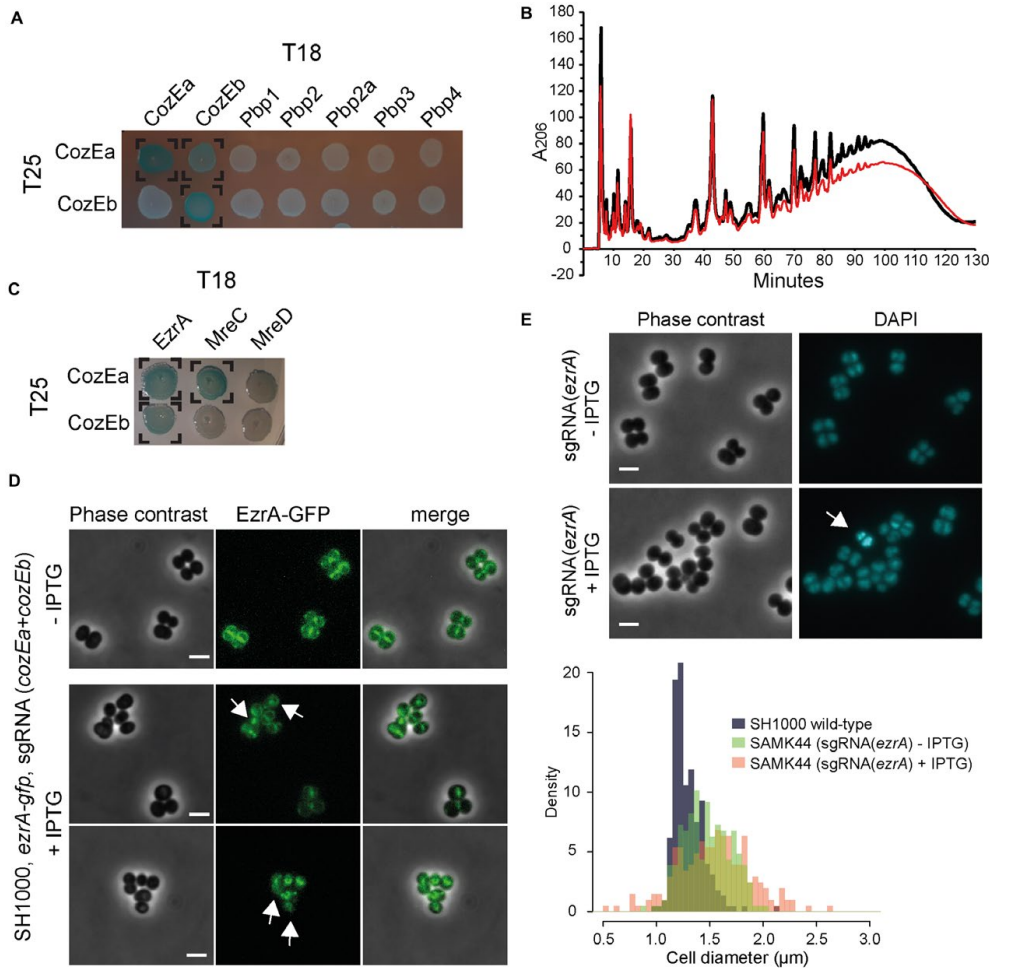


Fig. 5. CozEa and CozEb interact with EzrA, but do not alter cell wall synthesis.

A. Bacterial two-hybrid analyses of interactions between CozEa and CozEb fused to the T25 domain with proteins fused to the T18. Positive interactions are observed as blue colonies and marked with brackets. See Fig. S7 for control experiments. All interaction results were repeated at least five times.

B. Cell wall muropeptide composition of SAMK15 control cells (black) and GS1167 depletion cells (red) induced with 150 mM IPTG for 4 hours as analyzed with UHPLC. See Fig. S7 for control experiments.

C. Bacterial two-hybrid analyses of interactions between CozEa and CozEb fused to the T25 domain with EzrA, MreC and MreD fused to the T18 domain. Positive interactions are observed as blue colonies and marked with brackets. See Fig. S7 for control experiments. All interaction results were repeated at least five times.

D. Localization of EzrA-GFP without and with induction of CozEa/CozEb-depletion. The upper panel shows uninduced cells and two lower panels show representative cells after induction of CRISPRi with 400 μM IPTG. The arrows point to examples of cells where EzrA-GFP localization seems to be perturbed. The scale bars are 2 μm.

E. Phenotype of *ezrA* knockdown. Phase contrast micrographs and DAPI signal are shown for SAMK44 (CRISPRi targeting *ezrA*) with or without induction with 300 μM IPTG. The arrows point to cells with aberrant nucleoid staining. The scale bars are 2 μm. The lower panel shows cell diameter histograms of wild-type SH1000 cells as well as induced and non-induced SAMK44 cells. Both induced and non-induced cells are significantly larger than wild-type cells (Kolmogorov-Smirnov test, $P < 0.05$), with high proportion of the cells with diameters larger than 1.5 μm (7.9% for wild-type compared to 43.9% for non-induced and 55.1% for induced, $n > 100$ for all strains).

PBP2a (MecA) from *S. aureus* COL, but we could not find any interactions with the CozE proteins (Fig. 5A). Next, we analyzed the mucopeptide composition of peptidoglycan derived from strain the GS1167 (ΔcozEa with depleted *cozEb*), to see whether the cell wall architecture was altered in this mutant. However, the mucopeptide composition of GS1167 was similar to the wild-type (Fig. 5B). This suggests that CozEa and CozEb affect positioning and timing of cell division and cross-wall synthesis, but that the cell wall synthesis pathway is unaltered.

We further analyzed whether CozEa and CozEb could interact with a selection of other key cell cycle proteins using bacterial two-hybrid assays (Fig. 5C, S1 Table, Fig. S7). CozE^{Spn} has been shown to interact with MreC^{Spn}, MreD^{Spn} and DivIVA^{Spn} (Fenton *et al.*, 2016; Straume *et al.*, 2017). We detected an interaction between CozEa and MreC, however, this was not the case for CozEb. No interactions with MreD or DivIVA were observed for any of the combinations (Fig. 5C, S1 Table). The only protein we could identify that interacted with both CozEa and CozEb was the early cell division protein EzrA. Among the other proteins tested, we also found that CozEa and GpsB interacted, however, not CozEb and GpsB. A full overview of all tested bacterial two-hybrid interactions are given in S1 Table.

The positive two-hybrid interactions suggest that CozEa and CozEb may mediate cell division control via interactions with EzrA. CozEa and CozEb both displayed a membrane localization in *S. aureus* SH1000, with no apparent enrichment in the septal region (Fig. S9). Depletion of *cozEa* and *cozEb* expression in cells expressing a chromosomal *ezrA-gfp* fusion (Lund *et al.*, 2018), indicates that EzrA-GFP localization may be perturbed in the absence of CozE proteins (Fig. 5D). Furthermore, knock-down of *ezrA* using the CRISPRi system leads to similar phenotypes as cells lacking CozEa and CozEb (Fig. 5E) with variable cell sizes and nucleoid staining. This is fully in line with previous results of *ezrA* deletions and knock-down mutants in *S. aureus* (Jorge *et al.*, 2011; Steele *et al.*, 2011). Note that the cell size effect is observed also, but to a lesser extent, when no IPTG is added, reflecting leaky expression from the P_{lac} promoter. Abnormal DAPI staining pattern was also observed in the cells after IPTG induction, although this phenotype appear to be less pronounced in the *ezrA* knockdown cells (5.5 % of cells, n = 200) compared to cells depleted of CozEa and CozEb. It should also be noted that the growth rate was not severely affected upon induction of *ezrA* knockdown (Fig. S6), suggesting that *ezrA* is not essential for normal growth under these conditions (Bottomley *et al.*, 2014).

The division ring is mislocalized in S. pneumoniae cells depleted of CozE^{Spn}

The results above demonstrate that CozEa and CozEb play functionally overlapping roles in controlling cell division in *S. aureus*, and both genes can be deleted individually. As mentioned above, a single protein CozE^{Spn} (SPD_0768 in strain D39 and Spr0777 in strain R6), is shown to be essential for growth and proper cell morphology in *S. pneumoniae* (Fenton *et al.*, 2016; Straume *et al.*, 2017). To investigate whether the EzrA-interactions detected here were specific for *S. aureus* or also relevant in *S. pneumoniae*, we used bacterial two-hybrid assays to test the interaction between CozE^{Spn} and EzrA^{Spn}. Just like the staphylococcal proteins, a strong interaction was found between the corresponding pneumococcal proteins (Fig. 6A). Strikingly, while EzrA localized to midcell in wild-type *S. pneumoniae* (Fig. 6B and C), the protein is clearly mislocalized in cells where *cozE^{Spn}* was depleted (Fig. 6D).

S. aureus cozEa and cozEb can complement the $\Delta\text{cozE}^{\text{Spn}}$ phenotype of S. pneumoniae

In order to gain further insight into functional conservation of CozE proteins between *S. aureus* and *S. pneumoniae*, we tested whether CozEa or CozEb could functionally complement the essential CozE^{Spn} in *S. pneumoniae*. We created pneumococcal strains in which *cozEa* and *cozEb* were chromosomally integrated downstream of the ComRS-inducible promoter, P_{comX}. Induction of P_{comX} is achieved by addition of the peptide ComS to the growth medium; ComS is internalized where it activates the P_{comX}-binding transcriptional activator ComR (Berg *et al.*, 2011). Next, we attempted to delete the native *cozE^{Spn}* by allelic exchange with the Janus cassette (Sung *et al.*, 2001), with and without presence of the inducer ComS. A functional complementation with CozEa or CozEb in the pneumococcus would allow deletion of the *cozE^{Spn}* gene. Indeed, upon induction of *cozEa* or *cozEb* expression with 2 μM ComS, the native *cozE^{Spn}* could readily be deleted (Table 1). It should be noted that the CozEa and CozEb probably have a reduced functionality compared to CozE^{Spn}, as higher inducer concentrations were required to obtain correct transformants for the non-native CozE-proteins (Table 1). Additionally, CozEa seemed to function better than CozEb, since the number of transformants were higher for the former. Microscopy of the resulting strains further confirmed that the typical *cozE^{Spn}*-depletion phenotype in pneumococci, characterized by extensive chaining and slight rounding of cells (seen by reduced length and aspect ratio closer to 1) (Straume *et al.*, 2017), could be complemented by both CozEa or CozEb (Fig. S10).

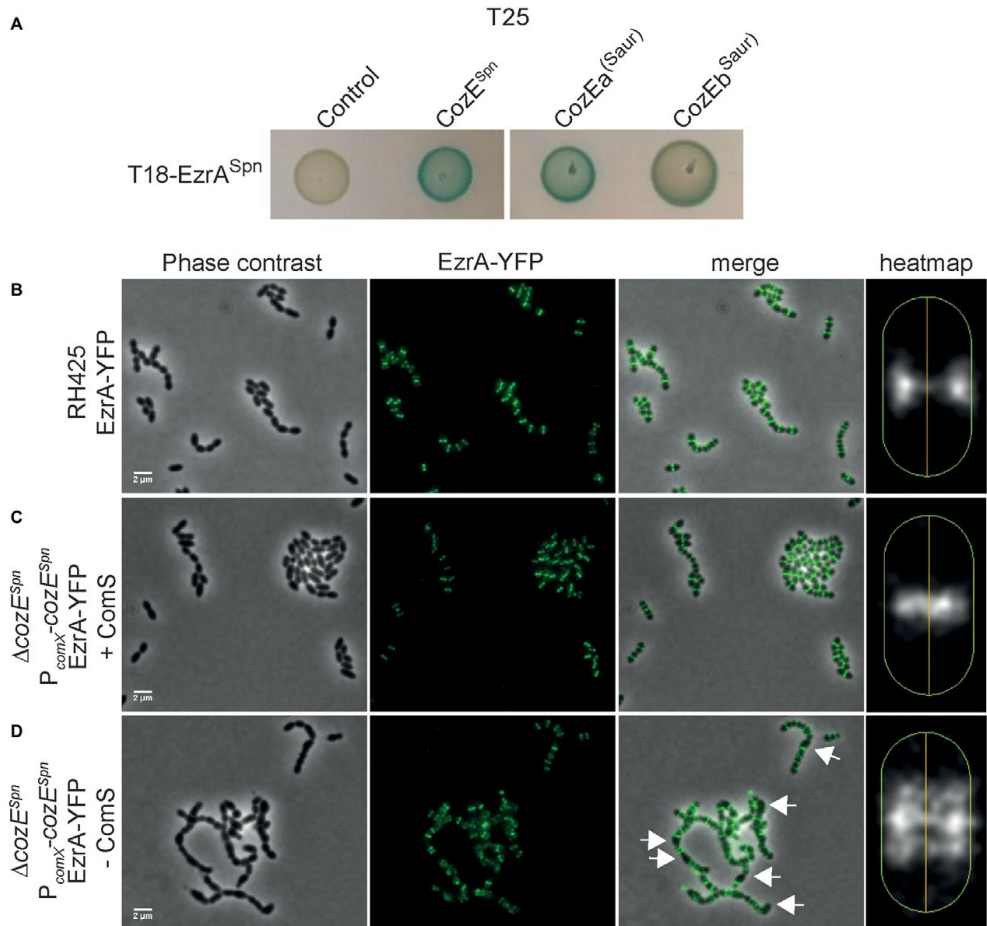


Fig. 6. CozE^{Spn} controls division ring formation in *S. pneumoniae*.

A. Bacterial two-hybrid assay showing interactions between EzrA^{Spn} and different CozE-proteins.

B–D. Localization of EzrA-YFP in *S. pneumoniae*. Phase contrast and fluorescence are shown individually and merged. The localization of EzrA-YFP in the cells are also shown as heatmaps, as generated using MicrobeJ. The heatmaps represent the localizations in >650 cells for each strain. EzrA-YFP localization was analyzed in RH425 wild-type (B) and a strain where the native *cozE*^{Spn} is deleted and instead expressed from the ComS-inducible promoter P_{comX} (Berg *et al.*, 2011). The *cozE*^{Spn}-depletion strain (Δ*cozE*^{Spn} and P_{comX}-*cozE*^{Spn}) was grown with (C) or without (D) inducer peptide ComS. The arrows point to examples of cells with mislocalized EzrA-YFP. The scale bars are 2 μm.

Finally, to get insights into how the staphylococcal proteins CozEa and CozEb could complement CozE^{Spn}, we analyzed by bacterial two-hybrid assays whether CozEa and CozEb could still interact with EzrA^{Spn} (Fig. 6A). Both CozEa and CozEb interact with EzrA^{Spn} in this assay. Thus, conservation of the interaction with EzrA could thus explain why CozEa and CozEb were functional in *S. pneumoniae*.

Discussion

The membrane protein CozE^{Spn} was recently identified as an essential regulator of cell elongation in oval shaped *S. pneumoniae* (Fenton *et al.*, 2016; Straume *et al.*, 2017). CozE proteins are widely conserved and present in the genome of bacteria from different phyla and of different morphologies (Fenton *et al.*, 2016). We here

Table 1. Complementation of $\Delta\text{cozE}^{\text{Spn}}$ in *S. pneumoniae* with CozEa and CozEb.

Complementation	Colonies/ml/ng ^a		
	0 μM ComS	0.2 μM ComS	2 μM ComS
$P_{\text{comX}}\text{-CozE}^{\text{Spn}}$	595 (0/8) ^b	>2000 (8/8)	>2000 (8/8)
$P_{\text{comX}}\text{-CozEa}$	65 (0/8)	580 (3/8)	>2000 (8/8)
$P_{\text{comX}}\text{-CozEb}$	71 (0/8)	77 (0/8)	45 (6/8)

^anumber of colonies on the plate after 16 h (per 1 ml transformation mix per ng DNA) when the respective strains were transformed with the DNA fragment $\Delta\text{cozE}^{\text{Spn}}::P\text{-rpsL-kan}$ (Janus cassette). Transformants were selected with kanamycin. Eight colonies for each transformation were checked by PCR, and the number of true $\Delta\text{cozE}^{\text{Spn}}$ verified by PCR per 8 colonies are indicated in brackets.

^bWhen transforming with the $\Delta\text{cozE}^{\text{Spn}}::P\text{-rpsL-kan}$ cassette, small sized colonies are observed also without complementation. However, these are not true $\Delta\text{cozE}^{\text{Spn}}$ deletions when checked by PCR. In these colonies, cozE^{Spn} has moved to another chromosomal location (data not shown) and the strain has probably acquired suppressor mutations as previously observed.

show that the two CozE-homologs of *S. aureus*, which we named CozEa and CozEb, play overlapping roles to control proper cell cycle progression in these spherical cells.

While the deletion of either *cozEa* or *cozEb* has only minor effects, both genes cannot be deleted at the same time. To confirm the synthetic relationship between *cozEa* and *cozEb*, we developed a CRISPRi system for *S. aureus* to allow knockdown of expression of essential genes. Recent reports have already shown the suitability of using CRISPR/dCas9 for knockdown of genes in *S. aureus* (Dong *et al.*, 2017; Zhao *et al.*, 2017). The plasmid-based CRISPR/dCas9-derived system we developed here contains several unique features compared to the published ones (Dong *et al.*, 2017; Zhao *et al.*, 2017): (i) Knockdown is inducible by addition of IPTG, since dCas9 expression is driven by the IPTG-inducible promoter. (ii) The plasmid harbouring the sgRNA construct is relatively small (5.8 kb), thus allowing easy replacement of target sequences by inverse PCR. (iii) Multi-sgRNA plasmids, allowing simultaneous knockdown of several genes, can be constructed by combining existing sgRNA plasmids using BglBrick assembly (Anderson *et al.*, 2010) (Fig. S2).

Using the CRISPRi system, we could construct combined deletion/depletion strains or double-depletion strains to study cells depleted of CozE proteins. Since all the different strains depleted of CozE proteins showed the same phenotypes, we could exclude that the conservative substitution in the gene *thil* (detected by whole genome resequencing, see results) played any functional role. Low levels of CozEa and CozEb proteins have pleiotropic effects on the staphylococcal cells, including abnormal cell size homeostasis and nucleoid staining, frequent lysis and, most strikingly, the thickened cell wall and compromised timing and positioning of cell division (Fig. 4). Wild-type *S. aureus* cells divide in consecutive, perpendicular planes, i.e. the new septum is formed perpendicular to the previous and splitting of daughter cells (Monteiro *et al.*,

2018) (popping) finishes before the next septum is formed (Pinho *et al.*, 2013; Monteiro *et al.*, 2015; Zhou *et al.*, 2015). However, cells lacking CozEa and CozEb can initiate septum formation asynchronously in only one of the daughter cells before the previous division cycle finishes and non-perpendicular septa were also observed, resulting in elongated cells. This is reminiscent of elongating staphylococcal FtsZ mutant strains (Fig. 4) (Pereira *et al.*, 2016) or staphylococci treated with antibiotics targeting the cell wall or cell division (Pinho *et al.*, 2000, Sieradzki and Tomasz, 2006; Lund *et al.*, 2018).

Despite having misplaced and thicker septa than wild-type, the cell wall composition does not appear to be altered in the CozEa/CozEb-depleted cells and the membrane proteins CozEa or CozEb are not directly interacting with any of the PBPs of *S. aureus*. An interaction between CozEa and MreC was detected, however, neither CozEa nor CozEb could interact with MreD. Although the CozEa-MreC interaction may be important for directing peptidoglycan synthesis, like in *S. pneumoniae*, it is worth noting MreC and MreD are non-essential in *S. aureus* (Tavares *et al.*, 2015). The significance of the CozEa-MreC interaction thus remains unknown.

CozEa and CozEb might compromise cell division coordination and autolytic splitting by interfering directly with key cell division proteins. The detailed mechanism of action remains to be determined, but we show that CozEa and CozEb could interact with one of the early cell division proteins, namely EzrA, in two-hybrid interaction assays. The EzrA-GFP localization in *S. aureus* cells lacking CozEa and CozEb also seems to be perturbed (Fig. 5D). Interaction with EzrA could thus be a plausible way for CozEa and CozEb to mediate cell division control. EzrA is one of the first proteins binding to the Z-ring in the initiation of cell division. EzrA was identified as a negative regulator of FtsZ formation in *B. subtilis* (Levin *et al.*, 1999), and is thought to be important for the switch between elongation and division growth in *B. subtilis* via

protein-protein interactions with penicillin-binding proteins (Claessen *et al.*, 2008). EzrA plays a similar role in *S. pneumoniae* (Rued *et al.*, 2017). In *S. aureus*, EzrA is involved in a large number of protein-protein interactions. Bacterial two-hybrid interactions have been shown between EzrA and FtsZ, DivIB, DivIC, FtsA, FtsL, Pbp1-3, SepF, GpsB, RodA (Steele *et al.*, 2011) and DivIVA (Bottomley *et al.*, 2017). Although some of these interactions may be false positives, it clearly suggests that EzrA is a central protein for proper cell cycle progression and cell wall synthesis in *S. aureus*. It has indeed been shown that EzrA plays a key role in staphylococcal cell size homeostasis; different levels of EzrA in the cells influence the cell size (Jorge *et al.*, 2011; Steele *et al.*, 2011). We also observed the same when *ezrA* was targeted using the CRISPRi system (Fig. 5). Furthermore, lack of EzrA causes mislocalization of other key cell division proteins such as FtsZ, GpsB and PBPs (Jorge *et al.*, 2011; Steele *et al.*, 2011). Thus, disrupting the localization or functionality of EzrA, which may be the case in cells lacking CozEa and CozEb, will therefore likely have large pleiotropic effects on different cell cycle processes, and is consistent with the results of the current study. Note, however, that there are conflicting results in the literature regarding the essentiality of *ezrA* (Jorge *et al.*, 2011; Steele *et al.*, 2011). The results from our CRISPRi depletion suggest that *ezrA* is non-essential for growth under our experimental conditions. Thus, it is likely that CozEa/CozEb have other roles in *S. aureus* yet to be identified. Since the CozEa-EzrA and CozEb-EzrA interactions were found by testing a collection of proteins in a heterologous bacterial two-hybrid assay, there may be important CozEa/CozEb interaction partners that we have not yet identified. It also remains to be determined whether the abnormal nucleoid-staining pattern is directly affected by CozEa/CozEb, or if this is an indirect effect of the compromised cell division control.

Our results also show that the influence of CozE on cell division observed in *S. aureus* was conserved in ovococcal *S. pneumoniae*. Just like in *S. aureus*, CozE^{Spn} could interact with EzrA^{Spn} in bacterial two-hybrid assays and depletion of CozE^{Spn} in *S. pneumoniae* caused aberrant cell division placement as observed by mislocalization of EzrA^{Spn}-GFP. In line with this, EzrA^{Spn} interacts with FtsZ^{Spn}, GpsB^{Spn} and DivIVA^{Spn} and is important for coordination of septal and peripheral cell wall synthesis in ovococcal *S. pneumoniae* cells (Fleurie *et al.*, 2014; Rued *et al.*, 2017). Depletion of *ezrA*^{Spn} expression in *S. pneumoniae* (Fig. 5) also resulted in cells with variable sizes and nucleoid staining pattern as well as multiple or misplaced septa (Liu *et al.*, 2017). Notably, both *cozEa* and *cozEb* could complement the Δ *cozE*^{Spn} in *S. pneumoniae*, although the functionality of the staphylococcal proteins were reduced compared to the native CozE^{Spn}.

CozE^{Spn} was identified as an essential regulator of cell elongation in *S. pneumoniae*, working through interactions with the MreCD^{Spn} and PBP1a^{Spn} (Fenton *et al.*, 2016). *S. aureus* also appears to elongate slightly during the cell cycle, but little is known about this and a machinery for peripheral peptidoglycan synthesis is lacking (Monteiro *et al.*, 2015). The results presented here suggest that CozE proteins in bacteria have additional functionalities to what was found for CozE^{Spn} and that they may act at an earlier stage of cell division to mediate proper spatial and temporal control. During the bacterial cell cycle, DNA replication, chromosome segregation, cell division and cell wall synthesis need to be coordinated spatially and temporally. The uncontrolled cell division occurring in *S. aureus* cells lacking CozEa and CozEb, may thus result in the pleiotropic effects we observed, such as aberrant chromosome replication/segregation, cell lysis and variable cell sizes. Future studies are required to unravel in more detail the molecular mode of action by which CozE proteins work. The CozE-mediated control of cell division seems to be a conserved feature between spherical *S. aureus* and ovococcal *S. pneumoniae*. Since genes encoding these proteins are widespread and found in bacteria with different cellular morphologies (Fenton *et al.*, 2016), it will be interesting to unravel how CozE proteins function in bacterial cells of various shapes.

Experimental procedures

Bacterial strains, growth conditions and transformation

Bacterial strains used in this study are listed in S2 Table. *S. aureus* was routinely grown at 37°C in brain-heart-infusion (BHI) broth with shaking or on BHI agar plates at 37°C. When appropriate, 5 µg/ml erythromycin, 10 µg/ml chloramphenicol or 100 µg/ml spectinomycin was added for selection. For induction of gene expression, different concentrations of IPTG was added. *S. pneumoniae* was grown in C medium (Lacks and Hotchkiss, 1960) at 37°C without shaking or on Todd-Hewitt (TH) agar plates at 37°C. When appropriate, 400 µg/ml kanamycin, 200 µg/ml streptomycin or 100 µg/ml spectinomycin was added to the growth medium for selection. *Escherichia coli* was grown at 37°C in LB medium with shaking or on LA plates at 37°C with 100 µg/ml ampicillin or 50 µg/ml kanamycin added for selection.

Transformation of *E. coli* was performed with a standard heat shock protocol. *S. aureus* was transformed with electroporation using plasmid DNA isolated from *E. coli* DC10B (Monk *et al.*, 2012) or IM08B (Monk *et al.*, 2015). Preparation of electrocompetent cells and electroporation were performed essentially as described before (Lofblom *et al.*, 2007). Constructs were introduced into *S.*

pneumoniae using natural transformation as described before (Stamsås *et al.*, 2017).

Construction of plasmids for the CRISPRi system

Construction of plasmid pLOW-dCas9. The *dcas9* gene was amplified from plasmid pJWV102-dcas9 (Liu *et al.*, 2017) using primers mk41 and mk42. The fragment and the vector pLOW-ftsZ-m(sf)gfp were both digested with Sall and NotI and ligated to produce the pLOW-dCas9 construct where *dcas9* is placed downstream of an IPTG-inducible promoter. The ligation was transformed into *E. coli* IM08B with ampicillin selection and correct construct was verified by PCR and sequencing. All plasmids in this study are listed in S3 Table, while all primers are listed in S4 Table.

Constructions of plasmids expressing single guide RNA. The single guide RNA (sgRNA) construct, containing a transcriptionally isolated sgRNA (see Fig. 2) driven by a constitutive promoter, was cut out from vector pPEPX-sgRNA(*luc*) (Liu *et al.*, 2017) using PstI and BamHI. The fragment was ligated into the corresponding sites of vector pCG248 (Helle *et al.*, 2011) (thus removing the *xylltet* regulatory system from this vector) to produce pCG248-sgRNA(*luc*). The construct was verified by sequencing.

New sgRNAs were then made by replacing the 20 nt base-pairing region with an inverse PCR approach; using the pCG248-sgRNA(*luc*) as template, new sgRNA-plasmids were amplified using one reverse phosphorylated primer mk200 annealing immediately upstream of the sgRNA, combined with a gene-specific forward primer containing the base-pairing region as overhangs. The product was treated with DpnI to remove the template plasmid and ligated using T4 DNA ligase prior to transformation into *E. coli* IM08B with ampicillin selection. Constructs were verified by sequencing. The resulting plasmids were named pCG248-sgRNA(x), where x denotes the name of the gene to be targeted. Selection of the gene-specific base pairing region to be used was done using established criteria (Peters *et al.*, 2016; Liu *et al.*, 2017).

For construction of the double-sgRNAs targeting both *cozEa* and *cozEb*, the fragment containing the sgRNA(*cozEb*) was cut out from the plasmid pCG248-sgRNA(*cozEb*) using restriction sites PstI and BamHI. The resulting fragment was ligated into the PstI and BglII sites of plasmid pCG248-sgRNA(*cozEa*). The resulting plasmid, pCG248-sgRNA(*cozEa-cozEb*), expresses two sgRNAs targeting both *cozEa* and *cozEb*. See also Fig. S2.

CRISPR interference. In order to obtain *S. aureus* strains for CRISPRi, the plasmid pLOW-dCas9 was first introduced with erythromycin selection. Then, in a second step, the sgRNA-containing plasmid pCG248(x),

was introduced with combined chloramphenicol and erythromycin selection (in order to retain both plasmids). Cells were then grown in the presence of IPTG to induce expression of *dcas9*.

S. aureus plasmid and strain construction

Construction of strain with constitutive GFP expression. A fragment containing a spectinomycin resistance gene and a gene encoding a monomeric superfolder GFP, *m(sf)gfp*, was first assembled by overlap extension PCR. The spectinomycin resistance cassette was amplified from pCN55 (Charpentier *et al.*, 2004) using primers mk203 and mk204. The *m(sf)gfp* gene was amplified from plasmid pMK17 (Kjos *et al.*, 2016) using primer im84 and im2. The primers mk204 and im84 contain overlapping sequence, and the *spc-m(sf)gfp* fragment could then be assembled in a second amplification step with outer primers mk203 and im2. The resulting fragment contains EcoRI sites on both ends introduced by overhangs in the primers. The fragment was digested with EcoRI and ligated into the corresponding site of plasmid pMAD-int2-luc. The ligation was transformed in *E. coli* IM08B with ampicillin selection. The resulting construct, pMAD-int2-luc-spc-gfp, was verified by PCR and sequencing. The temperature sensitive pMAD-derivative vector (Arnaud *et al.*, 2004) was transformed in *S. aureus* RN4220 at 30°C with erythromycin and X-gal selection. Integration of the plasmid into the chromosome and excision to construct the integration of P3-luc-spc-gfp in the *int*-locus (Fagerlund *et al.*, 2014) was performed as described (Arnaud *et al.*, 2004) with spectinomycin selection.

Construction of Δ *cozEa::spc* and Δ *cozEb::spc*. Vectors for deletion of *cozEa* and *cozEb* were made in pMAD. The constructions *cozEa::spc* and *cozEb::spc* were first assembled by overlap extension PCR as follows: The spectinomycin resistance cassette (*spc*) was amplified from plasmid pCN55 using primers mk188 and mk189. The *cozEa* upstream region was amplified with primers mk182 and mk184 and the downstream fragment with primers mk185 and mk187. The three fragments were assembled using overlap extension PCR and amplified using the outer primers mk183 and mk186. The outer primers contain restriction sites for NcoI and BamHI, and the *cozEa*_{up} – *spc* – *cozEa*_{down} fragment was ligated into the NcoI and BamHI sites of pMAD. The ligation was transformed into *E. coli* IM08B and correct transformants containing the pMAD-*cozEa::spc* plasmid were verified by PCR and sequencing.

pMAD-*cozEb::spc* plasmid was constructed in a similar way. The *spc* fragment was amplified in the same manner as above. The *cozEb* up- and downstream regions were amplified using primers mk190 and mk192, and mk193 and mk195 respectively. The resulting fragments were fused by overlap extension PCR using primers mk191 and mk194, and the resulting fragment (*cozEb*_{up} – *spc*

– *cozEb_down*), was ligated into the NcoI and BamHI sites of pMAD.

Finally, the pMAD-*cozEa::cam* plasmid was constructed by amplifying the upstream region with primers mk183 and mk259 and the downstream region with primers mk260 and mk186. A chloramphenicol resistance cassette was amplified from plasmid pRAB11 (Helle *et al.*, 2011), using primers mk257 and mk258. The fragments were fused by overlap extension PCR and ligated into the NcoI and BamHI sites of pMAD.

Construction of the deletion strains was done as previously described for the temperature sensitive pMAD system (Arnaud *et al.*, 2004). Briefly, the plasmids were transformed into *S. aureus* SH1000 with erythromycin selection with incubation at permissive temperature of 30°C. X-gal was also added to the transformation plates and blue colonies were re-streaked once at 30°C. One colony was then picked and grown in medium without selection at 30°C for 2 h before the tube was transferred to non-permissive temperature for plasmid replication (43°C) for 6 h. The culture was then plated on TSA with spectinomycin and X-gal at 43°C. White colonies, where double crossover had taken place to replace the gene of interest with the spectinomycin cassette, were re-streaked on two separate plates to verify that they were spectinomycin resistant and erythromycin sensitive. Correct constructs were further verified by PCR and sequencing. The Δ *cozEa::spc* deletion strain was named SAMK24 and the Δ *cozEb::spc* deletion strain SAMK21.

Construction of pLOW-*cozEa-m(sf)gfp* and pLOW-*cozEb-m(sf)gfp*. *m(sf)gfp*, was first inserted into the plasmid pLOW-FtsZ-GFP (Liew *et al.*, 2011) (replacing the *gfp* gene). The *m(sf)gfp* gene with linker was amplified from plasmid pMK17 (Kjos *et al.*, 2016) using primers im1 and im2 and ligated into the BamHI and EcoRI sites of plasmid pLOW-FtsZ-GFP. The resulting construct, pLOW-*ftsZ-m(sf)gfp*, was verified by PCR and sequencing. To construct pLOW-*cozEa-m(sf)gfp* and pLOW-*cozEb-m(sf)gfp*, *ftsZ* was replaced with *cozEa* or *cozEb* in this vector. *cozEa* was amplified using primers im10 and im11, while *cozEb* was amplified using primers im12 and im13, both using genomic DNA from SH1000 as template. The fragments were digested with Sall and BamHI and ligated into the respective sites of vector pLOW-*ftsZ-m(sf)gfp*. The constructs were verified by PCR and sequencing.

Strain construction for *S. pneumoniae*

Construction of P_{comX} -*cozE*^{Spn}, P_{comX} -*cozEa*, P_{comX} -*cozEb* and deletion of *cozE*^{Spn}. The ectopic P_{comX} -*cozE*^{Spn} construct integrated in the *cpsO-cpnN* locus of *S. pneumoniae* has been described previously (Straume *et al.*, 2017).

For construction of P_{comX} -*cozEa* and P_{comX} -*cozEb*, primers gs693/gs694 were used to amplify the *cozEa* gene and primers GS691/GS692 were used to amplify the *cozEb* gene, both using genomic DNA from *S. aureus* SH1000 as template. Using strain *S. pneumoniae* SPH131 as template, the P_{comX} and 800 bp upstream region in the *cpsO-cpnN* locus were amplified with primers khb31/khb33 and the *cpsO-cpnN* downstream fragment was amplified with primers khb34/khb36. The three fragments contain overlapping sequences introduced in the primers, and they were assembled by overlap extension PCR to create P_{comX} -*cozEa* and P_{comX} -*cozEb*. The constructs were transformed into strain SPH131 (containing a Janus cassette in the *cpsO-cpnN* locus) and transformants were selected on plates with streptomycin. The resulting strains were named GS1169 and GS1170.

The native pneumococcal *cozE*^{Spn} (*spr0777*) gene was replaced with a Janus cassette in strains GS1169, GS1170 and KHB432 as described before (Straume *et al.*, 2017). Since *spr0777* is essential, different concentrations of the transcription inducer ComS (0, 0.2 and 2 μ M) were added during all transformation steps to induce expression of the various *cozE* genes from the P_{comX} promoter. Transformants were selected on plates containing kanamycin. The number of colonies were counted and the transformants were screened for the presence of the pneumococcal *cozE*^{Spn} gene with primers gs337 and gs338 for each ComS concentration.

Construction of *ezrA*^{Spn}-*yfp*. An *ezrA-yfp_spc* fragment was assembled by overlap extension PCR. The *ezrA_up* fragment was amplified from *S. pneumoniae* R6 using primers mk288 and mk289, while the *ezrA_down* fragment was amplified using primers mk292 and mk293. The *yfp_spc* fragment was amplified from strain MK123 using primers mk290 and mk291. Due to overhangs in the primers, the three fragments could be assembled using outer primers mk301 and mk302, to produce the *ezrA-yfp_spc* fragment, which integrates in the pneumococcal chromosome to replace the native *ezrA* gene with an *ezrA-yfp* fusion gene. The fragment was transformed into *S. pneumoniae* and transformants were selected on plates with spectinomycin. Correct transformants were verified by PCR.

Total RNA isolation, cDNA synthesis and qPCR

Overnight cultures were diluted to OD₆₀₀ = 0.05 in 20 ml BHI containing 10 μ g/ml chloramphenicol and 5 μ g/ml erythromycin. There were two cultures of each strain, one of them was induced with 150 μ M IPTG. Cells were harvested from 10 ml culture at OD₆₀₀ = 0.4 by centrifugation at 4000 \times g at 4°C for one minute, and the pellets were immediately frozen in liquid nitrogen. The cells were lysed by mechanical disruption in Lysing Matrix B, 2 mL tubes (MP Biomedicals) by FastPrep@-24

(MP Biomedicals). The disruption was done at maximum speed for 3×20 seconds, with cooling on ice between the runs. Total RNA was extracted using RNeasy Mini kit following the manufacturers' description (Qiagen). Eluted RNA was treated with DNase I for removal of residual DNA, following the description of the manufacturer (Invitrogen). Thereafter, DNase was removed by Phenol-chloroform extraction. cDNA was synthesized using SuperscriptTM III Reverse Transcriptase (Invitrogen). Twenty-five ng cDNA was used as template for qPCR performed with PowerUpTM SYBRTM Green Master Mix (Applied Biosystems) in a StepOne Plus machine (Applied Biosystems). The setup included triplicates for each of the target genes for every sample. Primers im126 and im127 were used to target the reference gene, *pta* (Valihrach and Demnerova, 2012). Primers im130 and im131 were used to target *cozEa*, and primers im132 and im133 to target *cozEb*. The differential expression of *cozEa* and *cozEb* between non-induced and induced conditions was calculated according to the Pfaffl-method (Pfaffl, 2001).

Bacterial two-hybrid analysis

Construction of plasmids. Genes of interest were fused in frame to either 5' end or 3' end of either the T18 or the T25 domain of adenylate cyclase from *Bordetella pertussis* using the four vectors (pKT25, pKNT25, pUT18, pUT18C) provided by the manufacturer (Euromedex). Primers used for amplification of the genes are listed in S4 Table. The amplified fragments were digested (restriction sites indicated in the S4 Table) and ligated into the corresponding restriction sites in the vectors. Ligations were transformed into *E. coli* XL1-Blue cells, and selected on 1% glucose LA plates containing either 50 µg/ml kanamycin or 100 µg/ml ampicillin. Correct plasmids were verified by PCR and sequencing.

Bacterial two-hybrid assays (Karimova *et al.*, 2005) were performed as described by the manufacturer (Euromedex). Briefly, two plasmids, one containing a fusion to the T18 domain and the other a fusion to the T25 domain, were co-transformed into *E. coli* BTH101. The transformants were selected on LA plates containing 50 µg/ml kanamycin and 100 µg/ml ampicillin for selection. Five random colonies were picked per assay and grown in liquid LB containing kanamycin and ampicillin to OD₆₀₀ 0.3, before 2.5 µl of the cell culture was spotted on LA plates supplemented with 50 µg/ml kanamycin, 100 µg/ml ampicillin, 40 µg/ml of X-gal and 0.5 mM IPTG. The plates were incubated protected from light at 30°C for 20 to 48 h. Positive interactions are indicated by appearance of blue colonies, while white colonies indicate no interaction. All interaction assays were repeated with at least five independent replicates.

Isolation of peptidoglycan and HPLC-analysis

Strains GS1167 and SAMK15 were inoculated in 60 ml BHI containing 10 µg/ml chloramphenicol and 5 µg/ml erythromycin. At OD₆₀₀ 0.2 these cells were transferred to 1.5 liters of BHI containing 10 µg/ml chloramphenicol, 5 µg/ml erythromycin and 150 µM IPTG. When reaching OD₆₀₀ = 0.3, cells were harvested at 8000 ×g for 10 min. Peptidoglycan was isolated according to the protocol described by Vollmer (Vollmer, 2007). The isolated peptidoglycan was lyophilized and resuspended in water to a final concentration of 50 mg/ml.

HPLC analysis of muropeptides was performed as described by Vollmer (Vollmer, 2007) and Carvalho *et al.* (Carvalho *et al.*, 2015) with minor changes. Briefly, to remove cell wall teichoic acids, ten milligrams of purified peptidoglycan were treated with 1.5 ml 48 % hydrofluoric acid (HF) at 4°C for 48 hours with gentle mixing. The HF-treated peptidoglycan was collected by centrifugation at 20 000 ×g for 30 minutes and washed two times with 1.5 ml of dH₂O, once with 1.5 ml of 50 mM Tris-HCl (pH 7.4) and finally twice with 1.5 ml of dH₂O. One mg of HF-treated peptidoglycan was digested with 5000 U mutanolysin at 37°C for 18–20 h in a final volume of 100 µl containing 12.5 mM NaH₂PO₄ (pH 5.5). The sample was boiled for 20 min before insoluble material was removed by centrifugation at 20 000 ×g for 30 min. The supernatant was added with 0.5 M Na-borate pH 9.0 (1:1 volume) and treated with 1–2 mg of Na-borohydride for 30 min at room temperature to reduce the sugars. The reaction was stopped by adjusting the pH to 2.0 using 20 % phosphoric acid. Muropeptides were separated on a C18 column (Vydac 218TP C18 5 mm, Grace Davison Discovery Sciences) at 52°C using a linear 155-min gradient of methanol from 5–30 % in 0.1 M NaH₂PO₄ (pH 2.0) at a flow rate of 0.5 ml/min. Eluted muropeptides were detected at 206 nm.

Phase contrast and fluorescence microscopy

Microscopy was performed on a Zeiss AxioObserver with ZEN Blue software. Images were captured with an ORCA-Flash4.0 V2 Digital CMOS camera (Hamamatsu Photonics) through a 100x PC objective. For fluorescence microscopy, HPX 120 Illuminator (Zeiss) was used as a light source. Image analysis was performed using MicrobeJ (Ducret *et al.*, 2016) and plotting was done in RStudio.

Transmission electron microscopy

Strains SH1000, SAMK21 and SAMK24 were grown to OD₆₀₀ = 0.4 prior to sample preparation. GS1167 and SAMK15 were pre-grown to OD₆₀₀ = 0.1, after which the cultures were diluted 64-fold in medium with or without

150 µg/ml IPTG and grown until $OD_{600} = 0.3$. Cells were fixed by adding a solution of 4 % paraformaldehyd (w/v) and 5 % glutardialdehyd (w/v) in 1 x PBS pH 7.4 to the cell culture in a 1:1 ratio. The fixation mix was incubated 1 hour in room temperature and kept overnight at 4°C. The next day the cells were washed three times in PBS and three times in cacodylate buffer (CaCo) before being post-fixed for one hour in 1% OsO_4 in 0.1 M CaCo. Cells were washed three times in CaCo buffer, infiltrated in 3% agarose and washed again three times in CaCo buffer. The samples were then dehydrated in a gradient series of 70%, 90%, 96% and 100% ethanol (15 min for each ethanol concentration). Infiltration in LR White resin was then performed in multiple steps; LR White resin:EtOH in a ratio 1:3 was first incubated overnight, then a ratio of 1:1 for 7 h, a ratio of 3:1 overnight and finally 100% LR White resin overnight. Then the samples were embedded in 100% LR White resin at 60°C for 72 h. Thin sections were made and stained with uranyl acetate and potassium permanganate. The samples were analyzed in a FEI MORGAGNI 268 electron microscope.

Growth assays

Growth assays were performed in a Synergy H1 Hybrid Reader (BioTek) microtiter plate reader at 37°C. Five ml of cell culture were grown to exponential phase, $OD_{600} = 0.4$ before being harvested, resuspended in fresh BHI medium and diluted to $OD_{600} = 0.05$. Appropriate antibiotics were always present. Each well in the microtiter plate was added 280 µl diluted cell culture. IPTG (150 µM) was added to the wells when appropriate. Measurements of OD_{600} were taken every 10th min throughout growth.

Genome resequencing and analysis

Genomic DNA was isolated from *S. aureus* SH1000, SAMK21 and SAMK24 using the NucleoBond AXG 100 kit (Macherey-Nagel). For *S. aureus* SH1000, library for sequencing was created using the Nextera XT DNA library preparation kit (Illumina), and the sequencing was performed using an in-house Illumina MiSeq. For SAM21 and SAMK24, PCR-free library preparation and sequencing (HiSeq4000 PE151) was performed by BGI Hong Kong. Sequences assembly to the *S. aureus* NCTC8325 reference genome and SNP detection were done using Geneious version 10.1 (Kearse *et al.*, 2012).

Acknowledgements

We would like to thank Lene C. Hermansen at the Imaging Center, NMBU, for help with transmission electron microscopy, Davide Porcellato, NMBU, for help with genome sequencing and Simon J. Foster and Katarzyna

Wacnik, University of Sheffield, for providing the strain SH4639 (SH1000, *ezrA-gfp*). The work was funded by the Research Council of Norway (www.forskningradet.no, grant number 250976 awarded to M.K.).

Conflict of interest

The authors declare no conflicts of interest.

Author contributions

I.M., J.W.V., L.S.H. and M.K. conceived the study. G.A.S., I.M. D.S., Z.S. and M.K. performed experiments. G.A.S., I.M. and M.K. wrote the manuscript. D.S., J.W.V., L.S.H. edited the manuscript.

References

- Anderson, J.C., Dueber, J.E., Leguia, M., Wu, G.C., Goler, J.A., Arkin, A.P., and Keasling, J.D. (2010) BglBricks: A flexible standard for biological part assembly. *J Biol Eng* **4**: 1.
- Arnaud, M., Chastanet, A., and Debarbouille, M. (2004) New vector for efficient allelic replacement in naturally non-transformable, low-GC-content, gram-positive bacteria. *Appl Environ Microbiol* **70**: 6887–6891.
- Beilharz, K., Novakova, L., Fadda, D., Branny, P., Massidda, O., and Veening, J.W. (2012) Control of cell division in *Streptococcus pneumoniae* by the conserved Ser/Thr protein kinase StkP. *Proc Natl Acad Sci U S A* **109**: E905–913.
- Berg, K.H., Björnstad, T.J., Straume, D., and Håvarstein, L.S. (2011) Peptide-regulated gene depletion system developed for use in *Streptococcus pneumoniae*. *J Bacteriol* **193**: 5207–5215.
- Bikard, D., Jiang, W., Samai, P., Hochschild, A., Zhang, F., and Marraffini, L.A. (2013) Programmable repression and activation of bacterial gene expression using an engineered CRISPR-Cas system. *Nucleic Acids Res* **41**: 7429–7437.
- Bottomley, A.L., Kabli, A.F., Hurd, A.F., Turner, R.D., Garcia-Lara, J., and Foster, S.J. (2014) *Staphylococcus aureus* DivIB is a peptidoglycan-binding protein that is required for a morphological checkpoint in cell division. *Mol Microbiol* **94**: 1041–1064.
- Bottomley, A.L., Liew, A.T.F., Kusuma, K.D., Peterson, E., Seidel, L., Foster, S.J., and Harry, E.J. (2017) Coordination of chromosome segregation and cell division in *Staphylococcus aureus*. *Front Microbiol* **8**: 1575.
- Carvalho, F., Atilano, M. L., Pombinho, R., Covas, G., Gallo, R. L., Filipe, S. R., *et al.* (2015) L-rhamnosylation of *Listeria monocytogenes* wall teichoic acids promotes resistance to antimicrobial peptides by delaying interaction with the membrane. *PLoS Pathog* **11**: e1004919.
- Charpentier, E., Anton, A.I., Barry, P., Alfonso, B., Fang, Y., and Novick, R.P. (2004) Novel cassette-based shuttle vector system for gram-positive bacteria. *Appl Environ Microbiol* **70**: 6076–6085.
- Claessen, D., Emmins, R., Hamoen, L.W., Daniel, R.A., Errington, J., and Edwards, D.H. (2008) Control of the cell elongation-division cycle by shuttling of PBP1 protein in *Bacillus subtilis*. *Mol Microbiol* **68**: 1029–1046.

- Dong, X., Jin, Y., Ming, D., Li, B., Dong, H., Wang, L., *et al.* (2017) CRISPR/dCas9-mediated inhibition of gene expression in *Staphylococcus aureus*. *J Microbiol Methods* **139**: 79–86.
- Ducret, A., and Grangeasse, C. (2017) Bacterial physiology: Wrapping the cell in a CozE shell. *Nat Microbiol* **2**: 16262.
- Ducret, A., Quardokus, E.M., and Brun, Y.V. (2016) MicrobeJ, a tool for high throughput bacterial cell detection and quantitative analysis. *Nat Microbiol* **1**: 16077.
- Fagerlund, A., Granum, P.E., and Håvarstein, L.S. (2014) *Staphylococcus aureus* competence genes: mapping of the SigH, ComK1 and ComK2 regulons by transcriptome sequencing. *Mol Microbiol* **94**: 557–579.
- Fenton, A.K., Mortaji, L.E., Lau, D.T., Rudner, D.Z., and Bernhardt, T.G. (2016) CozE is a member of the MreCD complex that directs cell elongation in *Streptococcus pneumoniae*. *Nat Microbiol* **2**: 16237.
- Fleurie, A., Lesterlin, C., Manuse, S., Zhao, C., Cluzel, C., Lavergne, J. P., *et al.* (2014) MapZ marks the division sites and positions FtsZ rings in *Streptococcus pneumoniae*. *Nature* **516**: 259–262.
- Fleurie, A., Manuse, S., Zhao, C., Campo, N., Cluzel, C., Lavergne, J. P., *et al.* (2014) Interplay of the serine/threonine-kinase StkP and the paralogs DivIVA and GpsB in pneumococcal cell elongation and division. *PLoS Genet* **10**: e1004275.
- Foster, T.J., Geoghegan, J.A., Ganesh, V.K., and Hook, M. (2014) Adhesion, invasion and evasion: the many functions of the surface proteins of *Staphylococcus aureus*. *Nat Rev Microbiol* **12**: 49–62.
- Grice, E.A., and Segre, J.A. (2011) The skin microbiome. *Nat Rev Microbiol* **9**: 244–253.
- Helle, L., Kull, M., Mayer, S., Marincola, G., Zelder, M. E., Goerke, C., *et al.* (2011) Vectors for improved Tet repressor-dependent gradual gene induction or silencing in *Staphylococcus aureus*. *Microbiology* **157**: 3314–3323.
- Holeckova, N., Doubravova, L., Massidda, O., Molle, V., Buriankova, K., Benada, O., *et al.* (2014) LocZ is a new cell division protein involved in proper septum placement in *Streptococcus pneumoniae*. *MBio* **6**: e01700.
- Jorge, A.M., Hoiczky, E., Gomes, J.P., and Pinho, M.G. (2011) EzrA contributes to the regulation of cell size in *Staphylococcus aureus*. *PLoS One* **6**: e27542.
- Karimova, G., Dautin, N., and Ladant, D. (2005) Interaction network among *Escherichia coli* membrane proteins involved in cell division as revealed by bacterial two-hybrid analysis. *J Bacteriol* **187**: 2233–2243.
- Kearse, M., Moir, R., Wilson, A., Stones-Havas, S., Cheung, M., Sturrock, S., *et al.* (2012) Geneious Basic: an integrated and extendable desktop software platform for the organization and analysis of sequence data. *Bioinformatics* **28**: 1647–1649.
- Kjos, M., Miller, E., Slager, J., Lake, F. B., Gericke, O., Roberts, I. S., *et al.* (2016) Expression of *Streptococcus pneumoniae* bacteriocins is induced by antibiotics via regulatory interplay with the competence system. *PLoS Pathog* **12**: e1005422.
- Lacks, S., and Hotchkiss, R.D. (1960) A study of the genetic material determining an enzyme in *Pneumococcus*. *Biochim Biophys Acta* **39**: 508–518.
- Levin, P.A., Kurtser, I.G., and Grossman, A.D. (1999) Identification and characterization of a negative regulator of FtsZ ring formation in *Bacillus subtilis*. *Proc Natl Acad Sci U S A* **96**: 9642–9647.
- Liew, A.T., Theis, T., Jensen, S.O., Garcia-Lara, J., Foster, S. J., Firth, N., *et al.* (2011) A simple plasmid-based system that allows rapid generation of tightly controlled gene expression in *Staphylococcus aureus*. *Microbiology* **157**: 666–676.
- Liu, X., Gallay, C., Kjos, M., Domenech, A., Slager, J., van Kessel, S. P., *et al.* (2017) High-throughput CRISPRi phenotyping identifies new essential genes in *Streptococcus pneumoniae*. *Mol Syst Biol* **13**: 931.
- Lofblom, J., Kronqvist, N., Uhlen, M., Stahl, S., and Wernerus, H. (2007) Optimization of electroporation-mediated transformation: *Staphylococcus carnosus* as model organism. *J Appl Microbiol* **102**: 736–747.
- Lund, V. A., Wacnik, K., Turner, R. D., Cotterell, B. E., Walther, C. G., Fenn, S. J., *et al.* (2018) Molecular coordination of *Staphylococcus aureus* cell division. *Elife* **7**: e32057.
- Monk, I.R., Shah, I.M., Xu, M., Tan, M.W., and Foster, T.J. (2012) Transforming the untransformable: Application of direct transformation to manipulate genetically *Staphylococcus aureus* and *Staphylococcus epidermidis*. *MBio* **3**: e00277.
- Monk, I.R., Tree, J.J., Howden, B.P., Stinear, T.P., and Foster, T.J. (2015) Complete bypass of restriction systems for major *Staphylococcus aureus* lineages. *MBio* **6**: e00308.
- Monteiro, J.M., Fernandes, P.B., Vaz, F., Pereira, A.R., Tavares, A.C., Ferreira, M.T., *et al.* (2015) Cell shape dynamics during the staphylococcal cell cycle. *Nat Commun* **6**: 8055.
- Monteiro, J. M., Pereira, A. R., Reichmann, N. T., Saraiva, B. M., Fernandes, P. B., Veiga, H., *et al.* (2018) Peptidoglycan synthesis drives an FtsZ-treadmilling-independent step of cytokinesis. *Nature* **554**: 528–532.
- Pang, T., Wang, X., Lim, H.C., Bernhardt, T.G., and Rudner, D.Z. (2017) The nucleoid occlusion factor Noc controls DNA replication initiation in *Staphylococcus aureus*. *PLoS Genet* **13**: e1006908.
- Pereira, A.R., Hsin, J., Krol, E., Tavares, A.C., Flores, P., Hoiczky, E., *et al.* (2016) FtsZ-dependent elongation of a coccoid bacterium. *MBio* **7**: e00908.
- Pereira, S.F., Henriques, A.O., Pinho, M.G., de Lencastre, H., and Tomasz, A. (2007) Role of PBP1 in cell division of *Staphylococcus aureus*. *J Bacteriol* **189**: 3525–3531.
- Pereira, S.F., Henriques, A.O., Pinho, M.G., de Lencastre, H., and Tomasz, A. (2009) Evidence for a dual role of PBP1 in the cell division and cell separation of *Staphylococcus aureus*. *Mol Microbiol* **72**: 895–904.
- Peters, J.M., Colavin, A., Shi, H., Czarny, T.L., Larson, M. H., Wong, S., *et al.* (2016) A comprehensive, CRISPR-based functional analysis of essential genes in bacteria. *Cell* **165**: 1493–1506.
- Pfaffl, M.W. (2001) A new mathematical model for relative quantification in real-time RT-PCR. *Nucleic Acids Res* **29**: e45.
- Pinho, M.G., de Lencastre, H., and Tomasz, A. (2000) Cloning, characterization, and inactivation of the

- gene *pbpC*, encoding penicillin-binding protein 3 of *Staphylococcus aureus*. *J Bacteriol* **182**: 1074–1079.
- Pinho, M.G., and Errington, J. (2003) Dispersed mode of *Staphylococcus aureus* cell wall synthesis in the absence of the division machinery. *Mol Microbiol* **50**: 871–881.
- Pinho, M.G., and Errington, J. (2004) A *divIVA* null mutant of *Staphylococcus aureus* undergoes normal cell division. *FEMS Microbiol Lett* **240**: 145–149.
- Pinho, M.G., Kjos, M., and Veening, J.W. (2013) How to get (a)round: Mechanisms controlling growth and division of coccoid bacteria. *Nat Rev Microbiol* **11**: 601–614.
- Qi, L.S., Larson, M.H., Gilbert, L.A., Doudna, J.A., Weissman, J.S., Arkin, A.P., and Lim, W.A. (2013) Repurposing CRISPR as an RNA-guided platform for sequence-specific control of gene expression. *Cell* **152**: 1173–1183.
- Rasigade, J.P., and Vandenesch, F. (2014) *Staphylococcus aureus*: A pathogen with still unresolved issues. *Infect Genet Evol* **21**: 510–514.
- Rued, B.E., Zheng, J.J., Mura, A., Tsui, H.T., Boersma, M.J., Mazny, J.L., et al. (2017) Suppression and synthetic-lethal genetic relationships of Δ *gpsB* mutations indicate that GpsB mediates protein phosphorylation and penicillin-binding protein interactions in *Streptococcus pneumoniae* D39. *Mol Microbiol* **103**: 931–957.
- Sieradzki, K., and Tomasz, A. (2006) Inhibition of the autolytic system by vancomycin causes mimicry of vancomycin-intermediate *Staphylococcus aureus*-type resistance, cell concentration dependence of the MIC, and antibiotic tolerance in vancomycin-susceptible *S. aureus*. *Antimicrob Agents Chemother* **50**: 527–533.
- Stamsås, G.A., Straume, D., Ruud Winther, A., Kjos, M., Frantzen, C.A., and Håvarstein, L.S. (2017) Identification of EloR (Spr1851) as a regulator of cell elongation in *Streptococcus pneumoniae*. *Mol Microbiol* **105**: 954–967.
- Steele, V.R., Bottomley, A.L., Garcia-Lara, J., Kasturiarachchi, J., and Foster, S.J. (2011) Multiple essential roles for EzrA in cell division of *Staphylococcus aureus*. *Mol Microbiol* **80**: 542–555.
- Straume, D., Stamsås, G.A., Berg, K.H., Salehian, Z., and Håvarstein, L.S. (2017) Identification of pneumococcal proteins that are functionally linked to penicillin-binding protein 2b (PBP2b). *Mol Microbiol* **103**: 99–116.
- Sung, C.K., Li, H., Claverys, J.P., and Morrison, D.A. (2001) An *rpsL* cassette, janus, for gene replacement through negative selection in *Streptococcus pneumoniae*. *Appl Environ Microbiol* **67**: 5190–5196.
- Tavares, A.C., Fernandes, P.B., Carballido-Lopez, R., and Pinho, M.G. (2015) MreC and MreD proteins are not required for growth of *Staphylococcus aureus*. *PLoS One* **10**: e0140523.
- Valihrach, L., and Demnerova, K. (2012) Impact of normalization method on experimental outcome using RT-qPCR in *Staphylococcus aureus*. *J Microbiol Methods* **90**: 214–216.
- van Raaphorst, R., Kjos, M., and Veening, J.W. (2017) Chromosome segregation drives division site selection in *Streptococcus pneumoniae*. *Proc Natl Acad Sci U S A* **114**: E5959–E5968.
- Veiga, H., Jorge, A.M., and Pinho, M.G. (2011) Absence of nucleoid occlusion effector Noc impairs formation of orthogonal FtsZ rings during *Staphylococcus aureus* cell division. *Mol Microbiol* **80**: 1366–1380.
- Vollmer, W. (2007) Preparation and analysis of pneumococcal murein (peptidoglycan). In *Molecular Biology of Streptococci*. Hakenbeck, R., and Chhatwal, S. (eds). Norfolk: Horizon Bioscience, pp. 531–536.
- Zhao, C., Shu, X., and Sun, B. (2017) Construction of a gene knockdown system based on catalytically inactive ("dead") Cas9 (dCas9) in *Staphylococcus aureus*. *Appl Environ Microbiol* **83**: e00291–17.
- Zheng, J.J., Perez, A.J., Tsui, H.T., Massidda, O., and Winkler, M.E. (2017) Absence of the KhpA and KhpB (JAG/EloR) RNA-binding proteins suppresses the requirement for PBP2b by overproduction of FtsA in *Streptococcus pneumoniae* D39. *Mol Microbiol*. **106**: 793–814.
- Zhou, X., Halladin, D.K., Rojas, E.R., Koslover, E.F., Lee, T.K., Huang, K.C., and Theriot, J.A. (2015) Bacterial division. Mechanical crack propagation drives millisecond daughter cell separation in *Staphylococcus aureus*. *Science* **348**: 574–578.

Supporting information

Additional supporting information may be found in the online version of this article at the publisher's web site.

Supplementary Information

CozEa and CozEb play overlapping and essential roles in controlling cell division in *Staphylococcus aureus*

Gro Anita Stamsås^{1†}, Ine Storaker Myrbråten^{1†}, Daniel Straume¹, Zhian Salehian¹, Jan-Willem Veening²,
Leiv Sigve Håvarstein¹, Morten Kjos^{1*}

¹ Faculty of Chemistry, Biotechnology and Food Science, Norwegian University of Life Sciences, Ås, Norway.

² Department of Fundamental Microbiology, Faculty of Biology and Medicine, University of Lausanne, Lausanne, Switzerland.

* Correspondence. E-mail morten.kjos@nmbu.no, Tel. +47 67232951, Fax +47 64965901.

† These authors contributed equally to this work.

Content:

Fig. S1 – Fig. S10

and

Table S1 – Table S4

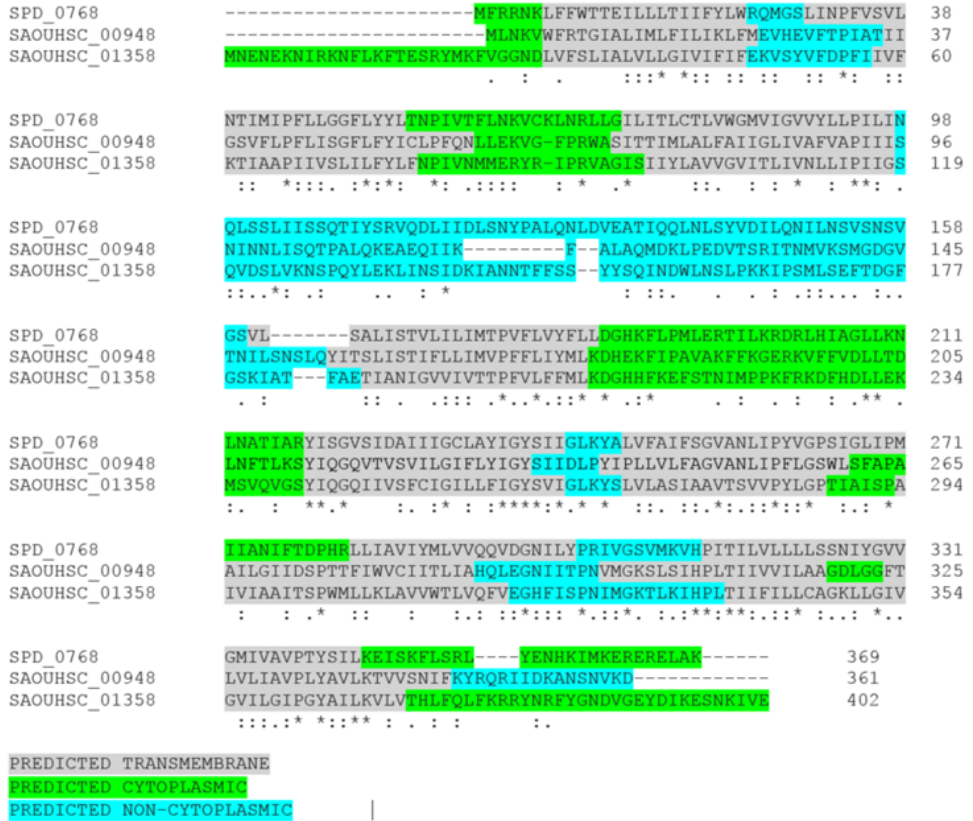


Fig. S1. Sequence alignments of CozE^{Spn} (SPD_0768), CozEa (SAOUHSC_00948) and CozEb (SAOUHSC_01358). The alignment was constructed using Clustal Omega (Sievers *et al.*, 2011). Transmembrane predictions were performed using Phobius and is indicated with colors in the alignment.

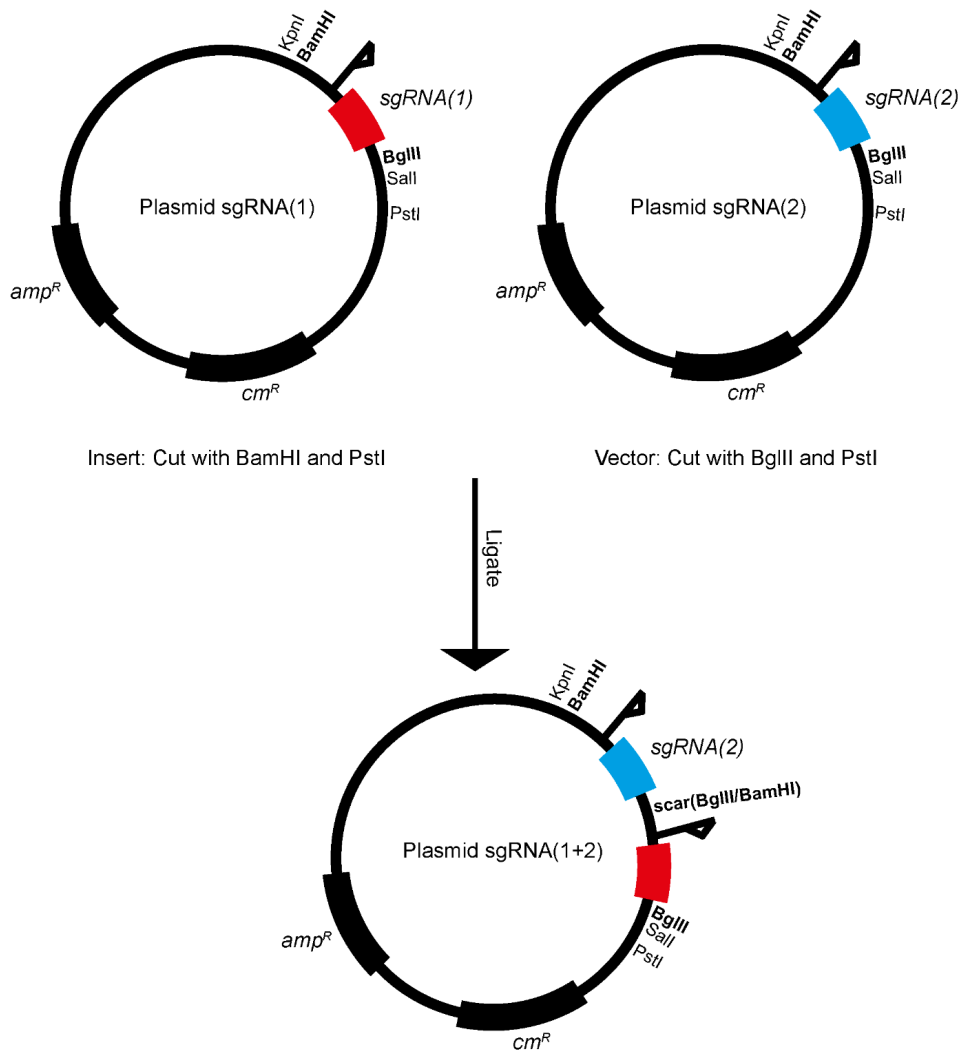


Fig. S2. Schematic view of the construction of multi-sgRNA plasmids by BglBrick cloning. The two sgRNA constructs are fused using the compatible BglII and BamHI restriction sites. BglII/BamHI ligation results in a 6 nt scar sequence (GGATCT) which is not recognized by restriction enzymes. Extra sgRNAs can therefore be added sequentially to the same plasmids using the same enzymes.

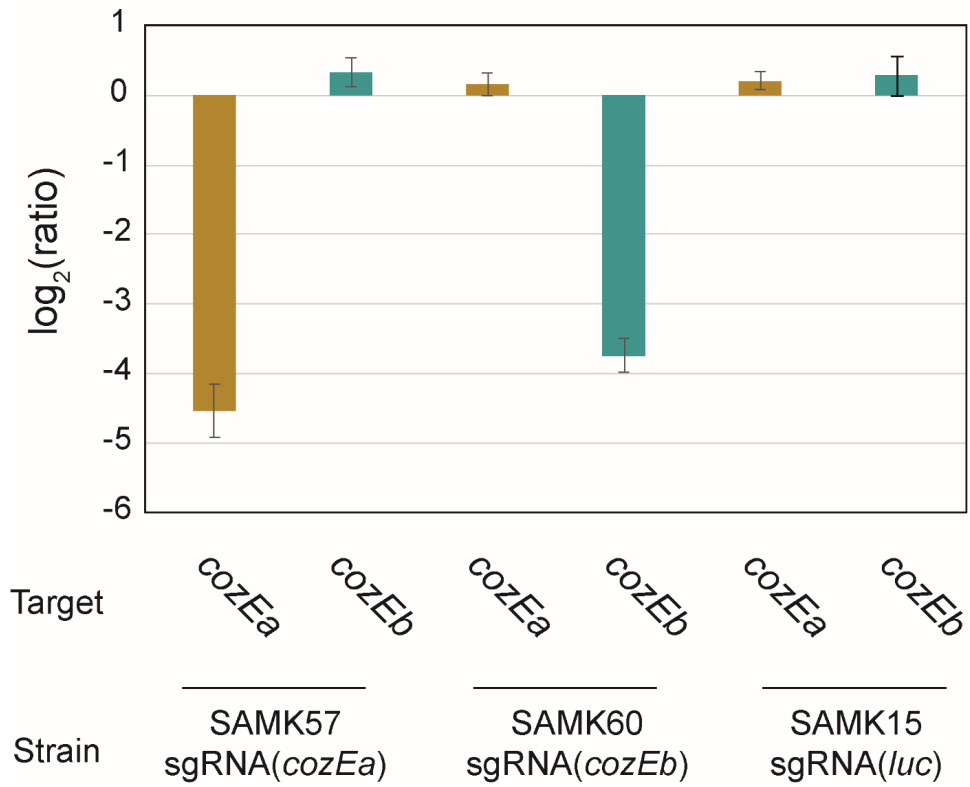


Fig. S3. Differential expression of *cozEa* and *cozEb* in induced (150 μ M IPTG) and non-induced strains as determined using qPCR. Strains with sgRNA targeting either *cozEa* (strain SAMK57), *cozEb* (strain SAMK60) or none of them (strain SAMK15) were used. Differential expression was calculated according to the Pfaffl-method using *pta* as reference gene.

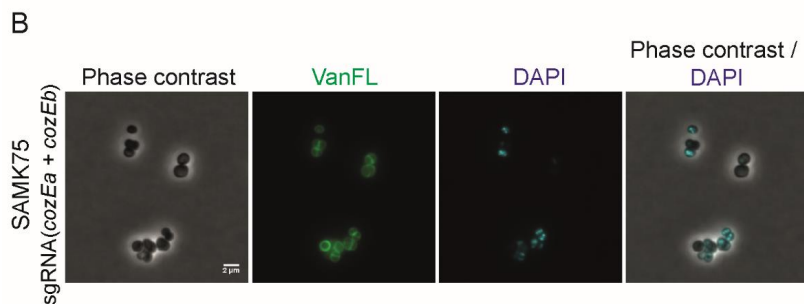
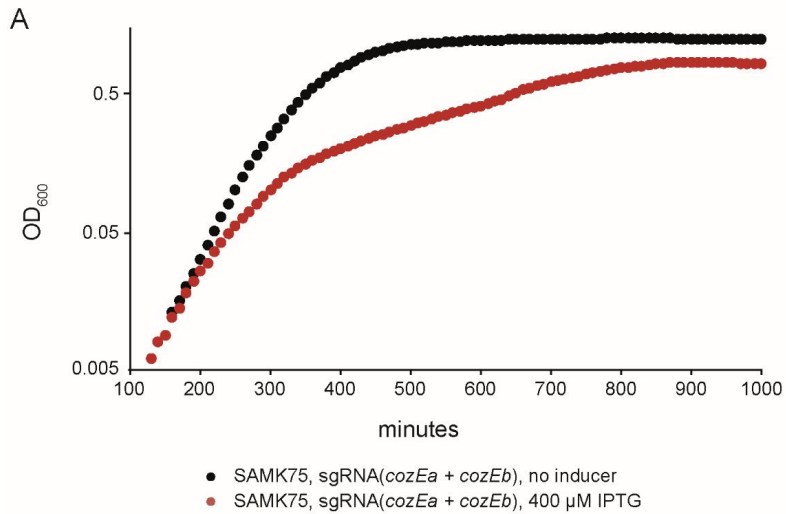


Fig. S4. Double sgRNA strain SAMK75, in which *cozEa* and *cozEb* are depleted simultaneously using the CRISPRi system.

A. Growth curves of SAMK75 grown without inducer (black) or with 400 μM IPTG (red).

B. The cells were grown in the presence of 400 μM IPTG for induction of *dcas9* expression for 4 hours.

The scale bar is 2 μm.

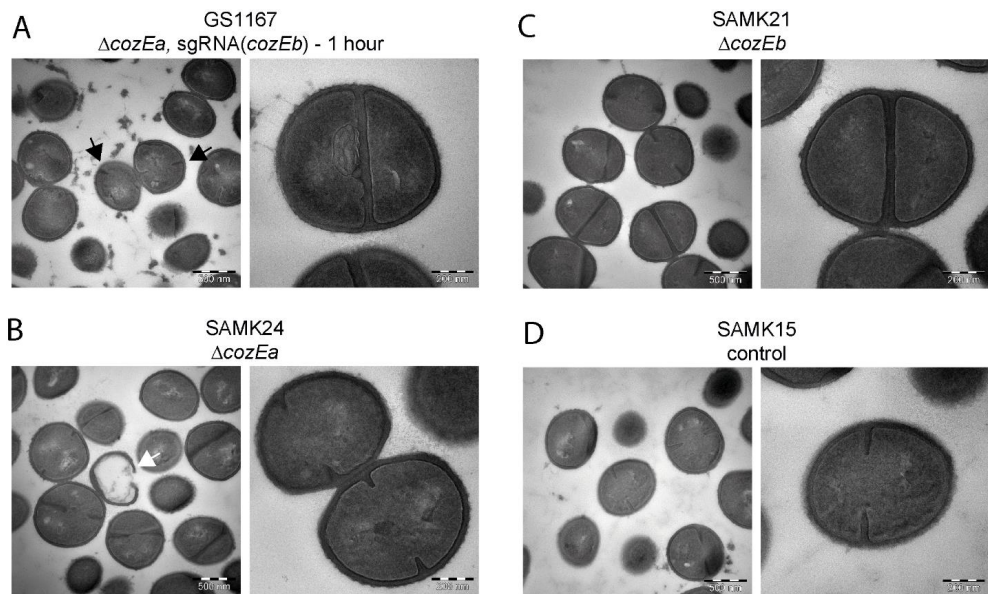


Fig. S5. Transmission electron micrographs.

A. Strain GS1167 depleted for 1 hour. The black arrows point to uncoordinated septum initiation.

B. Strain SAMK24 (ΔcozEa). Lysed cell is marked with a white arrow.

C. Strain SAMK21 (ΔcozEb).

D. Strain SAMK15 control cells carrying a non-targeting sgRNA.

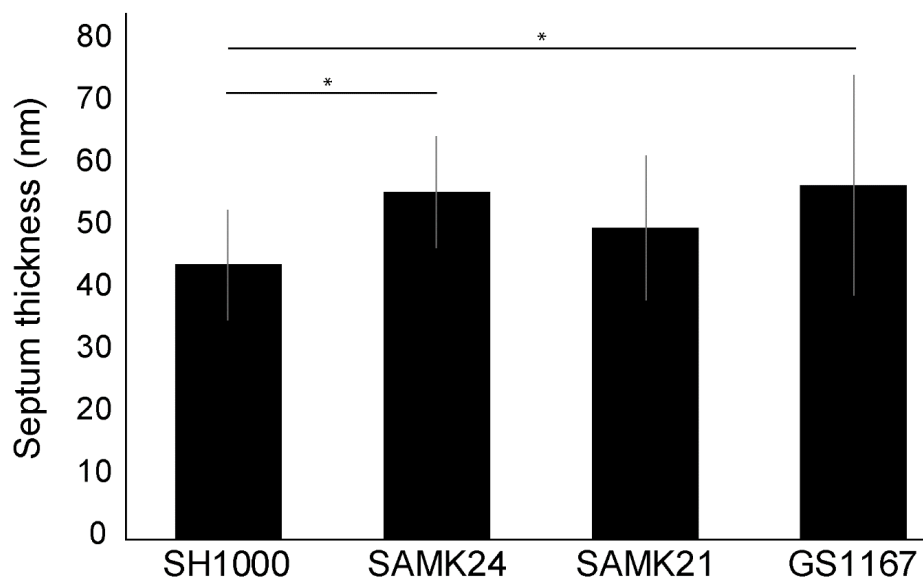
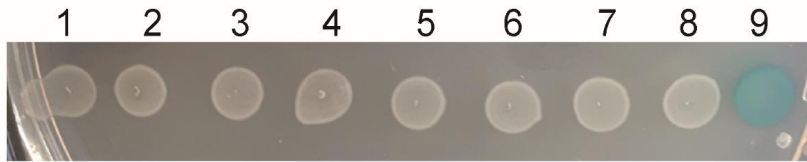


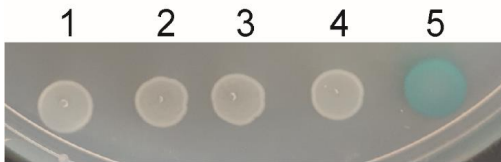
Fig. S6. Septum thickness. Wild-type cells (SH1000) compared to ΔcozEa (SAMK24), ΔcozEb (SAMK21) and $\Delta\text{cozEa}::\text{spc}$ with depleted cozEb (GS1167). Septum thickness was measured from TEM-images ($n > 20$ for each strain). Statistically significant differences ($P < 0.05$, two-sample t-test) are indicated by an asterisk.

A



1. pKT25 (empty vector) + CozEa-T18
2. pKT25 (empty vector) + CozEb-T18
3. pKT25 (empty vector) + T18-Pbp1
4. pKT25 (empty vector) + T18-Pbp2
5. pKT25 (empty vector) + T18-Pbp2a
6. pKT25 (empty vector) + T18-Pbp3
7. pKT25 (empty vector) + Pbp4-T18
8. pKT25 (empty vector) + pUT18 (empty vector) (negative control)
9. pKT25-zip + pUT18C-zip (positive control)

B



1. pKT25 (empty vector) + EzrA-T18
2. pKT25 (empty vector) + T18-MreC
3. pKT25 (empty vector) + MreD-T18
4. pKT25 (empty vector) + pUT18 (empty vector) (negative control)
5. pKT25-zip + pUT18C-zip (positive control)

Fig. S7. Control experiment for bacterial two-hybrid assays.

A. Controls related to Fig. 5A.

B. Controls related to Fig. 5B.

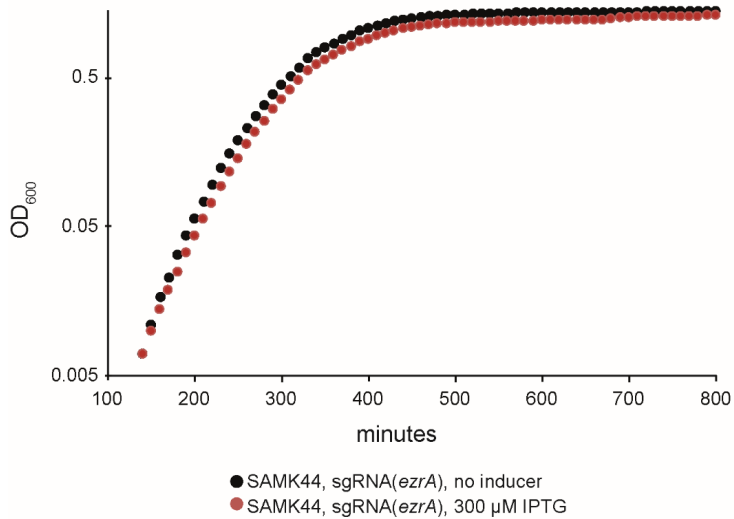


Fig. S8. Growth curve of *ezrA* depletion strain. Strain SAMK44 containing the *ezrA* depletion construct was grown without (black) or with (red) 300 μM IPTG.

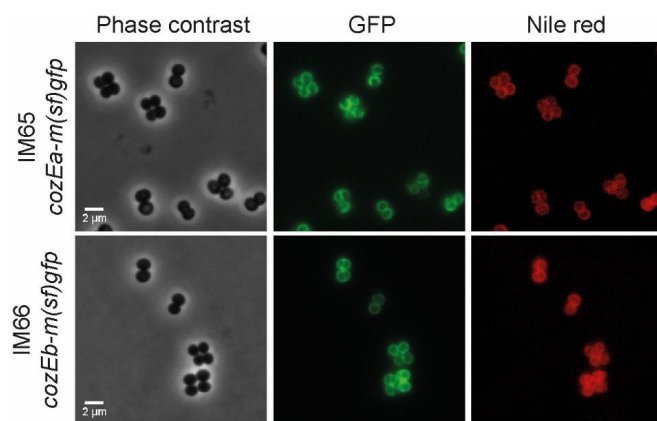


Fig. S9. Localization of CozEa-m(sf)GFP and CozEb-m(sf)GFP in *S. aureus* SH1000. Cells were stained with Nile Red to visualize the cell membrane.

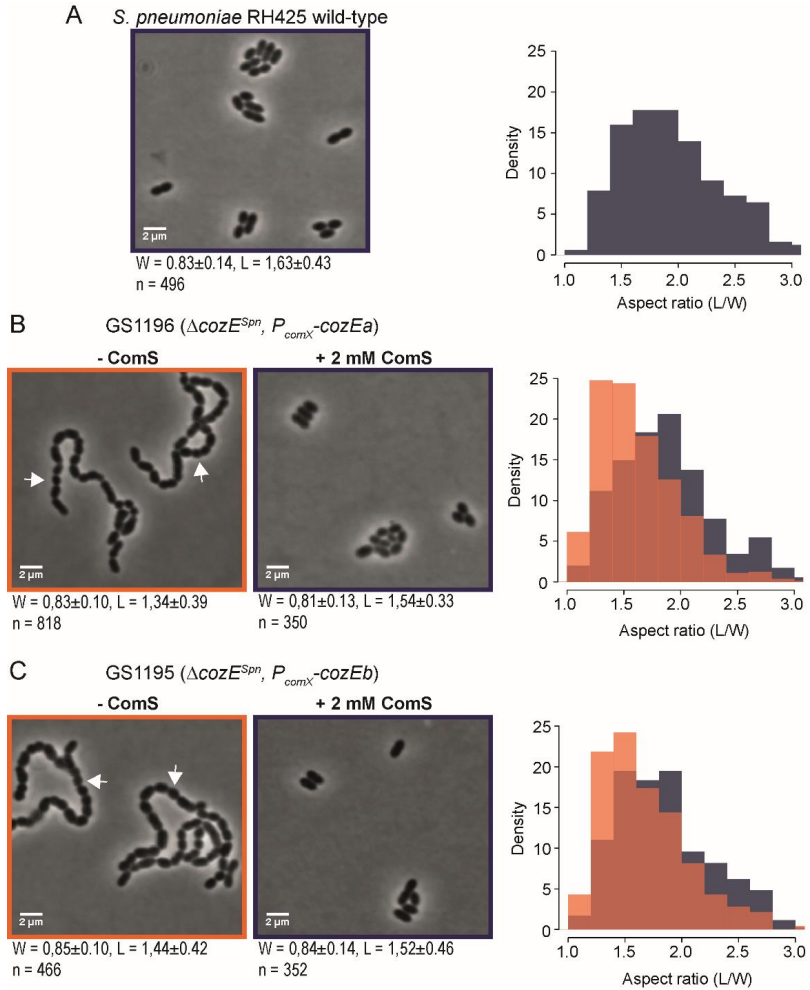


Fig. S10 Phase contrast images demonstrating complementation of $\Delta\text{cozE}^{\text{Spn}}$ with staphylococcal proteins CozEa and CozEb. Length and width measurements (\pm standard deviation) and the number of cells measured are indicated below the images. In addition, histograms of the aspect ratio for each strain is plotted in the right panel.

A. Wild-type *S. pneumoniae* RH425 cells.

B. Strain GS1196 cells incubated without or with ComS for 4 hours. In the histogram, orange bars represents cells without ComS and gray bars cells with ComS.

C. Strain GS1195 incubated with or without ComS for 4 hours. In the histogram, orange bars represents cells without ComS and gray bars cells with ComS.

When ComS is not present (left panel in B and C), the typical *cozE*-depletion phenotypes with extensive chaining and occasional rounding of cells (arrowhead) are observed. The scale bars are 2 μm . Cell width (W) and length (L) as measured using MicrobeJ is indicated below the images (\pm standard deviation) as well as number of cells calculated (n).

Supporting tables (S1 Table – S4 Table)

Table S1. Overview of bacterial two-hybrid assays performed with CozEa and CozEb in this study^a.

	T25-CozEa	CozEa-T25	T25- CozEb	CozEb-T25	T25-PBP1	T25-PBP2	T25-PBP2a	T25-PBP3	PBP4-T25	T25-MreC	MreD-T25	DnaA-T25	EzrA-T25	T25-GpsB	GpsB-T25	T25-DivIVA	DivIVA-T25
T18-CozEa	+	+	+	-	-	-	-	-	-	-	-	-	-	-	-	-	-
CozEa-T18	+	+	+	-	-	-	-	-	-	-	-	-	-	-	-	-	-
CozEb-T18	+	-	+	+	-	-	-	-	-	-	-	-	-	-	-	-	-
T18-PBP1	-	-	-	-	+	+	+	+	+	NT	NT	NT	NT	NT	NT	NT	NT
T18-PBP2	-	-	-	-	+	NT	NT	NT	NT	NT	NT	NT	NT	NT	NT	NT	NT
T18-PBP2a	-	-	-	-	+	NT	NT	NT	NT	NT	NT	NT	NT	NT	NT	NT	NT
T18-PBP3	-	-	-	-	+	NT	NT	NT	NT	NT	NT	NT	NT	NT	NT	NT	NT
PBP4-T18	-	-	-	-	+	NT	NT	NT	NT	NT	NT	NT	NT	NT	NT	NT	NT
T18-MreC	+	-	-	-	+	NT	NT	NT	NT	NT	-	NT	NT	NT	NT	NT	NT
T18-MreD	-	-	-	-	NT	NT	NT	NT	NT	+	-	NT	NT	NT	NT	NT	NT
MreD-T18	-	-	-	-	NT	NT	NT	NT	NT	+	-	NT	NT	NT	NT	NT	NT
DnaA-T18	-	-	-	-	NT	NT	NT	NT	NT	NT	NT	NT	NT	NT	NT	NT	NT
FtsZ-T18	-	-	-	-	NT	NT	NT	NT	NT	NT	NT	NT	NT	NT	NT	NT	NT
EzrA-T18	+	+	+	+	NT	NT	NT	NT	NT	NT	NT	NT	NT	NT	NT	NT	NT
T18-GpsB	-	-	-	-	NT	NT	NT	NT	NT	NT	NT	NT	NT	NT	NT	NT	NT
GpsB-T18	+	-	-	-	NT	NT	NT	NT	NT	NT	NT	NT	NT	NT	NT	NT	NT

^a “+” means positive interaction detected in the two-hybrid assay. “NT” denotes “not tested.”

S2 Table. Strains used in this study

Name	Genotype ^{a,b}	Source
<i>S. aureus</i>		
SH1000	<i>rbsU</i> ⁺ derivative of strain NCTC8325-4	(Horsburgh <i>et al.</i> , 2002)
RN4220	Restriction deficient derivative of NCTC8325-4	(Kreiswirth <i>et al.</i> , 1983)
SAMK13	SH1000 carrying pLOW- <i>dcas9</i> , ery ^t	This work
SAMK15	SH1000 carrying pLOW- <i>dcas9</i> and pCG248-sgRNA(<i>luc</i>), ery ^t , cam ^f	This work
SAMK21	SH1000, Δ <i>cozEb::spc</i> , spc ^f	This work
SAMK24	SH1000, Δ <i>cozEa::spc</i> , spc ^f	This work
SAMK56	RN4220, <i>int2::luc-spc-gfp</i> carrying pLOW- <i>dcas9</i> and pCG248-sgRNA(<i>m(sf)gfp</i>)	This work
GS.1163	SH1000, Δ <i>cozEb::spc</i> carrying pLOW- <i>dcas9</i> and pCG248-sgRNA(<i>cozEa</i>), spc ^f , ery ^t , cam ^f	This work
GS.1167	SH1000, Δ <i>cozEa::spc</i> carrying pLOW- <i>dcas9</i> , pCG248-sgRNA(<i>cozEb</i>), spc ^f , ery ^t , cam ^f	This work
SAMK27	SH1000 carrying pLOW- <i>dcas9</i> , pCG248-sgRNA(<i>dnaA</i>), ery ^t , cam ^f	This work
SAMK20	SH1000 carrying pLOW- <i>dcas9</i> , pCG248-sgRNA(<i>pbp1</i>), ery ^t , cam ^f	This work
SAMK44	SH1000 carrying pLOW- <i>dcas9</i> , pCG248-sgRNA(<i>ezrA</i>), ery ^t , cam ^f	This work
SAMK57	SH1000 carrying pLOW- <i>dcas9</i> , pCG248-sgRNA(<i>cozEa</i>), ery ^t , cam ^f	This work
SAMK60	SH1000 carrying pLOW- <i>dcas9</i> , pCG248-sgRNA(<i>cozEb</i>), ery ^t , cam ^f	This work
SAMK75	SH1000, pLOW-dCas9, sgRNA(<i>cozEa+cozEb</i>), ery ^t , cam ^f	This work
SH4639	SH1000, <i>ezrA-gfp</i> , kan ^f	(Lund <i>et al.</i> , 2018)
MK1443	SH1000, <i>ezrA-gfp</i> , pLOW-dCas9, sgRNA(<i>cozEa+cozEb</i>), kan ^f , ery ^t , cam ^f	This work
IM65	SH1000 carrying pLOW- <i>cozEa-m(sf)gfp</i> , ery ^t	This work
IM66	SH1000 carrying pLOW- <i>cozEb-m(sf)gfp</i> , ery ^t	This work
<i>E. coli</i>		
BTH101	Strain used for BACTH analysis	Euromedex
XL1-Blue	Host strain	Agilent
IM08B	DH10B, Δ <i>dcm</i> , P _{help} - <i>hsdMS</i> , P _{N25} - <i>hsdS</i> (strain expressing the <i>S. aureus</i> CC8 specific methylation genes)	(Monk <i>et al.</i> , 2015)
DC10B	DH10B, Δ <i>dcm</i>	(Monk <i>et al.</i> , 2012)
<i>S. pneumoniae</i>		
RH425	R6 derivative, streptomycin resistant, Δ <i>comA::ermAM</i> , ery ^t , sm ^f	(Johnsborg <i>et al.</i> , 2008)
SPH131	Δ <i>comA</i> , P1::P _{comR} :: <i>comR</i> , P _{comX} :: <i>Janus</i> , ery ^t , kan ^f	(Berg <i>et al.</i> , 2011)
KHB432	Δ <i>comA</i> , P1::P _{comR} :: <i>comR</i> , P _{comX} :: <i>cozE^{Spn}</i> (spr0777), ery ^t , sm ^f	(Straume <i>et al.</i> , 2017), lab collection

SPH355	$\Delta comA$, P1::P _{comR} ::comR, P _{comX} ::cozE ^{Spn} , $\Delta cozE^{Spn}$::DEL, ery ^r , sm ^r	(Straume <i>et al.</i> , 2017)
GS1169	$\Delta comA$, P1::P _{comR} ::comR, P _{comX} ::cozEb (SAOUHC_01358), ery ^r , sm ^r	This work
GS1170	$\Delta comA$, P1::P _{comR} ::comR, P _{comX} ::cozEa (SAOUHSC_00948), ery ^r , sm ^r	This work
GS1193	$\Delta comA$, P1::P _{comR} ::comR, P _{comX} ::cozEb, $\Delta cozE^{Spn}$::Janus, ery ^r , kan ^r	This work
GS1194	$\Delta comA$, P1::P _{comR} ::comR, P _{comX} ::cozEa, $\Delta cozE^{Spn}$::Janus, ery ^r , kan ^r	This work
GS1195	$\Delta comA$, P1::P _{comR} ::comR, P _{comX} ::cozEb, $\Delta cozE^{Spn}$, ery ^r , sm ^r	This work
GS1196	$\Delta comA$, P1::P _{comR} ::comR, P _{comX} ::cozEa, $\Delta cozE^{Spn}$, ery ^r , sm ^r	This work
GS1214	$\Delta comA$, $\Delta ezrA::ezrA-yfp-spc$, ery ^r , sm ^r , spc ^r	This work
GS1215	$\Delta comA$, P1::P _{comR} ::comR, P _{comX} ::cozE ^{Spn} , $\Delta cozE^{Spn}$::Janus, $\Delta ezrA::ezrA-yfp-spc$, ery ^r , kan ^r , spc ^r	This work

^a ery; erythromycin, spc; spectinomycin, kan; kanamycin, sm; streptomycin, cam; chloramphenicol

^b Janus contains a *kan::rpsL*⁺ cassette (Sung *et al.*, 2001).

S3 Table. Plasmids used in this study

Name	Description^{a,b}	Reference
pLOW	Plasmid for IPTG-inducible expression of proteins in <i>S. aureus</i> , amp ^r , ery ^r	(Liew <i>et al.</i> , 2011)
pLOW-FtsZ-GFP	<i>ftsZ-gfp</i> fusion downstream of P _{lac} promoter, amp ^r , ery ^r	(Liew <i>et al.</i> , 2011)
pLOW- <i>ftsZ-m(sf)gfp</i>	<i>ftsZ-m(sf)gfp</i> fusion downstream of P _{lac} promoter, amp ^r , ery ^r	This work
pLOW- <i>cozEa-m(sf)gfp</i>	<i>cozEa-m(sf)gfp</i> fusion downstream of P _{lac} promoter, amp ^r , ery ^r	This work
pLOW- <i>cozEb-m(sf)gfp</i>	<i>cozEb-m(sf)gfp</i> fusion downstream of P _{lac} promoter, amp ^r , ery ^r	This work
pMAD	Vector for allelic replacement in Gram-positive bacteria, amp ^R ,	(Arnaud <i>et al.</i> , 2004)
pCG248	<i>E. coli/S. aureus</i> shuttle vector, amp ^r , cam ^r	(Helle <i>et al.</i> , 2011)
pRAB11	<i>E. coli/S. aureus</i> shuttle vector	(Helle <i>et al.</i> , 2011)
pCN55	<i>E. coli/S. aureus</i> shuttle vector	(Charpentier <i>et al.</i> , 2004)
pMK17	<i>bgaA'</i> , <i>tet'</i> , P _{Zn} -MCS-linker- <i>m(sf)gfp</i> ' <i>bgaA</i>	(van Raaphorst <i>et al.</i> , 2017)
pMAD-int2-luc-spc-gfp	Vector for integrations of constitutively expressed luc-spc-gfp, amp ^r , spc ^r , ery ^r .	This work
pJWV102-dcas9	<i>dcas9</i> (cas9 gene derived from <i>S. pyogenes</i>) downstream of a zinc-inducible promoter.	(Liu <i>et al.</i> , 2017)
pLOW-dcas9	<i>dcas9</i> downstream of P _{lac} promoter	This work
pMAD-cozEa::spc	Vector for allelic replacement of <i>cozEa</i>	This work
pMAD-cozEb::spc	Vector for allelic replacement of <i>cozEb</i>	This work
pMAD-cozEa::cm	Vector for allelic replacement of <i>cozEa</i>	This work
<i>sgRNA plasmids</i>		
pPEPX-sgRNA(<i>luc</i>)	Transcriptionally isolated sgRNA(<i>luc</i>) construct downstream of constitutive promoter	(Liu <i>et al.</i> , 2017)
pCG248-sgRNA(<i>luc</i>)	For constitutive expression of sgRNA(<i>luc</i>), amp ^r , cam ^r	This work.
pCG248-sgRNA(<i>cozEa</i>)	For constitutive expression of sgRNA(<i>cozEa</i>), amp ^r , cam ^r	This work
pCG248-sgRNA(<i>cozEb</i>)	For constitutive expression of sgRNA(<i>cozEb</i>), amp ^r , cam ^r	This work
pCG248-sgRNA(<i>cozEa+cozEb</i>)	For constitutive expression of sgRNA(<i>cozEa</i> and <i>cozEn</i>), amp ^r , cam ^r	This work
pCG248-sgRNA(<i>dnaA</i>)	For constitutive expression of sgRNA(<i>dnaA</i>), amp ^r , cam ^r	This work
pCG248-sgRNA(<i>pbp1</i>)	For constitutive expression of sgRNA(<i>pbp1</i>), amp ^r , cam ^r	This work
pCG248-sgRNA(<i>ezrA</i>)	For constitutive expression of sgRNA(<i>ezrA</i>), amp ^r , cam ^r	This work
pCG248-sgRNA(<i>gfp</i>)	For constitutive expression of sgRNA(<i>gfp</i>), amp ^r , cam ^r	This work
<i>Plasmids used for BACTH analysis.</i>		
pKT25	Plasmid used for BACTH analyses	Euromedex
pKNT25	Plasmid used for BACTH analyses	Euromedex
pUT18	Plasmid used for BACTH analyses	Euromedex
pUT18C	Plasmid used for BACTH analyses	Euromedex

pUT18- <i>cozEb</i>	pUT18 containing <i>cozEb</i>	This work
pKT25- <i>cozEb</i>	pKT25 containing <i>cozEb</i>	This work
pKNT25- <i>cozEb</i>	pKNT25 containing <i>cozEb</i>	This work
pUT18C- <i>cozEa</i>	pUT18C containing <i>cozEa</i>	This work
pUT18- <i>cozEa</i>	pUT18 containing <i>cozEa</i>	This work
pKT25- <i>cozEa</i>	pKT25 containing <i>cozEa</i>	This work
pKNT25- <i>cozEa</i>	pKNT25 containing <i>cozEa</i>	This work
pUT18- <i>ezrA</i>	pUT18 containing <i>ezrA</i>	This work
pKNT25- <i>ezrA</i>	pKNT25 containing <i>ezrA</i>	This work
pUT18- <i>dnaA</i>	pUT18 containing <i>dnaA</i>	This work
pKNT25- <i>dnaA</i>	pKNT25 containing <i>dnaA</i>	This work
pKT25- <i>mreC</i>	pKT25 containing <i>mreC</i>	This work
pUT18C- <i>mreC</i>	pUT18C containing <i>mreC</i>	This work
pUT18C-link_ <i>mreD</i>	pUT18C containing a linker between T18 and <i>mreD</i>	This work
pKNT25-link_ <i>mreD</i>	pKNT25 containing a linker between T25 and and <i>mreD</i>	This work
pUT18-link_ <i>mreD</i>	pUT18 containing a linker between T18 and and <i>mreD</i>	This work
pUT18- <i>ftsZ</i>	pUT18 containing <i>ftsZ</i>	This work
pKT25- <i>pbp1</i>	pKT25 containing <i>pbp1</i>	This work
pUT18C- <i>pbp1</i>	pUT18C containing <i>pbp1</i>	This work
pKT25- <i>pbp2</i>	pKT25 containing <i>pbp2</i>	This work
pUT18C- <i>pbp2</i>	pUT18C containing <i>pbp2</i>	This work
pKT25- <i>pbp2a</i>	pKT25 containing <i>pbp2a</i>	This work
pUT18C- <i>pbp2a</i>	pUT18C containing <i>pbp2a</i>	This work
pKT25- <i>pbp3</i>	pKT25 containing <i>pbp3</i>	This work
pUT18C- <i>pbp3</i>	pUT18C containing <i>pbp3</i>	This work
pKNT25- <i>pbp4</i>	pKNT25 containing <i>pbp4</i>	This work
pUT18- <i>pbp4</i>	pUT18 containing <i>pbp4</i>	This work
pKT25- <i>gpsB</i>	pKT25 containing <i>gpsB</i>	This work
pKNT25- <i>gpsB</i>	pKNT25 containing <i>gpsB</i>	This work
pUT18- <i>gpsB</i>	pUT18 containing <i>gpsB</i>	This work
pUT18C- <i>gpsB</i>	pUT18C containing <i>gpsB</i>	This work
pKT25- <i>divIVA</i>	pKT25 containing <i>divIVA</i>	This work
pKNT25- <i>divIVA</i>	pKNT25 containing <i>divIVA</i>	This work

^a amp; ampicillin, ery; erythromycin, spe; spectinomycin, cam; chloramphenicol

^b Janus contains a *kan::rpsL*⁺ cassette (Sung *et al.*, 2001).

S4 Table. Primers used in this study.

Name	Sequence 5' -> 3', reference^a
<i>Primers for construction of pMAD deletion vectors</i>	
mk182_0948_up_F_check	GCAAATAACGCTGGCACTTC
mk183_0948_up_F_NcoI	ACGTCCATGGCCATAAAATGGTACAACGGCTG
mk184_0948_up_R_over_aad9	GATCCTAGGTGGGCCCAAT TAACATAAACGATGTTCTCCT
mk185_0948_down_F_over_aad9	CTCGAGCGGCCGCATAGT AGGACTAATTCTGTGGATGTC
mk186_0948_down_R_BamHI	ACGTGGATCCCTGGGATTAGATATTCTATCCGT
mk187_0948_down_R_check	CAAACATTTATCGTTGTAATACGT
mk188_aad9_up_F	ATTGGGCCACCTAGGATC
mk189_aad9_down_R	ACTATGCGGCCGCTCGAG
mk190_1358_up_F_check	ACTTTCAAGTTAGACATTTCCGA
mk191_1358_up_F_NcoI	ACGTCCATGGACAACAATGTCGTAGTATGTAC
mk192_1358_up_R_over_aad9	GATCCTAGGTGGGCCCAAT ACTTCATATACCGTGATTCCGGT
mk193_1358_down_F_over_aad9	CTCGAGCGGCCGCATAGTGGTGCTTATAATGTTGGGCAG
mk194_1358_down_R_BamHI	ACGTGGATCCCTCGGGTGGTCTAACCATTTGA
mk195_1358_down_R_check	GCGTCAACAATTACACCACAG
mk257_cmR_F	ACGAAAATTGGATAAAAGTGGGA
mk258_cmR_R	ATTATCTCATATTATAAAAGCCAG
mk259_0948_up_R_over_cmR	TCCCACTTTATCCAATTTTCGTAAACATAAACGATGTTCTCCT
mk260_0948_down_F_over_cmR	CTGGCTTTTATAATATGAGATAATAGGACTAATTCTGTGGATGTC
<i>Primers for construction of dCas9 construct</i>	
mk41_cas9_f_Sall_KpnI_XhoI	ACTCCTCGAGTCGACGGTACCAAAGAGGAGAAAGGATCTATG
mk42_cas9_R_NotI_XhoI	GACCCCTCGAGCGGCCGCTTATTAGTCACCTCCTAGCTGAC
<i>Primers for construction of sgRNA constructs</i>	
mk200_Phospho-sgRNA_promoter_R	TATAGTTATTATACCAGGGGGACAGTGC
mk202_For_dnaA	AGACAACATCAAATAAGATTGCTGTTTAAAGAGCTATGCTGGAAACAG
mk15_For_pbp1	TCATATATCTTTCCTCGTTCGTGTTTAAAGAGCTATGCTGGAAACAG
mk205_For_0948	TAATCAGAGCGATGCCAGTTGTTTAAAGAGCTATGCTGGAAACAG
mk206_For_1358	AAACTTCATATACCGTGATTGTTTAAAGAGCTATGCTGGAAACAG
mk207_For_sfgfp	CCGTCAAGCTCAACGAGAATGTTTAAAGAGCTATGCTGGAAACAG
mk210_For_ezrA	TTATGGATTTTTTCTCCACGTTTAAAGAGCTATGCTGGAAACAG
<i>Primers used for construction of constitutive gfp expression in S. aureus</i>	
mk203_spc_F_EcoRI	ACGTGAATTCTATATGAACATAATCAACGAGGT
mk204_spcR_over_GFP	TTTATTGCTCGAGGTCGACGATAGCCTAATTGAGAGAAGTTTC
im84_m(sf)gfp_F_Sall_XhoI_RB S	ATCGTCGACCTCGAGCAATAAAACTAGGAGGAAATTTAAATGTCAAAAGGAGAAGAGCTGTTTC
im2_m(sf)gfp_R_NotI_EcoRI	AGTGAATTCGCGGCCGCTTACTTATAAAGCTCATCCATGCC
<i>Primers for construction of coxEa- m(sf)gfp and coxEb-m(sf)gfp fusions</i>	
im1_linker-PP_F_BamHI	ATCGGATCCCGGATCTGGTGAGAGAAGCTGCA
im2_m(sf)gfp_R_NotI_EcoRI	AGTGAATTCGCGGCCGCTTACTTATAAAGCTCATCCATGCC
im10_SA0948_F_XhoI_Sall_RBS	ATCCTCGAGGTCGACCAATAAAACTAGGAGGAAATTTAAATGTTAAACAAGGTTTGGTTCC
im11_SA0948_R_BamHI	TCCGGGGATCCAGTCCTTAACACTTACTGTTTGCT

mk269_ezrA_rev_KpnI	GATCGGT <u>ACCC</u> GTTGCTTAATAA <u>ACTTCTTCTT</u> CAAT
mk270_dnaA_for_BamHI	GATCGGATCCCTCGGAAAAAGAAATTTGGGAAAAAG
mk271_dnaA_rev_KpnI	GATCGGT <u>ACCC</u> GATACATTTCTTATTTCTTTTTCAAGA
mk272_1358_for_BamHI	GATCGGATCCCAATGAAAAATGAAAAAGAAATATAAGAAAG
mk273_1358_rev_KpnI	GATCGGT <u>ACCC</u> GTTCAACTATTTTATTACTTTCTTTAA
gs649-mreC_fwd_XbaI	GATCTCTAGAGCTTAAGTTTTTTAAAAATAACAAATTAATTG
gs650-mreC_rev_EcoRI	GATCGAATTC <u>T</u> TATTTATCCCTGCTTTCATCATC
gs651-mreD_fwd_XbaI	GATCTCTAGAGATGCGTACACTGTATTATTTTTTG
gs652-mreD_rev_linker_EcoRI	GATCGAATTCGAGGTTCTCTCTCCACTTCTCTCTCTCCCAT TGACGACGTTTCATGTC
gs656-cozEB_fwd_BamHI	GATCGGATCCCATGAATGAAATGAAAAGAATATAAG
gs657-cozEB_rev_EcoRI	GATCGAATTCGATTCAACTATTTTATTACTTTCTTTAATA
gs658-cozEA_fwd_XbaI	GATCTCTAGAGTTAAACAAGTTTGGTTCCGAAC
gs659-cozEA_rev_EcoRI	GATCGAATTC <u>T</u> TTAGTCTTAACATTACTGTTTGC
gs660-cozEA_rev_EcoRI	GATCGAATTCGATTAGTCTTAACATTACTGTTTGC
gs661-cozEA_fwd_XbaI	GATCTCTAGAGATGTTAAACAAGTTTGGTTCCG
gs662-cozEA_rev_EcoRI	GATCGAATTCGAGTCTTAACATTACTGTTTGCCTT
gs663-pbp1_fwd_XbaI	GATCTCTAGAGGCGAAGAAAAATTAATAAATAAAAAA
gs664-pbp1_rev_EcoRI	GATCGAATTC <u>T</u> TTAGTCCGACTTATCCTTGTGAG
gs665-pbp2_fwd_pstI	GATCCTGCAGGGACGAAAAACAAAGGATCTTCTC
gs666-pbp2_rev_BamHI	GATCGGATCCCTCTTAGTTGAATATACCTGTTAATCC
gs667-pbp2_fwd_pstI	GATCCTGCAGGACGAAAAACAAAGGATCTTCTC
gs668-pbp3_fwd_BamHI	GATCGGATCCCTAAAAAGACTAAAAAGAAAAATCAAATG
gs669-pbp3_rev_EcoRI	GATCGAATTC <u>T</u> TTATTGTCTTTGTCTTATTTTTATC
gs670-pbp4_fwd_XbaI	GATCTCTAGAGATGAAAAATTAATATCTATTATCATC
gs671-pbp4_rev_EcoRI	GATCGAATTCGATTTTCTTTTTCTAAATAAACGATTG
gs688-mreD_fwd_linker_XbaI	GATCTCTAGAGGGAGGAGGAGGAAGTGGAGGAGGAGGAACCAT GCGTACACTGTATTATTTTTTG
gs689-mreD_rev_EcoRI	GATCGAATTC <u>T</u> CCATTGACGACGTTTCATGTC
gs695-pbp2a_BamHI	GATCGGATCCCAAAAAGATAAAAATTTGTTCCACTTATT
gs696-pbp2a_EcoRI	GATCGAATTC <u>T</u> TATTCATCTATATCGTATTTTTATTAC
gs711-gpsB_fwd_BamHI	GATCGGATCCCTCAGATGTTTCATTGAAATTATCAG
gs712-gpsB_rev_KpnI	GATCGGT <u>ACCC</u> GTTTACCAATACAGCTTTTTCTAAG
gs713-divIVA_fwd_BamHI	GATCGGATCC <u>CC</u> TTTTACACCAATGAAATTAAG
gs714-divIVA_rev_KpnI	GATCGGT <u>ACCC</u> GCTTCTTAGTTGTTTCTGAATCATTG

^a No reference is indicated for the primers made for this work

References

- Arnaud, M., A. Chastanet & M. Debarbouille, (2004) New vector for efficient allelic replacement in naturally nontransformable, low-GC-content, gram-positive bacteria. *Appl Environ Microbiol* **70**: 6887-6891.
- Berg, K.H., T.J. Bjørnstad, D. Straume & L.S. Håvarstein, (2011) Peptide-regulated gene depletion system developed for use in *Streptococcus pneumoniae*. *J Bacteriol* **193**: 5207-5215.
- Charpentier, E., A.I. Anton, P. Barry, B. Alfonso, Y. Fang & R.P. Novick, (2004) Novel cassette-based shuttle vector system for gram-positive bacteria. *Appl Environ Microbiol* **70**: 6076-6085.
- Helle, L., M. Kull, S. Mayer, G. Marincola, M.E. Zelder, C. Goerke, C. Wolz & R. Bertram, (2011) Vectors for improved Tet repressor-dependent gradual gene induction or silencing in *Staphylococcus aureus*. *Microbiology* **157**: 3314-3323.
- Horsburgh, M.J., J.L. Aish, I.J. White, L. Shaw, J.K. Lithgow & S.J. Foster, (2002) SigmaB modulates virulence determinant expression and stress resistance: characterization of a functional *rsbU* strain derived from *Staphylococcus aureus* 8325-4. *J Bacteriol* **184**: 5457-5467.
- Johnsborg, O., V. Eldholm, M.L. Bjørnstad & L.S. Håvarstein, (2008) A predatory mechanism dramatically increases the efficiency of lateral gene transfer in *Streptococcus pneumoniae* and related commensal species. *Mol Microbiol* **69**: 245-253.
- Kreiswirth, B.N., S. Lofdahl, M.J. Betley, M. O'Reilly, P.M. Schlievert, M.S. Bergdoll & R.P. Novick, (1983) The toxic shock syndrome exotoxin structural gene is not detectably transmitted by a prophage. *Nature* **305**: 709-712.
- Liew, A.T., T. Theis, S.O. Jensen, J. Garcia-Lara, S.J. Foster, N. Firth, P.J. Lewis & E.J. Harry, (2011) A simple plasmid-based system that allows rapid generation of tightly controlled gene expression in *Staphylococcus aureus*. *Microbiology* **157**: 666-676.
- Liu, X., C. Gallay, M. Kjos, A. Domenech, J. Slager, S.P. van Kessel, K. Knoop, R.A. Sorg, J.R. Zhang & J.W. Veening, (2017) High-throughput CRISPRi phenotyping identifies new essential genes in *Streptococcus pneumoniae*. *Mol Syst Biol* **13**: 931.
- Lund, V.A., K. Wacnik, R.D. Turner, B.E. Cotterell, C.G. Walther, S.J. Fenn, F. Grein, A.J. Wollman, M.C. Leake, N. Olivier, A. Cadby, S. Mesnage, S. Jones & S.J. Foster, (2018) Molecular coordination of *Staphylococcus aureus* cell division. *Elife* **7**.
- Monk, I.R., I.M. Shah, M. Xu, M.W. Tan & T.J. Foster, (2012) Transforming the untransformable: application of direct transformation to manipulate genetically *Staphylococcus aureus* and *Staphylococcus epidermidis*. *MBio* **3**.
- Monk, I.R., J.J. Tree, B.P. Howden, T.P. Stinear & T.J. Foster, (2015) Complete bypass of restriction systems for major *Staphylococcus aureus* lineages. *MBio* **6**: e00308-00315.
- Sievers, F., A. Wilm, D. Dineen, T.J. Gibson, K. Karplus, W. Li, R. Lopez, H. McWilliam, M. Remmert, J. Soding, J.D. Thompson & D.G. Higgins, (2011) Fast, scalable generation of high-quality protein multiple sequence alignments using Clustal Omega. *Mol Syst Biol* **7**: 539.
- Straume, D., G.A. Stamsås, K.H. Berg, Z. Salehian & L.S. Håvarstein, (2017) Identification of pneumococcal proteins that are functionally linked to penicillin-binding protein 2b (PBP2b). *Mol Microbiol* **103**: 99-116.
- Sung, C.K., H. Li, J.P. Claverys & D.A. Morrison, (2001) An *rpsL* cassette, janus, for gene replacement through negative selection in *Streptococcus pneumoniae*. *Appl Environ Microbiol* **67**: 5190-5196.
- van Raaphorst, R., M. Kjos & J.W. Veening, (2017) Chromosome segregation drives division site selection in *Streptococcus pneumoniae*. *Proc Natl Acad Sci U S A* **114**: E5959-E5968.

PAPER II

The function of CozE proteins is linked to lipoteichoic acid biosynthesis in *Staphylococcus aureus*

Maria Disen Barbuti, Ine Storaker Myrbråten, Gro Anita Stamsås, Maria Victoria Heggenhougen, Daniel Straume and Morten Kjos*.

Faculty of Chemistry, Biotechnology and Food Science, Norwegian University of Life Sciences, Ås, Norway.

* Corresponding author: Morten Kjos, morten.kjos@nmbu.no.

Abstract

Teichoic acids, and in particular lipoteichoic acids (LTA), found in the cell envelope of *Staphylococcus aureus*, are important virulence factors and modulators of antibiotic susceptibility. These anionic polymers are also critical for cell integrity and proper cell division. The paralogous membrane proteins CozEa and CozEb have previously been reported to have overlapping and essential roles during cell division in *S. aureus*. By further investigating the CozEa and CozEb functionality in methicillin-sensitive- and methicillin-resistant *S. aureus* (MSSA and MRSA), we here discovered a link between these proteins and biosynthesis of LTA. We found that deletion of *cozEa* or *cozEb* had opposite effects on the growth of LTA depleted cells. The LTA polymers are attached to the membrane via glycolipid anchors, and we show that the proteins involved in synthesis and flipping of the glycolipid anchor modulated the essentiality of CozE-proteins. While the essentiality of CozE proteins was increased in cells devoid of glycolipid synthesis (\DeltaugtP), the essentiality was alleviated in cells lacking the flippase activity (\DeltaltaA). Furthermore, we found that CozEb had an impact on the length of LTA in *S. aureus*. This study clearly demonstrates a link between CozE proteins and LTA biosynthesis in *S. aureus*, although the exact mechanism explaining this relationship needs further investigation.

Introduction

Staphylococcus aureus is a Gram-positive, spherical bacterium that can cause a wide range of infectious diseases. Among the major factors contributing to its colonisation, infection, and immune evasion are the anionic teichoic acid (TA) polymers (Rajagopal & Walker, 2017; Xia et al., 2010). TAs also modulate the susceptibility to antibiotics in *S. aureus*, and the TA biosynthesis pathways are therefore attractive as potential anti-virulence and antibiotic targets (Pasquina et al., 2013; Xia et al., 2010).

Along with peptidoglycan, TAs are the major constituents of the cell wall of *S. aureus*. TAs are mainly composed of repeating units of ribitol phosphate (RboP) or glycerol phosphate (GroP), that are either covalently linked to peptidoglycan (wall teichoic acids, WTAs) or anchored to the cytoplasmic membrane (LTAs). While LTA is more important than WTA for cell viability, deletion mutants of genes involved in either pathways can be made, however, it is not possible to delete both pathways simultaneously (Oku et al., 2009; Santa Maria et al., 2014).

LTAs in *S. aureus* consist of poly-GroP chains anchored to the cytoplasmic membrane via the glycolipid anchor diglucosyl-diacylglycerol (Glc₂DAG) (Fig. 2A). Glc₂DAG is synthesized in the cytoplasm by the glycosyltransferase UgtP (also called YpfP), which transfers two glucose moieties from uridine diphosphate glucose (UDP-Glc) to DAG (Kiriukhin et al., 2001). Glc₂DAG is translocated to the outer membrane leaflet by the multi-membrane spanning protein LtaA (Grundling & Schneewind, 2007a; Zhang et al., 2020). Lastly, the LTA synthase LtaS, polymerizes the poly-GroP backbone chain by transferring GroP units, derived from the head group of phosphatidylglycerol (Ptd-Gro; GroP linked to DAG), to the Glc₂DAG on the outside surface of the membrane (Grundling & Schneewind, 2007b), leaving extracellular DAG as by-product. LTA polymers are often further modified by D-alanylation, by the action of the DltABCD system, and/or glycosylation, which modulates their properties and functions (Kho & Meredith, 2018; Rismondo et al., 2021)

The LTA synthase LtaS is considered essential for growth in *S. aureus*, as deletions of *ltaS*, in which LTA synthesis is completely abolished, are associated with suppressor mutations (Bæk et al., 2016; Corrigan et al., 2011). Cells with deletions in the genes required for synthesis and flipping of the glycolipid anchor, *ΔugtP* or *ΔltaA*, are however still viable (Hesser et al., 2020a; Kiriukhin et al., 2001). In *ΔugtP* cells, which completely lack the Glc₂DAG anchor, LtaS can initiate LTA synthesis directly on Ptd-Gro (Kiriukhin et al., 2001; Reichmann & Grundling, 2011). *ΔltaA* mutants have been demonstrated to produce a mixture of LTAs linked to both Ptd-Gro and Glc₂DAG (Grundling & Schneewind, 2007a); thus, there must be a yet unknown mechanism

that can translocate Glc₂DAG produced by UgtP to the outer membrane in the absence of LtaA. In both \DeltaugtP and \DeltaltaA backgrounds, LTA length control is lost as a result of lack of the Glc₂DAG anchor, resulting in cells that produce abnormally long LTA polymers (Hesser et al., 2020b).

Importantly, several studies suggest a link between LTA synthesis and cell division in *S. aureus*. Deletion of genes in the LTA biosynthetic pathway results in enlarged cells with severe division and morphological defects, suggested to be caused by changes in length and abundance of LTA (Hesser et al., 2020a; Kiriukhin et al., 2001). Furthermore, UgtP, LtaA and LtaS, have all been shown to interact with each other as well as multiple cell division and cell wall synthesis proteins (e.g., EzrA, FtsA, FtsW, PBP1-PBP4) (Reichmann et al., 2014), and LtaS has been demonstrated to mainly accumulate at the septum in *S. aureus*, indicating that LTA is primarily produced at the division site (Reichmann et al., 2014).

CozE (coordinator of zonal elongation) is a family of multi-transmembrane proteins that are broadly distributed across the bacterial kingdom (Fenton et al., 2016). CozE was first studied in *Streptococcus pneumoniae*, where it was shown to direct peptidoglycan synthesis to midcell for zonal elongation via interactions with the bifunctional class A PBP1a and the MreCD complex (Ducret & Grangeasse, 2017; Fenton et al., 2016; Straume et al., 2017). Recently, a CozE-paralog in *S. pneumoniae*, named CozEb, was found to be part of the same complex as CozE (Stamsås et al., 2020). Individual deletions of *cozE* and *cozEb* in *S. pneumoniae* generated different phenotypes with regard to cell shape and growth inhibition, and while CozEb was not required for correct localisation of PBP1a, overexpression of this protein could compensate for deletion of *cozE*, suppressing both growth and morphology defects, thus indicating a complex interplay between the two paralogs.

In *S. aureus*, the two CozE-paralogs, CozEa and CozEb, have been studied in the strain SH1000 where they are important for proper coordination of cell division (Stamsås et al., 2018). While neither *cozEa* nor *cozEb* were essential when deleted individually, a synthetic lethal phenotype was observed; a double deletion strain could not be obtained and knockdown of *cozEa* in $\Delta cozEb$ (or vice versa) resulted in significantly reduced growth, aberrant septal placement and cell shapes, frequent cell lysis and a non-homogeneous nucleoid staining. CozEa and CozEb were found to interact with, and modulate the localization of, the cell division regulator EzrA, suggesting that this interaction may be important for the coordination of cell division in this bacterium (Stamsås et al., 2018).

In this work, we demonstrate that there is a link between biosynthesis of LTA and CozE proteins in both MSSA and MRSA strains. We show that the two CozE

proteins have unique functionalities, as CozEb, but not CozEa, modulate the lengths of LTAs. The results presented here give insights into hitherto unknown functions of the transmembrane CozE proteins.

Results

The overlapping role of CozEa and CozEb is conserved in different *S. aureus* strains

In a previous work, we studied the effects of *cozEa* and *cozEb* on growth and cell morphology in *S. aureus* SH1000 and showed that the two genes were synthetic lethal and possessed overlapping functions (Stamsås et al., 2018). We here initially set out to investigate the functional conservation of *cozEa* and *cozEb* across different *S. aureus* strains and characterize the phenotypes in more detail. In the MSSA strain NCTC8325-4, $\Delta\textit{cozEa}::\textit{spc}$ and $\Delta\textit{cozEb}::\textit{spc}$ mutants were constructed by allelic replacement using the temperature-sensitive pMAD-vector (Arnaud et al., 2004), while the *cozEa::Tn* and *cozEb::Tn* mutants in the community associated (CA)-MRSA USA300 strain JE2 were obtained from the Nebraska collection (Fey et al., 2013). Growth- and microscopy analysis displayed similar phenotypes as observed before: single deletions of either *cozEa* or *cozEb* did not alter growth compared to wild-types in these strains (Fig. 1A, Fig. S1A). The cell size distributions were not severely altered, although the JE2 $\Delta\textit{cozEa}$ cells, as well as both NCTC8325-4 mutants, on average were slightly smaller compared to their wild types (Fig. 1B-C, Fig. S2, Fig. S3). To identify possible changes in cell wall synthesis or septum placement, the cells were labelled with fluorescent vancomycin (VanFL), which binds to D-Ala-D-Ala of non-crosslinked peptidoglycan throughout the cell wall. However, no obvious differences were observed between the mutants and the wild-types (Fig. 1B, Fig. S2). Likewise, cell cycle phase distribution analyses (as determined from VanFL labelled cells; Fig. 1D) (Monteiro et al., 2015) did not reveal differences between the mutants and wild-type cells (Fig. 1E, Fig. S2). Thus, the mutants in JE2 and NCTC8325-4 were similar to their respective wild-types in this single-cell analysis, which is consistent with the results from *S. aureus* SH1000 (Stamsås et al., 2018).

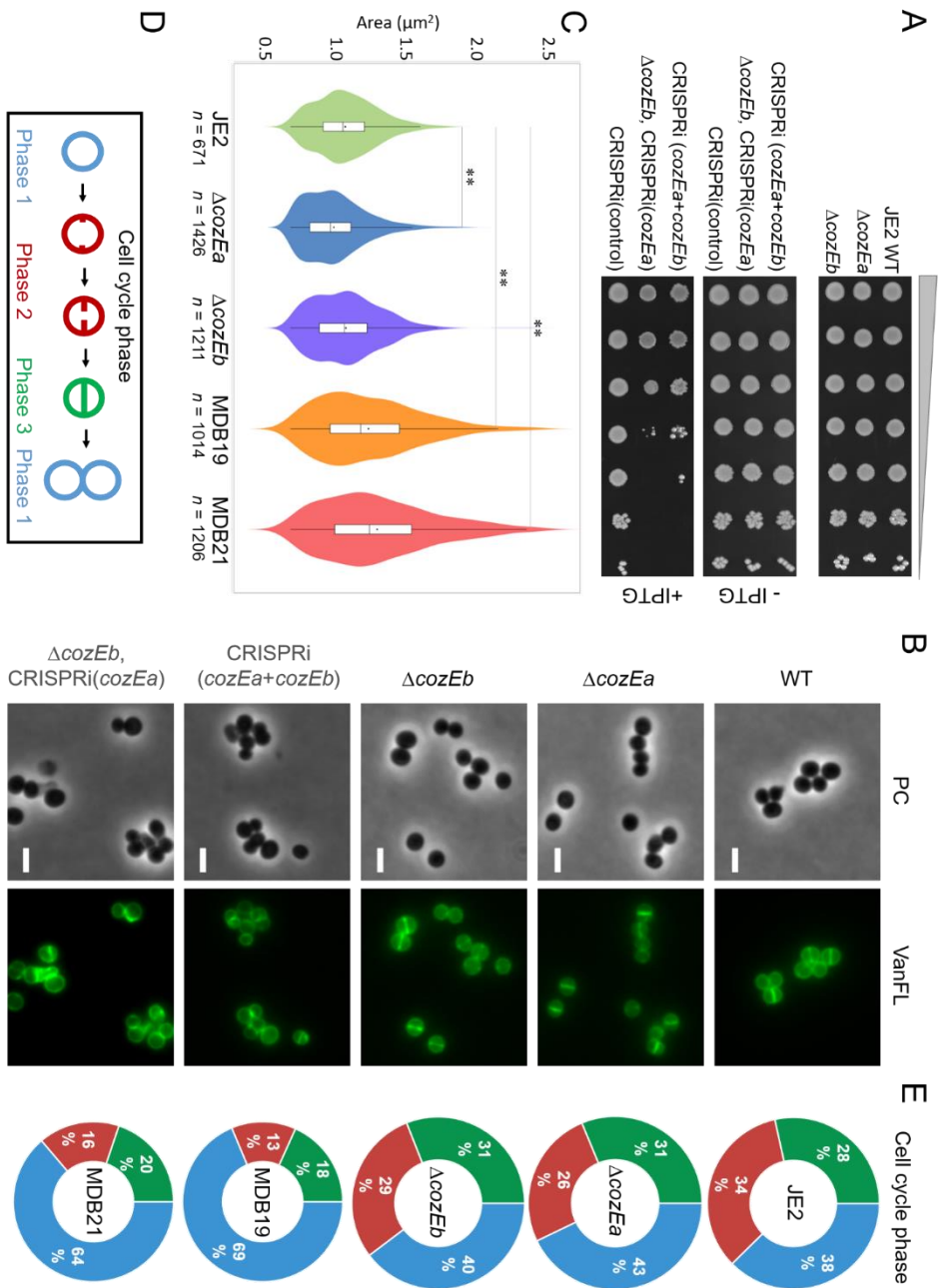


Fig. 1. The phenotypes of *cozEa* and *cozEb* in *S. aureus* JE2. (A) Growth assays of JE2, $\Delta\text{cozEa}::Tn$ and $\Delta\text{cozEb}::Tn$, as well as for CRISPRi double knockdown strain CRISPRi(*cozEa+cozEb*) (MDB19) and combined knockout/knockdown strain $\Delta\text{cozEb}+\text{CRISPRi}(\text{cozEa})$ (MDB21). A CRISPRi-strain with non-targeting sgRNA was used as control (MDB44). Strains were grown over night and 10-fold dilutions were spotted onto agar plates. IPTG was added to the plates

for the CRISPRi-strains, as indicated. **(B)** Micrographs showing phase contrast and VanFL staining of the same strains as in (A). CRISPRi strains grown in medium with IPTG to induce the CRISPRi-system. Scale bars, 2 μm . **(C)** Box plot of the cell areas of JE2 ($1.09 \pm 0.22 \mu\text{m}^2$), $\Delta\text{cozEa}::\text{Tn}$ ($1.01 \pm 0.22 \mu\text{m}^2$), $\Delta\text{cozEb}::\text{Tn}$ ($1.09 \pm 0.24 \mu\text{m}^2$), MDB19 ($1.25 \pm 0.36 \mu\text{m}^2$) and MDB21 ($1.31 \pm 0.39 \mu\text{m}^2$). The cell areas were determined using MicrobeJ. Significant differences between the strains are indicated with asterisks (** indicates two-tailed P-value, $p < 0.01$, derived from a Mann Whitney test in MicrobeJ). The number of cells analyzed in each case is indicated in the figure. **(D)** Schematic outline of different cell cycle phases (distributions in panel E). Cells in phase 1 are in the initial cell cycle phase before initiation of septum formation, cells in phase 2 have initiated synthesis of the division septum, and the cells in the final cell cycle stage (phase 3) have a complete septum. **(E)** Distribution of cell cycle phases for JE2, $\Delta\text{cozEa}::\text{Tn}$, $\Delta\text{cozEb}::\text{Tn}$, MDB19 and MDB21, indicating the percentage of cells in each phase. The distributions were obtained by manual counting the different cell phases of 100-150 random VanFL stained cells from each strain.

As reported previously (Stamsås et al., 2018), a double $\Delta\text{cozEa}\Delta\text{cozEb}$ deletion strain could not be obtained. We therefore used an established two-plasmid CRISPR interference (CRISPRi) system for knockdown of gene expression, in which an IPTG-inducible dCas9 is expressed from one plasmid and the gene-specific sgRNA is constitutively expressed from the other plasmid (Stamsås et al., 2018). Similar to what was observed in the SH1000 strain, knockdown of *cozEa* and *cozEb* at the same time or as combined deletion-depletion strain (ΔcozEb , CRISPRi(*cozEa*) and vice versa) in JE2 and NCTC8325-4 caused a clear reduction in growth (Fig. 1A, Fig. S1). These strains also had perturbed cell sizes compared to the wild-type cells and single *cozEa/cozEb* deletions (Fig. 1B-C, Fig. S2, Fig. S3). By investigating their cell cycle phases, we observed an over-representation of phase 1 cells and under-representation of phase 2 and phase 3 cells compared to the wild-type (Fig. 1D, Fig. S2). This confirms that cell division coordination is disturbed in cells lacking both CozE proteins (Stamsås et al., 2018), and specifically indicates that initiation of septum synthesis is inhibited in these cells.

There is a synthetic genetic link between the *cozE* genes and genes involved in LTA synthesis

Mutants lacking both their CozE proteins displayed phenotypes such as morphological abnormalities and impaired control of septum formation (Fig. 1, Fig. S2) (Stamsås et al., 2020), resembling that of *S. aureus* mutants with defects in LTA biosynthesis (*AltaS*, *AltaA* and *AugtP*) (Grundling & Schneewind, 2007a; Grundling & Schneewind, 2007b; Hesser et al., 2020a; Kiriukhin et al., 2001; Oku et al., 2009) (Fig. 2A). In this context it is also interesting to note that in a study by Corrigan et al. (2011), re-sequencing of *ltaS* deletion mutants resulted in the identification of

potential suppressor mutations (both nonsense and a missense mutation) in *cozEb* (SAOUHSC_01358). Together, this prompted us to investigate a potential link between CozE proteins and LTA synthesis.

Three sgRNA plasmids, each targeting an LTA synthase or modification gene (*ugtP-ltaA*, *ltaS*, or *dltABCD*), were made. UgtP and LtaA are encoded within the same operon and were therefore depleted together. The same is true for DltABCD which together are responsible for the TA D-alanylation. No reduction in growth rate was observed upon depletion of DltABCD in a wild-type background, although the cells entered stationary phase at a slightly lower optical density than non-depleted cells (MDB93, Fig. 2B). Knockdown of *ugtP-ltaA* and *ltaS*, on the other hand, caused a reduction in growth, with somewhat more dramatic effects for *ugtP-ltaA* (MDB35) compared to *ltaS* (MDB85).

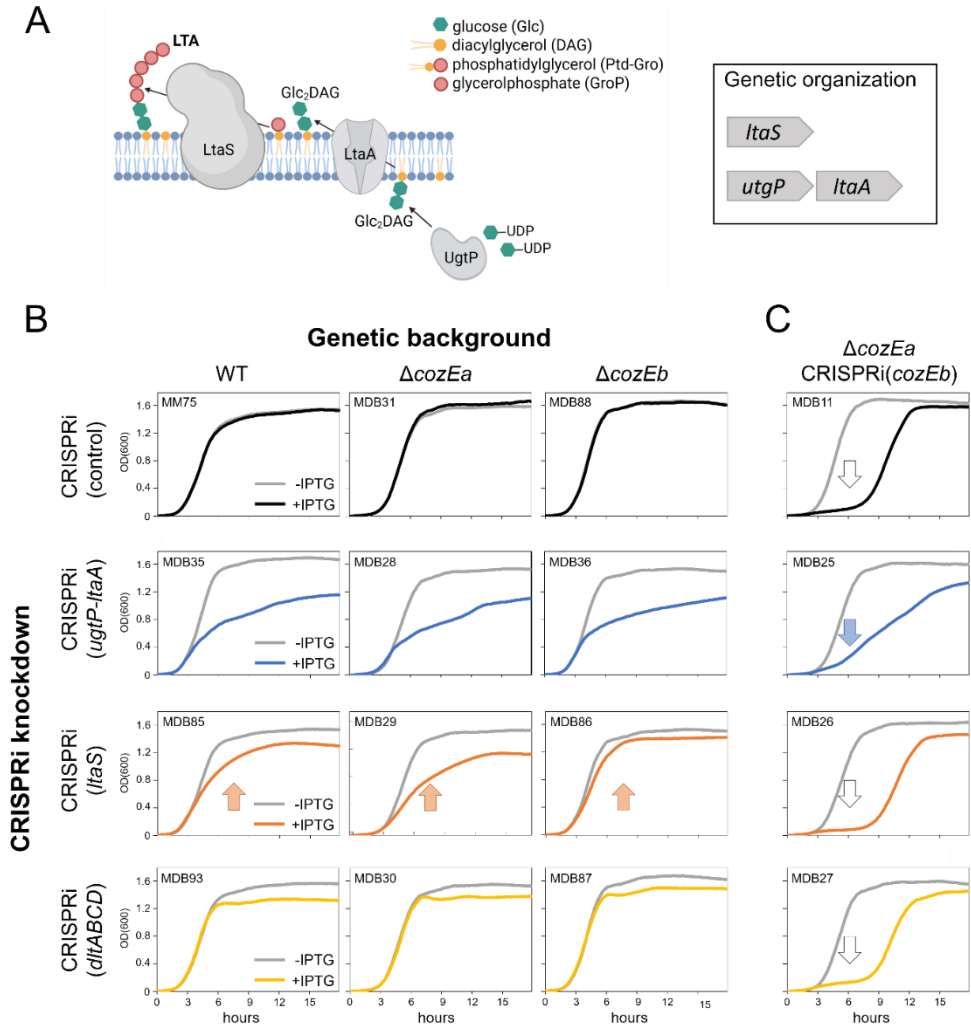


Fig. 2. A synthetic genetic relationship between *cozE* genes and genes involved in LTA biosynthesis. **(A)** Schematic overview of the LTA biosynthetic pathway. UgtP (also known as YpfP) synthesizes the glycolipid anchor Glc₂DAG from UDP-glucose and diacylglycerol (DAG), which is flipped to the outer membrane leaflet by LtaA. LtaS then synthesizes the LTA polymer by transferring glycerolphosphates (from phosphatidylglycerol, Ptd-Gro) to the glycolipid anchor. The genetic organization of *ItaS*, *utgP* and *ItA* is indicated in the box. **(B)** Growth assays to identify possible genetic interactions between *cozE* genes and the LTA biosynthetic pathway. *utgP-ltaA*, *ItaS* or *dltABCD* were knocked down by CRISPRi in either NCTC8325-4 wild-type, Δ *cozEa* or Δ *cozEb* backgrounds. **(C)** Growth assays of mutants where *utgP-ltaA*, *ItaS* or *dltABCD* is knocked down along with both *cozE* proteins. In B and C, the graphs represent averages from triplicate measurements. Cells were grown with or without IPTG, as indicated by the colors. The orange arrows point to growth differences observed between the genetic backgrounds, wild-type, Δ *cozEa* or Δ *cozEb*, in which LtaS was depleted. The blue arrow points to the altered growth pattern observed in strain MDB25 (Δ *cozEa* CRISPRi(*cozEb+utgP-ltaA*)) as compared to MDB11 (Δ *cozEa* CRISPRi(*cozEb*)), MDB26 (Δ *cozEa* CRISPRi(*cozEb+ItaS*)) and MDB27 (Δ *cozEa* CRISPRi(*cozEb+dltABCD*)) (white arrows).

The growth patterns of the resulting strains were then analysed in ΔcozEa and ΔcozEb genetic backgrounds, to see whether the presence of LTA affected the viability of cells lacking CozEa or CozEb (Fig. 2B). For the *dltABCD*- and *ugtP-ltaA* knockdown experiments, no clear changes in growth patterns were observed in ΔcozEa (strain MDB30 and MDB28) nor ΔcozEb (strain MDB87 and MDB36) backgrounds compared to the wild-type (strain MDB93 and MDB35). In contrast, the growth reduction observed for LtaS depleted cells (strain MDB85), was partially alleviated in a ΔcozEb mutant (MDB86). This is in line with the result from Corrigan et al. (2011), assuming that the observed *cozEb* suppressors are loss-of-function mutants. Interestingly, we also observed that growth reduction by LtaS depletion was more severe in the ΔcozEa mutant (strain MDB29) compared to the wild-type (Fig. 2B). Microscopy analysis, however, showed that the severe abnormal cell size and cell division defect in LtaS depleted cells were not significantly changed by the lack of either CozE proteins (Fig. 3A and B). Thus, while the CozE proteins affected growth of LtaS depleted cells (Fig. 2B), LtaS (and thus LTA) is essential for proper cell division both in the presence and absence of CozE proteins.

We further went on to study the growth phenotypes when both CozEa and CozEb were depleted at the same time as the LTA biosynthesis genes (Fig. 2C). As before, depletion of both CozEa and CozEb in a wild-type background resulted in severe growth defects with the growth being almost fully abolished for 10 h (strain MDB11). The same expected growth defect was observed in the cells where LtaS or DltABCD was depleted together with CozEa and CozEb (strain MDB26 and MDB27, Fig. 2C). Note that these strains started growing rapidly after about 10 h. This is most probably caused by reduced functionality of the CRISPRi system after 10 h in this experimental setup. Interestingly, however, when both CozE proteins were depleted together with UgtP and LtaA, a completely different growth pattern was observed (MDB25, blue arrow, Fig. 2C). The growth defect of the control strain (MDB11) was partially rescued, suggesting that the detrimental effect of lacking both CozEa and CozEb is partly alleviated when UgtP and/or LtaA is removed. As mentioned above, the growth defects observed by *ugtP-ltaA* depletion was not worsened in single ΔcozEa or ΔcozEb knockouts (MDB35, MDB28 and MDB36, Fig. 2B). Hence, these results show that the combined function of CozEa and CozEb is affected by the presence of UgtP and/or LtaA.

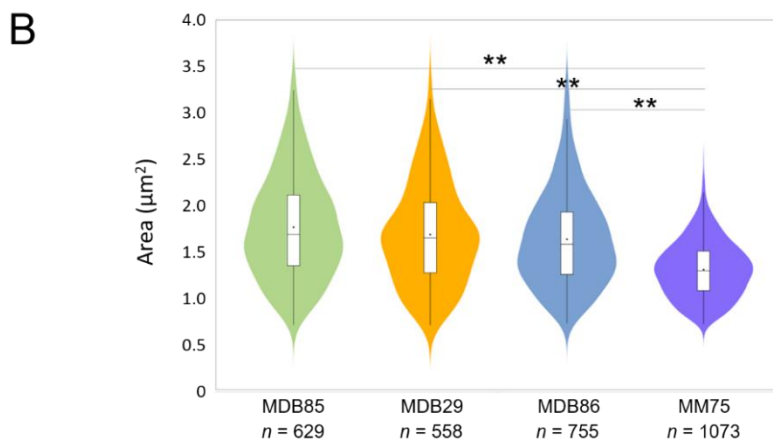
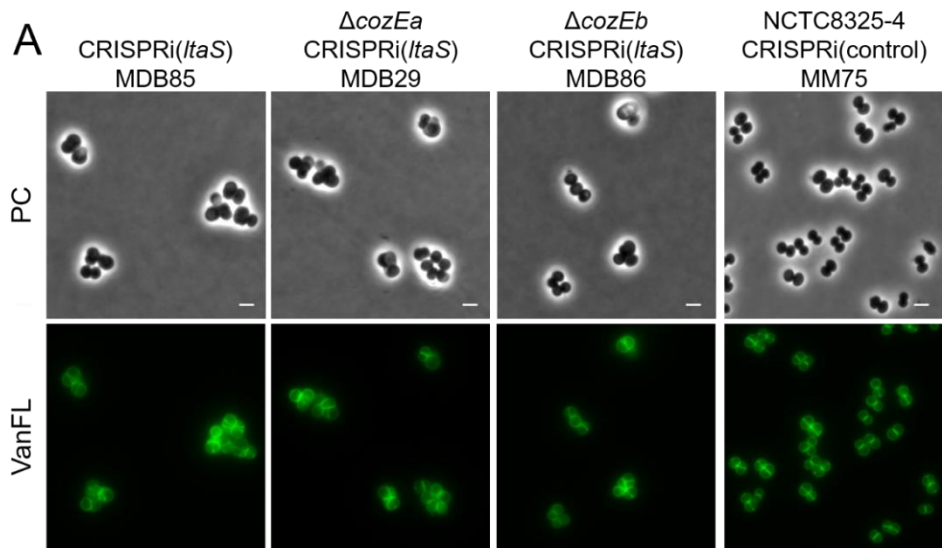


Fig. 3. *LtaS* depletion in *S. aureus* NCTC8325-4. **(A)** Phase contrast micrographs and fluorescent images from labelling with VanFL of *LtaS* depletion in wild-type background (MDB85), in Δ *cozEa* background (MDB29) and in Δ *cozEb* background (MDB86). The NCTC8325-4 CRISPRi control strain (MM75) with a non-targeting sgRNA was included for comparison. Strains were grown in the presence of IPTG for induction of the CRISPRi-system. Scale bars, 2 µm. **(B)** Box plot of cell areas for the same strains as in A (MDB85; $1.76 \pm 0.55 \mu\text{m}^2$, MDB29; $1.68 \pm 0.55 \mu\text{m}^2$, MDB86; $1.63 \pm 0.51 \mu\text{m}^2$, MM75; $1.30 \pm 0.31 \mu\text{m}^2$). The cell areas were determined using MicrobeJ. Significant differences between the mutants are indicated with asterisks (** indicates two-tailed P-value, $p < 0.01$, derived from a Mann Whitney test in MicrobeJ). The number of cells analyzed in each case is indicated in the figure.

LtaA and UgtP modulate the essentiality of CozE proteins

To further understand how *ugtP-ltaA* knockdown alleviated the growth inhibition of CozEab depleted cells, JE2 strains with single deletions of *ugtP* ($\DeltaugtP::Tn$) and *ltaA* ($\DeltaltaA::Tn$) were obtained from the Nebraska library (Fey et al., 2013). The CRISPRi systems to target *cozEa*, *cozEb* or both *cozEa* and *cozEb* simultaneously, were transformed into these strains. Both $\DeltaugtP::Tn$ and $\DeltaltaA::Tn$ grew almost as the wild-type under the tested conditions and no changes in growth were observed upon knockdown of the individual *cozE* genes in the JE2 \DeltaugtP or \DeltaltaA cells (Fig. S4). Strikingly, however, knockdown of *cozEa* and *cozEb* simultaneously, in \DeltaugtP or \DeltaltaA caused dramatic, but opposite, alterations to the growth patterns (Fig. 4A). In the \DeltaugtP mutant, depletion of both CozE proteins (MDB45) resulted in a synthetic sick phenotype with reduced growth compared to the cells depleted of only the CozE proteins (MDB19). On the contrary, in the \DeltaltaA mutant, depletion of both CozE proteins simultaneously had no negative effect on growth (MDB46). Thus, the CozE proteins appear to have lost their importance when the flippase LtaA is absent. The same growth pattern was observed both in liquid cultures and when cells were spotted on agar.

To further confirm these intriguing, opposite growth alterations observed in the \DeltaugtP and \DeltaltaA JE2 mutants, we conducted the same analysis in *S. aureus* NCTC8325 cells. An *S. aureus* NCTC8325 \DeltaltaA strain was obtained (Zhang et al., 2020), and a $\DeltaugtP::spc$ mutant strain was constructed in the same strain background. In contrast to JE2 (Fig. 4A), severe growth reduction was observed for both \DeltaltaA , and in particular \DeltaugtP , in the NCTC8325 background (Fig. 4B). Clearly, however, the same CozE-mediated growth patterns were observed in the NCTC8325 strains (Fig. 4B): double depletion of CozEa and CozEb was detrimental for growth in a wild-type background (MDB75), and while the growth was further reduced in \DeltaugtP (MDB84), \DeltaltaA alleviated this effect (MDB76) (Fig. 4B).

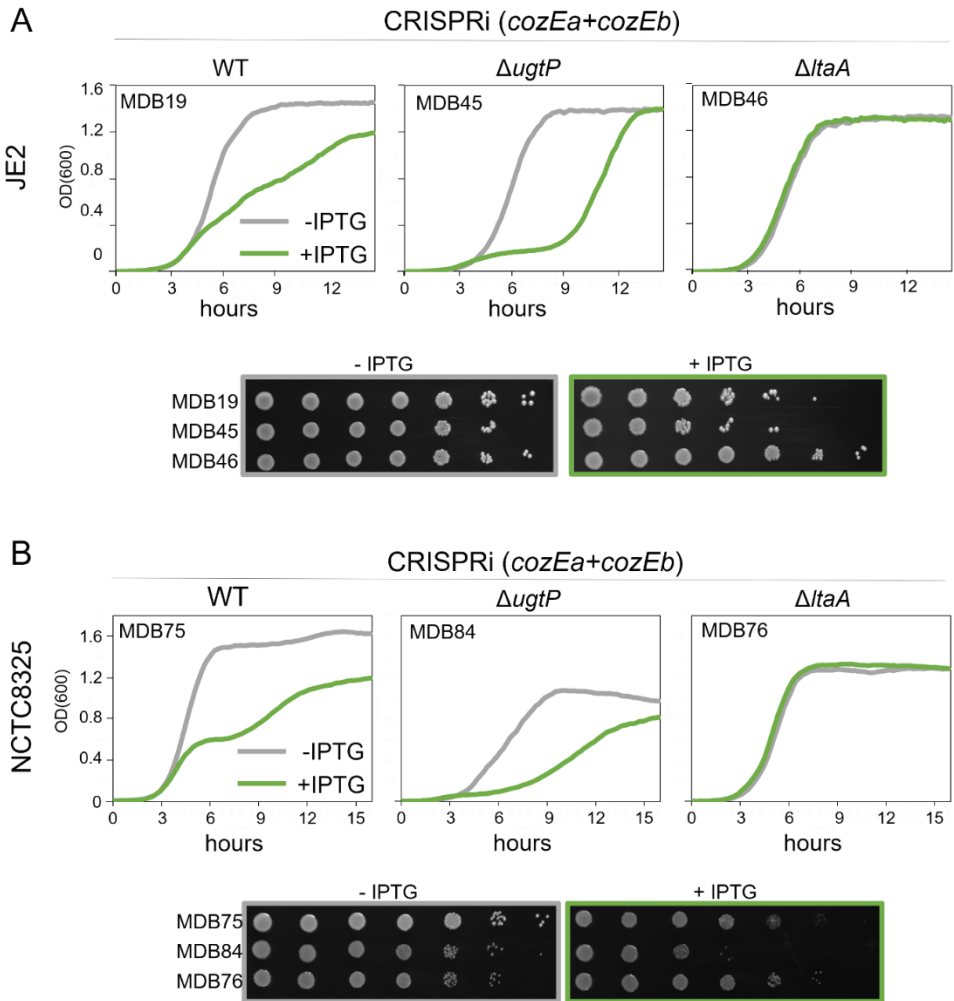


Fig. 4. Growth of double *CozE* depletion strains in different genetic backgrounds of *S. aureus* JE2 and NCTC8325. Growth of (A) JE2 and (B) NCTC8325, with wild-type, \DeltaugtP and \DeltaltaA genetic backgrounds, with or without depletion of *CozEa* and *CozEb* in liquid cultures (top panels) or on agar plates (bottom panels). Cells were grown in the presence or absence of IPTG, as indicated by the colors. Strain names are indicated in the figure.

Single cell analyses of the combined mutants further corroborated the pairwise synthetic genetic interaction between *ugtP*, *ltaA* and *cozE* genes (Fig. 5). The mis-regulation of septal synthesis and cell size defects observed in cells lacking both *cozEa* and *cozEb* were further elevated when also *UgtP* was absent, as observed by phase contrast imaging and staining with VanFL (MDB19 and MDB45, Fig. 5A and B). On the other hand, in the \DeltaltaA cells, depletion of *CozEa* and *CozEb* did not result in

such changes observed by VanFL labelling (Fig. 5A), and the cell size distribution was more similar to the control cells (MDB46 and MDB44, Fig. 5B). We also stained these cells with DAPI to visualize the nucleoids, since perturbed DAPI staining was previously observed for *S. aureus* with double depletion of CozEa and CozEb (Stamsås et al., 2018). As expected, cells with highly intense DAPI signals were observed for the double CozE depleted strain, as well as for the strain also lacking UgtP, while this phenotype was rescued in the $\Delta ltaA$ background which had a DAPI staining pattern similar to the wild-type (Fig. 5A).

Finally, we performed transmission electron microscopy (TEM) on the same strains. As observed before (Stamsås et al., 2018), cells depleted of both CozE proteins displayed a large fraction of lysed cells (Fig. S5A) and misplaced and abnormal septa (Fig. 6A), and this phenotype was further aggravated in a $\Delta ugtP$ background (Fig. 6B, Fig. S5B). However, in the $\Delta ltaA$ genetic background, the double *cozE* knockdown had a wild-type like appearance, with few lysed cells and virtually no misplaced septa (Fig. 6C and Fig. S5C). Together this shows that, in a genetic background where UgtP is absent, and no Glc₂DAG precursor is produced, CozE proteins seem to be more essential than in a wild-type background. On the other hand, in a strain background where LtaA is lacking, and thus the flipping of Glc₂DAG to the outer membrane leaflet is reduced, the CozE proteins seem to have partially lost their functional importance.

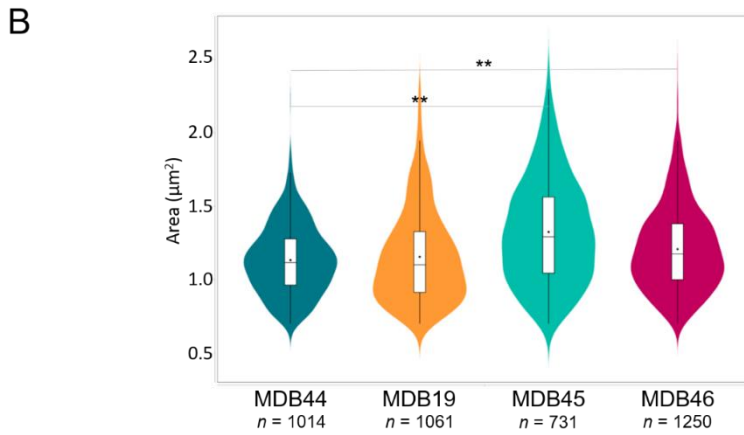
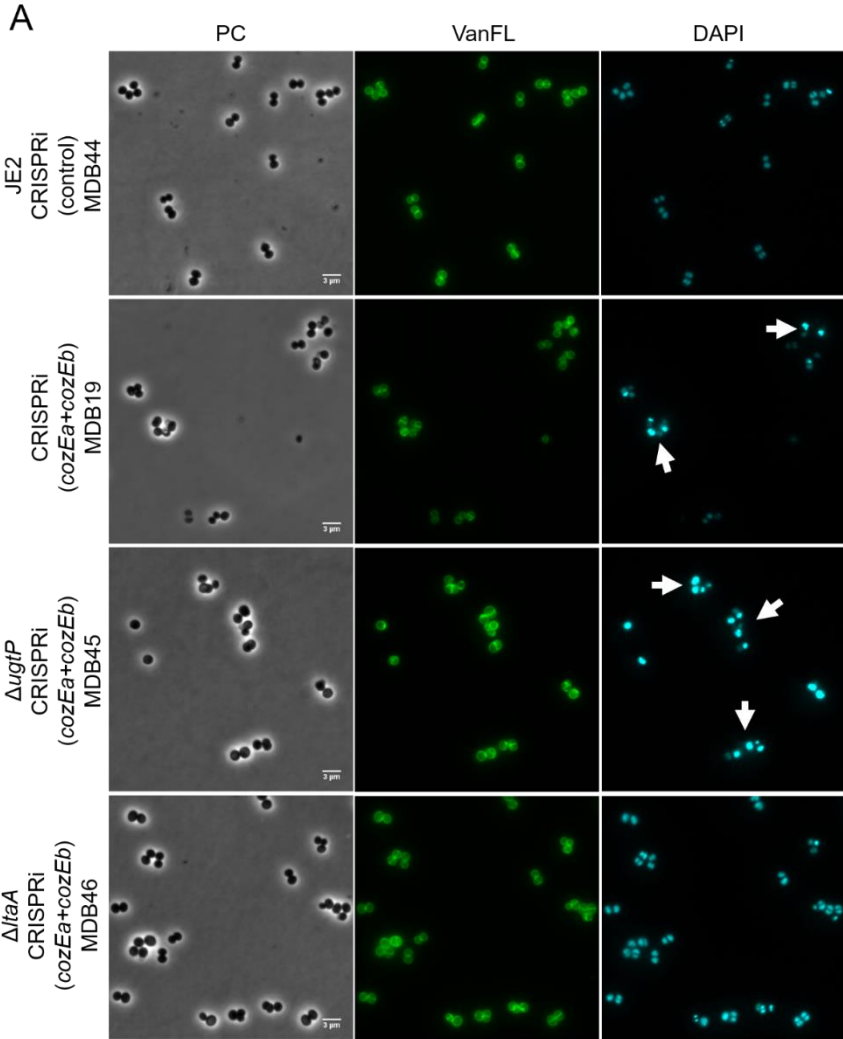


Fig. 5. Microscopy analysis of *S. aureus* JE2 wild-type and \DeltaugtP and $\Delta ltaA$ mutants depleted of CozEa and CozEb. A CRISPRi non-targeting control strain was also included. **(A).** Phase contrast (PC) images are shown along with fluorescence images from labelling with VanFL and DAPI. JE2 carrying a CRISPRi-system with no target was used as a control. Scale bar, 3 μm . **(B)** Box plot of cell areas of the same cells (MDB44; $1.13 \pm 0.25 \mu\text{m}^2$, MDB19; $1.15 \pm 0.25 \mu\text{m}^2$, MDB45; $1.32 \pm 0.35 \mu\text{m}^2$, MDB46; $1.21 \pm 0.28 \mu\text{m}^2$). The cell areas were determined using MicrobeJ. Significant differences between the strains are indicated with asterisks (** indicates two-tailed P-value, $p < 0.01$, derived from a Mann Whitney test in MicrobeJ). The number of cells analyzed in each case is indicated in the figure.

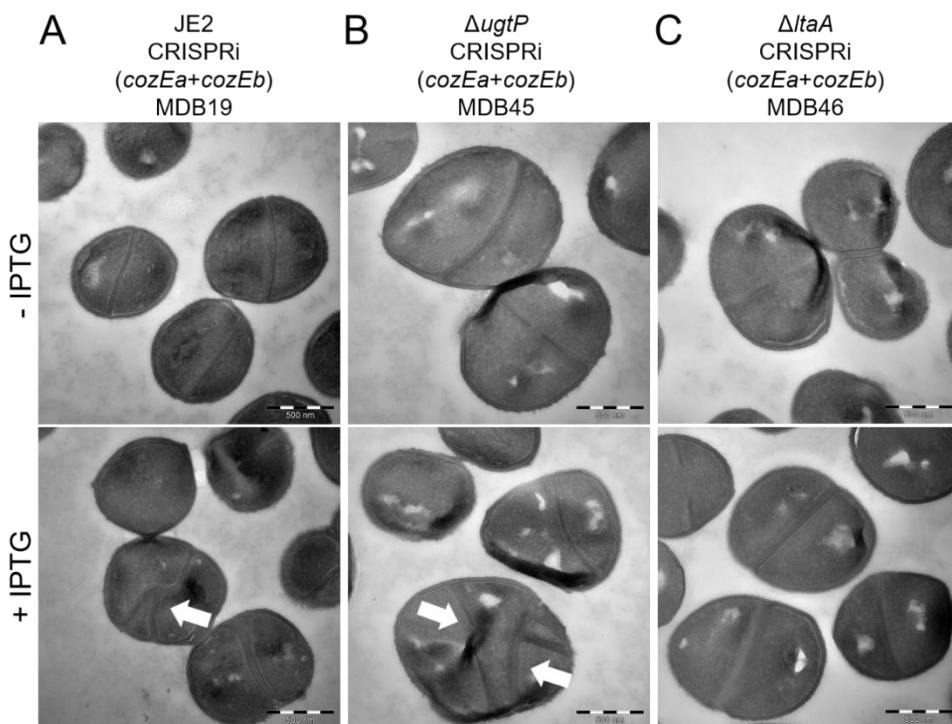


Fig. 6. TEM images of *S. aureus* JE2 **(A)** wild-type cells, **(B)** \DeltaugtP and **(C)** $\Delta ltaA$ mutants with uninduced or induced depletion of CozEa and CozEb. Arrows point to cells with aberrant septum formation. Scale bars, 500 nm.

CozEb, but not CozEa, affects LTA polymer length

The results above demonstrate an intriguing genetic link between LTA biosynthesis and the CozE proteins. Previous studies have demonstrated that *S. aureus* *ugtP* and *ltaA* deletion mutants displayed growth defects due to production of abnormally long LTA, as a result of the loss of glycolipid anchors (Hesser et al., 2020a; Hesser et al., 2020b). To determine if CozEa and CozEb could influence the LTA length in *S. aureus*, the relative lengths of LTA polymers of exponential phase *S. aureus* were analyzed. Cell lysates were separated by SDS-PAGE and LTA were detected by immunoblotting using an anti-LTA antibody. Interestingly, although slightly, the LTA polymers were consistently longer in the Δ *cozEb* mutants, but not in the Δ *cozEa* mutants. The same observation was made for both NCTC8325-4 and JE2 (Fig. 7A and B). The LTA size in the Δ *cozEa* mutants appear rather similar to the wild-type for both NCTC8325-4 and JE2 (Fig. 7A and B). The LTA size does not increase further in the Δ *cozEb* background combined with CRISPRi(*cozEa*) knockdown (Fig 7A). Furthermore, complementation of the Δ *cozEb* strains, by ectopic expression of *cozEa* and/or *cozEb* from plasmids pRAB11-*cozEa* and pRAB11-*cozEb*, showed that expression of *cozEb*, but not *cozEa* could recover the LTA to wild-type lengths (Fig. 7C and D). The quantity of LTA polymers produced in the cells did not seem to be clearly affected by deletion in either of the *cozE* genes, as indicated by similar band intensities in the immunoblots in >5 repeated assays (Fig. 7). Although it should be noted that the increase of LTA polymer length in the *cozEb* mutant appears to be less dramatic compared to a strain lacking both UgtP and LtaA (Fig. 7A), these results clearly show that CozEb has a role in controlling LTA polymer length in *S. aureus*.

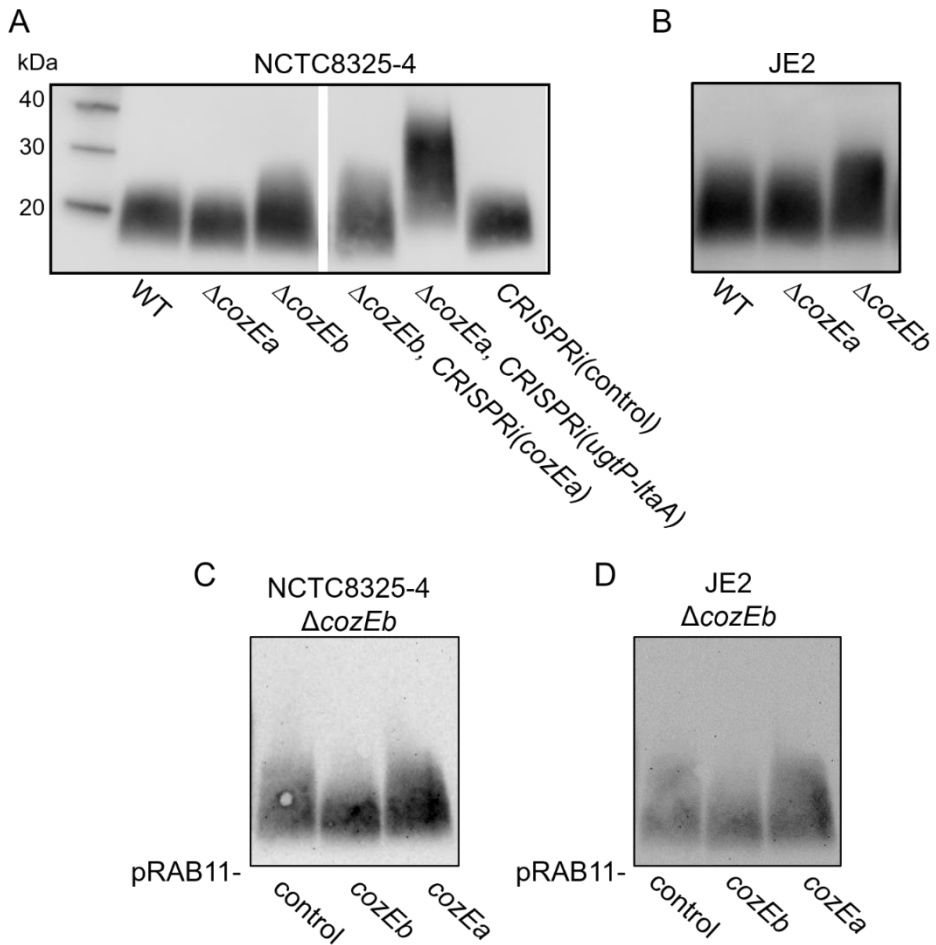


Fig. 7. Immunoblots using anti-LTA antibodies on whole cell extracts. **(A)** NCTC8325-4 wild-type, ΔcozEa , ΔcozEb , the combined knockout/knockdown strains ΔcozEb CRISPRi(*cozEa*) and ΔcozEa CRISPRi(*ugtP-ltaA*), and the CRISPRi-control strain (MM75). **(B)** JE2 wild-type, ΔcozEa and ΔcozEb strains. Complementation experiments in **(C)** NCTC8325-4 and **(D)** JE2. The plasmids pRAB11-*cozEb* and pRAB11-*cozEa*, as well as a pRAB11 control plasmid, were introduced into the ΔcozEb mutants. Expression of the plasmid-located genes was induced by addition of 0.004 $\mu\text{g/ml}$ aTc.

CozE and the membrane localization of UgtP

Using GFP-fusions expressed from plasmids, we have previously reported that CozEa and CozEb localizes to the membrane of *S. aureus* without any enrichment in the division septum. We further confirmed and studied this in more detail here by chromosomally integrating *cozEa-gfp* and *cozEb-gfp* fusion genes in their native loci in NCTC8325-4 (Fig. 8A). Fluorescence microscopy revealed an uneven, spotty localization in the membrane of both proteins. Interestingly, Reichmann et al. (2014) has demonstrated that UgtP has a similar uneven localization in the membrane of *S. aureus*. UgtP is a 391 amino acids long protein without any predicted transmembrane segments, and the mechanism responsible for the recruitment of UgtP to the membrane, which is independent of its UDP-Glc substrate, is therefore still unknown (Reichmann et al., 2014). Given that *cozEa* and *cozEb* display genetic interactions with LTA biosynthetic genes and that lack of CozEb results in longer LTA polymers, in a similar fashion as cells lacking UgtP, we hypothesized that the CozE proteins could be involved in the recruitment of UgtP to the membrane. To test this, we constructed a strain with a chromosomally integrated ectopic copy of *gfp-ugtP* expressed from its own promoter. Fluorescence microscopy of the resulting strain indeed show that UgtP have a spotty localisation in the bacterial membrane in NCTC8325-4 (Fig. 8B). We then performed single and double knockdown of *cozEa* and *cozEb* in the *gfp-ugtP* expressing strain. Membrane-enriched localization of GFP-UgtP was still observed in all of these strains (Fig. 8B). Bacterial two-hybrid assays, performed to identify potential protein-protein interactions, did also not reveal any direct interaction between UgtP and the CozE proteins (Fig. 8C). Together these results suggest that neither CozEa nor CozEb are localizing UgtP to the membrane via direct protein-protein interactions.

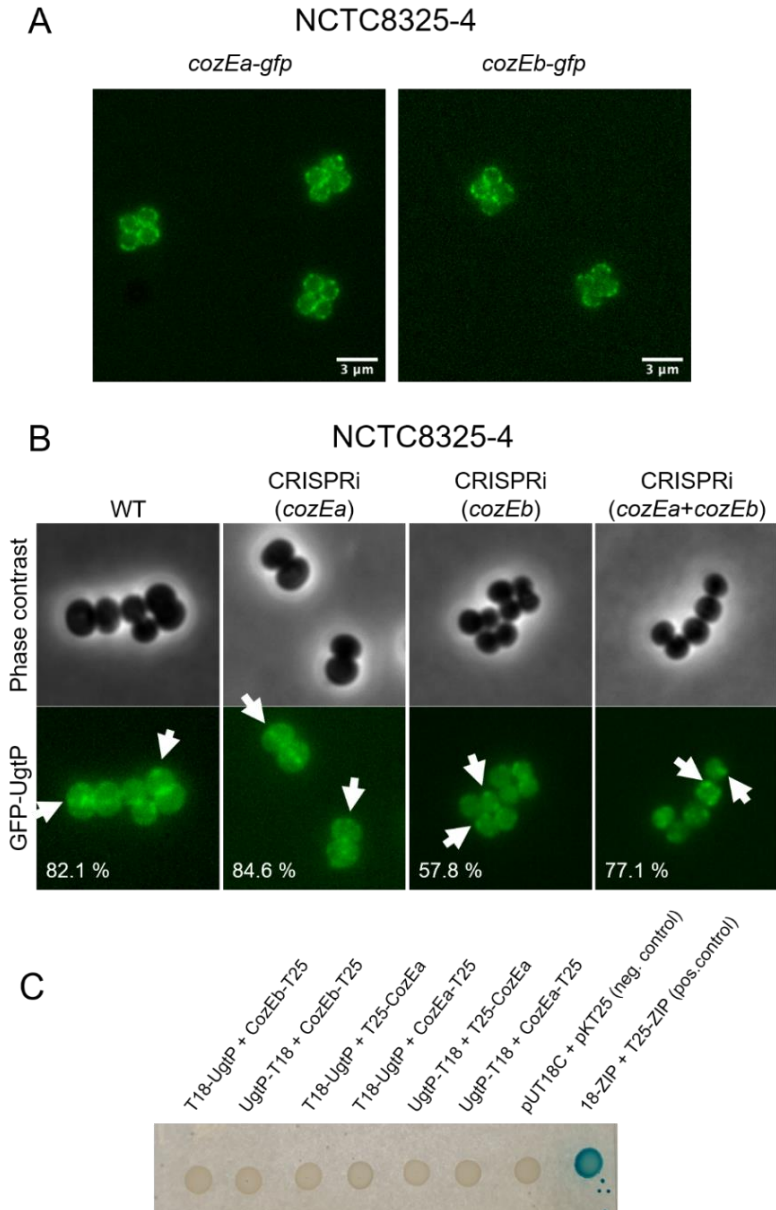


Fig. 8. CozE proteins do not directly influence the membrane-localization of UgtP. **(A)** Localization of CozEa-GFP and CozEb-GFP in *S. aureus* NCTC8325-4. The fusion proteins were expressed from their native, chromosomal loci. **(B)** Localization of GFP-UgtP in NCTC8325-4 wild-type (MDB77), as well as cells depleted of CozEa (MDB89), CozEb (MDB90) or both (MDB79). Phase contrast- and fluorescence images are shown. Arrows point to spots with membrane-localized GFP-UgtP. **(C)** Bacterial two-hybrid interaction assays between CozEa or CozEb and UgtP. Fusions of the proteins to either the T18 or K25 domain of adenylate cyclase were expressed in *E. coli* according to established protocols (Karimova et al., 1998). Blue color indicates positive interaction. Positive and negative controls are included.

Discussion

CozEa and CozEb are two homologous membrane proteins that constitute a synthetic lethal gene pair, whose function(s) are essential for cell growth and division across different *S. aureus* strains. In this work, we have further investigated their cellular roles. In line with what was previously observed for *S. aureus* SH1000, we here show that CozEa and CozEb together play an important role for cell growth and spatiotemporal coordination of cell division in the MRSA strain JE2 and MSSA laboratory strain NCTC8325-4. VanFL-based cell cycle analysis of CozE depleted strains show an enrichment of cells without septa (phase 1), implying that these cells may have a delayed initiation of septal synthesis and further confirms the effect on cell division and septum formation reported previously (Stamsås et al., 2018).

While it is the combined function of CozEa and CozEb that results in the severe single cell phenotypes (Fig. 1, Fig. S1, Fig. S2 and Fig. S3), we here demonstrate for the first time that CozEa and CozEb in fact have unique properties in *S. aureus*. This is shown (i) in the LtaS depletion strains, where deletion of *cozEa* and *cozEb* had opposite effects on growth, (ii) as deletion of *cozEb*, but not *cozEa*, resulted in longer LTA polymers. The notion of the unique functionality of these paralogs is indeed supported by a phylogenetic analysis of CozE proteins from 28 different species within the *Staphylococcaceae* family (Fig. S6). This demonstrates that each species encodes two CozE proteins, and that within the genera *Staphylococcus* and *Micrococcus*, the two proteins clusters into two separate subgroups, corresponding to CozEa and CozEb (Fig. S6). The conserved phylogenetic division across the family indicates that the function of CozEa and CozEb are unique and conserved among *genera*. It should be noted that, CozE proteins from more distantly related genera (within the *Jeotgalicoccus*, *Salinicoccus*, and *Nosocomiicoccus*) do not display this subclassification, but instead clusters in a separate group closer to CozEa. This indicate that the CozEb function may be unique for the *Staphylococcus* and *Micrococcus* genera. Furthermore, knowing that the two CozE homologs in *S. pneumoniae* have unique properties (Stamsås et al., 2020), it is not surprising that the same is also true for the *S. aureus* homologs.

Importantly, we here identified a link between the CozE proteins and lipoteichoic acid biosynthesis. Mutants with defects in LTA biosynthetic genes are known to display cell division defects and increased lysis in *S. aureus* (Grundling & Schneewind, 2007a; Hesser et al., 2020a; Kiriukhin et al., 2001), and these phenotypes are consistent with the alterations observed in mutants lacking both CozE proteins. Furthermore, we here also observed some intriguing genetic interactions. Firstly, as

mentioned above, CozEa and CozEb have opposite effects on the growth of cells depleted of the LTA synthase LtaS. The growth defect resulting from LtaS depletion in wild-type background, is aggravated in ΔcozEa , while we found that deletion of *cozEb* partially rescues the growth defect of LtaS depletion. This latter result is in line with Corrigan et al. (2011), who identified both missense- and nonsense mutations in the *cozEb* gene when *ltaS* was deleted. Thus, in cells completely lacking LTA, the function of CozEa thus seems to become more important, while the function of CozEb is detrimental for growth in this background. It should be noted, however, that depletion of LtaS still resulted in highly aberrant cell morphologies and cell division defects in both the ΔcozEa and ΔcozEb backgrounds, demonstrating that LTA synthesis is required for normal cell division in all these strains. Secondly, and more noticeable, when the flippase LtaA is deleted, resulting in reduced flipping of the glycolipid anchor Glc₂DAG, the essentiality of CozEa and CozEb appears to be alleviated. *cozEa/cozEb* and *ltaA* thus display a synthetic viable genetic relationship. The opposite seems to be true for ΔugtP cells, in which synthesis of the glycolipid anchor is lacking completely. In these cells, CozEa and CozEb are more essential than in wild-type background.

Currently, we do not understand all the molecular basis for the reported observations. While the ΔugtP mutant cannot produce the Glc₂DAG glycolipid, the ΔltaA mutant still synthesizes Glc₂DAG on the inner membrane leaflet and produce a mixture of LTAs linked to both Ptd-DAGs and Glc₂DAGs. Although these cells lack the LtaA flippase activity, there must exist another yet unknown mechanism that can translocate Glc₂DAG to the outer membrane leaflet (Grundling & Schneewind, 2007a). In cells lacking, or with reduced levels of, the Glc₂DAG on the extracellular side (such as ΔugtP and ΔltaA), the cells can use Ptd-Gro as alternative starter unit for LTA synthesis (Kiriukhin et al., 2001). LTA polymers formed on Ptd-Gro are longer than those formed on Glc₂DAG, and the starter unit ratio Glc₂DAG/Ptd-Gro affects the polymer length (Hesser et al., 2020b). Based on the observed genetic interactions, involving *ugtP* and *ltaA*, along with the longer LTA polymers observed for ΔcozEb , it is tempting to speculate that CozE proteins may be affecting processes related to synthesis or flipping of LTA starter units. If this is the case, lack of CozE proteins would change the lipid distribution and homeostasis of the membrane and influence synthesis of LTA. Such a mechanism could also explain why CozE proteins are so widely distributed in bacteria (since the same lipids are found across bacterial phyla), but at the same time result in variable phenotypes between species (since lipid composition and function may vary between species). This could also explain why overexpression of staphylococcal CozE proteins could complement the phenotype of

cozE deletion in *S. pneumoniae* in our previous study (Stamsås et al., 2018). However, this hypothesis has to be further investigated experimentally, for instance by analysing lipid levels and differences in lipids between bilayers. Furthermore, this hypothesis does not fully explain why the depletion of both CozE proteins had opposite effects in Δ *ltaA* and Δ *utgP* mutants.

CozE proteins are distributed throughout the membrane similarly to UgtP and LtaA, but unlike LtaS that predominantly accumulates at the cell division site (Reichmann et al., 2014). UgtP, the enzyme synthesizing the LTA glycolipid anchor, was shown previously (Reichmann et al., 2014), and here, to have a spotty localization in the membrane in *S. aureus* (reminiscent of CozE proteins), but the membrane targeting mechanism for this cytoplasmic protein is unknown. We therefore hypothesized that CozEb (and/or CozEa) might play a role in recruiting UgtP to the cytoplasmic membrane, since the loss of membrane localization could result in partial loss of function for UgtP, consistent with the longer LTA polymers found in both Δ *utgP* (Hesser et al., 2020a; Hesser et al., 2020b) and Δ *cozEb* mutants. However, no direct interaction between UgtP and CozE proteins were detected and GFP-UgtP still localized to the membrane in CozE depleted cells (Fig. 8B). On the other hand, it should be noted that upon quantification of the fraction of cells with membrane-enriched localization (Fig. 8), we found that while 75.9 (\pm 6.2) % of the wild-type cells (n = 190) had such localization, this was reduced to 51.4 (\pm 6.4) % (n = 237) in CozEb depleted cells. The CozEa depletion (74.1 (\pm 10.4) % membrane localized GFP-UgtP, n = 246) and the double CozE-depletion (65.4 (\pm 11.7) %, n = 179), however, were more similar to wild type. Together this suggest that the activity of CozE in fact may have an effect on the membrane localization of GFP-UgtP, but this is most likely not mediated via direct protein-protein interactions. The localization of the UgtP-homologue in *Bacillus subtilis* has been shown to depend on its substrate UDP-Glc, although the subcellular localization is dynamic and influenced by growth conditions (Chien et al., 2012; Nishibori et al., 2005; Weart et al., 2007). The UDP-Glc dependency for localizing UgtP is probably not the same for *S. aureus* (Reichmann et al., 2014). It is thus possible that CozEb affects another protein(s) or molecule(s) that are responsible for the recruitment of UgtP to the membrane, however, future research is needed to solve this question.

It has previously been shown in *S. pneumoniae* that CozE proteins are involved in spatiotemporal localization of peptidoglycan synthesis through their interaction and control of the bifunctional class A PBP (Fenton et al., 2016; Stamsås et al., 2020). However, no interactions have been found between CozEa/CozEb and any of the PBPs found in *S. aureus* (Stamsås et al., 2018). The early cell division protein

EzrA, which is important for linking Z-ring formation and the cell wall synthesis machinery, is the only protein found to have a direct interaction to both CozEa and CozEb. The CozE proteins in *S. aureus* therefore may affect peptidoglycan synthesis via this interaction (Stamsås et al., 2018; Steele et al., 2011). It is indeed well established that there are also tight links between LTA biosynthetic proteins and proteins involved in cell division in *S. aureus*, including EzrA (Reichmann et al., 2014). In this context, it should also be noted that in *B. subtilis*, changes in the UgtP activity directly affected the assembly of the division ring and UgtP has been suggested to function as a metabolic sensor governing cell size in this bacterium (Weart et al., 2007). Thus, the connections between LTA and cell division are widespread, and future research should aim to decipher these connections in detail to understand whether the disturbance of cell division in the double CozE knockdown are direct or indirect as a result of effects on LTA synthesis or lipid homeostasis (see hypothesis above).

In this work we show that the CozE proteins, and CozEb in particular, affect LTA biosynthesis in *S. aureus*. While the exact mechanisms remain elusive, the results further improve our understanding of the complex pathways linking LTA biosynthesis and cell division. Furthermore, given the importance of TA for viability and pathogenicity, understanding the role of CozE proteins in this pathway, can potentially uncover a novel antibiotic- or anti-virulence target in these pathogens.

Methods

Bacterial strains and growth conditions

Strains used in this work are listed in Table S1. *S. aureus* strains NCTC8325-4 and JE2-USA300 (called JE2 here) were standardly grown in BHI medium with shaking or on BHI agar plates at 37°C. *Escherichia coli* strain IM08B was grown in LB with shaking or on LA plates at 37°C. When appropriate, antibiotics were added for selection: 100 µg/ml ampicillin and/or 50 µg/ml kanamycin for *E. coli*, 100 µg/ml spectinomycin, 5 µg/ml erythromycin and/or 10 µg/ml chloramphenicol for *S. aureus*. Isopropyl β-D-1-thiogalactopyranoside (IPTG; 500 µM) and anhydrotetracycline (aTc; 0.004 µg/ml) were added for induction of transcription when needed.

For transformation of *E. coli*, chemically competent cells were prepared using calcium-chloride treatment followed by transformation with heat shock according to standard protocols. *S. aureus* strains were transformed by electroporation with plasmids isolated from *E. coli* IM08B as described previously (Lofblom et al., 2007).

Strain construction

A list of all strains constructed in this work are shown in Table S1. Primers used for cloning are shown in Table S2. All constructs were verified by PCR and sequencing.

Deletion of *cozEa* and *cozEb* (*cozEa::spc* and *cozEb::spc*). Deletion of *cozEa* and *cozEb* in *S. aureus* NCTC8325-4 was done using the temperature-sensitive pMAD system, following the same approach as described before (Stamsås et al., 2018).

Deletion of *ugtP* (*ugtP::spc*). pMAD- Δ *ugtP::spc* was constructed to allow deletion of *ugtP* from the chromosome of *S. aureus*. Three fragments were initially amplified (using primers in Table S2): (1) the *ugtP* upstream sequence (*ugtP_up*), (2) a spectinomycin resistance cassette (*spc*), and (3) the *ugtP* downstream sequence (*ugtP_down*). gDNA from *S. aureus* NCTC8325-4 was used as template DNA for amplification of both *ugtP_up* and *ugtP_down*, while pCN55 (Charpentier et al., 2004) was the template for amplification of *spc*. The primers were designed with overlapping sequences to allow fusion of the three fragments by overlap extension PCR. The resulting fragment was digested with BamHI (introduced with outer primer mk506) and NcoI (naturally occurring restriction site near the 5' end of the fragment) and ligated into the corresponding sites of pMAD. The plasmid was verified by PCR and sequencing and the standard pMAD protocol (Arnaud et al., 2004) was used to replace *ugtP* with the *spc*-marker. Note that the *ugtP*-fragment was amplified without any terminator sequence to avoid downstream effect on transcription of *ltaA*.

Chromosomal integration of P_{ugtP} -*gfp-ugtP spc* in an ectopic locus. The *gfp-ugtP* fusion gene, driven by the *ugtP*-promoter, was integrated into a neutral locus (between genes SAOUHSC_03046 and SAOUHSC_03047) on the *S. aureus* NCTC8325-4 chromosome using the pMAD-system. To construct the plasmid pMAD- P_{ugtP} -*gfp-ugtP_spc*, *gfp* was first fused to *ugtP* by restriction cloning; *ugtP* was amplified from gDNA of *S. aureus* NCTC8325-4 and ligated into the NcoI and BamHI restriction sites of pLOW-*m(sf)gfp*-SAOUHSC_1477 to produce plasmid pLOW-*gfp-ugtP*. Then, four fragments constituting the insert of the pMAD- P_{ugtP} -*gfp-ugtP_spc* plasmids were amplified: (1) The upstream integration region ("ori_up"), (2) the *ugtP*-promotor (" P_{ugtP} "), (3) the "*gfp-ugtP*", and (4) a spectinomycin resistance cassette spliced with the DNA sequence downstream of the target gene ("*spc*+ori_down"). Both ori_up and P_{ugtP} were amplified using gDNA from *S. aureus* NCTC8325-4 as template, while purified pLOW-*gfp-ugtP* and pMAD-ori-*parS* were used as template DNA for amplification of *gfp-ugtP* and *spc*+ori_down, respectively. Primers are shown in Table

S2. The fragments were spliced by overlap extension PCR and ligated into pMAD using the EcoRI and Sall restriction sites introduced by the outer primers. The standard pMAD protocol (Arnaud et al., 2004) was used to integrate the construct into the chromosome of *S. aureus* NCTC8325-4.

Construction of pRAB11 complementation plasmids

The genes of *cozEa*, *cozEb* and *lacA* (control) were amplified from gDNA of *S. aureus* SH1000 with primers (found in Table S2) containing KpnI and EcoRI as overhang. Purified PCR products and the plasmid pRAB11 (Helle et al., 2011) were digested with KpnI and EcoRI, and subsequently ligated using T4 DNA Ligase. Ligation mixtures were transformed into *E. coli* IM08B and verified by PCR and sequencing before being electroporated to *S. aureus*.

CRISPR interference

The two-plasmid CRISPR interference system was used as described previously (Stamsås et al., 2018). Strains were transformed with a plasmid carrying an IPTG-inducible *dcas9* (pLOW-*dcas9*) and a plasmid carrying the gene-specific sgRNA with constitutive expression (pCG248-sgRNA(*xxx*) or pVL2336-sgRNA(*xxx*), where *xxx* denotes the target gene). The sgRNA plasmids were constructed using inverse PCR in pCG248 (Stamsås et al., 2018) or Golden Gate cloning in plasmid pVL2336 (unpublished) using oligos in Table S2.

Construction of chromosomally integrated *cozEa-gfp* and *cozEb-gfp* fusions

Chromosomal fusions of *cozEa-gfp* and *cozEb-gfp* in their native loci were made using the pMAD-vector. For construction of pMAD-*cozEa-gfp_spc*, the *cozEa-gfp* fusion was amplified from plasmid pLOW-*cozEa-gfp* using primers mk432 and mk433, while the *spc*-cassette and the *cozEa* downstream region was amplified from plasmid pMAD-*cozEa::spc* using primers mk188 and mk434. The two fragments were fused by overlap extension PCR and ligated into pMAD using the NcoI and Sall restriction sites introduced in the primers. Similarly, for pMAD-*cozEb-gfp_spc*, the *cozEb-gfp* fusion was amplified from plasmid pLOW-*cozEb-gfp* using primers mk435 and mk433, while the *spc*-cassette and the *cozEb* downstream region was amplified from plasmid pMAD-*cozEb::spc* using primers mk188 and mk436. The two fragments were fused by overlap extension PCR and ligated into pMAD using the NcoI and Sall restriction sites introduced in the primers. A standard pMAD protocol (Arnaud et al., 2004) was used for chromosomal integration of the fusions.

Growth assays in liquid media

The bacterial strains to be monitored were firstly grown overnight in BHI medium with the respective antibiotics. They were then diluted 1:1000 in fresh BHI medium with the respective antibiotics and inducers added when appropriate. Bacteria were then applied to a 96-well microtiter plate and incubated in a plate reader at 37°C for 18-20 h. OD₆₀₀ measurements were taken every 10 minutes. The plate was shaken for 2-5 seconds before every measurement. All growth curves in this work are the mean value of three replicate measurements.

Spotting assays to analyze growth on plates

Cells grown overnight in BHI medium were serially 10-fold diluted in fresh medium with antibiotics and IPTG for induction (when appropriate). Each overnight culture and its serial dilutions were spotted onto the appropriate BHI agar plates with a volume of 2 µl. The plates were incubated at 37°C for 17 to 20 h. Images of the plates were captured using a Gel Doc™ XR+ Imager (Bio-Rad Laboratories).

Epifluorescence- and phase contrast microscopy

For microscopy analysis, strains were first grown overnight in BHI medium with the respective antibiotics. The overnight cultures were diluted 1:1000 in fresh BHI medium containing the proper antibiotics and incubated until OD₆₀₀ reached 0.4. Inducers were added when necessary. The cells were stained with fluorescent vancomycin (VanFL, in which BODIPY is linked to a vancomycin molecule [Invitrogen]) or DAPI (Invitrogen) when appropriate, at final concentrations of 0.8 µg/ml and 7.5 µg/ml, respectively. Bacterial cells were immobilised on agarose pads (1.2 %) before imaging on a Zeiss AxioObserver with ZEN Blue software. The bacteria were visualized with the 100× phase contrast objective, and the pictures were captured using the ORCA-Flash4.0 V3 Digital CMOS camera (Hamamatsu Photonics K.K.).

The distribution of cell sizes among different *S. aureus* strains were determined using MicrobeJ. A stack of phase contrast images of the strain to be analyzed were segmented in MicrobeJ and images were manually examined to discard and/or add cells that were incorrectly segmented. In addition to analysing cell sizes, the cell cycle of the bacteria was also analysed by manual counting the different cell phases (phase 1, 2 or 3) of 100-150 random cells from each strain based on VanFL staining.

Transmission electron microscopy

The bacterial strains to be visualised by TEM were first grown overnight in BHI medium with the respective antibiotics and then diluted 1:1000 in BHI with antibiotics and IPTG added when necessary. The diluted bacterial cultures were incubated at 37°C until they reached an OD₆₀₀ of 0.3. Each of the bacterial cultures (10 ml) were carefully mixed with 10 ml fixation solution, containing 2 % (v/v) paraformaldehyde, 0.1 M cacodylate (CaCo) buffer and 1.25 % (v/v) glutaraldehyde solution (grade I). The tubes were incubated at room temperature for 1 h, followed by incubation at 4°C overnight. The next day, the cells were centrifugated at 5000 × *g* at 4°C for 5 min, and subsequently washed three times with PBS, pH 7.4, and three times with 0.1 M CaCo buffer. The cells were subjected for post-fixation for 1 h with 1 % OsO₄ in 0.1 M CaCo. The CaCo-washing steps were repeated prior to dehydration, involving 10 min incubation steps at increasing concentrations of ethanol (70 %, 90 %, 96 % and 100 %). The samples were next infiltrated with LR White by multiple incubation steps with increasing concentration of embedding media (mixed with EtOH). First, overnight with a 1:3 ratio between LR White and EtOH, second; approximately 4 h with the ratio 1:1, third; 4 h with the ratio 3:1, and finally overnight with only LR White. Lastly, incubation overnight with 100 % LR White at 60°C made the embedding media polymerize into a hard block. All sample blocks were sectioned, 60 nm thin, and stained with uranyl acetate and potassium permanganate. A FEI Morgagni™ 268 Transmission electron microscope were used for examination of the cells. Images of the bacteria were captured using a Veleta CCD camera (Olympus Corporation) with an exposure time of ~1000 ms.

Lipoteichoic acid detection with anti-LTA antibodies

Cells grown overnight in TSB medium were diluted 1:1000 in medium with antibiotics and IPTG for induction (when appropriate). The cultures were incubated at 37°C until they reached an OD₆₀₀ between 0.6 and 0.8, except for MDB45 (JE2 *ΔugtP* CRISPRi(*cozEa+cozEb*)) which was only grown to OD₆₀₀ = 0.28 due to slow growth rate and high degree of cell lysis. The cultures were normalized to an OD₆₀₀ of 0.6 and then harvested by centrifugation at 5400 × *g* for 3 min at 4°C. Detection of LTA was done essentially as described before (Hesser et al., 2020a). The pellets were resuspended in 50 µl staphylococcal lysis buffer (50 mM Tris-HCl pH 7.4, 150 mM sodium chloride and 200 µg/ml lysostaphin) and incubated at 37°C for 10 min. The suspensions were then added 50 µl 4× SDS loading buffer and boiled at 95°C for 30 min. The cell lysates were subsequently centrifuged at 16 000 × *g* for 10 min to pellet cellular debris. The supernatants (60 µl) were transferred to clean tubes containing

60 µl dH₂O. The diluted suspensions were lastly added 0.5 µl proteinase K (20 mg/ml) and incubated at 50°C for 2 h. The samples were separated with SDS-PAGE using a 4-20 % Mini-PROTEAN TGX acrylamide gel (Bio-Rad). Blotting onto a PVDF membrane was performed using a Trans-Blot Turbo System (Bio-Rad). Afterwards, the membrane was blocked in 5 % skimmed milk for one hour at room temperature, before being washed with PBST and incubated for one hour with an anti-LTA primary antibody (Hycult) (diluted 1:4000 in PBST). Next, the membrane was washed three times to remove unbound antibodies, and then incubated for another hour with the anti-Mouse IgG HRP-conjugate (Promega) secondary antibody (diluted 1:5000 in PBST). After incubation, unbound antibodies were removed by washing the membrane 3 times with PBST. Detection was performed using the SuperSignal™ West Pico PLUS Chemiluminescent Substrate kit (Thermo Fisher Scientific). Images of the membrane were captured using an Azure Imager c400 (Azure Biosystems).

Bacterial two-hybrid assays

Both construction of plasmids and procedure for bacterial two-hybrid assays were performed as described (Stamsås et al., 2018). Primers used for plasmid construction are found in Table S2. The assay utilizes adenylate cyclase from *Bordetella pertussis* to detect possible protein interactions by making gene fusions to the T18 or T25 domains of adenylate cyclase (Karimova et al., 1998) in the vectors pKT25, pKNT25, pUT18 or pUT18C (Euromedex). *E. coli* XL1-Blue were used for transformation, and isolated plasmids (with T18 and T25 domains) were co-transformed to *E. coli* BTH101 with kanamycin and ampicillin as selection markers. Five colonies were picked, grown to visible growth, and spotted on plates with the selection markers and additionally 40 µg/ml X-gal and 0.5 mM IPTG. After incubation at 30°C (kept dark) for 20-48 h, plates were inspected, where blue colonies indicated a positive interaction, and white colonies the opposite.

Acknowledgments

We would like to thank the Xue Liu and the Veening lab (University of Lausanne, Switzerland) for the NCTC8325 *ΔltaA* strain. Marita Torrisen Mårli and Zhian Salehian for help with strain construction, and the NMBU Imaging Center for help with transmission electron microscopy.

References

- Arnaud, M., Chastanet, A. & Debarbouille, M. (2004). New vector for efficient allelic replacement in naturally nontransformable, low-GC-content, Gram-positive bacteria. *Appl Environ Microbiol*, 70 (11): 6887-6891. doi: 10.1128/AEM.70.11.6887-6891.2004.
- Bæk, K. T., Bowman, L., Millership, C., Dupont Søgaard, M., Kaeffer, V., Siljamäki, P., Savijoki, K., Varmanen, P., Nyman, T. A., Grundling, A., et al. (2016). The cell wall polymer lipoteichoic acid becomes nonessential in *Staphylococcus aureus* cells lacking the ClpX chaperone. *mBio*, 7 (4): e01228-16. doi: 10.1128/mBio.01228-16.
- Charpentier, E., Anton, A. I., Barry, P., Alfonso, B., Fang, Y. & Novick, R. P. (2004). Novel cassette-based shuttle vector system for Gram-positive bacteria. *Appl Environ Microbiol*, 70 (10): 6076-6085. doi: 10.1128/aem.70.10.6076-6085.2004.
- Chien, A. C., Zareh, S. K., Wang, Y. M. & Levin, P. A. (2012). Changes in the oligomerization potential of the division inhibitor UgtP co-ordinate *Bacillus subtilis* cell size with nutrient availability. *Mol Microbiol*, 86 (3): 594-610. doi: 10.1111/mmi.12007.
- Corrigan, R. M., Abbott, J. C., Burhenne, H., Kaeffer, V. & Gründling, A. (2011). c-di-AMP is a new second messenger in *Staphylococcus aureus* with a role in controlling cell size and envelope stress. *PLoS Pathogens*, 7 (9): e1002217-e1002217. doi: 10.1371/journal.ppat.1002217.
- Ducret, A. & Grangeasse, C. (2017). Bacterial physiology: Wrapping the cell in a CozE shell. *Nat Microbiol*, 2: 16262. doi: 10.1038/nmicrobiol.2016.262.
- Fenton, A. K., Mortaji, L. E., Lau, D. T., Rudner, D. Z. & Bernhardt, T. G. (2016). CozE is a member of the MreCD complex that directs cell elongation in *Streptococcus pneumoniae*. *Nat Microbiol*, 2: 16237. doi: 10.1038/nmicrobiol.2016.237.
- Fey, P. D., Endres, J. L., Yajjala, V. K., Widhelm, T. J., Boissy, R. J., Bose, J. L. & Bayles, K. W. (2013). A genetic resource for rapid and comprehensive phenotype screening of nonessential *Staphylococcus aureus* genes. *mBio*, 4 (1): e00537-12. doi: 10.1128/mBio.00537-12.
- Grundling, A. & Schneewind, O. (2007a). Genes required for glycolipid synthesis and lipoteichoic acid anchoring in *Staphylococcus aureus*. *J Bacteriol*, 189 (6): 2521-2530. doi: 10.1128/jb.01683-06.
- Grundling, A. & Schneewind, O. (2007b). Synthesis of glycerol phosphate lipoteichoic acid in *Staphylococcus aureus*. *Proc Natl Acad Sci U S A*, 104 (20): 8478-8483. doi: 10.1073/pnas.0701821104.
- Helle, L., Kull, M., Mayer, S., Marincola, G., Zelder, M. E., Goerke, C., Wolz, C. & Bertram, R. (2011). Vectors for improved Tet repressor-dependent gradual gene induction or silencing in *Staphylococcus aureus*. *Microbiology*, 157 (Pt 12): 3314-3323. doi: 10.1099/mic.0.052548-0.
- Hesser, A. R., Matano, L. M., Vickery, C. R., Wood, B. M., Santiago, A. G., Morris, H. G., Do, T., Losick, R. & Walker, S. (2020a). The length of lipoteichoic acid polymers controls *Staphylococcus aureus* cell size and envelope integrity. *J Bacteriol*, 202 (16): e00149-20. doi: 10.1128/JB.00149-20.

- Hesser, A. R., Schaefer, K., Lee, W. & Walker, S. (2020b). Lipoteichoic acid polymer length is determined by competition between free starter units. *Proc Natl Acad Sci U S A*, 117 (47): 29669-29676. doi: 10.1073/pnas.2008929117.
- Karimova, G., Pidoux, J., Ullmann, A. & Ladant, D. (1998). A bacterial two-hybrid system based on a reconstituted signal transduction pathway. *Proc Natl Acad Sci U S A*, 95 (10): 5752-5756. doi: 10.1073/pnas.95.10.5752.
- Kho, K. & Meredith, T. C. (2018). Salt-induced stress stimulates a lipoteichoic acid-specific three-component glycosylation system in *Staphylococcus aureus*. *J Bacteriol*, 200 (12): e00017-18. doi: 10.1128/JB.00017-18.
- Kiriukhin, M. Y., Debabov, D. V., Shinabarger, D. L. & Neuhaus, F. C. (2001). Biosynthesis of the glycolipid anchor in lipoteichoic acid of *Staphylococcus aureus* RN4220: role of Ypfp, the diglycosyldiacylglycerol synthase. *J Bacteriol*, 183 (11): 3506-3514. doi: 10.1128/JB.183.11.3506-3514.2001.
- Lofblom, J., Kronqvist, N., Uhlen, M., Stahl, S. & Wernerus, H. (2007). Optimization of electroporation-mediated transformation: *Staphylococcus carnosus* as model organism. *J Appl Microbiol*, 102 (3): 736-747. doi: 10.1111/j.1365-2672.2006.03127.x.
- Monteiro, J. M., Fernandes, P. B., Vaz, F., Pereira, A. R., Tavares, A. C., Ferreira, M. T., Pereira, P. M., Veiga, H., Kuru, E., VanNieuwenhze, M. S., et al. (2015). Cell shape dynamics during the staphylococcal cell cycle. *Nat Commun*, 6: 8055. doi: 10.1038/ncomms9055.
- Nishibori, A., Kusaka, J., Hara, H., Umeda, M. & Matsumoto, K. (2005). Phosphatidylethanolamine domains and localization of phospholipid synthases in *Bacillus subtilis* membranes. *J Bacteriol*, 187 (6): 2163-2174. doi: 10.1128/JB.187.6.2163-2174.2005.
- Oku, Y., Kurokawa, K., Matsuo, M., Yamada, S., Lee, B. L. & Sekimizu, K. (2009). Pleiotropic roles of polyglycerolphosphate synthase of lipoteichoic acid in growth of *Staphylococcus aureus* cells. *J Bacteriol*, 191 (1): 141-151. doi: 10.1128/JB.01221-08.
- Pasquina, L. W., Santa Maria, J. P. & Walker, S. (2013). Teichoic acid biosynthesis as an antibiotic target. *Curr Opin Microbiol*, 16 (5): 531-537. doi: 10.1016/j.mib.2013.06.014.
- Rajagopal, M. & Walker, S. (2017). Envelope structures of Gram-positive bacteria. *Curr Top Microbiol Immunol*, 404: 1-44. doi: 10.1007/82_2015_5021.
- Reichmann, N. T. & Grundling, A. (2011). Location, synthesis and function of glycolipids and polyglycerolphosphate lipoteichoic acid in Gram-positive bacteria of the phylum Firmicutes. *FEMS Microbiol Lett*, 319 (2): 97-105. doi: 10.1111/j.1574-6968.2011.02260.x.
- Reichmann, N. T., Picarra Cassona, C., Monteiro, J. M., Bottomley, A. L., Corrigan, R. M., Foster, S. J., Pinho, M. G. & Grundling, A. (2014). Differential localization of LTA synthesis proteins and their interaction with the cell division machinery in *Staphylococcus aureus*. *Mol Microbiol*, 92 (2): 273-286. doi: 10.1111/mmi.12551.
- Rismondo, J., Gillis, A. & Grundling, A. (2021). Modifications of cell wall polymers in Gram-positive bacteria by multi-component transmembrane glycosylation systems. *Curr Opin Microbiol*, 60: 24-33. doi: 10.1016/j.mib.2021.01.007.
- Santa Maria, J. P., Jr., Sadaka, A., Moussa, S. H., Brown, S., Zhang, Y. J., Rubin, E. J., Gilmore, M. S. & Walker, S. (2014). Compound-gene interaction mapping

- reveals distinct roles for *Staphylococcus aureus* teichoic acids. *Proc Natl Acad Sci U S A*, 111 (34): 12510-12515. doi: 10.1073/pnas.1404099111.
- Stamsås, G. A., Myrbråten, I., Straume, D., Salehian, Z., Veening, J.-W., Håvarstein, L. S. & Kjos, M. (2018). CozEa and CozEb play overlapping and essential roles in controlling cell division in *Staphylococcus aureus*. *Mol Microbiol*, 109 (5): 615-632. doi: 10.1101/256560.
- Stamsås, G. A., Restelli, M., Ducret, A., Freton, C., Garcia, P. S., Håvarstein, L. S., Straume, D., Grangeasse, C. & Kjos, M. (2020). A CozE homolog contributes to cell size homeostasis of *Streptococcus pneumoniae*. *mBio*, 11 (5): e02461-20. doi: 10.1128/mBio.02461-20.
- Steele, V. R., Bottomley, A. L., Garcia-Lara, J., Kasturiarachchi, J. & Foster, S. J. (2011). Multiple essential roles for EzrA in cell division of *Staphylococcus aureus*. *Mol Microbiol*, 80 (2): 542-55. doi: 10.1111/j.1365-2958.2011.07591.x.
- Straume, D., Stamsås, G. A., Berg, K. H., Salehian, Z. & Håvarstein, L. S. (2017). Identification of pneumococcal proteins that are functionally linked to penicillin-binding protein 2b (PBP2b). *Mol Microbiol*, 103 (1): 99-116. doi: 10.1111/mmi.13543.
- Weart, R. B., Lee, A. H., Chien, A. C., Haeusser, D. P., Hill, N. S. & Levin, P. A. (2007). A metabolic sensor governing cell size in bacteria. *Cell*, 130 (2): 335-47. doi: 10.1016/j.cell.2007.05.043.
- Xia, G., Kohler, T. & Peschel, A. (2010). The wall teichoic acid and lipoteichoic acid polymers of *Staphylococcus aureus*. *Int J Med Microbiol*, 300 (2-3): 148-54. doi: 10.1016/j.ijmm.2009.10.001.
- Zhang, B., Liu, X., Lambert, E., Mas, G., Hiller, S., Veening, J. W. & Perez, C. (2020). Structure of a proton-dependent lipid transporter involved in lipoteichoic acids biosynthesis. *Nat Struct Mol Biol*, 27 (6): 561-569. doi: 10.1038/s41594-020-0425-5.

Supplementary information

The function of CozE proteins is linked to lipoteichoic acid biosynthesis in *Staphylococcus aureus*

Disen Barbuti, Myrbråten et al.

Supplementary Figures

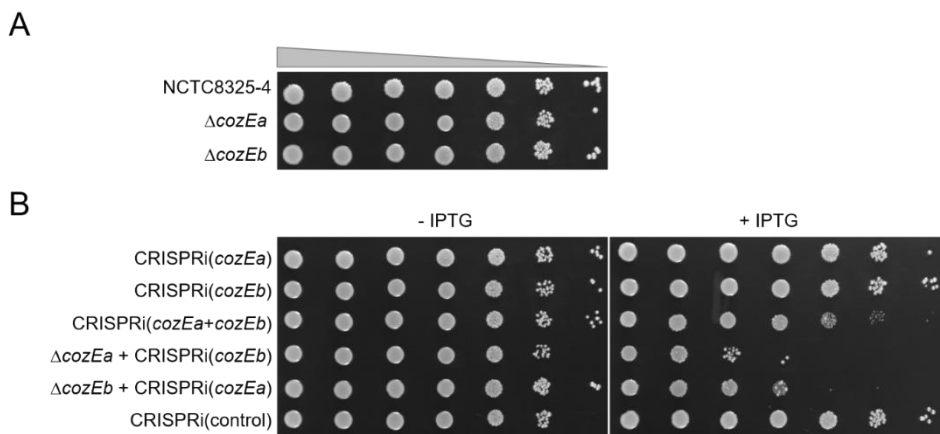


Fig. S1. Growth assays in *S. aureus* NCTC8325-4. **(A)** Growth assays for NCTC8325-4, ΔcozEa (MDB2) and ΔcozEb (MDB3). **(B)** Growth assays for NCTC8325-4 single knockdown strains CRISPRi(*cozEa*) (MDB14) and CRISPRi(*cozEb*) (MDB15), double knockdown strain CRISPRi(*cozEa+cozEb*) (MDB13) and combined knockout/knockdown strains ΔcozEa + CRISPRi(*cozEb*) (MDB11) and ΔcozEb + CRISPRi(*cozEa*) (MDB12). Strains were grown over night and 10-fold dilutions of the strains were spotted onto agar plates. IPTG was added to the plates for the CRISPRi-strains, as indicated.

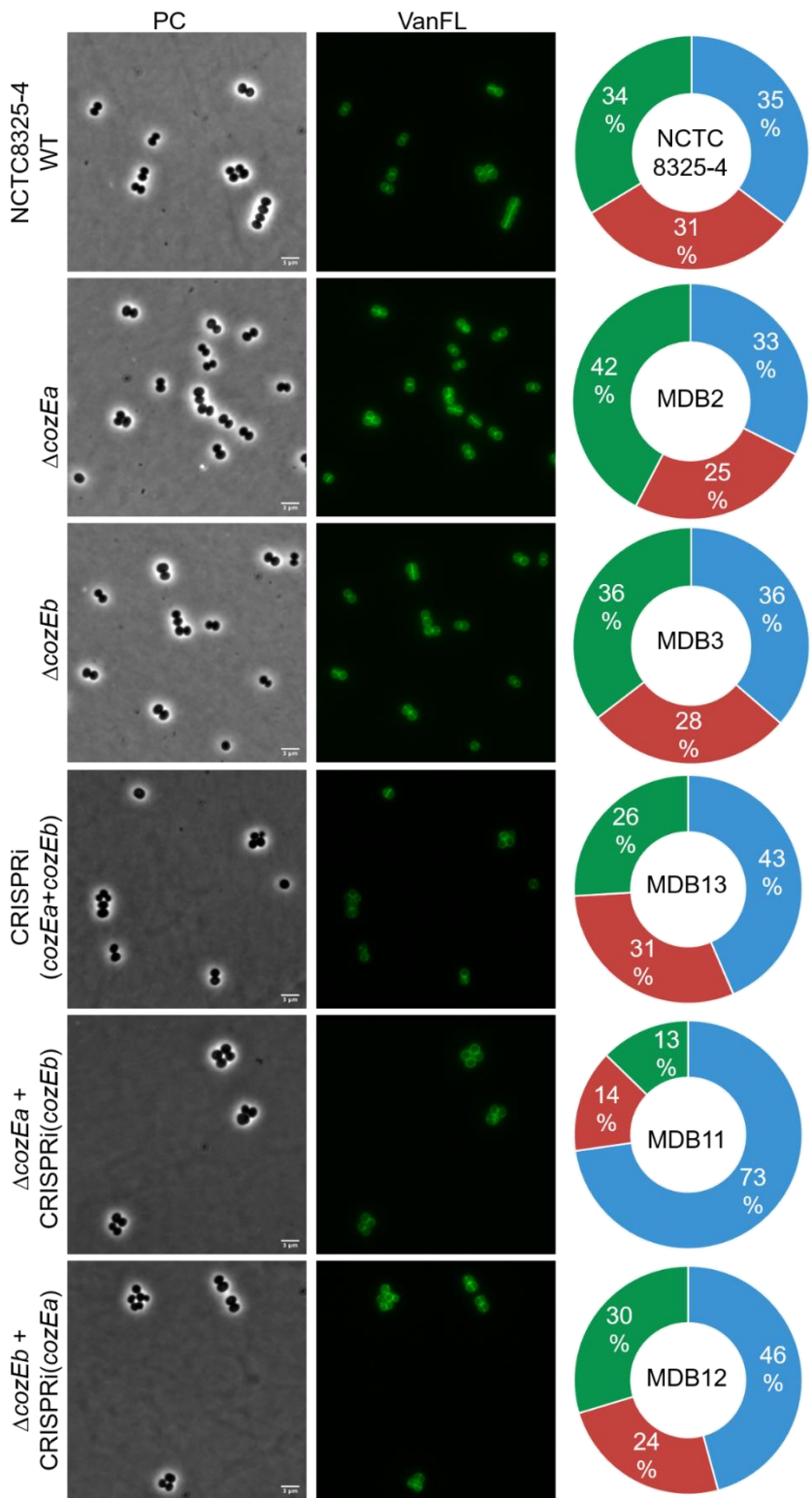


Fig. S2. Micrographs and cell cycle analysis of *cozE* single and double mutants in *S. aureus* NCTC8325-4. Phase contrast (PC)- and fluorescence micrographs from VanFL labelling are shown for of NCTC8325-4 wild-type, deletion mutants $\Delta cozEa$ (MDB2) and $\Delta cozEb$ (MDB3), as well as double knockdown strain CRISPRi(*cozEa+cozEb*) (MDB13) and combined knockout/knockdown strains $\Delta cozEa$ +CRISPRi(*cozEb*) (MDB11) and $\Delta cozEb$ +CRISPRi(*cozEa*) (MDB12). The CRISPRi strains were induced with 500 μ M IPTG. Scale bars, 3 μ m. White arrows point to cells with perturbed size and/or morphologies. Cell size analysis of the strains are shown in Fig. S3. Distribution of cell cycle phases based on VanFL staining for the strains are shown in the rightmost column. See Fig. 1D in the main article for schematic overview of the different phases analysed. The cell cycle data was obtained by manual counting the different cell phases of 100-150 random VanFL stained cells from each strain.

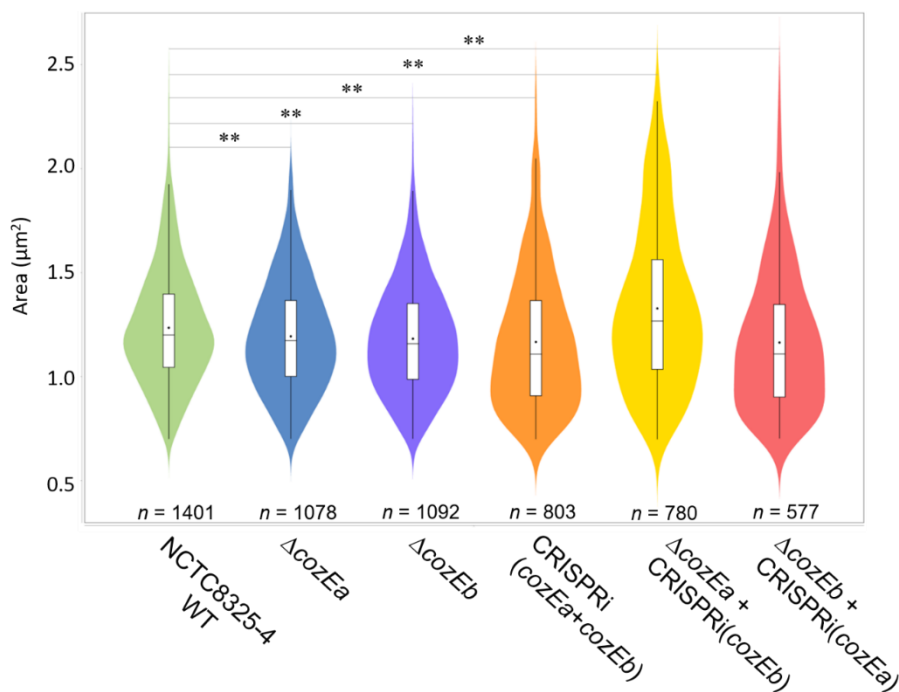


Fig. S3. Cell area of *S. aureus* NCTC8325-4 strains. Box plots of cell areas of cells from micrographs in Fig. S2; NCTC8325-4 wild-type ($1.24 \pm 0.27 \mu\text{m}^2$), $\Delta cozEa$ (MDB2; $1.19 \pm 0.26 \mu\text{m}^2$), $\Delta cozEb$ (MDB3; $1.18 \pm 0.27 \mu\text{m}^2$), CRISPRi(*cozEa+cozEb*) (MDB13; $1.17 \pm 0.32 \mu\text{m}^2$), $\Delta cozEa$ +CRISPRi(*cozEb*) (MDB11; $1.33 \pm 0.39 \mu\text{m}^2$) and $\Delta cozEb$ +CRISPRi(*cozEa*) (MDB12; $1.16 \pm 0.33 \mu\text{m}^2$). Cell areas were measured using MicrobeJ. The number of cells analyzed for each strain is indicated. Significant differences between the strains are indicated with asterisks (** indicates two-tailed P-value, $p < 0.01$, derived from a Mann Whitney test in MicrobeJ).

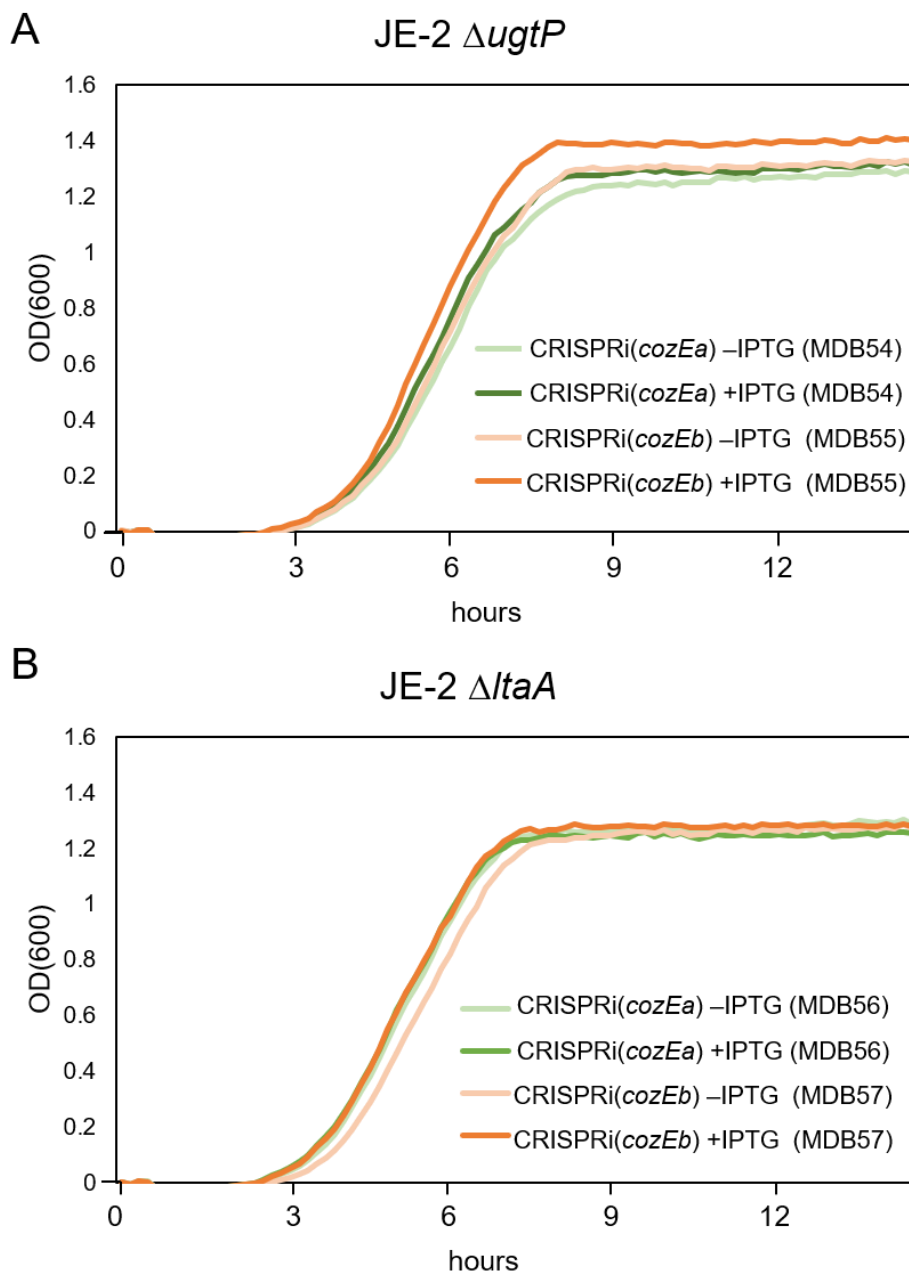


Figure S4. Growth curves of JE2 Δ ugtP (**A**) and Δ ltaA (**B**) with depletion of CozEa or CozEb, individually. The CRISPRi system was induced with 500 μ M IPTG when indicated.

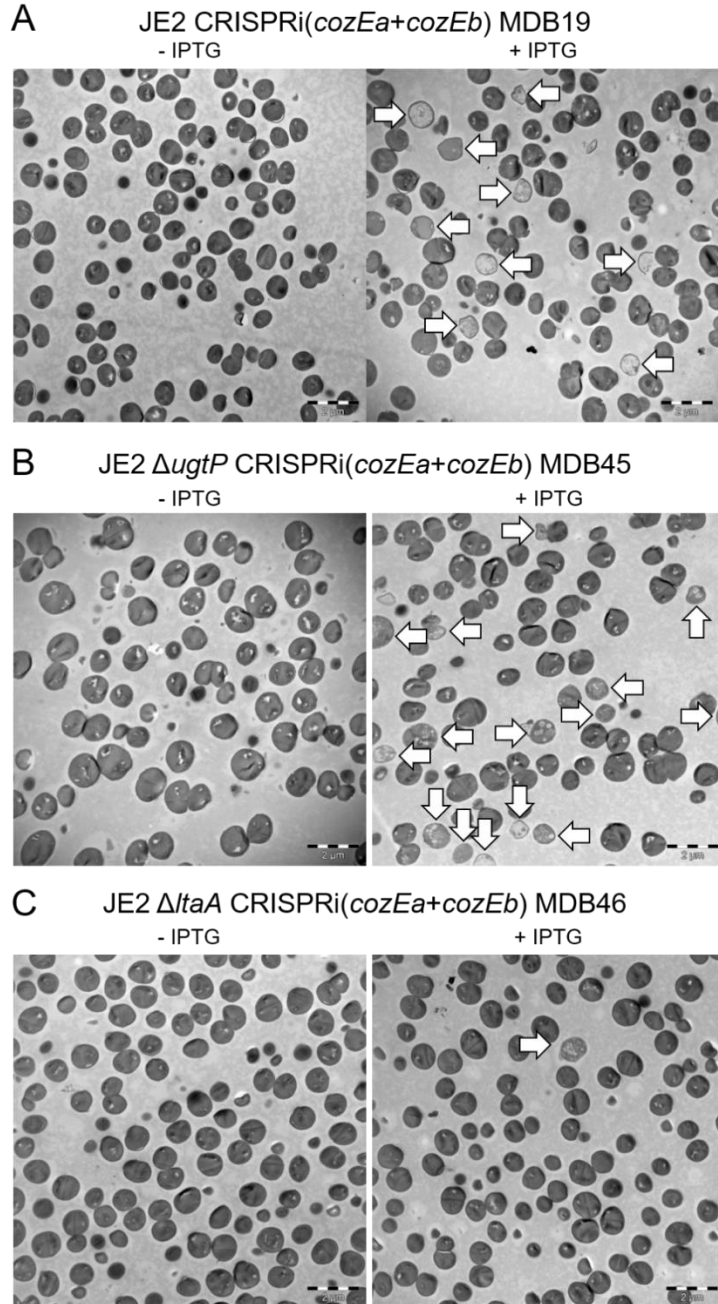


Figure S5. TEM micrographs of *cozEa/cozEb* knockdown in JE2 wild-type (**A**), Δ *ugtP* (**B**) and Δ *ltaA* (**C**) in which both *CozEa* and *CozEb* were depleted. Arrows point to lysed cells, and demonstrate extensive lysis in the control cells and Δ *ugtP* background. Cultures were induced with 500 μ M IPTG when indicated. Scale bars, 2 μ m.

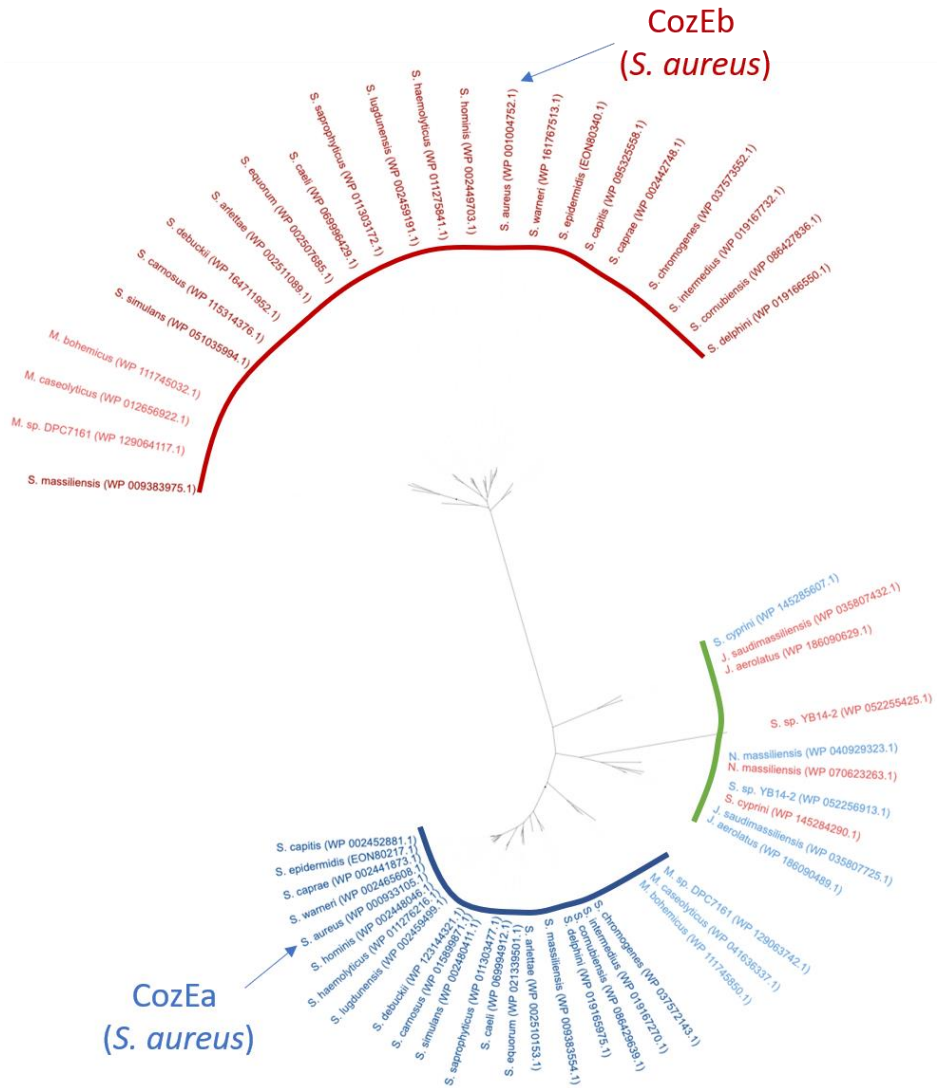


Fig. S6. Phylogenetic distribution of CozE proteins in the *Staphylococcaceae* family (species from genera *Staphylococcus*, *Macrococcus*, *Jeotgalicoccus*, *Salinicoccus*, and *Nosocomiicoccus*). A maximum likelihood phylogenetic tree was constructed from a Clustal Omega sequence alignment of CozE homologs from *Staphylococcaceae* using IQ-TREE. The phylogenetic tree was finally visualised and annotated using iTOL. The CozE proteins from species belonging to the genus *Staphylococcus* distributed into two phylogenetically separate CozEa (marked in blue) and CozEb (marked in red) subgroups. Each *Staphylococcus* and *Macrococcus* genome encode one protein from each subgroup. The CozE sequences from *Jeotgalicoccus*, *Salinicoccus*, and *Nosocomiicoccus* genomes clustered together in another subgroup which is closer to the CozEa subgroup than the CozEb subgroup (marked by a green line). Arrows point at the *S. aureus* CozE proteins.

Supplementary Tables

Table S1. Strains and mutants used in this work.

	Genotype and characteristics^a	Reference
Strain name		
<i>S. aureus</i> NCTC8325-4		
MDB1/ NCTC8325-4	MSSA-lab strain.	(Novick, 1967)
MDB2	NCTC8325-4 Δ <i>cozEa</i> , <i>spc</i> ^r	This work
MDB3	NCTC8325-4 Δ <i>cozEb</i> , <i>spc</i> ^r	This work
MH225	MDB1 carrying pLOW-dCas9_extra_ <i>lacO</i> , <i>ery</i> ^r	Lab collection
MH223	MDB2 carrying pLOW-dCas9_extra_ <i>lacO</i> , <i>ery</i> ^r	This work
MH224	MDB3 carrying pLOW-dCas9_extra_ <i>lacO</i> , <i>ery</i> ^r	This work
MDB11	MH223 carrying pCG248-sgRNA(<i>cozEb</i>), <i>ery</i> ^r , <i>cam</i> ^r	This work
MDB12	MH224 carrying pCG248-sgRNA(<i>cozEa</i>), <i>ery</i> ^r , <i>cam</i> ^r	This work
MDB13	MH225 carrying pCG248-sgRNA(<i>cozEa+cozEb</i>), <i>ery</i> ^r , <i>cam</i> ^r	This work
MDB14	MH225 carrying pCG248-sgRNA(<i>cozEa</i>), <i>ery</i> ^r , <i>cam</i> ^r	This work
MDB15	MH225 carrying pCG248-sgRNA(<i>cozEb</i>), <i>ery</i> ^r , <i>cam</i> ^r	This work
MM75	MH225 carrying pVL2336-sgRNA(control), <i>ery</i> ^r , <i>cam</i> ^r	Lab collection
MK1582	NCTC8325-4, but with <i>gfp</i> fused to the 3' end of <i>cozEa</i> , <i>spc</i> ^r	This work
MK1584	NCTC8325-4, but with <i>gfp</i> fused to the 3' end of <i>cozEb</i> , <i>spc</i> ^r	This work
MDB25	MH223 carrying pCG248-sgRNA(<i>cozEb+ugtP-ltaA</i>), <i>ery</i> ^r , <i>cam</i> ^r	This work
MDB26	MH223 carrying pCG248-sgRNA(<i>cozEb+ltaS</i>), <i>ery</i> ^r , <i>cam</i> ^r	This work
MDB27	MH223 carrying pCG248-sgRNA(<i>cozEb+dltA</i>), <i>ery</i> ^r , <i>cam</i> ^r	This work
MDB28	MH223 carrying pVL2336-sgRNA(<i>ugtP-ltaA</i>), <i>ery</i> ^r , <i>cam</i> ^r	This work
MDB29	MH223 carrying pVL2336-sgRNA(<i>ltaS</i>), <i>ery</i> ^r , <i>cam</i> ^r	This work
MDB30	MH223 carrying pVL2336-sgRNA(<i>dltA</i>), <i>ery</i> ^r , <i>cam</i> ^r	This work
MDB31	MH223 carrying pCG248-sgRNA(control), <i>ery</i> ^r , <i>cam</i> ^r	This work
MDB35	MH225 carrying pVL2336-sgRNA(<i>ugtP-ltaA</i>), <i>ery</i> ^r , <i>cam</i> ^r	This work
MDB36	MH224 carrying pVL2336-sgRNA(<i>ugtP-ltaA</i>), <i>ery</i> ^r , <i>cam</i> ^r	This work
MDB58	MDB3 carrying pRAB11- <i>cozEa</i> , <i>cam</i> ^r	This work
MDB62	MDB3 carrying pRAB11- <i>cozEb</i> , <i>cam</i> ^r	This work
MDB63	MDB3 carrying pRAB11- <i>lacA</i> , <i>cam</i> ^r	This work
MDB77	MDB1, but with <i>gfp</i> fused to the 5' end of <i>ugtP</i> , <i>spc</i> ^r	This work
MDB78	MDB77 carrying pLOW-dCas9_extra_ <i>lacO</i> , <i>ery</i> ^r	This work
MDB79	MDB78 carrying pCG248-sgRNA(<i>cozEa+cozEb</i>), <i>ery</i> ^r , <i>cam</i> ^r	This work
MDB85	MH225 carrying pVL2336-sgRNA(<i>ltaS</i>), <i>ery</i> ^r , <i>cam</i> ^r	This work
MDB86	MH224 carrying pVL2336-sgRNA(<i>ltaS</i>), <i>ery</i> ^r , <i>cam</i> ^r	This work
MDB89	MDB78 carrying pCG248-sgRNA(<i>cozEa</i>), <i>ery</i> ^r , <i>cam</i> ^r	This work
MDB90	MDB78 carrying pCG248-sgRNA(<i>cozEb</i>), <i>ery</i> ^r , <i>cam</i> ^r	This work

<i>S. aureus</i> NCTC8325		
MDB68/ NCTC8325	MSSA-lab strain	Lab collection
MDB69/ VL3222	NCTC8325 Δ <i>ltaA</i> , <i>spc</i> ^r	(Zhang et al., 2020)
MDB70	MDB68 carrying pLOW-dCas9_extra_ <i>lacO</i> , <i>ery</i> ^r	This work
MDB71	MDB69 carrying pLOW-dCas9_extra_ <i>lacO</i> , <i>ery</i> ^r	This work
MDB75	MDB70 carrying pCG248-sgRNA(<i>cozEa+cozEb</i>), <i>ery</i> ^r , <i>cam</i> ^r	This work
MDB76	MDB71 carrying pCG248-sgRNA(<i>cozEa+cozEb</i>), <i>ery</i> ^r , <i>cam</i> ^r	This work
MDB80	NCTC8325 <i>DugtP</i> , <i>spc</i> ^r	This work
MDB81	MDB80 carrying pLOW-dCas9_extra_ <i>lacO</i> , <i>ery</i> ^r	This work
MDB84	MDB81 carrying pCG248-sgRNA(<i>cozEa+cozEb</i>), <i>ery</i> ^r , <i>cam</i> ^r	This work
<i>S. aureus</i> JE2		
JE2	Wild-type, MRSA strain	(Fey et al., 2013)
NE779	JE2 Δ <i>cozEb</i> , <i>ery</i> ^r	(Fey et al., 2013)
NE1270	JE2 Δ <i>cozEa</i> , <i>ery</i> ^r	(Fey et al., 2013)
NE1663	JE2 <i>DugtP</i> , <i>ery</i> ^r	(Fey et al., 2013)
NE462	JE2 Δ <i>ltaA</i> , <i>ery</i> ^r	(Fey et al., 2013)
MDB16	JE2 carrying pLOW-dCas9_aad9, <i>spc</i> ^r	This work
MDB17	MDB16 carrying pCG248-sgRNA(<i>cozEa</i>), <i>spc</i> ^r , <i>cam</i> ^r	This work
MDB18	MDB16 carrying pCG248-sgRNA(<i>cozEb</i>), <i>spc</i> ^r , <i>cam</i> ^r	This work
MDB19	MDB16 carrying pCG248-sgRNA(<i>cozEa+cozEb</i>), <i>spc</i> ^r , <i>cam</i> ^r	This work
MDB20	MDB10 carrying pLOW-dCas9_aad9, <i>spc</i> ^r	This work
MDB21	MDB20 carrying pCG248-sgRNA(<i>cozEa+cozEb</i>), <i>spc</i> ^r , <i>cam</i> ^r	This work
MDB41	NE1663 carrying pLOW-dCas9_aad9, <i>spc</i> ^r	This work
MDB42	NE462 carrying pLOW-dCas9_aad9, <i>spc</i> ^r	This work
MDB44	MDB16 carrying pCG248-sgRNA(<i>luc</i>), <i>spc</i> ^r , <i>cam</i> ^r	This work
MDB45	MDB41 carrying pCG248-sgRNA(<i>cozEa+cozEb</i>), <i>spc</i> ^r , <i>cam</i> ^r	This work
MDB46	MDB42 carrying pCG248-sgRNA(<i>cozEa+cozEb</i>), <i>spc</i> ^r , <i>cam</i> ^r	This work
MDB47	MDB41 carrying pCG248-sgRNA(<i>luc</i>), <i>spc</i> ^r , <i>cam</i> ^r	This work
MDB48	MDB42 carrying pCG248-sgRNA(<i>luc</i>), <i>spc</i> ^r , <i>cam</i> ^r	This work
MDB54	MDB41 carrying pCG248-sgRNA(<i>cozEa</i>), <i>spc</i> ^r , <i>cam</i> ^r	This work
MDB55	MDB41 carrying pCG248-sgRNA(<i>cozEb</i>), <i>spc</i> ^r , <i>cam</i> ^r	This work
MDB56	MDB42 carrying pCG248-sgRNA(<i>cozEa</i>), <i>spc</i> ^r , <i>cam</i> ^r	This work
MDB57	MDB42 carrying pCG248-sgRNA(<i>cozEb</i>), <i>spc</i> ^r , <i>cam</i> ^r	This work
MDB59	NE779 carrying pRAB11- <i>cozEa</i> , <i>cam</i> ^r	This work
MDB60	NE779 carrying pRAB11- <i>cozEb</i> , <i>cam</i> ^r	This work
MDB61	NE779 carrying pRAB11- <i>lacA</i> , <i>cam</i> ^r	This work

<i>E. coli</i>		
IM08B	DH10B, Δdcm, Phelp-hsdMS, PN25-hsdS (strain expressing the <i>S. aureus</i> CC8 specific methylation genes)	(Monk et al., 2015)
XL-1	Host strain	Agilent
Plasmid name		
pLOW-dCas9_aad9, amp ^r		(Myrbråten et al., 2021)
pLOW-dCas9, amp ^r		(Stamsås et al., 2018)
pLOW-m(sf)gfp-SA1477, amp ^r		(Myrbråten et al., 2021)
pLOW-m(sf)gfp-ugtP, amp ^r		This work
pLOW-cozEa-gfp		(Stamsås et al., 2018)
pLWO-cozEb-gfp		(Stamsås et al., 2018)
pCG248-sgRNA(<i>cozEa</i>), amp ^r		(Stamsås et al., 2018)
pCG248-sgRNA(<i>cozEb</i>), amp ^r		(Stamsås et al., 2018)
pCG248-sgRNA(<i>cozEa+cozEb</i>), amp ^r		(Stamsås et al., 2018)
pCG248-sgRNA(<i>cozEb+ugtP-ltaA</i>), amp ^r		This work
pCG248-sgRNA(<i>cozEb+ltaS</i>), amp ^r		This work
pCG248-sgRNA(<i>cozEb+dltA</i>), amp ^r		This work
pVL2336-sgRNA(<i>ugtP-ltaA</i>), amp ^r		This work
pVL2336-sgRNA(<i>ltaS</i>), amp ^r		This work
pVL2336-sgRNA(<i>dltA</i>), amp ^r		Laboratory stock
pCG248-sgRNA(control), amp ^r (control sgRNA-plasmid)		(Stamsås et al., 2018)
pLOW-m(sf)gfp-SA1477, amp ^r		(Myrbråten et al., 2021)
pLOW-m(sf)gfp-ugtP, amp ^r		This work
pRAB11- <i>cozEa</i> , amp ^r		This work
pRAB11- <i>cozEb</i> , amp ^r		This work
pRAB11- <i>lacA</i> , amp ^r (control plasmid)		This work
pMAD, amp ^r		(Arnaud et al., 2004)
pMAD-ori- <i>parS</i> , amp ^r		Laboratory stock
pMAD-Δ <i>ugtP::spc</i> , amp ^r		This work
pMAD- <i>gfp_ugtP_spc</i> , amp ^r		This work

pMAD- <i>cozEa::spc</i> , amp ^r	(Stamsås et al., 2018)
pMAD- <i>cozEb::spc</i> , amp ^r	(Stamsås et al., 2018)
pMAD- <i>cozEa-m(sf)gfp</i> , amp ^r	This work
pMAD- <i>cozEb-m(sf)gfp</i> , amp ^r	This work
pUT18C- <i>ugtP</i>	This work
pUT18- <i>ugtP</i>	This work
pKNT25- <i>cozEb</i>	(Stamsås et al., 2018)
pKT25- <i>cozEa</i>	(Stamsås et al., 2018)
pKNT25- <i>cozEa</i>	(Stamsås et al., 2018)
pCN55, amp ^r	(Charpentier et al., 2004)

a. *spc*^r = spectinomycin resistant, *ery*^r = erythromycin resistant, *cam*^r = chloramphenicol resistant, and *amp*^r = ampicillin resistant.

Table S2. Primers used in this work.

Primer name	Sequence 5'-3' ^a	Description ^b
Primers to check for the presence of <i>cozEa</i>		
im17	ATCGGT <u>ACCC</u> CAATAAAACTAGGAGGAAATTTAAATGT TAAACAAGGTTTGGTTCC	<i>cozEa</i> F w/ KpnI RS
im18	GATGA <u>ATTC</u> TTAGTCCTTAACATTACTGTTTG	<i>cozEa</i> R w/ EcoRI RS
Primers to check for the deletion of <i>cozEa</i>		
mk188	ATTGGGCCACCTAGGATC	F upstream of <i>cozEa</i> deletion
mk187	CAAACATTTATCGTTGTAATACGT	R downstream of <i>cozEa</i> deletion
Primers to check for the presence of <i>cozEb</i>		
GS653	GATCGGATCCCAATGAAAATGAAAAGAATATAAGAAA G	<i>cozEb</i> F w/BamHI RS
GS654	GATCGAATCCTTTATTCAACTATTTTATTACTTTCTTT A	<i>cozEb</i> R
Primers to check for the deletion of <i>cozEb</i>		
mk188	ATTGGGCCACCTAGGATC	F upstream of <i>cozEb</i> deletion
mk195	GCGTCAACAATTACACCACAG	R downstream of <i>cozEb</i> deletion
Primers to check for the presence of <i>ItaA</i>		
mdb10	ACGTG <u>GATCCG</u> AAAGGTTTCCTTTATATGCAAG	<i>ItaA</i> F w/ BamHI RS
mdb11	ACGTGA <u>ATTC</u> CGTTTAAACCTTACTTAGCTTTT	<i>ItaA</i> R w/ EcoRI RS
Primers to check for the presence of pCG248 plasmids		
mk26	GGATAACCGTATTACGCCT	pCG248 F
mk25	AAATCTCGAAAATAATAGAGGGA	pCG248 R
Primers to check for the presence of pRAB11 plasmids		
mk23	GGATCCCTCGAGTTCATG	pRAB11 F
mk24	GGGATGTGCTGCAAGCGA	pRAB11 R
Primers to check for the presence of pMAD plasmids		
im156	AATCTAGCTAATGTTACGTTACA	pMAD F
mk177	GATGCCGCCGGAAGCGAG	pMAD R
Primers for construction of pLOW-<i>gfp-ugtP</i>		
mdb9	ACGTG <u>GATCCG</u> TTACTCAAATAAAAAGATATTGA	<i>ugtP</i> F w/ BamHI RS

mdb2	ACGTGAATTCATGATTAGCGTAATTATTTAACG	<i>ugtP</i> R w/ EcoRI RS
Primers for construction of pMAD-<i>gfp-ugtP_spc</i>		
mdb3	ACCTGAATTCGGTATCGCTAGCGATGGCT	ori_up F w/ EcoRI RS
mdb4	TCGAACCCCGATGTTGTCC	ori_up R
mdb5	CGACAACATCGGGGTTGACAATATGTTTATTATACACGT	P _{ugtP} F overlapping ori_up
mdb6	GTGAACAGCTCTTCTCCTTTTGACATTAATAGCCACCC TCCGTTAG	P _{ugtP} R overlapping <i>gfp</i>
mk48	ATGTCAAAGGAGAAGAGCTGTTTAC	<i>gfp</i> F
mdb7	GATCCTAGGTGGGCCAATTTATTTAACGAAGAATCTTGCATATAAAG	<i>ugtP</i> R overlapping <i>spc</i>
mk188	ATTGGGCCACCTAGGATC	<i>spc</i> F
mdb8	AGGTGTCGACATTGGTGGTATCGCTGTTGC	Ori_down R w/ Sall RS
Primers for construction of pMAD-Δ<i>ugtP::spc</i>		
mk501	CAACGCCTCGCAGTCGTCC	<i>ugtP</i> _up F
mk502	TTTCCGTTAATCAAATTGCTCATTAAATAGCCACCCTCCGTTAG	<i>ugtP</i> _up R overlapping <i>spc</i>
mk503	ATGAGCAATTTGATTAACGGAAA	<i>spc</i> F
mk504	CTAATTGAGAGAAGTTTCTATAG	<i>spc</i> R
mk505	CTATAGAACTTCTCTCAATTAGAAAATTAAGTATGCTACACAGAC	<i>ugtP</i> _down F overlapping <i>spc</i>
mk506	ACGTGGATCCGATAGCTAAAGCGATAATCCAC	<i>ugtP</i> _down R w/ BamHI RS
Primers for construction of bacterial two-hybrid (BACTH) constructs		
mk488	GCAGGTCGACAGGAAACAGCTATGGTTACTCAAATAAAAAGATA	ugtPSa_F_Sall
mk499	TAGAGGATCCCTTAAACGAAGAATCTTGCATATAAAG	ugtPSa_R_BamHI
im228	TAGAGGATCCCTCTTAAACGAAGAATCTTGCATATAAAG	ugtP_R_BamHI
mk500	ATCGGGATCCCGTTACTCAAATAAAAAGATATTGA	ugtPSa_F_BamHI
mdb2	ACGTGAATTCATGATTAGCGTAATTATTTAACG	mdb2_ugtP_r_pLOW_EcoRI
Primers for construction of pRAB11-constructs		
im17	ATCGGTACCCAATAAAAAGTAGGAGGAAATTTAAATGT TAAACAAGGTTTGGTTCC	0948_F_KpnI_RBS
im18	GATGAATTCCTTAGTCCTTAACATTACTGTTTG	0948_R_EcoRI
im19	ATCGGTACCCAATAAAAAGTAGGAGGAAATTTAAATGATGAAAATGAAAAGAATATAAG	1358_F_KpnI_RBS
im20	GATGAATTCCTTATTCAACTATTTTATTACTTTCTT	SA1358_R_EcoRI
im21	ATCGGTACCCAATAAAAAGTAGGAGGAAATTTAAATGGCGATTATTATTGGTTTCAG	lacA_F_KpnI_RBS
im22	GATGAATTCCTTAGCACATTTTATTAAGCATATC	lacA_R_EcoRI

Primers for chromosomal fusions of <i>cozEa-gfp</i> and <i>cozEb-gfp</i>		
mk432	ACGT <u>CCATGG</u> ATGTTAAACAAGTTTGGTTCC	cozEa_F_NcoI
mk433	GATCCTAGGTGGGCCCAATTTACTTATAAAGCTCATCC ATGCC	gfp_R_over aad9
mk188	ATTGGGCCACCTAGGATC	aad9_F
mk434	ACGT <u>GTCGACT</u> GGGATTAGATATTCTATCCGT	cozEa_down_R_Sall
mk435	ACGT <u>CCATGG</u> ATGAAAATGAAAAGAATATAAGAAAG	cozEb_F_NcoI
mk436	ACGT <u>GTCGACT</u> CGGGTGGTCTAACCATTTGA	cozEb_down_R_Sall

a. The restriction sites are underlined.

b. F = forward primer, R = reverse primer, and RE = restriction site.

References

- Arnaud, M., Chastanet, A. & Debarbouille, M. (2004). New vector for efficient allelic replacement in naturally nontransformable, low-GC-content, Gram-positive bacteria. *Appl Environ Microbiol*, 70 (11): 6887-6891. doi: 10.1128/AEM.70.11.6887-6891.2004.
- Charpentier, E., Anton, A. I., Barry, P., Alfonso, B., Fang, Y. & Novick, R. P. (2004). Novel cassette-based shuttle vector system for Gram-positive bacteria. *Appl Environ Microbiol*, 70 (10): 6076-6085. doi: 10.1128/aem.70.10.6076-6085.2004.
- Fey, P. D., Endres, J. L., Yajjala, V. K., Widhelm, T. J., Boissy, R. J., Bose, J. L. & Bayles, K. W. (2013). A genetic resource for rapid and comprehensive phenotype screening of nonessential *Staphylococcus aureus* genes. *mBio*, 4 (1): e00537-12. doi: 10.1128/mBio.00537-12.
- Monk, I. R., Tree, J. J., Howden, B. P., Stinear, T. P. & Foster, T. J. (2015). Complete bypass of restriction systems for major *Staphylococcus aureus* lineages. *MBio*, 6 (3): e00308. doi: 10.1128/mBio.00308-15.
- Myrbråten, I. S., Stamsås, G. A., Chan, H., Morales Angeles, D., Knutsen, T. M., Salehian, Z., Shapaval, V., Håvarstein, L. S., Straume, D. & Kjos, M. (2021). SmdA is a novel cell morphology determinant in *Staphylococcus aureus*. *Manuscript*.
- Novick, R. (1967). Properties of a cryptic high-frequency transducing phage in *Staphylococcus aureus*. *Virology*, 33 (1): 155-166. doi: 10.1016/0042-6822(67)90105-5.
- Stamsås, G. A., Myrbråten, I., Straume, D., Salehian, Z., Veening, J.-W., Håvarstein, L. S. & Kjos, M. (2018). CozEa and CozEb play overlapping and essential roles in controlling cell division in *Staphylococcus aureus*. *Mol Microbiol*, 109 (5): 615-632. doi: 10.1101/256560.
- Zhang, B., Liu, X., Lambert, E., Mas, G., Hiller, S., Veening, J. W. & Perez, C. (2020). Structure of a proton-dependent lipid transporter involved in lipoteichoic acids biosynthesis. *Nat Struct Mol Biol*, 27 (6): 561-569. doi: 10.1038/s41594-020-0425-5.

PAPER III

SmdA is a novel cell morphology determinant in *Staphylococcus aureus*

Ine S. Myrbråten¹, Gro A. Stamsås¹, Helena Chan^{2,3}, Danae Morales Angeles¹, Tiril Mathiesen Knutsen¹, Zhian Salehian¹, Volha Shapaval⁴, Daniel Straume¹ and Morten Kjos¹.

¹Faculty of Chemistry, Biotechnology and Food Science, Norwegian University of Life Sciences, Ås, Norway.

²Structural Cellular Biology Unit, Okinawa Institute of Science and Technology, Okinawa, Japan.

³The ithree institute, University of Technology Sydney, Broadway, NSW, Australia.

⁴Faculty of Science and Technology, Norwegian University of Life Sciences, Ås, Norway.

Abstract

Cell division and cell wall synthesis in staphylococci need to be precisely coordinated and controlled to allow the cell to multiply while maintaining their nearly spherical shape. The mechanisms ensuring correct placement of the division plane and synthesis of new cell wall have been studied intensively, however, hitherto unknown factors and proteins are likely to play a role in this complex interplay. Starting from a subcellular localization- and gene knockdown screen of essential genes with unknown functions in *Staphylococcus aureus*, we identified a protein with major influence on cell morphology in *S. aureus*. The protein, here named SmdA (for staphylococcal morphology determinant A), is a membrane-protein with septum-enriched localization. By *smdA* silencing and overexpression, we demonstrate by using different microscopy techniques that SmdA is critical for cell division processes, including septum formation and cell splitting. We also identified conserved residues in SmdA that are critical for functionality. Pulldown- and bacterial two-hybrid interaction experiments showed that SmdA interacts with several known cell division- and cell wall synthesis proteins, including penicillin binding proteins (PBPs) and EzrA. Notably, SmdA also affects susceptibility to cell wall targeting antibiotics, particularly in methicillin-resistant *S. aureus* (MRSA). Together, our results show that *S. aureus* is dependent on balanced amounts of membrane-attached SmdA in order to carry out proper cell division.

Introduction

Most bacteria are surrounded by a shape-determining cell envelope which protects against lysis and interacts with the extracellular milieu. The cell envelope of the opportunistic, Gram-positive pathogen *Staphylococcus aureus* consists of a thick layer of peptidoglycan (PG) along with teichoic acids (TA) and cell wall-associated surface proteins. During a bacterial cell cycle, synthesis of PG and TA needs to be precisely regulated and coordinated with cell division, DNA replication and chromosome segregation. Tight control of these processes is critical for staphylococcal cells to maintain their integrity and nearly spherical shape as they multiply, and they are therefore attractive targets for antimicrobials (Sass & Brötz-Oesterhelt, 2013). Exactly how such control is mediated in *S. aureus* is still not fully established, and hitherto unknown factors may be involved. In this work we describe a new staphylococcal cell morphology determinant.

Staphylococcal cell division is initiated by assembly of the Z-ring, consisting of polymerized FtsZ-proteins, that localizes to the future division septa (Pinho et al., 2013). The Z-ring functions as a scaffold for cell division- and cell wall synthesis proteins which together constitute the divisome (Errington et al., 2003). Cell division in *S. aureus* occurs in alternating orthogonal planes, meaning that the new cell division plane is always perpendicular to the previous (Saraiva et al., 2020). Timely and spatial control of localization of the Z-ring assembly is most likely linked with chromosome segregation and DNA replication, involving proteins such as the nucleoid occlusion factor Noc, which ensures that the cells do not establish new septa across the chromosomes (Veiga et al., 2011), and CcrZ, which connects initiation of DNA replication to cell division (Gallay et al., 2021). The chromosomes and chromosome segregation also contribute to establish a physical barrier allowing the Z-ring only to be formed in an angle perpendicular to the previous division plane (Saraiva et al., 2020).

The Z-ring directs the synthesis of new PG in *S. aureus* to the septum. Synthesis of PG starts in the cytoplasm, where UDP-MurNAc-pentapeptide is first synthesized and then attached to the membrane by the enzyme MraY to form the PG precursor lipid I (Barreteau et al., 2008; Bouhss et al., 2007). A pentaglycine side chain is attached to produce lipid II-Gly₅ (Rohrer & Berger-Bächi, 2003), which is flipped to the outer leaflet of the membrane by MurJ (Monteiro et al., 2018; Sham et al., 2014) where it is incorporated into the existing PG mesh by transpeptidation (TP) and transglycosylation (TG) reactions. Specifically, the shape, elongation, division and sporulation (SEDS) proteins, FtsW and RodA with TG activity, work in pairs with

monofunctional transpeptidases, the penicillin binding proteins PBP1 and PBP3, respectively (Meeske et al., 2016; Reichmann et al., 2019). While the PBP1-FtsW pair is essential and performs the septal cross wall synthesis, the non-essential PBP3-RodA pair is responsible for the slight elongation occurring in *S. aureus*. Additionally, *S. aureus* possesses two other PBPs; the bifunctional PBP2 with both TG and TP activity, whose role is essential in *S. aureus*, and the low-molecular weight PBP4, which controls the degree of PG crosslinks (Atilano et al., 2010; Pinho & Errington, 2005; Wyke et al., 1981). Finally, MRSA strains have an additional PBP, PBP2A, a transpeptidase with low-affinity for β -lactam antibiotics (Hartman & Tomasz, 1984; Ubukata et al., 1985). In the final step of division, PG hydrolases break bonds in PG for remodeling and daughter cell splitting. The major, bifunctional autolysin Atl, together with Sle1, for which expression are regulated by the two-component system WalkR, are the primary enzymes responsible for hydrolyzing the septal PG to allow splitting of daughter cells (Dubrac et al., 2007; Nega et al., 2020; Oshida et al., 1995; Thalsø-Madsen et al., 2019). The actual cross wall splitting is a mechanical process occurring within milliseconds (Monteiro et al., 2015; Zhou et al., 2015).

The spatiotemporal control of cell division and PG synthesis is directly and indirectly influenced by several factors. One of these is the anionic TA polymers, the second major component of the cell wall, which are either covalently linked to the PG (wall teichoic acids, WTA), or linked via a lipid-anchor to the plasma membrane (lipoteichoic acids, LTA). Mutations in enzymes involved in either WTA or LTA biosynthesis result in cells of abnormal shape and lack of septum synthesis control, probably via different mechanisms (Atilano et al., 2010; Brown et al., 2013; Hesser et al., 2020). Furthermore, proteases, chaperones and secretion proteins, involved in production, folding and/or secretion of cell cycle proteins, may also directly or indirectly affect coordination of cell division and septum formation in *S. aureus*. For example, Clp-protease complexes can target both FtsZ and Sle1, and thereby have major effects on these processes (Feng et al., 2013; Jensen et al., 2019; Silber et al., 2020).

Evidently, cell shape maintenance and control of cell division and septum formation are a complex interplay between many cellular processes where unknown key factors are yet to be discovered. We here identified a hitherto novel protein named SmdA (for staphylococcal morphology determinant A). We show that the levels of the membrane-attached SmdA protein is critical for maintaining normal division progression and morphology in *S. aureus*, as silencing or overexpression of *smdA* resulted in defective cell division, septal cross wall synthesis, as well as increased sensitivity towards cell wall targeting antibiotics.

Results

Knockdown phenotyping- and subcellular localization analysis of essential staphylococcal proteins

Cell cycle factors often have a specific subcellular localization, and their mutants result in cells with obvious cell division defects such as altered cell sizes, cell clustering and lack of spherical cell morphologies. To identify novel proteins potentially involved in the cell cycle and morphology control in *S. aureus*, we therefore performed a combined knockdown- and subcellular localization analysis of 27 essential staphylococcal proteins with no annotated functions (Chaudhuri et al., 2009; Santiago et al., 2015; Valentino et al., 2014) (Text S1). Using *S. aureus* SH1000 as the host strain, fluorescent fusions of the selected proteins to monomeric superfolder green fluorescent protein (m(sf)GFP) were expressed using the low copy-number plasmid pLOW (Liew et al., 2011), and their subcellular localization were analyzed by fluorescence microscopy. Knockdown strains were constructed using an established CRISPR interference (CRISPRi) system (Stamsås et al., 2018), and investigated by phase contrast- and fluorescence microscopy (Text S1). An overview of the growth (Fig. S1) and single cell knockdown phenotypes (Fig. S2), as well as the subcellular localization of the proteins (Fig. S3), is found in Table S1 and Text S1. From this screen, we observed that knockdown of the membrane-attached protein SAOUHSC_01908, whose m(sf)GFP-fusion appeared to be enriched in the septum (Fig. S3, see below), resulted in cells of variable sizes that formed large clusters (Fig. S2, see below). Nucleoid staining with 4',6-diamidino-2-phenylindole (DAPI) in this knockdown strain also appeared abnormal with highly variable intensities and degree of nucleoid condensation (Fig. S2). As these are characteristics previously observed for bacterial proteins involved in cell division processes, we set out to further characterize the functional roles of SAOUHSC_01908 (here named SmdA) in *S. aureus*.

SmdA is a conserved staphylococcal membrane protein

SmdA is a protein of 302 amino acids and is fully conserved in species within the *Staphylococcaceae* family (Fig. S4). The protein has a predicted N-terminal transmembrane helix and a C-terminal cytoplasmic part with partial homology to a so-called nuclease related domain (NERD) (PF08375, $E = 1.08 \cdot 10^{-5}$) (Fig. 1A). The domain was named based on distant similarities to endonucleases, and is found in bacterial, archaeal, as well as plant proteins (Grynberg & Godzik, 2004). However, the functional role of NERD in bacteria have to our knowledge never been studied. SmdA

has been found to be essential in transposon mutagenesis studies in *S. aureus* (Chaudhuri et al., 2009; Valentino et al., 2014). Growth analysis of SmdA CRISPRi knockdown (hereafter SmdA^{down}) in *S. aureus* SH1000 in rich medium at 37°C resulted in reduction in growth compared to the control strain when spotted on agar plates (Fig. 1B), however, the growth rate in liquid medium was not affected (Fig. S5A). Similarly, for *S. aureus* NCTC8325-4, HG001 and the MRSA strain COL, SmdA^{down} resulted in reduced growth on agar plates (Fig. 1B), but no significant growth reduction was observed in liquid medium, except for HG001 (Fig. S5A). By RT-PCR we verified that the expression of *smdA* was indeed fully knocked down by the CRISPRi system in *S. aureus* SH1000 (Fig. S5B). Since the SmdA^{down} strains were still viable, we attempted to construct deletion mutants of *smdA* by allelic replacement with a spectinomycin resistance cassette using the pMAD-vector (Arnaud et al., 2004). However, even after prolonged incubation we were not able to obtain the deletion mutant in *S. aureus* SH1000, NCTC8325-4 or COL. We therefore used the CRISPRi system in the different *S. aureus* strains to study the phenotypes of SmdA further.

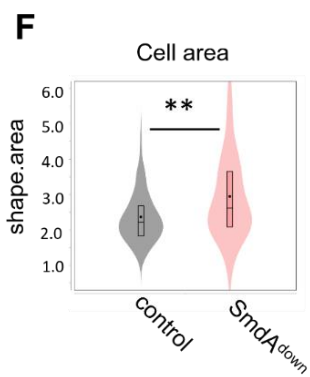
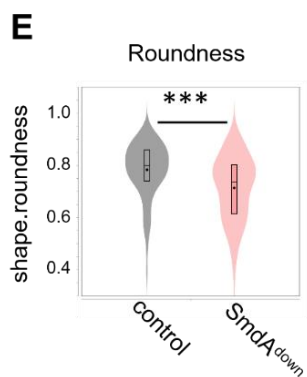
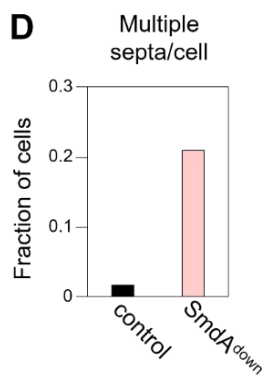
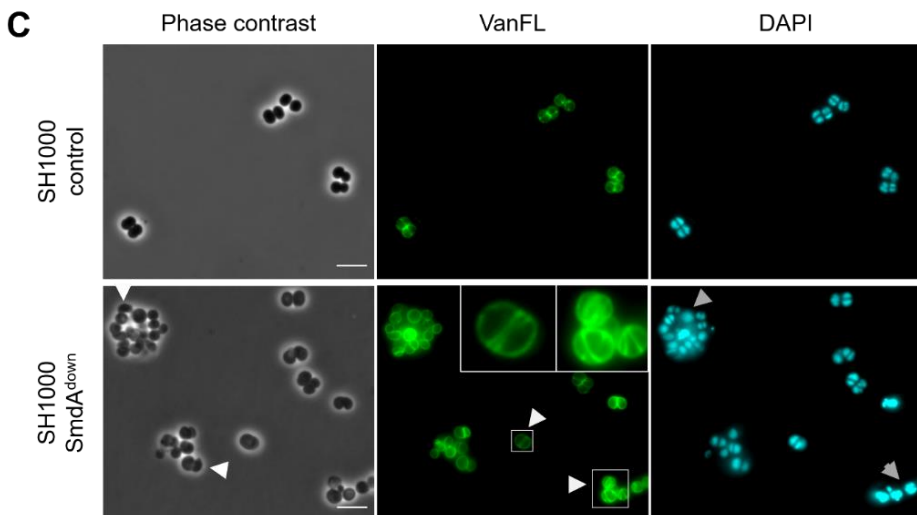
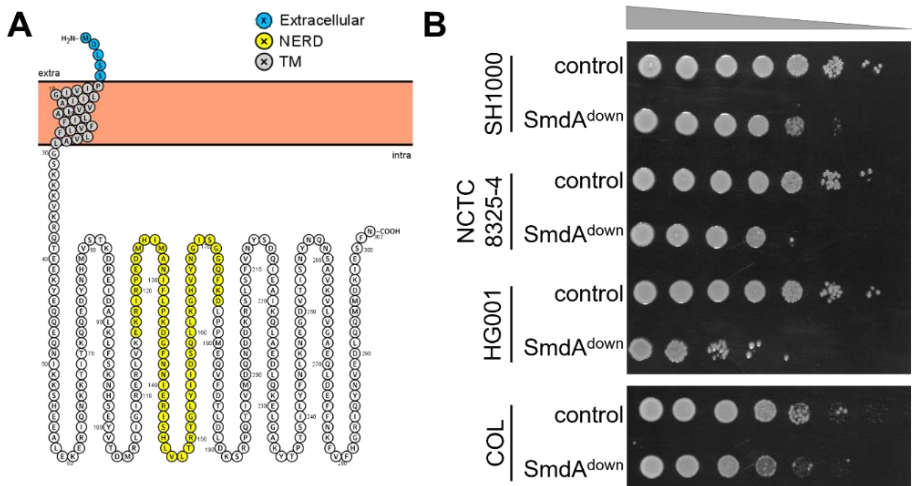


Fig. 1. Phenotypes resulting from depletion of SmdA. (A) Predicted topology of SmdA using Protter (Omasits et al., 2014). SmdA is predicted to have one transmembrane (TM) helix with a short extracellular N-terminus and a large intracellular domain. The sequence with predicted similarity to the NERD domain is highlighted in yellow. (B) Growth on solid media of SmdA knockdown strains (SmdA^{down}) in *S. aureus* SH1000 (IM269), NCTC8325-4 (IM311), HG001 (IM312) and COL (IM294). Strains carrying a non-targeting sgRNA were used as controls (IM284, IM307, IM313 and IM295 for the respective strains). From non-induced overnight cultures, 10-fold dilution series were made and spotted onto plates with 300 μ M isopropyl- β -D-thiogalactopyranoside (IPTG). (C) SmdA^{down} (IM269) and control strain (IM284) analyzed by phase contrast- and fluorescence microscopy of cells labelled with the nucleoid marker DAPI and the cell wall label VanFL. White arrows point at mis-shaped cells and cells with perturbed septum formation, and grey arrows point at cells with abnormal nucleoid signals. Magnified insets of representative cells are shown for the VanFL micrographs. Scale bars, 5 μ m. (D) Fraction of cells with multiple septa per cell for the SmdA^{down} strain IM269 (n = 225) and the non-target control strain IM284 (n = 242) are plotted. (E) Cell roundness, as determined using MicrobeJ, was used as a measure of the morphology of the cells. Spherical cells will have values close to 1. Cell roundness measures for the control strain IM284 (n = 198) and the SmdA^{down} strain IM269 (n = 191) are plotted. (F) Cell area (in μ m²) as determined using MicrobeJ of the control strain IM284 (n = 198) and the SmdA^{down} strain IM269 (n = 191). In E and F, significant differences between the distributions are indicated by asterisks (***, P < 0.0001). P-values were derived from a Mann-Whitney test.

Depletion and overexpression of SmdA results in cells with highly aberrant cell shapes

During the initial screen, we observed that SmdA^{down} in *S. aureus* SH1000 resulted in clusters containing cells of variable sizes. The knockdown experiment was repeated, and exponentially growing cells were stained with fluorescent vancomycin (VanFL, binds to non-crosslinked stem peptides throughout the cell wall) and DAPI and investigated by microscopy. SmdA^{down} indeed resulted in severe phenotypic defects (Fig. 1C); increased cell clustering and a large fraction of cells with multiple septa (20.1 % for SmdA^{down} as opposed to 1.6 % for the control strain, Fig. 1D) and abnormal, non-spherical morphology (Fig. 1E). The SmdA^{down} cells were also significantly larger than the control strain (Fig. 1F). Furthermore, the nucleoid signal visualized by DAPI staining, appeared very heterogeneous in SmdA^{down} with a large fraction of cells having highly intense signal (25.7 %, n = 225), as opposed to the control (5.8 %, n = 242). This phenotype has been observed previously in staphylococci with cell division defects (Stamsås et al., 2018).

Transmission- and scanning electron microscopy (TEM and SEM) were used to obtain more detailed images of the defects in morphology and septal placement found in SmdA^{down} cells. Strikingly, SmdA depleted *S. aureus* SH1000 displayed highly aberrant septum formation (Fig. 2A). In addition to lysis, cells with several non-perpendicular- or parallel septa were frequently observed, resulting in cells, or small

cell clusters, with aberrant morphologies (Fig. 2A). This was also evident from the SEM micrographs, which showed clustered cells with various morphologies (Fig. 2B). Similar phenotypes from TEM and SEM analyses were observed for the NCTC8325-4, HG001 and COL strains, with the HG001 strain being more affected by SmdA^{down} than the other two (Fig. S6 and Fig. S7).

Since reduced levels of SmdA led to defects in cell division and morphology of *S. aureus*, we next wondered whether overexpression of SmdA would affect the cells. An ectopic copy of *smdA* was placed behind an IPTG-inducible promoter in the plasmid pLOW (Liew et al., 2011) and expressed in *S. aureus* NCTC8325-4. As for SmdA^{down}, the nucleoid and cell walls were stained with DAPI and VanFL (Fig. S8). Although less evident than for SmdA^{down}, overexpression of SmdA also resulted in clusters of cells with several septa per cell as defined by VanFL staining (Fig. S8) (3.9 %, n = 181 for SmdA overexpression, compared to 20.1 % for SmdA^{down}, and 1.6 % for the control). Together, these knockdown- and overexpression analyses clearly demonstrated that septum formation and splitting in *S. aureus* are dependent on proper levels of SmdA.

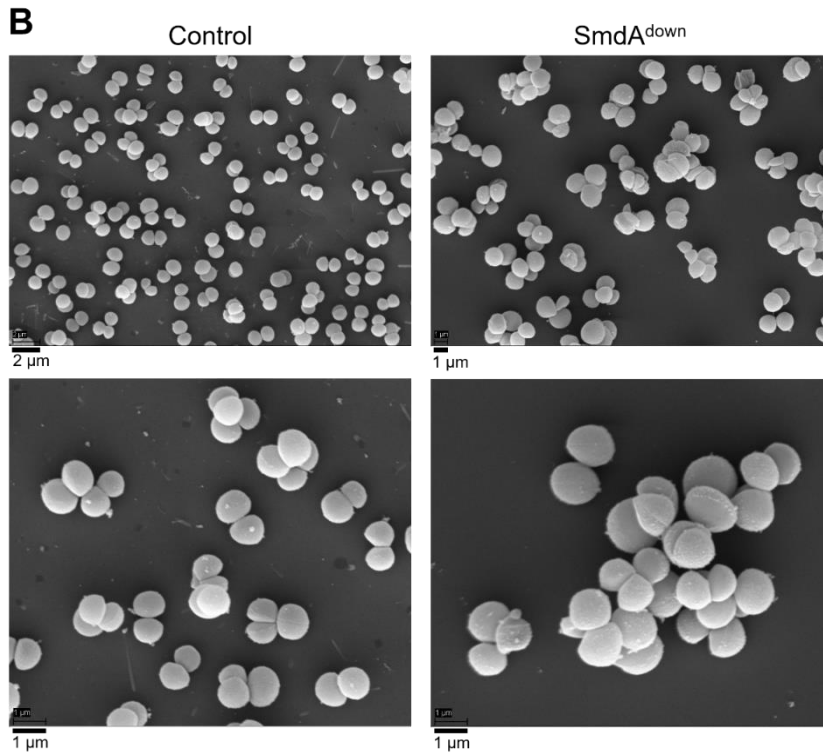
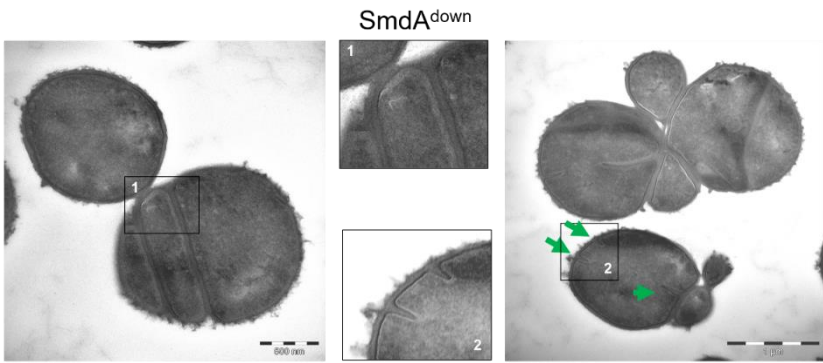
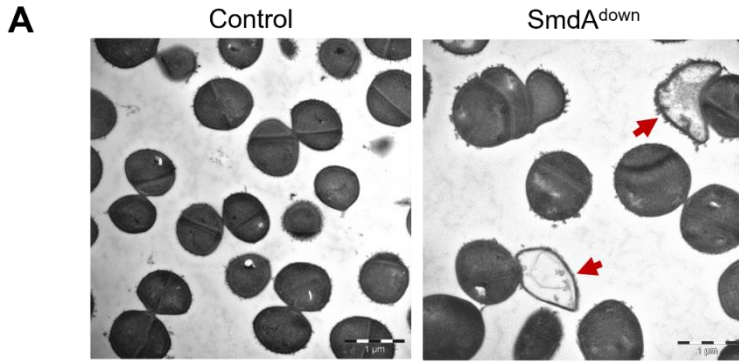


Fig. 2. SmdA^{down} in *S. aureus* SH1000 visualized by electron microscopy. (A) Transmission electron- and (B) scanning electron micrographs of SH1000 CRISPRi control strain (IM284) and SH1000 SmdA^{down} (IM269). In (A), red arrows in the TEM micrographs point at lysed cells. Representative examples of cells with parallel septa or multiple septa are shown. Green arrows point to initiation of septum synthesis at multiple sites within the same cell. Different magnifications are shown, indicated by the scale bars.

Depletion of SmdA results in increased sensitivity towards antimicrobials targeting cell wall synthesis

Given the negative effect SmdA depletion had on cell morphology and -division, we reasoned that reduced expression of SmdA could influence the sensitivity of *S. aureus* to cell wall targeting antibiotics. To test this, SmdA^{down} strains were treated with PBP-targeting β -lactams (oxacillin, cefotaxime, ceftazidime and imipenem), the glycopeptide vancomycin (blocking cell wall synthesis by targeting the terminal D-Ala-D-Ala on the stem peptides of nascent PG (Reynolds, 1989)), tunicamycin (targeting TarO and MraY, enzymes involved in the early stages of synthesis of WTA and PG, respectively (Campbell et al., 2011)) and Congo Red (inhibitor of the LTA biosynthesis enzyme LtaS (Vickery et al., 2018)) (Table 1). Two antibiotics with alternative targets; tetracycline (targeting protein synthesis) and ciprofloxacin (a quinolone targeting DNA synthesis), were also included.

For the methicillin-susceptible *S. aureus* (MSSA) strain SH1000, a two-fold reduction in minimum inhibitory concentration (MIC), compared to the control, was observed for oxacillin and ceftazidime in SmdA^{down}. More notably, in the MRSA strain COL, SmdA^{down} sensitized the COL strain towards all β -lactams with a 2- to 8-fold reduction in MIC compared to the control (Table 1). SmdA depletion did not seem to significantly influence vancomycin susceptibility. Strikingly, however, we observed that SmdA^{down} cells became highly sensitive towards tunicamycin, with a 64-fold reduction in MIC compared to the control for *S. aureus* SH1000 and >4-fold reduction for COL. The increased susceptibility towards tunicamycin suggests that SmdA may influence processes related to TA synthesis, as the primary target of this antibiotic is TarO, the first enzyme in the WTA biosynthesis pathway (Price & Tsvetanova, 2007; Swoboda et al., 2010). We therefore also tested the tunicamycin sensitivity of the NCTC8324-5 and HG001 SmdA^{down} strains, which also showed increased susceptibility towards tunicamycin (HG001; 125-fold reduced MIC and NCTC8325-4; 4-fold reduced). The SmdA^{down} strains also displayed increased sensitivity towards Congo Red. Furthermore, SmdA depletion in *S. aureus* SH1000 led to a 2- to 4-fold reduction in MIC against tetracycline, compared to the control, however, depletion of

SmdA in COL did not change its sensitivity towards tetracycline or ciprofloxacin (Table 1).

Table 1. Minimum inhibitory concentration (MIC, in µg/ml) of different antimicrobials when SmdA is depleted in *S. aureus* SH1000 and COL.

Antibiotics	<i>S. aureus</i> SH1000 (MSSA)			<i>S. aureus</i> COL (MRSA)		
	SmdA ^{down}	Control	Fold change	SmdA ^{down}	Control	Fold change
Oxacillin	0.12	0.24	2	64-128	256	2-4
Cefotaxime	2	2	1	50	400	8
Cefoxitin	1	2	2	47-94	188	2-4
Imipenem	0.016	0.016	1	150	>300	>2
Vancomycin	2.5	2.5	1	2.5	2.5	1
Tetracycline	0.05	0.1-0.2	2-4	≥64	≥64	1
Ciprofloxacin	0.32	0.32	1	0.32	0.32	1
Tunicamycin	0.094	6	64	24	>96	>4
Congo Red	256	>1024	>4	512-1024	>1024	≥2

SmdA has no major effects on the TA biosynthetic pathways

The increased sensitivity to tunicamycin and Congo Red in SmdA^{down} strains, prompted us to study whether there were any major alterations in the TA in these cells. Notably, the SmdA^{down} strain displayed morphologies reminiscent of what has previously been reported for cells depleted of TA, i.e., with larger cell sizes, cells with irregular septum formations and reduced splitting (Campbell et al., 2011; Campbell et al., 2012; Hesser et al., 2020; Santa Maria et al., 2014). It has previously been shown that there is a synthetic lethal relationship between the WTA and LTA biosynthetic pathways (Oku et al., 2009; Santa Maria et al., 2014), and it could therefore be hypothesized that hypersensitivity to tunicamycin could result from deficient LTA biosynthesis in the *smdA* mutants. Using an anti-LTA antibody, we compared the quantity and lengths of LTA in the SmdA^{down}- and control strains for SH1000, NCTC8325-4, HG001 and COL (Fig. S9A). No consistent changes in LTA amounts or lengths were observed between the SmdA depletions and the controls in the four strains tested. Furthermore, we could not detect any release of LTA into the medium in the depletion strains, indicating that the stability of LTA (Mikkelsen et al., 2021) is intact (Fig. S9B). We therefore conclude that no major alterations in the LTA synthesis seem to occur upon SmdA depletion.

WTA has been shown to protect cells from the LTA-inhibitor Congo Red. Without WTA, cells became hypersensitive towards Congo Red (MIC of $<4 \mu\text{g/ml}$ for *tarO* deletion mutants and $>1024 \mu\text{g/ml}$ for wild-type cells) (Suzuki et al., 2012). Although to a much lesser degree, SmdA depletion strains were also more sensitive to Congo Red compared to the controls (Table 1), and we therefore looked into whether WTA could be disturbed in a SmdA^{down} strain. In TEM images, WTA can be seen as a dark, high-density layer in the septa of staphylococcal cells. By comparing strains with depletions of TarO and SmdA, using TEM, it was evident that the former lacked this dark, high-density layer, while it was still present in the SmdA^{down} strain, suggesting that WTA was still produced (Fig. S10A). We also performed Fourier transform infrared spectroscopy (FTIR), which has been used before to detect differences in the composition of WTA due to variable glycosylation patterns (Grunert et al., 2018; Mikkelsen et al., 2021). As expected, changes in the FTIR spectra were evident in the polysaccharide region ($1200 \text{ cm}^{-1} - 800 \text{ cm}^{-1}$) for the TarO^{down} strain compared to the control, with the most significant differences recorded for the peaks at 1076 cm^{-1} , 1048 cm^{-1} , 1033 cm^{-1} and $1000 - 970 \text{ cm}^{-1}$, representing α - and β -glycosidic bonds in WTA (Grunert et al., 2018). However, no changes were observed between SmdA^{down} and the control (Fig. S10B). Together, these results suggest that SmdA has no major effect on the WTA biosynthetic pathway.

SmdA is important in several stages of staphylococcal cell division

To identify potential protein interaction partners of SmdA, we next performed a protein pulldown experiment using GFP-trapping with a chromosomal *smdA-m(sf)gfp* fusion strain. Interestingly, the major staphylococcal autolysin Atl, as well as the bifunctional PBP2 were identified, along with 12 other proteins (Table S2). The experiment was repeated in a strain with plasmid-based expression of SmdA-m(sf)GFP, and this setup resulted in an extended list of proteins that were pulled down, probably due to the elevated expression of SmdA-m(sf)GFP. Selecting the proteins for which at least 10 unique peptides were detected and with a fold change of >2 compared to the control, resulted in a list of 58 proteins (Table S2). Several proteins with activity involved in protein folding, secretion and/or degradation (e.g., FtsH, PrsA, SpsB, ClpB, ClpC, SecD) were identified in this assay, in addition to the penicillin-binding proteins PBP1, PBP2, PBP3 and the early division protein EzrA. All the 14 proteins identified in the initial experiment were also pulled down in the second experiment.

Bacterial two-hybrid analyses of the SmdA-PBP1-3 and SmdA-EzrA were performed to see whether these interactions could be reproduced in a heterologous

system. The proteins were fused either N- or C-terminally to the domains of adenylate cyclase, an enzyme which catalyzes the production of cyclic adenosine monophosphate (cAMP) and eventually induction of β -galactosidase activity when brought in proximity by interaction between the target proteins. Indeed, SmdA interacted with PBP2, as well as PBP1, PBP3 and EzrA in the two-hybrid assays (Fig. 3A). By expressing a version of SmdA without its N-terminal membrane domain (SmdA Δ TMH), we also show that the observed interactions between SmdA and the PBPs in this assay occur via the transmembrane segment, while the interaction with EzrA was not abolished in SmdA Δ TMH. The latter notion show that EzrA interacts with the intracellular domain of SmdA (Fig. 1A).

The observed interactions between SmdA and PBPs may suggest that SmdA is somehow important for proper localization of PBPs, and thus localization of PG insertion in *S. aureus* (Fig. 1 and Fig. 2). With the VanFL approach used above (Fig. 1C), non-crosslinked PG throughout the cell surface was labelled. To determine more precisely the sites of active PG synthesis, *S. aureus* NCTC8325-4 SmdA^{down}, as well as SmdA overexpression cells, were therefore instead pulse-labelled for 90 sec with the fluorescent D-amino acid 7-hydroxycoumarincarboxylamino-D-alanine (HADA), a molecule which is integrated into PG by the specific activity of transpeptidases (Radkov et al., 2018). In the control cells, the expected midcell-localized band was observed (Fig. 3B). However, in the SmdA^{down} strain, we observed a more diffuse HADA signal with PG synthesis often occurring at several sites within the cell, forming patterns visible as crosses or Y-shapes (Fig. 3C). Similar observations were made in the cells overexpressing SmdA, although with a lower frequency of cells with abnormal labelling (Fig. 3D-E). Thus, the site of active transpeptidation (by PBP1-3) is indeed mis-localized when the levels of SmdA is altered.

Moreover, we also studied whether SmdA could affect the localization of EzrA by knocking down *smdA* in a strain expressing a chromosomal *ezrA-gfp* fusion (Fig. 3F). Indeed, abnormal localization patterns for EzrA-GFP was observed with similar frequency as the abnormal HADA labelling (Fig. 3G). These results thus suggest that SmdA affect the localization of the entire *S. aureus* divisome.

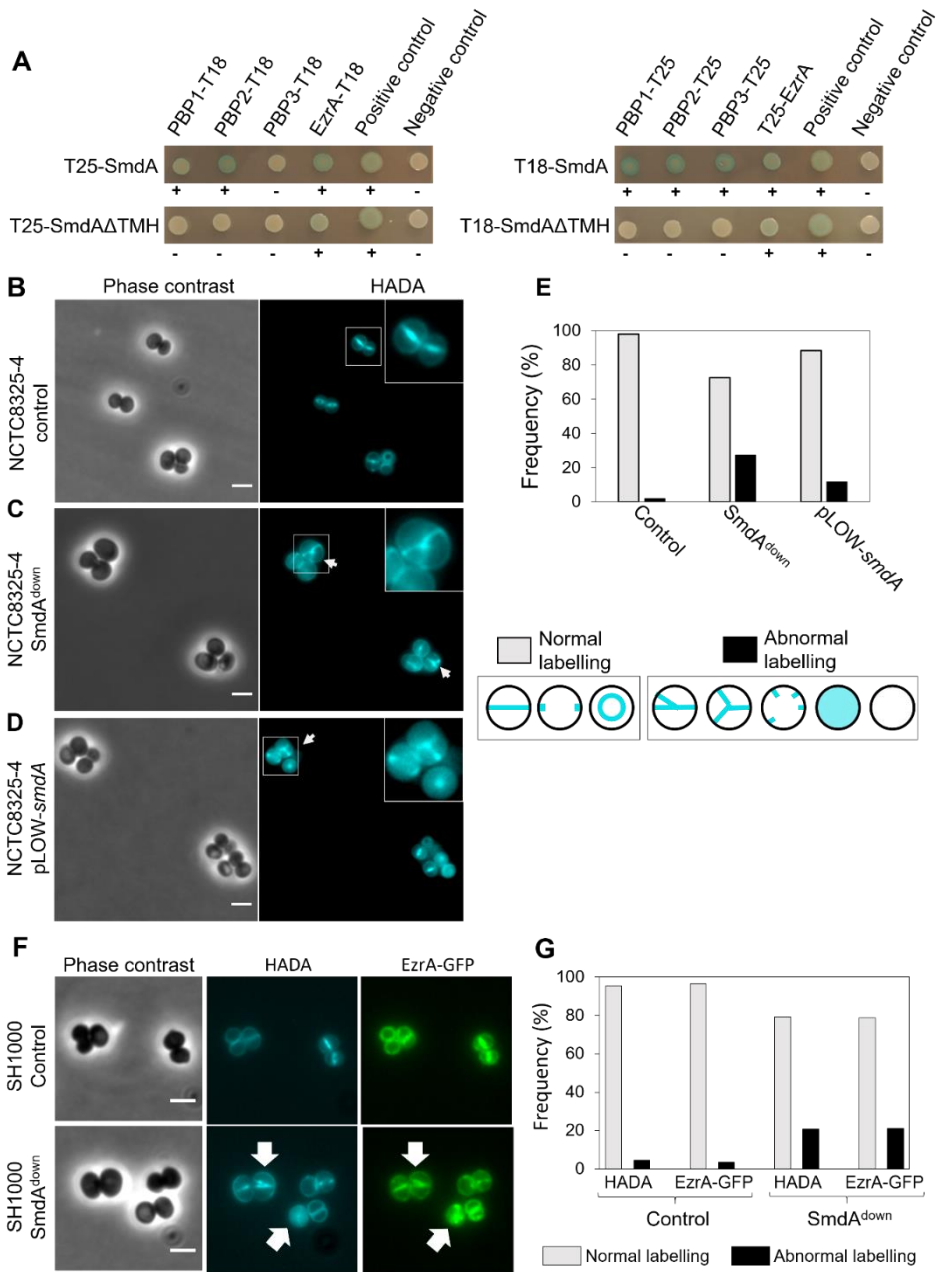


Fig. 3. SmdA interacts with important cell division proteins and is necessary for proper localization of EzrA and peptidoglycan synthesis. (A) Protein-protein interactions tested with bacterial two-hybrid assay, where SmdA and SmdAΔTMH were tested against PBP1, PBP2, PBP3 and EzrA. The proteins were fused either N- or C-terminally to the T18 or T25 domains as indicated. Blue colonies and plus signs indicate positive interactions and white colonies and minus signs negative interactions. (B-D). Micrographs of HADA labelled *S. aureus* NCTC8325-4

with depletion and overexpression of SmdA. Arrows point at cells with misplaced septum synthesis. Scale bars, 2 μ m. **(B)** CRISPRi control strain, IM307 **(C)** SmdA^{down} strain, IM311 and **(D)** SmdA overexpression strain, MK1866. **(E)** Frequency plot of cells with normal or abnormal HADA labelling pattern. Categorization of normal or abnormal labelling patterns are indicated. The number of cells analyzed were 259, 179 and 189 for B, C and D, respectively. **(F)** Micrographs showing co-localization of EzrA-GFP and HADA incorporation in *S. aureus* SH1000 strains with (MK1952) or without (MK1953) knockdown of SmdA. Phase contrast- and fluorescence images of HADA labelling and GFP (EzrA-GFP) are shown. Scale bars, 2 μ m. Arrows points to cells with abnormal localization of both HADA and EzrA-GFP. **(G)** Frequencies of cells (from F) with normal or abnormal localization of HADA and EzrA-GFP are plotted. The number of cells analyzed were 285 (for MK1953) and 298 (for MK1952).

Furthermore, the major autolysin Atl was also pulled down with SmdA. Atl is a secreted multidomain enzyme, which is processed to an acetylmuramyl-L-alanine amidase and β -N-acetylglucosaminidase, involved in septal cross wall splitting resulting in daughter cell separation (Oshida et al., 1995). Micrographs of SmdA^{down} cells showed that they have reduced cross wall splitting, a phenotype also observed in *atl* mutants and WalkR depleted cells (Biswas et al., 2006; Dubrac et al., 2007). WalkR is the two-component regulatory system controlling the expression of *atl* and other cell wall hydrolases (Dubrac et al., 2007). To assess the cross wall splitting phenotype in more detail, we performed Triton X-100-induced autolysis assays on the cultures. Indeed, reduced autolysis was observed in SmdA^{down} cells, demonstrating reduced autolytic activity (Fig. 4A). The lysostaphin sensitivity was also reduced (Fig. 4B), suggesting alterations in the cell wall affecting the lytic properties of this enzyme. It should be noted that the resistance towards Triton X-100- and lysostaphin-induced autolysis in the SmdA^{down} strain was clearly less compared to the control strain where *walR*, and thus all the regulated autolysins, was knocked down.

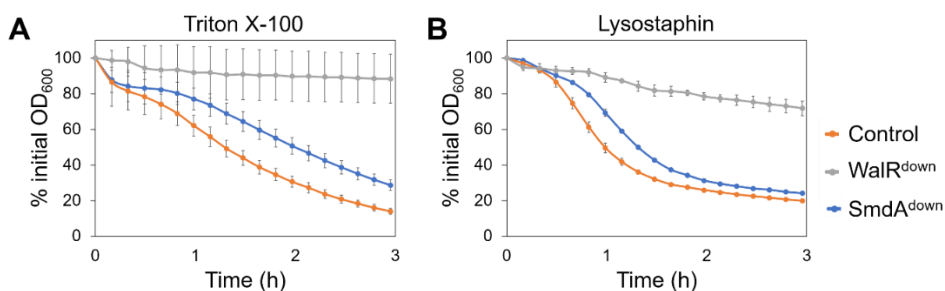


Fig. 4. Autolysis of *S. aureus* SH1000 depletion strains (control = IM284; WalR^{down} = IM293; SmdA^{down} = IM269) measured in presence of **(A)** 0.5 % Triton X-100 and **(B)** 100 ng/ml lysostaphin. Results presented as % of initial OD₆₀₀. Error bars represent standard error calculated from 4 technical replicates.

SmdA localizes to the septum after FtsZ

The initial screen showed that the SmdA-m(sf)GFP fusion protein displayed a septum-enriched signal when expressed ectopically from the low copy-number plasmid pLOW (Fig. 5A and Fig. S3). In order to analyze the localization with native expression levels, a chromosomally integrated version of SmdA-m(sf)GFP was made, in which *m(sf)gfp* was fused to the C-terminus end of *smdA*. Localization analyses in these cells further confirmed the septum-enriched localization of the fusion protein (Fig. 5A), with an average septum/periphery fluorescence signal ratio of 3.4 (n = 52). To visualize the localization of SmdA relative to the cell division process, we used FtsZ as a marker. Expression of *ftsZ*-fusion genes in the *smdA-m(sf)gfp* chromosomal fusion strain, however, only resulted in strains with extremely poor growth, suggesting that the cells did not tolerate such double-labelling. Instead, we therefore created a double-labelled strain in which SmdA-mYFP and FtsZ-mKate2 were co-expressed from plasmids while the native *smdA* and *ftsZ* were still present on the chromosome. Structured illumination microscopy (SIM) analysis showed that SmdA is localized around in the membrane when the Z-ring is formed (Fig. 5B), and that a septum-enriched localization occurs as the septal cross wall is being synthesized. This is further confirmed by stimulated emission depletion (STED) microscopy analysis (Fig. 5C). STED imaging also revealed that there is no apparent co-localization of SmdA-mYFP and FtsZ-mKate2 in newborn cells before FtsZ-constriction initiates. Combined, the localization of SmdA is reminiscent of the localization of PBPs in *S. aureus* (Monteiro et al., 2018), but appears to localize to the septal area after the early divisome proteins such as EzrA (Jorge et al., 2011; Lund et al., 2018).

The SmdA protein is attached to the membrane by a single transmembrane helix (Fig. 1A). To verify the significance of the SmdA membrane attachment for its localization, we ectopically expressed a version of SmdA without the transmembrane helix (SmdA Δ TMH). As expected, the N-terminal truncated SmdA Δ TMH-m(sf)GFP localized to the cytoplasm of the cells (Fig. 5A).

During this latter experiment, we noticed that SmdA Δ TMH-m(sf)GFP overexpression led to cells with obvious morphology defects. In fact, overexpression of SmdA Δ TMH (without the GFP-tag) (Fig. 6A) strikingly resulted in a more extreme phenotype than overexpression of full length SmdA (Fig. 3D, Fig. S8). The cells were often inflated or with a bean-shaped appearance (Fig. 6A). HADA pulse labelling of these cells revealed a highly abnormal cell wall incorporation pattern, with the fluorescent signal forming both condensed clumps and Y-shapes in different directions in almost 50 % of the cells (Fig. 6A and B). This demonstrates that the membrane attachment is critical for the localization and function of SmdA.

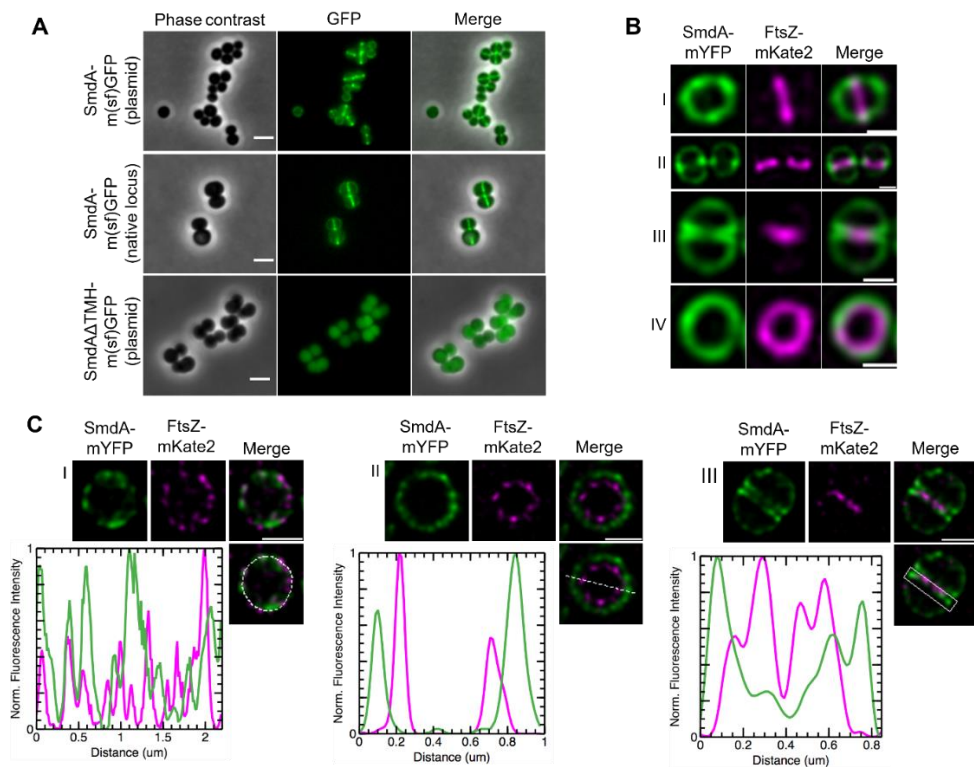


Fig. 5. Subcellular localization analysis of SmdA. (A) Micrographs of cells with induced expression of SmdA-m(sf)GFP from plasmid (top panel, IM104), native chromosomal expression of the SmdA-m(sf)GFP fusion protein (middle panel, IM308), and expression of SmdAATMH-m(sf)GFP from plasmid (bottom panel, IM373). Scale bars, 2 μm . (B) SIM images of fixed *S. aureus* SH1000 with plasmid-expressed SmdA-mYFP and FtsZ-mKate2 (HC060). (B-I) Side-view of a cell showing that FtsZ localizes at septum before arrival of SmdA. As cell division progresses, (B-II) SmdA concentrates at sites where septum formation is initiated, and (B-III) displays a septal localization at the two septal membranes as FtsZ constricts and septum formation proceeds. (B-IV) Top-view of a cell showing the FtsZ-ring inside of the SmdA-ring. All scale bars, 0.5 μm . (C) STED images of fixed *S. aureus* SH1000 with plasmid-expressed SmdA-mYFP and FtsZ-mKate2 (HC060), where line scans show fluorescence intensity of selected areas. (C-I) At an early stage of cell division, the rings of both SmdA and FtsZ have a similar diameter, but do not overlap in their distribution, and a heterogeneous distribution with a patchy signal is observed. (C-II) Top-view of a cell as cell division progresses, with the FtsZ-ring laying inside of SmdA, approximately 100-150 nm apart from each other. (C-III) Side-view of a cell showing how FtsZ is located innermost, and how SmdA is located at the two septal membranes. Scale bars, 0.5 μm .

Conserved residues in the predicted NERD domain are critical for the function of SmdA

The functional importance of the NERD domain (Fig. 1A) has, to our knowledge, neither been studied nor verified previously in any bacterial protein. As mentioned, we observed that overexpression of SmdA Δ TMH led to severe phenotypic changes in the staphylococcal morphology (Fig. 6A). We decided to use this as a tool to gain insight into whether the predicted NERD domain is important for the function of SmdA. Multiple sequence alignment of SmdA proteins from different staphylococcal species (Fig. S4) revealed conserved residues in this domain, and site directed mutagenesis was used to create two versions of SmdA Δ TMH containing mutations in the NERD domain: one in which H145 was changed to Ala (mut1), and a second containing the mutations R150A and T151A (mut2). Furthermore, we also observed from the alignment that the C-terminus of SmdA is highly conserved (Fig. S4), and another C-terminal mutated variant was created (mut3; F280A, H281A). The three-dimensional structure of SmdA, predicted by AlphaFold (Jumper et al., 2021), suggests that the N-terminal part of the protein folds into a long α -helix and that the NERD is located within the C-terminal structured part of the protein (Fig. 6C-II). The positions of the mutated residues are indicated in the predicted structure (Fig. 6C-III). The mutated SmdA Δ TMH versions were overexpressed in a wild-type background. Expression of these mutated variants indeed partially, or fully, abolished the phenotypic defects observed when overexpressing the non-mutated SmdA Δ TMH version. HADA staining of _mut1 (H145A) showed septum placement and PG synthesis comparable to wild-type cells, while _mut2 (R150A, T151A) and _mut3 (F280A, H281A) also clearly reduced the functionality of the protein (Fig. 6A and B). Furthermore, the growth inhibition upon overexpression of SmdA Δ TMH (Fig. 6D) was also abolished when the mutated variants were expressed under the same conditions. This strongly suggests that the given residues in both the predicted NERD and the conserved C-terminus are important for the function of SmdA.

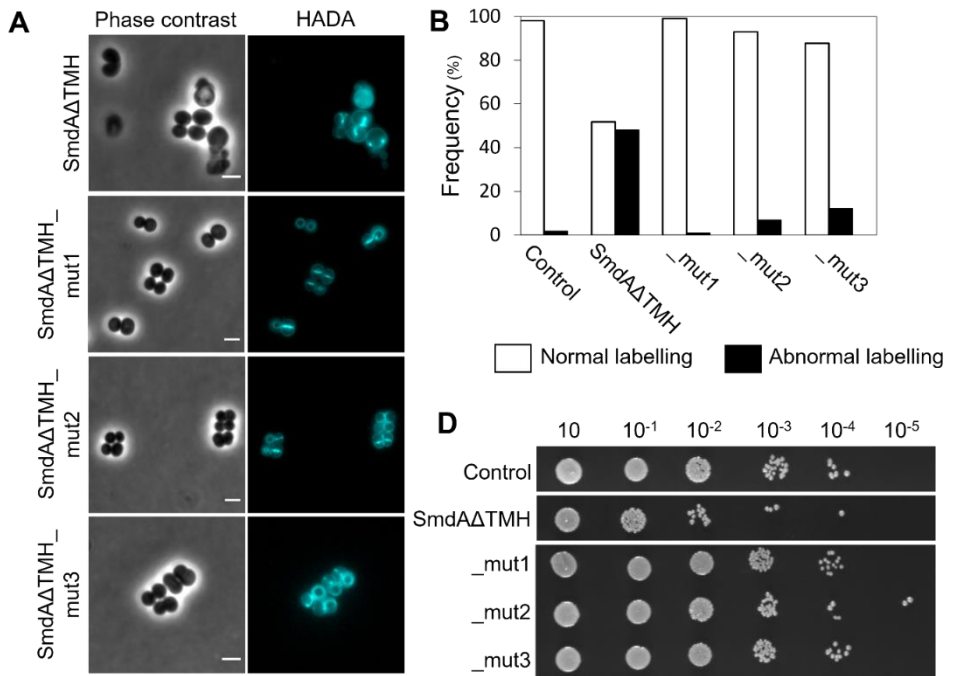


Fig. 6. Membrane attachment and conserved residues important for SmdA function. (A) HADA stained *S. aureus* NCTC8325-4 overexpressing SmdAΔTMH (MK1911), SmdAΔTMH_mut1 (IM377), _mut2 (IM378) and _mut3 (IM379). Scale bars, 2 μm. (B) The frequency of cells from panel A with normal or abnormal HADA staining is plotted. The number of cells plotted were 259 for the control (images not shown), 82 for SmdAΔTMH, 101 for _mut1, 113 for _mut2 and 122 for _mut3. (C) Structure of SmdA, predicted by AlphaFold (Jumper et al., 2021), where (C-I) shows the structure colored by a “per-residue confidence score” (pLDDT) with dark blue pLDDT > 90, light blue 90 > pLDDT > 70, and yellow 70 > pLDDT > 50, (C-II) shows the structured domain magnified with the predicted NERD colored in green and residues that have been mutated in red. (C-III) A magnified inset of (II) with annotated residues. (D) Growth assay on solid media of *S. aureus* NCTC8325-4 expressing SmdAΔTMH, SmdAΔTMH_mut1, _mut2 and _mut3.

Discussion

The results presented here provides the first functional insights into the conserved and essential staphylococcal protein SAOUHSC_01908, here named SmdA. SmdA, a protein conserved within the *Staphylococcaceae* family, is critical for maintaining cell morphology and for proper progression of cell division in different *S. aureus* strains (including MRSA and MSSA). Unbalanced levels, as well as loss of proper subcellular localization, of SmdA, results in severe cell morphology defects due to mis-localized cell division, uncontrolled cell wall synthesis, and lack of proper cross wall splitting.

Depletion of SmdA resulted in clearly reduced number of viable cells, while growth in liquid culture (biomass, as measured by OD₆₀₀) was not severely affected (Fig. 1, Fig. S5). Such a discrepancy between biomass and viable colonies has previously been observed in antibiotic-treated *S. aureus* SH1000 (Campbell et al., 2012), and this was ascribed to the combination of increased cell size and reduced daughter cell splitting in the culture. Larger cells and impaired cross wall splitting are indeed typical attributes of the SmdA^{down} cells as well, and most likely this explains the growth differences we observed in the two assays.

We observed that knockdown of SmdA increased the sensitivity of *S. aureus* to cell wall targeting antibiotics (Table 1). In *S. aureus*, many of the frequently used antibiotics are targeting cell wall synthesis, including β-lactams and glycolipids. The rise of both methicillin-resistant- and vancomycin-resistant *S. aureus* (MRSA and VRSA) have, however, made *S. aureus* infections more difficult to treat and novel anti-staphylococcal targets and strategies are needed. Targeting cell cycle proteins have been shown to re-sensitize resistant staphylococci towards existing antibiotics due to synergistic effects (Lee et al., 2011; Roemer et al., 2013; Tan et al., 2012). For example, inactivation of proteins involved in WTA synthesis sensitizes MRSA to β-lactams (Brown et al., 2012; Campbell et al., 2011). The same is also the case for a diversity of

factors contributing to cell division and cell wall biogenesis, including FtsZ, FtsA, PBP4 and most proteins involved in the PG synthesis pathway (Lee et al., 2011). The secretion-associated proteins SecDF and the chaperones PrsA and HtrA1 have also been tightly linked to β -lactam sensitivity (Quiblier et al., 2011; Roch et al., 2019), and recently, inactivation of the autolytic cell wall amidase Sle1 (Thalsø-Madsen et al., 2019), or the membrane proteins AuxA and AuxB (Mikkelsen et al., 2021), were shown to result in increased sensitivity to β -lactams. Mechanisms of re-sensitization in these cases vary and may be a result of weakened cell wall, as well as inactivation or mis-localization of PG synthesis, including the key resistance determinant PBP2A. The large number of factors affecting β -lactam sensitivity reflects the tight links between different processes involved in cell wall biogenesis. Our results suggest that SmdA most likely affects several steps in the cell division process, as we observed phenotypes and protein-protein interactions which linked SmdA to division ring formation, PG synthesis and cross wall splitting.

While the exact mechanism by which SmdA affect these processes remains to be determined, it is possible that SmdA influence the localization of cell division and cell wall synthesis via direct protein-protein interactions. This is supported by the SmdA-EzrA and SmdA-PBP1-3 interactions, combined with the abnormal localization of EzrA-GFP and HADA incorporation in SmdA^{down} cells. In fact, the division defects observed in SmdA^{down} cells are reminiscent of previous studies of *ezrA* null mutants, strains with point mutations in FtsZ or cells exposed to Z-ring inhibitors (Jorge et al., 2011; Lund et al., 2018; Pereira et al., 2016). However, the contribution of the identified interactions to the observed phenotypes must be investigated further, particularly since the subcellular localization of SmdA-m(sf)GFP does not appear to overlap with the Z-ring throughout the cell cycle and is instead more similar to the reported localization of PBPs (Jorge et al., 2011; Lund et al., 2018; Monteiro et al., 2018).

Lack of cross wall splitting is another prominent feature of the SmdA depleted cells. After septum formation, cells remain attached, forming clusters of mis-shaped cells. Indeed, the autolytic activity was reduced in the SmdA^{down} cells (Fig. 4). The major autolysin Atl was also pulled down together with SmdA-m(sf)GFP as one of the major hits. Atl is an extracellular processed protein whose amidase and glucosaminidase domains together process PG in the septum to allow splitting. It is possible that SmdA somehow influences the export or processing of Atl. In this context, it is interesting to note that proteases, foldases and chaperones (FtsH, PrsA, SpsB, ClpC, ClpB, HtrA1) were also pulled down with SmdA. It remains to be determined whether any of these interactions have any functional relevance,

however, perturbation of such pathways may have large consequences for cell division and septal placement as they are important for proper folding and secretion of key proteins involved in such processes. This has, for example, previously been demonstrated for the chaperone ClpX, which is critical for coordination of autolysins and cell division proteins (Jensen et al., 2019). Involvement in such a mechanism could also explain the pleiotropic phenotypes observed in SmdA^{down} cells, affecting several stages in the cell division process.

A part of the SmdA protein displays limited similarity to the so-called nuclease related domain (NERD). This domain, which is found in a broad range of bacterial species and in some archaea and plants, was initially identified on a virulence-plasmid from *Bacillus anthracis* (Grynberg & Godzik, 2004), and has later been suggested to belong to a superfamily of phosphodiesterases (Steczkiewicz et al., 2012). The majority of NERD proteins are single-domain proteins, but they are also occasionally found together with a kinase-, pseudokinase- or helicase domain (Kwon et al., 2019). The actual function of the NERD has, to our knowledge, however, not been studied experimentally. The results in this paper show that conserved residues in the predicted NERD are important for the functionality of SmdA, thus demonstrating for the first time a functional role of this domain. Although highly speculative at this point, it would be interesting if a cell division factor such as SmdA had DNA-interacting capabilities and thus forming a potential link between the membrane-associated cell division proteins and the nucleoid. Alterations in nucleoid labelling by DAPI was observed in the SmdA^{down} strain (Fig. 1C and Fig. S2), however, this is a phenotype observed for different cell division mutants (Stamsås et al., 2018) and does not necessarily infer a direct involvement of SmdA in the chromosome biology. It should also be noted that several of the most conserved residues of the NERD (Grynberg & Godzik, 2004) are not found in SmdA, suggesting a functional diversity within proteins harboring homology to this domain and implying that the NERD of SmdA may have functions unrelated to the nucleoid.

The staphylococcal genome encodes hundreds of essential proteins, which all represent potential target sites for antimicrobials. To be able to fully exploit the antibiotic target repertoire, it is critical to understand how essential proteins are involved and linked between different cell cycle processes. In this work, we identified and characterized SmdA as a novel factor essential for cell morphology and cell division in *S. aureus*. Based on the results presented here, future research should aim at pinpointing the molecular mechanism by which SmdA affect different stages of the cell division process. Finally, since SmdA depletion results in increased sensitivity to

β -lactams, it may as such also be a possible future target for combatting β -lactam resistance by re-sensitizing MRSA to these antibiotics.

Materials and Methods

Bacterial strains, growth conditions and transformations

Bacterial strains used in this study are listed in Table S3. *Escherichia coli* IM08B (Monk et al., 2015), *E. coli* XL1-Blue and *E. coli* BTH101 were grown in lysogeny broth (LB) at 30-37°C with shaking or on lysogeny agar (LA) plates at 30-37°C, with 100 μ g/ml ampicillin and/or 50 μ g/ml kanamycin for selection. *S. aureus* SH1000, RN4220, NCTC8325-4, HG001 and COL were grown in brain-heart infusion (BHI) broth or tryptic soy broth (TSB) at 37°C with shaking or on BHI/TSA plates at 37°C. For selection, 10 μ g/ml of chloramphenicol, 5 μ g/ml of erythromycin, 15 μ g/ml neomycin or 100 μ g/ml spectinomycin were added. For induction of gene expression, 50-300 μ M isopropyl β -D-1-thiogalactopyranoside (IPTG) or 2.5 ng/ml anhydrotetracycline (ATc) were added to the bacterial cultures.

A standard heat shock protocol was used for transformation of *E. coli* IM08B. Isolated plasmids from *E. coli* were transformed into *S. aureus* by electroporation. Preparation of electrocompetent *S. aureus* cells and electroporation were performed according to Löfblom et al. (2007).

Construction of GFP-fusion plasmids and strains for localization studies

To construct the library of fusion constructs for the subcellular localization screen, the Aureowiki database (www.aureowiki.med.uni-greifswald.de/Main_Page) and the Uniprot database (www.uniprot.org/) were initially used to identify potential transmembrane helices within the proteins. Based on this prediction, m(sf)GFP was fused to either the C- or N-terminus of the selected proteins to position the m(sf)GFP protein intracellularly. For all cloning experiments, fragments were amplified from *S. aureus* SH1000 genomic DNA, and cloning was performed with restriction digestion (enzymes from New England Biolabs [NEB]) and subsequent ligation using T4 DNA Ligase (NEB), unless otherwise stated. Ligation mixtures were transformed into *E. coli* IM08B, and consecutive isolated and sequence-verified plasmids were transformed into *S. aureus*. All strains and primers used in this study are listed in Table S3 and Table S4, respectively. Overview of genes included in the screen (and the results) is given in Table S1, in addition to information about whether a C- or N-terminal fusion was constructed for the subcellular localization screen.

Construction of pLOW-ftsZ-m(sf)gfp, pLOW-ftsZ-m(sf)gfp KpnI and pLOW-lacA-m(sf)gfp. Monomeric superfolder GFP, *m(sf)gfp*, was initially fused to *ftsZ* in the plasmid pLOW (Liew et al., 2011). *m(sf)gfp* was amplified from the plasmid pMK17 (van Raaphorst et al., 2017) using primers im1_linker_FP_F_BamHI and im2_m(sf)gfp_R_NotI_EcoRI. The amplified fragment encodes a linker sequence N-terminally of the *m(sf)gfp* gene. The fragment was digested with BamHI and EcoRI and subsequently ligated into the corresponding sites of the plasmid pLOW-*ftsZ-gfp* using Quick Ligase (NEB) to replace the original *gfp*-gene with the linker_m(sf)gfp sequence. To facilitate subsequent cloning, other versions of this plasmid were made. pLOW-*ftsZ-m(sf)gfp_KpnI*, containing a KpnI site in the linker sequence, was made in a similar fashion as described for pLOW-*ftsZ-m(sf)gfp*, except that im79_linker_FP_F_KpnI was used as forward primer for amplification of *m(sf)gfp*. Next, the plasmid pLOW-*lacA-m(sf)gfp* was constructed, where an NcoI site was inserted immediately upstream of the start codon. The *lacA* gene was amplified with primers im14_lacA_F_SalI_RBS_NcoI and im15_lacA_R_BamHI, the fragment was digested with Sall and BamHI and ligated into the corresponding sites of pLOW-*ftsZ-m(sf)gfp* to replace *ftsZ* with *lacA*.

Construction of C-terminal fusions to m(sf)gfp. The majority of the genes were amplified with primers having NcoI restriction site as overhang on the forward primer and BamHI restriction site as overhang on the reverse primer. The resulting fragments and the plasmid pLOW-*lacA-m(sf)gfp* were digested with NcoI and BamHI and ligated, resulting in plasmids pLOW-*x-m(sf)gfp*, where *x* represents the genes for C-terminal fusion in the library. A few genes already had one of the restriction sites sequences within the gene sequence and had to be constructed in a different manner. pLOW-*SAOUHSC_01756-m(sf)gfp* and pLOW-*SAOUHSC_01908-m(sf)gfp*, were constructed by including Sall and the RBS sequence as overhang on the forward primers. SAOUHSC_01244 and SAOUHSC_01782 had a BamHI restriction site sequence in their genes, so a KpnI restriction site was included as overhang on the reverse primers, and the fragment was ligated into pLOW-*ftsZ-m(sf)gfp_KpnI*.

Construction of N-terminal fusions to m(sf)gfp. For making N-terminal fusions, the plasmid pLOW-*m(sf)gfp-SAOUHSC_01477*, encoding a fusion gene with a flexible linker, was constructed initially. *m(sf)gfp* was amplified from pMK17 (van Raaphorst et al., 2017) with the primers im95_m(sf)gfp_F_SalI_RBS and im96_m(sf)gfp_R_linker_overlap. SAOUHSC_01477 was amplified with the primers

im97_SA1477_F_BamHI_linker-overlap and im98_SA1477_R_EcoRI_NotI. The forward primer im97 had overlapping sequence to the linker sequence in im96, followed by the BamHI restriction site. The two fragments, harboring overlapping sequences introduced in the primers, were fused together by overlap extension PCR using the outer primers im95 and im98. The resulting fragment was digested with Sall and EcoRI and ligated into the corresponding sites of pLOW-*ftsZ-gfp*. pLOW-*m(sf)gfp-SAOUHSC_01477* was then used as starting point for construction of N-terminal fusions for SAOUHSC_02151 and SAOUHSC_00957. SAOUHSC_02151 was amplified with the primers im99_SA2151_F_BamHI and im100_SA2151_R_EcoRI and digested with BamHI and EcoRI. SAOUHSC_00957 was amplified with the primers im101_SA0957_F_BglII and im102_SA0957_R_EcoRI and digested with BglII and EcoRI. Both digested fragments were then ligated into BamHI and EcoRI-digested pLOW-*m(sf)gfp-SAOUHSC_01477*.

Construction of pMAD-*smdA-m(sf)gfp_aad9* for chromosomal integration. To tag the chromosomal *smdA*, the plasmid pMAD-*smdA-flag_aad9* was constructed initially. The insert in this plasmid (*smdA-flag_aad9*) was assembled by overlap extension PCR (primers im147-im152 (Table S4), with the flag-tag sequence inserted by primer overhangs, and cloned into pMAD (Arnaud et al., 2004) using restriction enzymes MluI and BamHI and T4 DNA Ligase (NEB). The insert was designed so that the flag-tag could be removed using NotI and SpeI. The *m(sf)gfp* sequence was amplified from template pMK17 (van Raaphorst et al., 2017) using the primers im153 and im154. The PCR product was digested with NotI and SpeI and subsequently ligated with NotI- and SpeI-digested pMAD-*smdA-flag_aad9*. The ligation mix was transformed to *E. coli* IM08B, and the resulting plasmid, pMAD-*smdA-m(sf)gfp_aad9*, was verified by sequencing and transformed into electrocompetent *S. aureus* SH1000. Integration of *smdA-m(sf)gfp* in the native locus of *smdA* using the temperature-sensitive pMAD-system was carried out as previously described (Arnaud et al., 2004).

Construction of pHC-*ftsZ-mKate2*. *ftsZ-mKate2* was amplified from the plasmid pLOW-*ftsZ-mKate2*. pLOW-*ftsZ-mKate2* was made in a similar manner as described for pLOW-*ftsZ-m(sf)gfp*, but with reverse primer im5_mKate_R_NotI_EcoRI and MK119 (Kjos & Veening, 2014) as template for amplification of *mKate2*. Then, *ftsZ-mKate2* was amplified with primers USHC109 and USHC148, generating a product with Sall and MluI as overhang. The PCR product and the plasmid pSK9065 (Brzoska & Firth, 2013) were digested with Sall and MluI and thereafter ligated.

Construction of pLOW-smdA-mYFP. This plasmid was constructed by using pLOW-ftsZ-mYFP as starting point, made similarly as pLOW-ftsZ-m(sf)gfp, but with reverse primer im3_cfp_myfp_R_NotI_EcoRI and plasmid pMK20 (lab collection) as template for amplifying *mYFP*. The plasmids pLOW-SAOUHSC_01908-m(sf)gfp (described above) and pLOW-ftsZ-mYFP were digested with SalI and BamHI and subsequently ligated, resulting in pLOW-smdA-mYFP.

CRISPRi knockdown strains

For gene knockdown, the CRISPR interference (CRISPRi) system developed by Stamsås et al. (2018) were used. In this system, *dcas9* is placed downstream of an IPTG-inducible promoter in the plasmid pLOW-*dcas9*. A second plasmid is carrying the single guide RNA (pCG248-sgRNA(*x*), where *x* represents the targeted gene), which constitutively expresses the sgRNA, including the 20 nt base-pairing region specific for the gene to be knocked down. The pLOW-*dcas9* plasmid contains an erythromycin resistance gene, and the pCG248-sgRNA(*x*) plasmid a chloramphenicol resistance gene.

Construction of pCG248-sgRNA(*x*) plasmids. The gene-specific 20 nt sequences were replaced in the pCG248-sgRNA(*x*) plasmids using an inverse PCR approach as described earlier (Stamsås et al., 2018) or with a Golden Gate cloning approach. Primers used are found in Table S4.

Construction of pLOW-dCas9 aad9. The erythromycin resistance gene *ermC* in pLOW-*dcas9* was replaced with *aad9*, encoding a spectinomycin resistance cassette, in order to make the CRISPRi system compatible with the MRSA strain COL. The primers im183 and im184 were used to amplify the entire pLOW-*dcas9* plasmid, except the *ermC* gene. The *aad9* gene was amplified with primers im185 and im186 using pCN55 (Charpentier et al., 2004) as template, where im185 contained the sequence of im183 as overhang, and im186 the sequence of im184 as overhang. Thus, the two fragments had overlapping sequences and were fused using NEBuilder® HiFi DNA Assembly (NEB). The construct was transformed to *E. coli* IM08B, and the plasmid verified by PCR and sequencing. For CRISPRi in *S. aureus* COL, the pLOW-*dcas9_aad9* plasmid was used along with pCG248-sgRNA(*x*).

Construction of plasmids used for overexpression studies

Construction of pLOW-smdA and mutated versions. *smdA* was amplified from *S. aureus* genomic DNA using primers im77_SA1908_F_SalI_RBS and mk517_1908_R_NotI. The fragment was digested with SalI and NotI and ligated into the corresponding sites of plasmid pLOW-*dcas9* (Stamsås et al., 2018) to produce the plasmid pLOW-*smdA*, with IPTG-inducible overexpression of *smdA*. pLOW-*smdA*ΔTMH was constructed in a similar manner, except that primer mk518_1908_F_RBS_SalI was used instead of im77 to remove the 29 N-terminal amino acids of SmdA, predicted to encode the TMH and extracellular part. Site-directed mutagenesis in the two plasmids was performed by a two-step overlap extension PCR approach, where the mutations were introduced in the primers. The primers mk519 and mk520 were used for introducing mutation H145A (mut1), mut2 (R150A, R151A) was made with primers mk521 and mk522, and mut3 (F280A, H281A) with primers mk529 and mk530.

Phase contrast- and fluorescence microscopy analysis

Cultures were added to agarose pads and microscopy performed on a Zeiss AxioObserver with ZEN Blue software. An ORCAFlash4.0 V2 Digital complementary metal-oxide semiconductor (CMOS) camera (Hamamatsu Photonics) was used to capture images through a 100 × PC objective. HPX 120 Illuminator (Zeiss) was used as a light source for fluorescence microscopy. BODIPY™ FL vancomycin (VanFL) (Invitrogen) and DAPI (Invitrogen) were added for staining of DNA and cell wall, respectively. To label newly synthesized peptidoglycan, HADA (van Nieuwenhze group, Indiana University) was added actively growing cultures (OD₆₀₀ approximately 0.4) at a final concentration of 250 μM. The cells were incubated at 37°C for 90 sec and put on ice to stop growth. The cultures were pelleted by centrifugation at 10 000 × *g* at 4°C for 1 min, washed with cold 1 × PBS, pH 7.4 and finally resuspended in 25 μl PBS. Cells were subsequently added to agarose pads and analyzed.

Images were processed and prepared for publication using Fiji (Schindelin et al., 2012). For analysis of cell roundness, cell area and fluorescent labelling patterns, MicrobeJ (Ducret et al., 2016) was used to determine cell outlines. Outlines were corrected manually, when necessary. Cell area and roundness as a measure of morphology were calculated and plotted using MicrobeJ. After cell outline detection, categorization of cells into normal or abnormal labelling patterns were done manually using images from independent experiments.

Structured illumination microscopy (SIM) and stimulated emission depletion (STED) microscopy

Super-resolution SIM imaging was performed using a Zeiss ELYRA PS.1 microscope equipped with a 100 × 1.46 NA alpha plan apochromat oil immersion objective and a pco.edge sCMOS camera. Fluorescence images were acquired sequentially using 200–300 ms exposure times per image, for a total of 15 images per SIM reconstruction. All imaging was performed at room temperature (~23°C). Raw data were reconstructed using the SIM algorithms in ZEN 2011 SP7 software (black edition, Carl Zeiss). Brightfield images were captured using widefield imaging mode. Images had a final pixel size of 25 nm.

Gated STED (gSTED) images were acquired on a Leica TCS SP8 STED 3× system, using a HC PL Apo 100 × oil immersion objective with NA 1.40. Fluorophores were excited using a white excitation laser operated at 509 nm for mYFP and 563 nm for mKate2. A STED depletion laser line was operated at 592 nm and 775 nm for mYFP and mKate2, respectively, using a detection time-delay of 0.8–1.6 ns for both fluorophores. The total depletion laser intensity was in the order of 20–40 MW cm⁻² for all STED imaging. The final pixel size was 13 nm and scanning speed was 400 Hz. The pinhole size was set to 0.9 AU.

Images were processed and analyzed using Fiji (Schindelin et al., 2012). Line scans were analyzed using the Plot Profile function in Fiji, using a line width of 1.5. Fluorescence intensities were normalized to the highest value for each channel.

Scanning- and transmission electron microscopy analysis

Overnight cultures were diluted to approximately OD₆₀₀ = 0.1. When OD₆₀₀ reached 0.4, the cultures were diluted 1:250. Antibiotic and IPTG were added when appropriate. The cultures (10 ml) were grown to OD₆₀₀ = 0.3 and 1 volume of fixation solution, containing 5 % (w/v) glutaraldehyde and 4 % (w/v) paraformaldehyde in 1×PBS, pH 7.4, was added. The tubes were carefully inverted a few times and incubated for one hour at room temperature before being placed at 4°C overnight. The following day, the cultures were centrifugated at 5000 × *g*, and the pellets washed three times with PBS. Further preparations of samples to be analyzed with TEM were performed as described before (Stamsås et al., 2018).

Samples for SEM were, after washing with PBS, dehydrated with EtOH, essentially in the same manner as for sample preparations for TEM (Stamsås et al., 2018). The samples were subjected to critical point drying by exchanging the EtOH with CO₂. Then, the samples were coated with a conductive layer of Au-Pd before

being analyzed in a ZEISS EVO50 EP Scanning electron microscope. Images were analyzed and prepared using Fiji (Schindelin et al., 2012).

Growth assays

For monitoring growth in liquid media, cultures were initially pre-grown to exponential phase ($OD_{600} = 0.4$) by diluting overnight cultures. Thereafter, cultures were back diluted in fresh BHI medium to $OD_{600} = 0.05$ and a two-fold dilution series were made before adding the cultures to a 96-well microtiter plate. A final concentration of 300 μM IPTG was added for induction and antibiotics were added when appropriate. The cells were grown at 37°C, and measurements of OD_{600} were taken every 10th minute, with shaking 5 sec before each read, using either a Synergy™ H1 Hybrid Multi-Mode Reader (BioTek Instruments) or a Hidex Sense (Hidex Oy). The data are mean values from at least 3 technical replicates.

For examining growth on solid media, overnight cultures were pre-grown as described, and diluted 1:250 in BHI containing 300 μM IPTG, unless otherwise specified. When reaching exponential phase, OD_{600} were adjusted to 0.3 for all samples. A 10-fold dilution series were made for all strains, and 2 μl of each dilution were spotted on BHI agar containing proper antibiotics and 300 μM IPTG. The plates were incubated at 37°C for approximately 16 h, and pictures of the plates were captured in a Gel Doc™ XR + Imager (Bio-Rad).

Minimum inhibitory concentration (MIC) assays

The experiments were set up in 96-well microtiter plates with a total volume of 300 μl . A two-fold dilution series of the antibiotics were prepared in BHI containing selective antibiotics and IPTG when appropriate. The overnight cultures were diluted 1:1000 in BHI. The cells were grown at 37°C, and the plate was shaken for 5 sec before measurements of OD_{600} were taken every 10th min throughout the experiment, using either a Synergy™ H1 Hybrid Multi-Mode Reader (BioTek Instruments) or a Hidex Sense (Hidex Oy).

RNA isolation and RT-PCR

To verify that *smdA* expression was knocked down by CRISPRi, RNA was isolated from exponentially growing cultures of IM284 (SH1000, CRISPRi(control)), IM165 (SH000 CRISPRi(empty)) and IM269 (SH1000 CRISPRi(*smdA*)). Isolation of total RNA and cDNA synthesis were performed as previously described (Stamsås et al., 2018). A PCR reaction (30 cycles) was run with Phusion® High-Fidelity DNA polymerase (NEB).

The primer pairs im126/im127 and im137/im138 were used to target the reference gene *pta* (Valihrach & Demnerova, 2012) and *smdA*, respectively.

Detection of lipoteichoic acid (LTA) by Western blotting

Detection of LTA was performed by western blotting, and sample preparations were done according to descriptions found in Hesser et al. (2020). The samples were separated on a 4-20 % gradient Mini Protean TGX acrylamide gel (BioRad), and subsequently transferred to a polyvinylidene difluoride (PVDF) membrane by semi-dry electroblotting. The membrane was blocked for 1 h in 5 % (w/v) skim milk in PBST and placed overnight at 4°C. Next, the membrane was incubated for 1 h with α -LTA (Hycult) 1:4000 in PBST, washed three times (10 minutes each) with PBST before incubation for 1 h with α -Mouse IgG HRP Conjugate (Promega) secondary antibody (1:10 000 in PBST). The membrane was again washed three times and LTA bands were visualized by using SuperSignal™ West Pico PLUS Chemiluminescent substrate (Thermo Fisher Scientific) in an Azure Imager c400 (Azure Biosystems).

Same procedure as in (Mikkelsen et al., 2021) was performed for possible detection of LTA released to the medium. The supernatants, after harvesting cells during sample preparations, were kept. Supernatant samples were centrifugated for $16\,000 \times g$ for 10 min, and 75 μ l was mixed with 25 μ l $4 \times$ SDS-PAGE sample buffer. These samples were boiled for 30 min and applied on the 4-20 % Mini Protean TGX acrylamide gel. Thereafter, the same blotting procedure as described above was followed.

Fourier-transform infrared spectroscopy (FTIR) analysis

Cultures of the strains IM313 (HG001, CRISPRi(control)), IM312 (HG001, CRISPRi(*smdA*)) and IM357 (HG001, CRISPRi(*tarO*)) were initially pre-grown to exponential phase, back diluted to $OD_{600} = 0.05$ and induced with 300 μ M IPTG. The bacterial cells (1 ml) were harvested at $OD_{600} = 0.4$ by centrifugation at $5000 \times g$, 4°C, for 3 min. The pelleted cells were kept at -20°C prior to further processing. Pellets were resuspended in 40 μ l 0.1 % (w/v) NaCl, and 10 μ l of the suspensions were added to an IR-light-transparent silicon 384-well microplate (Bruker Optic, Germany), with three technical replicates for each sample. The plates were left to dry at room temperature for approximately 2 h. FTIR spectra were recorded in transmission mode using a high-throughput screening extension (HTS-XT) unit coupled to a Vertex 70 FTIR spectrometer (Bruker Optik GmbH, Leipzig, Germany). Spectra were recorded in the region 4000-500 cm^{-1} , with a spectral resolution of 6 cm^{-1} , a digital spacing of 1.928 cm^{-1} , and an aperture of 5 mm. For each spectrum, 64 scans were

averaged. The OPUS software (Bruker Optik GmbH, Leipzig, Germany) was used for data acquisition and instrument control. The obtained spectra were processed by taking second derivatives and extended multiplicative signal correction (EMSC) preprocessing in Unscrambler X version 11 (CAMO Analytics, Oslo, Norway). Results presented are averaged spectra from 3 biological replicates (each with 3 technical replicates) for the region with wavelengths between 1200 cm^{-1} and 800 cm^{-1} .

GFP-trap and liquid chromatography with tandem mass spectrometry (LC-MS/MS)

Cultures (*S. aureus* SH1000 wild-type, IM308 SH1000 *smdA-m(sf)gfp*, IM104 SH1000 pLOW-*smdA-m(sf)gfp* and IM164 SH1000 pLOW-*smdA-flag*) were pre-grown to exponential phase, back diluted to $\text{OD}_{600} = 0.05$ and induced if necessary. When reaching OD_{600} at 0.4, 80 ml of each culture were harvested by centrifugation at $4000 \times g$, 4°C for 3 min. Supernatants were decanted and pellets resuspended in cold TBS prior to transfer to 1.5 ml microcentrifuge tubes. Centrifugation was repeated for 1 min, and pelleted cells were stored at -80°C prior to further use.

For GFP-trap, cells were resuspended in 1 ml cold buffer containing 10 mM Tris pH 7.5, 150 mM NaCl, 1 mM PMSF, 6 $\mu\text{g/ml}$ RNase and 6 $\mu\text{g/ml}$ DNase. Suspensions were transferred to 2 ml lysing matrix B tubes (MP Biomedicals) containing $0.8 \text{ g} \leq 106 \mu\text{m}$ glass beads (Sigma-Aldrich) and subjected for mechanical lysis by agitation in a FastPrep-24™ (MP Biomedicals) for $3 \times 30 \text{ sec}$ at 6.5 m/s, with 1 min pause on ice between the runs. Tubes were centrifuged at $5000 \times g$, 4°C for 10 min, and supernatants transferred to new tubes. Concentrations were determined measuring A280 using NanoDrop™ 2000 (Thermo Fisher Scientific), where a small amount of the samples were added a final concentration of 1 % (w/v) SDS prior to measurements. GFP-Trap beads (25 μl per sample) (Chromotek) were washed three times with 500 μl cold Dilution/Wash buffer (10 mM Tris pH 7.5, 150 mM NaCl, 0.5 mM EDTA) and centrifuged at $2500 \times g$, 4°C for 5 min. Lysates were diluted in Dilution/Wash buffer to a final concentration of 1 mg in a total volume of 500 μl , before being transferred to GFP-Trap beads. Samples were placed in a Bio RS-24 Multi rotor (Biosan) at 4°C for 1 h. Then, samples were centrifuged at $2500 \times g$, 4°C for 5 min, supernatant removed, and beads washed three times with Dilution/Wash buffer. During last washing step, solutions were transferred to new tubes, and after centrifugation and removal of supernatant, beads were resuspended in 50 μl 5 % (w/v) SDS, 50 mM Tris pH 7.6. Tubes were incubated at 95°C for 5 min, and centrifuged at maximum speed for 30 sec. After standing at the bench a few minutes, 30-50 μl were transferred into new tubes. Samples were kept at -20°C and heated for

2 min at 95°C prior to the sample preparation method Suspension trapping (STrap), conducted as described by Zougman et al. (2014).

The peptide samples were analyzed by coupling a nano UPLC (nanoElute, Bruker) to a trapped ion mobility spectrometry/quadrupole time of flight mass spectrometer (timsTOF Pro, Bruker). The peptides were separated by an Aurora Series 1.6 µm C18 reverse-phase 25 cm × 75 µm analytical column with nanoZero and CaptiveSpray Insert (IonOpticks, Australia). The flow rate was set to 400 nl/min and the peptides were separated using a gradient from 2 % to 95 % acetonitrile solution (in 0.1 % (v/v) formic acid) over 120 minutes. The timsTOF Pro was ran in positive ion data dependent acquisition PASEF mode, with a mass range at 100-1700 m/z. The acquired spectra were analyzed against a *S. aureus* NCTC8325 proteome database.

Bacterial two-hybrid (BACTH) assays

Plasmid construction, and procedure for the BACTH assays, were conducted in a same manner as previously described (Stamsås et al., 2018), and primers used are listed in Table S4. Shortly, gene fusions of selected genes, to the T18 or T25 domains of adenylate cyclase form *Bordetella pertussis*, were made by restriction cutting and ligation in the plasmid vectors pKT25, pKNT25, pUT18 or pUT18C (Euromedex). *E. coli* XL1-Blue cells were used for transformation, and plasmids verified by sequencing before BACTH assays (Karimova et al., 1998) were set up according to the manufacturer (Euromedex). Co-transformation of plasmids containing fusion-genes of opposite domains, that is T25 in one plasmid and T18 in the other, were done in *E. coli* BTH101 with 50 µg/ml kanamycin and 100 µg/ml ampicillin as selection markers. Five random colonies were picked, grown in liquid LB to visible growth, and spotted on LA plates containing 40 µg/ml X-gal and 0.5 mM IPTG, in addition to the selection markers. Plates were incubated dark at 30°C for 20-48 h before being inspected, and blue colonies are an indication of positive interaction between tested genes. Presented results are representative for at least six independent replicates.

Acknowledgements

We would like to acknowledge the NMBU Imaging Center for help with electron microscopy, Morten Skaugen, NMBU, for running the LC-MS/MS, Maria Victoria Heggenhougen and Marita Torrissen Mårli (both NMBU) for providing strains and Henriette Olsen (NMBU) for help with FTIR. We acknowledge the van Nieuwenhze group, Indiana University, for providing HADA. The work is supported by grants from the Research Council of Norway (project number 250976) and JPI-AMR (project number 296906). Work in the Structural Cell Biology Unit (OIST) is supported by OIST core subsidy. Ine S. Myrbråten acknowledge support from “Pasteurlegatet”.

References

- Arnaud, M., Chastanet, A. & Débarbouillé, M. (2004). New vector for efficient allelic replacement in naturally nontransformable, low-GC-content, Gram-positive bacteria. *Applied and environmental microbiology*, 70 (11): 6887-6891. doi: 10.1128/AEM.70.11.6887-6891.2004.
- Atilano, M. L., Pereira, P. M., Yates, J., Reed, P., Veiga, H., Pinho, M. G. & Filipe, S. R. (2010). Teichoic acids are temporal and spatial regulators of peptidoglycan cross-linking in *Staphylococcus aureus*. *Proceedings of the national academy of sciences*, 107 (44): 18991-18996. doi: 10.1073/pnas.1004304107.
- Barreteau, H., Kovač, A., Boniface, A., Sova, M., Gobec, S. & Blanot, D. (2008). Cytoplasmic steps of peptidoglycan biosynthesis. *FEMS microbiology reviews*, 32 (2): 168-207. doi: 10.1111/j.1574-6976.2008.00104.x.
- Biswas, R., Voggu, L., Simon, U. K., Hentschel, P., Thumm, G. & Götz, F. (2006). Activity of the major staphylococcal autolysin Atl. *FEMS microbiology letters*, 259 (2): 260-268. doi: 10.1111/j.1574-6968.2006.00281.x.
- Bouhss, A., Trunkfield, A. E., Bugg, T. D. & Mengin-Lecreulx, D. (2007). The biosynthesis of peptidoglycan lipid-linked intermediates. *FEMS microbiology reviews*, 32 (2): 208-233. doi: 10.1111/j.1574-6976.2007.00089.x.
- Brown, S., Xia, G., Luhachack, L. G., Campbell, J., Meredith, T. C., Chen, C., Winstel, V., Gekeler, C., Irazoqui, J. E. & Peschel, A. (2012). Methicillin resistance in *Staphylococcus aureus* requires glycosylated wall teichoic acids. *Proceedings of the national academy of sciences*, 109 (46): 18909-18914. doi: 10.1073/pnas.1209126109.
- Brown, S., Santa Maria Jr, J. P. & Walker, S. (2013). Wall teichoic acids of Gram-positive bacteria. *Annual review of microbiology*, 67: 313-336. doi: 10.1146/annurev-micro-092412-155620.
- Brzoska, A. J. & Firth, N. (2013). Two-plasmid vector system for independently controlled expression of green and red fluorescent fusion proteins in *Staphylococcus aureus*. *Applied and environmental microbiology*, 79 (9): 3133-3136. doi: 10.1128/AEM.00144-13.

- Campbell, J., Singh, A. K., Santa Maria Jr, J. P., Kim, Y., Brown, S., Swoboda, J. G., Mylonakis, E., Wilkinson, B. J. & Walker, S. (2011). Synthetic lethal compound combinations reveal a fundamental connection between wall teichoic acid and peptidoglycan biosyntheses in *Staphylococcus aureus*. *ACS chemical biology*, 6 (1): 106-116. doi: 10.1021/cb100269f.
- Campbell, J., Singh, A. K., Swoboda, J. G., Gilmore, M. S., Wilkinson, B. J. & Walker, S. (2012). An antibiotic that inhibits a late step in wall teichoic acid biosynthesis induces the cell wall stress stimulon in *Staphylococcus aureus*. *Antimicrobial agents and chemotherapy*, 56 (4): 1810-20. doi: 10.1128/aac.05938-11.
- Charpentier, E., Anton, A. I., Barry, P., Alfonso, B., Fang, Y. & Novick, R. P. (2004). Novel cassette-based shuttle vector system for Gram-positive bacteria. *Applied and environmental microbiology*, 70 (10): 6076-6085. doi: 10.1128/AEM.70.10.6076-6085.2004.
- Chaudhuri, R. R., Allen, A. G., Owen, P. J., Shalom, G., Stone, K., Harrison, M., Burgis, T. A., Lockyer, M., Garcia-Lara, J., Foster, S. J., et al. (2009). Comprehensive identification of essential *Staphylococcus aureus* genes using Transposon-Mediated Differential Hybridisation (TMDH). *BMC genomics*, 10 (1): 291. doi: 10.1186/1471-2164-10-291.
- Dubrac, S., Boneca, I. G., Poupel, O. & Msadek, T. (2007). New insights into the WalK/WalR (YycG/YycF) essential signal transduction pathway reveal a major role in controlling cell wall metabolism and biofilm formation in *Staphylococcus aureus*. *Journal of bacteriology*, 189 (22): 8257-69. doi: 10.1128/jb.00645-07.
- Ducret, A., Quardokus, E. M. & Brun, Y. V. (2016). MicrobeJ, a tool for high throughput bacterial cell detection and quantitative analysis. *Nature microbiology*, 1 (7): 16077. doi: 10.1038/nmicrobiol.2016.77.
- Errington, J., Daniel, R. A. & Scheffers, D.-J. (2003). Cytokinesis in bacteria. *Microbiology and molecular biology reviews*, 67 (1): 52-65. doi: 10.1128/MMBR.67.1.52-65.2003.
- Feng, J., Michalik, S., Varming, A. N., Andersen, J. H., Albrecht, D., Jelsbak, L., Krieger, S., Ohlsen, K., Hecker, M., Gerth, U., et al. (2013). Trapping and proteomic identification of cellular substrates of the ClpP protease in *Staphylococcus aureus*. *Journal of proteome research*, 12 (2): 547-58. doi: 10.1021/pr300394r.
- Gallay, C., Sanselicio, S., Anderson, M. E., Soh, Y. M., Liu, X., Stamsås, G. A., Pellicciari, S., van Raaphorst, R., Dénéréaz, J., Kjos, M., et al. (2021). CcrZ is a pneumococcal spatiotemporal cell cycle regulator that interacts with FtsZ and controls DNA replication by modulating the activity of DnaA. *Nature microbiology*, 6 (9): 1175-1187. doi: 10.1038/s41564-021-00949-1.
- Grunert, T., Jovanovic, D., Sirisarn, W., Johler, S., Weidenmaier, C., Ehling-Schulz, M. & Xia, G. (2018). Analysis of *Staphylococcus aureus* wall teichoic acid glycoepitopes by Fourier Transform Infrared Spectroscopy provides novel insights into the staphylococcal glycode. *Scientific reports*, 8 (1): 1-9. doi: 10.1038/s41598-018-20222-6.
- Grynberg, M. & Godzik, A. (2004). NERD: a DNA processing-related domain present in the anthrax virulence plasmid, pXO1. *Trends in biochemical sciences*, 29 (3): 106-110. doi: 10.1016/j.tibs.2004.01.002.

- Hartman, B. J. & Tomasz, A. (1984). Low-affinity penicillin-binding protein associated with beta-lactam resistance in *Staphylococcus aureus*. *Journal of bacteriology*, 158 (2): 513-516. doi: 10.1128/jb.158.2.513-516.1984.
- Hesser, A. R., Matano, L. M., Vickery, C. R., Wood, B. M., Santiago, A. G., Morris, H. G., Do, T., Losick, R. & Walker, S. (2020). The length of lipoteichoic acid polymers controls *Staphylococcus aureus* cell size and envelope integrity. *Journal of bacteriology*, 202 (16): e00149-20. doi: 10.1128/JB.00149-20.
- Jensen, C., Bæk, K. T., Gallay, C., Thalsø-Madsen, I., Xu, L., Jousselin, A., Torrubia, F. R., Paulander, W., Pereira, A. R. & Veening, J.-W. (2019). The ClpX chaperone controls autolytic splitting of *Staphylococcus aureus* daughter cells, but is bypassed by β -lactam antibiotics or inhibitors of WTA biosynthesis. *PLoS pathogens*, 15 (9): e1008044. doi: 10.1371/journal.ppat.1008044.
- Jorge, A. M., Hoiczky, E., Gomes, J. P. & Pinho, M. G. (2011). EzrA contributes to the regulation of cell size in *Staphylococcus aureus*. *PLoS One*, 6 (11): e27542. doi: 10.1371/journal.pone.0027542.
- Jumper, J., Evans, R., Pritzel, A., Green, T., Figurnov, M., Ronneberger, O., Tunyasuvunakool, K., Bates, R., Žídek, A., Potapenko, A., et al. (2021). Highly accurate protein structure prediction with AlphaFold. *Nature*, 596 (7873): 583-589. doi: 10.1038/s41586-021-03819-2.
- Karimova, G., Pidoux, J., Ullmann, A. & Ladant, D. (1998). A bacterial two-hybrid system based on a reconstituted signal transduction pathway. *Proceedings of the national academy of sciences*, 95 (10): 5752-6. doi: 10.1073/pnas.95.10.5752.
- Kjos, M. & Veening, J. W. (2014). Tracking of chromosome dynamics in live *Streptococcus pneumoniae* reveals that transcription promotes chromosome segregation. *Molecular microbiology*, 91 (6): 1088-105. doi: 10.1111/mmi.12517.
- Kwon, A., Scott, S., Taujale, R., Yeung, W., Kochut, K. J., Eyers, P. A. & Kannan, N. (2019). Tracing the origin and evolution of pseudokinases across the tree of life. *Science signaling*, 12 (578): eaav3810. doi: 10.1126/scisignal.aav3810.
- Lee, S. H., Jarantow, L. W., Wang, H., Sillaots, S., Cheng, H., Meredith, T. C., Thompson, J. & Roemer, T. (2011). Antagonism of chemical genetic interaction networks resensitize MRSA to β -lactam antibiotics. *Chemical biology*, 18 (11): 1379-1389. doi: 10.1016/j.chembiol.2011.08.015.
- Liew, A. T., Theis, T., Jensen, S. O., Garcia-Lara, J., Foster, S. J., Firth, N., Lewis, P. J. & Harry, E. J. (2011). A simple plasmid-based system that allows rapid generation of tightly controlled gene expression in *Staphylococcus aureus*. *Microbiology*, 157 (3): 666-676. doi: 10.1099/mic.0.045146-0.
- Lund, V. A., Wacnik, K., Turner, R. D., Cotterell, B. E., Walther, C. G., Fenn, S. J., Grein, F., Wollman, A. J., Leake, M. C., Olivier, N., et al. (2018). Molecular coordination of *Staphylococcus aureus* cell division. *eLife*, 7: e32057. doi: 10.7554/eLife.32057.
- Löfblom, J., Kronqvist, N., Uhlén, M., Ståhl, S. & Wernérus, H. (2007). Optimization of electroporation-mediated transformation: *Staphylococcus carnosus* as model organism. *Journal of applied microbiology*, 102 (3): 736-747. doi: 10.1111/j.1365-2672.2006.03127.x.
- Meeske, A. J., Riley, E. P., Robins, W. P., Uehara, T., Mekalanos, J. J., Kahne, D., Walker, S., Kruse, A. C., Bernhardt, T. G. & Rudner, D. Z. (2016). SEDS proteins are a

- widespread family of bacterial cell wall polymerases. *Nature*, 537 (7622): 634-638. doi: 10.1038/nature19331.
- Mikkelsen, K., Sirisarn, W., Alharbi, O., Alharbi, M., Liu, H., Nøhr-Meldgaard, K., Mayer, K., Vestergaard, M., Gallagher, L. A. & Derrick, J. P. (2021). The novel membrane-associated auxiliary factors AuxA and AuxB modulate β -lactam resistance in MRSA by stabilizing lipoteichoic acids. *International journal of antimicrobial agents*, 57 (3): 106283. doi: 10.1016/j.ijantimicag.2021.106283.
- Monk, I. R., Tree, J. J., Howden, B. P., Stinear, T. P. & Foster, T. J. (2015). Complete bypass of restriction systems for major *Staphylococcus aureus* lineages. *mBio*, 6 (3): e00308-15. doi: 10.1128/mBio.00308-15.
- Monteiro, J. M., Fernandes, P. B., Vaz, F., Pereira, A. R., Tavares, A. C., Ferreira, M. T., Pereira, P. M., Veiga, H., Kuru, E. & VanNieuwenhze, M. S. (2015). Cell shape dynamics during the staphylococcal cell cycle. *Nature communications*, 6 (1): 1-12. doi: 10.1038/ncomms9055.
- Monteiro, J. M., Pereira, A. R., Reichmann, N. T., Saraiva, B. M., Fernandes, P. B., Veiga, H., Tavares, A. C., Santos, M., Ferreira, M. T., Macario, V., et al. (2018). Peptidoglycan synthesis drives an FtsZ-treadmilling-independent step of cytokinesis. *Nature*, 554 (7693): 528-532. doi: 10.1038/nature25506.
- Nega, M., Tribelli, P. M., Hipp, K., Stahl, M. & Götz, F. (2020). New insights in the coordinated amidase and glucosaminidase activity of the major autolysin (Atl) in *Staphylococcus aureus*. *Communications biology*, 3 (1): 1-10. doi: 10.1038/s42003-020-01405-2.
- Oku, Y., Kurokawa, K., Matsuo, M., Yamada, S., Lee, B.-L. & Sekimizu, K. (2009). Pleiotropic roles of polyglycerolphosphate synthase of lipoteichoic acid in growth of *Staphylococcus aureus* cells. *Journal of bacteriology*, 191 (1): 141-151. doi: 10.1128/JB.01221-08.
- Omasits, U., Ahrens, C. H., Müller, S. & Wollscheid, B. (2014). Protter: interactive protein feature visualization and integration with experimental proteomic data. *Bioinformatics*, 30 (6): 884-886. doi: 10.1093/bioinformatics/btt607.
- Oshida, T., Sugai, M., Komatsuzawa, H., Hong, Y.-M., Suginaka, H. & Tomasz, A. (1995). A *Staphylococcus aureus* autolysin that has an N-acetylmuramoyl-L-alanine amidase domain and an endo-beta-N-acetylglucosaminidase domain: cloning, sequence analysis, and characterization. *Proceedings of the national academy of sciences*, 92 (1): 285-289. doi: 10.1073/pnas.92.1.285.
- Pereira, A. R., Hsin, J., Król, E., Tavares, A. C., Flores, P., Hoiczky, E., Ng, N., Dajkovic, A., Brun, Y. V., VanNieuwenhze, M. S., et al. (2016). FtsZ-dependent elongation of a coccoid bacterium. *mBio*, 7 (5): e00908-16. doi: 10.1128/mBio.00908-16.
- Pinho, M. G. & Errington, J. (2005). Recruitment of penicillin-binding protein PBP2 to the division site of *Staphylococcus aureus* is dependent on its transpeptidation substrates. *Molecular microbiology*, 55 (3): 799-807. doi: 10.1111/j.1365-2958.2004.04420.x.
- Pinho, M. G., Kjos, M. & Veening, J.-W. (2013). How to get (a) round: mechanisms controlling growth and division of coccoid bacteria. *Nature reviews microbiology*, 11 (9): 601-614. doi: 10.1038/nrmicro3088.
- Price, N. P. & Tsvetanova, B. (2007). Biosynthesis of the tunicamycins: a review. *The journal of antibiotics*, 60 (8): 485-491. doi: 10.1038/ja.2007.62.

- Quiblier, C., Zinkernagel, A. S., Schuepbach, R. A., Berger-Bächli, B. & Senn, M. M. (2011). Contribution of SecDF to *Staphylococcus aureus* resistance and expression of virulence factors. *BMC microbiology*, 11: 72. doi: 10.1186/1471-2180-11-72.
- Radkov, A. D., Hsu, Y.-P., Booher, G. & VanNieuwenhze, M. S. (2018). Imaging bacterial cell wall biosynthesis. *Annual review of biochemistry*, 87: 991-1014. doi: 10.1146/annurev-biochem-062917-012921.
- Reichmann, N. T., Tavares, A. C., Saraiva, B. M., Jousselin, A., Reed, P., Pereira, A. R., Monteiro, J. M., VanNieuwenhze, M. S., Fernandes, F. & Pinho, M. G. (2019). SEDS-bPBP pairs direct lateral and septal peptidoglycan synthesis in *Staphylococcus aureus*. *Nature microbiology*, 4: 1368-1377. doi: 10.1038/s41564-019-0437-2.
- Reynolds, P. E. (1989). Structure, biochemistry and mechanism of action of glycopeptide antibiotics. *European journal of clinical microbiology & infectious diseases*, 8 (11): 943-950. doi: 10.1007/bf01967563.
- Roch, M., Lelong, E., Panasencko, O. O., Sierra, R., Renzoni, A. & Kelley, W. L. (2019). Thermosensitive PBP2a requires extracellular folding factors PrsA and HtrA1 for *Staphylococcus aureus* MRSA β -lactam resistance. *Communications biology*, 2: 417. doi: 10.1038/s42003-019-0667-0.
- Roemer, T., Schneider, T. & Pinho, M. G. (2013). Auxiliary factors: a chink in the armor of MRSA resistance to β -lactam antibiotics. *Current opinion in microbiology*, 16 (5): 538-548. doi: 10.1016/j.mib.2013.06.012.
- Rohrer, S. & Berger-Bächli, B. (2003). FemABX peptidyl transferases: a link between branched-chain cell wall peptide formation and β -lactam resistance in gram-positive cocci. *Antimicrobial agents and chemotherapy*, 47 (3): 837-846. doi: 10.1128/AAC.47.3.837-846.2003.
- Santa Maria, J. P., Jr., Sadaka, A., Moussa, S. H., Brown, S., Zhang, Y. J., Rubin, E. J., Gilmore, M. S. & Walker, S. (2014). Compound-gene interaction mapping reveals distinct roles for *Staphylococcus aureus* teichoic acids. *Proceedings of the national academy of sciences*, 111 (34): 12510-12515. doi: 10.1073/pnas.1404099111.
- Santiago, M., Matano, L. M., Moussa, S. H., Gilmore, M. S., Walker, S. & Meredith, T. C. (2015). A new platform for ultra-high density *Staphylococcus aureus* transposon libraries. *BMC genomics*, 16 (1): 1-18. doi: 10.1186/s12864-015-1361-3.
- Saraiva, B. M., Sorg, M., Pereira, A. R., Ferreira, M. J., Caulat, L. C., Reichmann, N. T. & Pinho, M. G. (2020). Reassessment of the distinctive geometry of *Staphylococcus aureus* cell division. *Nature communications*, 11 (1): 1-7. doi: 10.1038/s41467-020-17940-9.
- Sass, P. & Brötz-Oesterhelt, H. (2013). Bacterial cell division as a target for new antibiotics. *Current opinion in microbiology*, 16 (5): 522-530. doi: 10.1016/j.mib.2013.07.006.
- Schindelin, J., Arganda-Carreras, I., Frise, E., Kaynig, V., Longair, M., Pietzsch, T., Preibisch, S., Rueden, C., Saalfeld, S. & Schmid, B. (2012). Fiji: an open-source platform for biological-image analysis. *Nature methods*, 9 (7): 676-682. doi: 10.1038/nmeth.2019.
- Sham, L.-T., Butler, E. K., Lebar, M. D., Kahne, D., Bernhardt, T. G. & Ruiz, N. (2014). Bacterial cell wall. MurJ is the flippase of lipid-linked precursors for

- peptidoglycan biogenesis. *Science*, 345 (6193): 220-222. doi: 10.1126/science.1254522.
- Silber, N., Pan, S., Schäkermann, S., Mayer, C., Brötz-Oesterhelt, H. & Sass, P. (2020). Cell division protein FtsZ is unfolded for N-terminal degradation by antibiotic-activated ClpP. *mBio*, 11 (3): e01006-20. doi: 10.1128/mBio.01006-20.
- Stamsås, G. A., Myrbråten, I. S., Straume, D., Salehian, Z., Veening, J. W., Håvarstein, L. S. & Kjos, M. (2018). CozEa and CozEb play overlapping and essential roles in controlling cell division in *Staphylococcus aureus*. *Molecular microbiology*, 109 (5): 615-632. doi: 10.1111/mmi.13999.
- Steczkiewicz, K., Muszewska, A., Knizewski, L., Rychlewski, L. & Ginalski, K. (2012). Sequence, structure and functional diversity of PD-(D/E)XK phosphodiesterase superfamily. *Nucleic acids research*, 40 (15): 7016-7045. doi: 10.1093/nar/gks382.
- Suzuki, T., Campbell, J., Kim, Y., Swoboda, J. G., Mylonakis, E., Walker, S. & Gilmore, M. S. (2012). Wall teichoic acid protects *Staphylococcus aureus* from inhibition by Congo red and other dyes. *Journal of antimicrobial chemotherapy*, 67 (9): 2143-2151. doi: 10.1093/jac/dks184.
- Swoboda, J. G., Campbell, J., Meredith, T. C. & Walker, S. (2010). Wall teichoic acid function, biosynthesis, and inhibition. *ChemBioChem*, 11 (1): 35-45. doi: 10.1002/cbic.200900557.
- Tan, C. M., Therien, A. G., Lu, J., Lee, S. H., Caron, A., Gill, C. J., Lebeau-Jacob, C., Benton-Perdomo, L., Monteiro, J. M., Pereira, P. M., et al. (2012). Restoring methicillin-resistant *Staphylococcus aureus* susceptibility to β -lactam antibiotics. *Science translational medicine*, 4 (126): 126ra35. doi: 10.1126/scitranslmed.3003592.
- Thalsø-Madsen, I., Torrubia, F. R., Xu, L., Petersen, A., Jensen, C. & Frees, D. (2019). The Sle1 cell wall amidase is essential for β -lactam resistance in community-acquired methicillin-resistant *Staphylococcus aureus* USA300. *Antimicrobial agents and chemotherapy*, 64 (1): e01931-19. doi: 10.1128/AAC.01931-19.
- Ubukata, K., Yamashita, N. & Konno, M. (1985). Occurrence of a beta-lactam-inducible penicillin-binding protein in methicillin-resistant staphylococci. *Antimicrobial agents and chemotherapy*, 27 (5): 851-857. doi: 10.1128/AAC.27.5.851.
- Valentino, M. D., Foulston, L., Sadaka, A., Kos, V. N., Villet, R. A., Santa Maria, J., Lazinski, D. W., Camilli, A., Walker, S. & Hooper, D. C. (2014). Genes contributing to *Staphylococcus aureus* fitness in abscess-and infection-related ecologies. *mBio*, 5 (5): e01729-14. doi: 10.1128/mBio.01729-14.
- Valihrach, L. & Demnerova, K. (2012). Impact of normalization method on experimental outcome using RT-qPCR in *Staphylococcus aureus*. *Journal of microbiological methods*, 90 (3): 214-216. doi: 10.1016/j.mimet.2012.05.008.
- van Raaphorst, R., Kjos, M. & Veening, J.-W. (2017). Chromosome segregation drives division site selection in *Streptococcus pneumoniae*. *Proceedings of the national academy of sciences*, 114 (29): E5959-E5968. doi: 10.1073/pnas.1620608114.
- Veiga, H., Jorge, A. M. & Pinho, M. G. (2011). Absence of nucleoid occlusion effector Noc impairs formation of orthogonal FtsZ rings during *Staphylococcus aureus*

- cell division. *Molecular microbiology*, 80 (5): 1366-1380. doi: 10.1111/j.1365-2958.2011.07651.x.
- Vickery, C. R., Wood, B. M., Morris, H. G., Losick, R. & Walker, S. (2018). Reconstitution of *Staphylococcus aureus* lipoteichoic acid synthase activity identifies Congo red as a selective inhibitor. *Journal of the american chemical society*, 140 (3): 876-879. doi: 10.1021/jacs.7b11704.
- Wyke, A. W., Ward, J. B., Hayes, M. V. & Curtis, N. A. (1981). A role *in vivo* for penicillin-binding protein-4 of *Staphylococcus aureus*. *European journal of biochemistry*, 119 (2): 389-393. doi: 10.1111/j.1432-1033.1981.tb05620.x.
- Zhou, X., Halladin, D. K., Rojas, E. R., Koslover, E. F., Lee, T. K., Huang, K. C. & Theriot, J. A. (2015). Mechanical crack propagation drives millisecond daughter cell separation in *Staphylococcus aureus*. *Science*, 348 (6234): 574-578. doi: 10.1126/science.aaa1511.
- Zougman, A., Selby, P. J. & Banks, R. E. (2014). Suspension trapping (STrap) sample preparation method for bottom-up proteomics analysis. *Proteomics*, 14 (9): 1006-1000. doi: 10.1002/pmic.201300553.

Supplementary material

SmdA is a novel cell morphology determinant in *Staphylococcus aureus*

Myrbråten et al.

Supplementary Text

Text S1. A combined knockdown- and subcellular localization screen of essential proteins of unknown function in *Staphylococcus aureus*

Proteins involved in staphylococcal cell cycle processes, including cell division, cell wall synthesis, DNA replication and chromosome segregation, often have a distinct temporal and spatial localization pattern. Furthermore, knockout or knockdown of such proteins often results in characteristic phenotypic defects, such as cell size variation, cell clustering or abnormal DAPI staining patterns. To identify yet uncharacterized, essential genes involved in the staphylococcal cell cycle, we selected a set of 27 essential genes (Chaudhuri et al., 2009; Santiago et al., 2015; Valentino et al., 2014) with no annotated functions neither in the Uniprot database (www.uniprot.org, “uncharacterized”) nor in the Patric database (www.patricbrc.org, “hypothetical”) (Sept. 2016), and performed a combined knockdown- and subcellular localization screen of the selected proteins. Knockdown strains were made using an established CRISPRi-system (Stamsås et al., 2018), and phenotyping of the knockdown strains was done with growth assays (Fig. S1) and microscopy of cells fluorescently labelled with the nucleoid stain DAPI and cell wall binding fluorescent vancomycin (Fig. S2). Fluorescent fusion proteins were expressed by constructing either N- or C-terminal fusions to monomeric superfolder GFP (*m(sf)gfp*), and localization were determined by fluorescent microscopy (Fig. S3).

Due to recent publications, as well as poor annotation in databases, some of the selected genes included in our screen have already been described by others. These include the cell cycle regulator CcrZ (Gallay et al., 2021), DacA and GdpP which are involved in synthesis and degradation, respectively, of the secondary messenger cyclic-di-AMP (Corrigan et al., 2011), the wall teichoic acid biosynthesis proteins TarL, TarJ and TarO (Qian et al., 2006; Sewell & Brown, 2014), GatD, which is a

member of the peptidoglycan amidotransferase complex MurT/GatD (Münch et al., 2012), the toxin transporter protein PmtD (Chatterjee et al., 2013), and TsaB and TsaE involved in adenosine biosynthesis (Deutsch et al., 2012).

An overview of the strains and the results from the knockdown- and localization screen are shown in Table S1. In total 16 out of the 22 knockdown strains displayed reduced growth (Fig. S1). The lack of growth reduction in the remaining six strains may be a result of insufficient depletion of the proteins, or that these genes are not essential under the tested conditions. Many of the knockdowns of the non-annotated genes resulted in phenotypic differences as observed by (fluorescence) microscopy (Fig. S2), including cell clustering (SAOUHSC_01244 and _01908), variable cell sizes (SAOUHSC_00444, _01721, _01756, _01930 and _01908) and abnormal nucleoid staining (SAOUHSC_00444, _01627, _01477, _01700/1, _01756, _01930 and _01908). Most of the proteins did not have a specific subcellular localization, as they either localized throughout the cytoplasm or membrane, as predicted by *in silico* tools (Table S1). It is worth noting, however, that the predicted cytoplasmic proteins SAOUHSC_01782, _01244 and _01930 displayed a membrane-localization, while SAOUHSC_02720 appeared as foci (Fig. S3). Furthermore, SAOUHSC_00957 and _01908, which are predicted to encode membrane-localized proteins appeared to have a septal or septum-enriched signal (Fig. S3).

Supplementary Figures

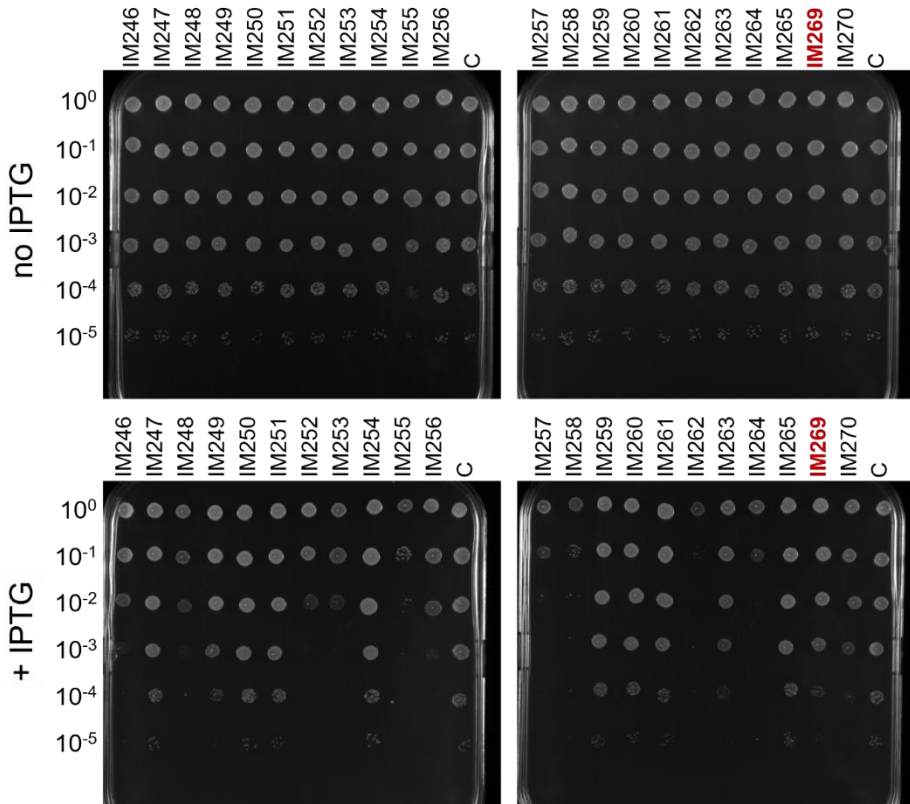


Fig. S1. Growth analysis of CRISPRi knockdown strains. A 10-fold dilution series were made for each strain before spotted on agar plates without or with IPTG (300 μ M) for induction of the CRISPRi system. Strain numbers are given on top of the figures. See Table S1 for locus tags corresponding to the different strains. The SmdA CRISPRi-strain IM269 is indicated in red.

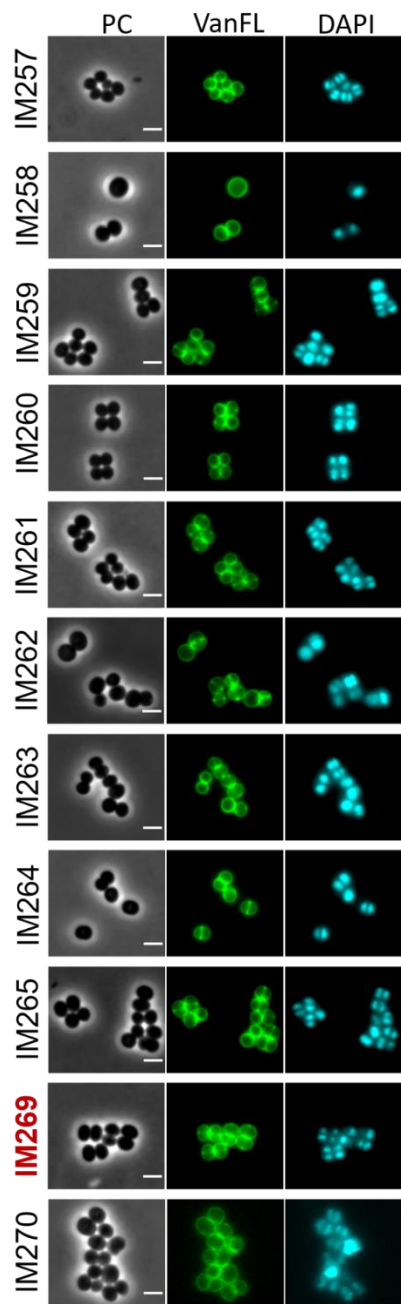
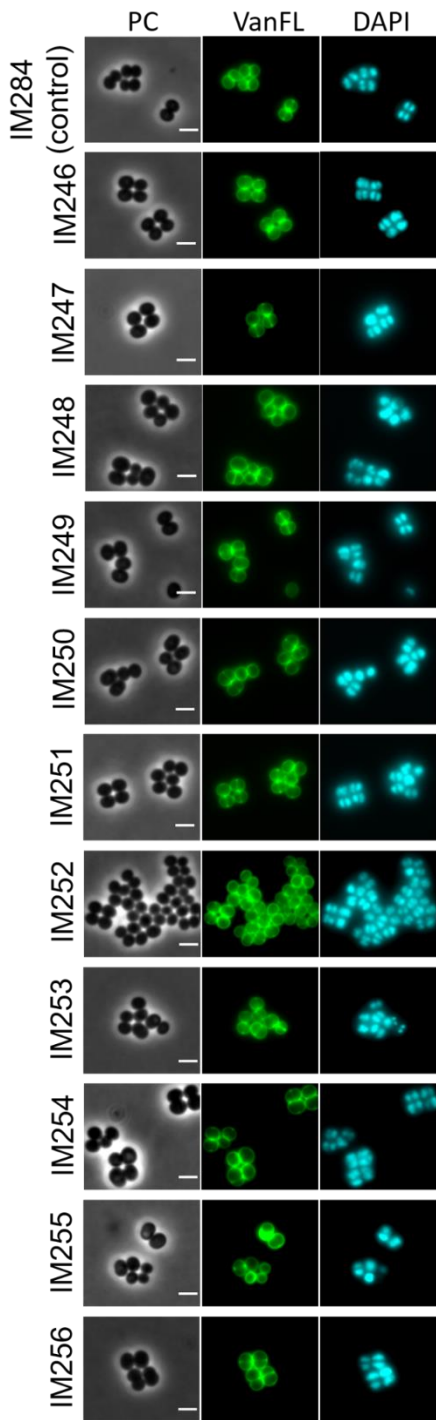


Fig. S2. Phenotyping of CRISPRi knockdown strains. The knockdown strains were labelled with DAPI (DNA stain) and fluorescent vancomycin (VanFL, cell wall stain), and visualized by fluorescence microscopy. Scale bars, 2 μ m. IM269, the SmdA knockdown strain, is highlighted in red. See Table S1 for locus tags corresponding to the different strain names.

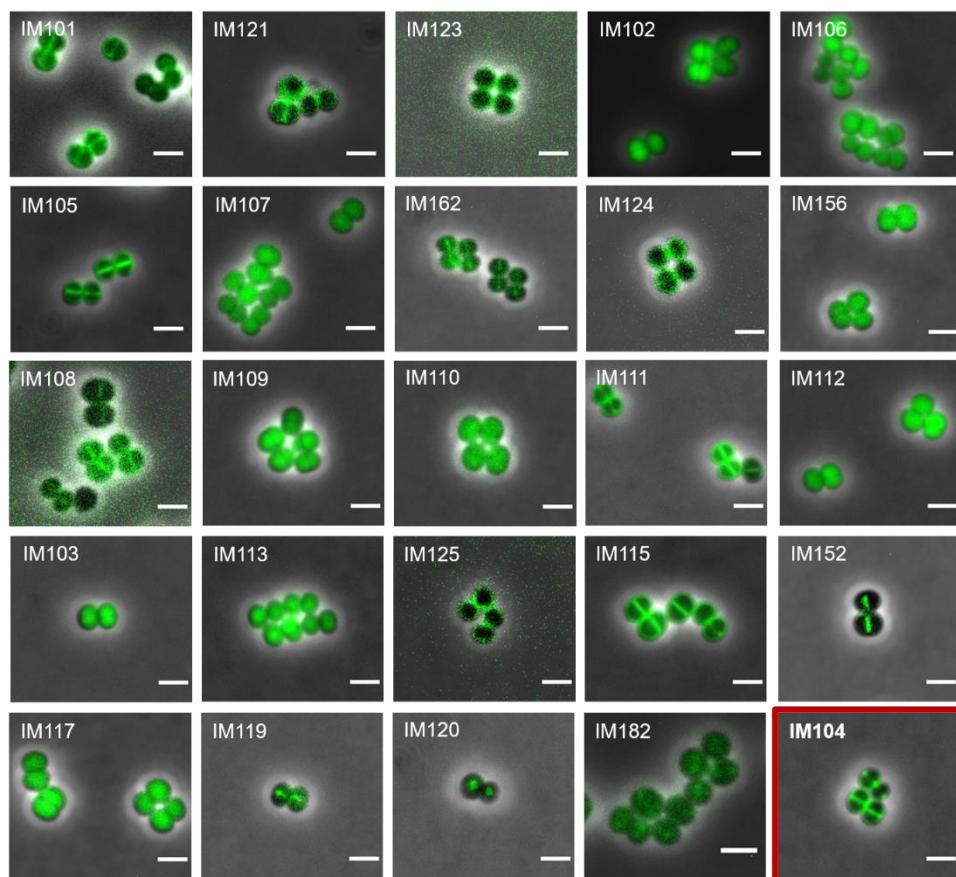


Fig. S3. Subcellular localization screen. Fluorescent fusion proteins were expressed in *S. aureus* SH1000 or RN4220 and analyzed by fluorescence microscopy. Scale bars, 2 μ m. Expression of SmdA-m(sf)GFP (IM104) is highlighted by a red square. Strain names are indicated. See Table S1 for locus tags and information about the fusion in the different strains.

```

Nosoc_WP_068130731 -----MSTELTEPLFTIWAALLLIVLISFL 26
Aliic_SEV88016 -----MNTDIFLDPPIFAVAALLVLVTLWFL 26
Salin_WP_020007446 -----MNTETFTNPVIVIAIVALLVAVSFL 26
Jeotg_WP_026866661 -----MNTETFTNPVIFIAIAVALLLIVLWFL 26
Auric_AQL56528 -----MNIINMDFDMIHWMIFGLALLLILLIFFI 30
Abyss_RPF57660 -----MNIINMDFDMIHWMIFGLALLLILLVFFI 30
Mepid_RAK44338 -----MSVVGSTLFFVVLIGLGLALLFFVLWL 28
Mcase_PKE19057 MGFYFLINLSKTMKLMFFFMKLIANIRKVRMSLSNLQPMHYIVLGLAARALLLFFVLF 60
Ssciu_WP_025905540 -----MSQLEPIHYGLIAAIVIAIFLIFLFF 26
Sinte_PNZ51430 -----MTQFCPMEIGLIAAIVWAALFFLFL 26
Schro_KDP13111 -----MSQLDPIQIGLIAVSVLALLFLVFL 26
Shyic_RTX86857 -----MCPLEIGLVAIVIAVIAVILFL 23
Saur_NCTC8325 -----MDLSSPIVIGLIAIAVIALIFFVFL 26
Ssimi_EHJ07687 -----MDFSSPIVIGLIAIAVIALIFFVFL 26
Swarn_PTI58951 -----MSLSSPIGIGLIAVAVIAIIFVFL 26
Scap_TPX81490 -----MSLSSPIVIGLIAVIAVIAIIFVFL 26
Mabsc_SLD57873 -----MDFSSPTVIGLIAVIAVIAVIAVFL 26
Sepid_KAB2218069 -----MDFSSPTVIGLIAVIAVIAVIAVFL 26
Sarle_EJY95024 -----MNSFCPIEIGLIAVIAVIAVIAVFL 26
Ssapr_EHY92709 -----MNSFCPIEIGLIAVIAVIAVIAVFL 26
Scarn_RTX88654 -----MNSFCPIEIGLIAVIAVIAVIAVFL 26
Slugd_ADC87241 -----MNSLCPMEIGLIAVIAVIAVIAVFL 26

```

```

Nosoc_WP_068130731 IYVVKHRNEVEENERLYKKKEETLIESYVKNQEDERMAHKKVESHVSHNEKYLEDDTLNNK 86
Aliic_SEV88016 VYFLKRNVRNKLTEEFDHEKQTLIEDYEATQEDRLSHKKEVSLNEKYNKDTQLNKR 86
Salin_WP_020007446 VYFLKRNVRNRLTLDIYSKEKGLIEKYESNQEEERLNHKEVSLNEKYNKDTQLNKR 86
Jeotg_WP_026866661 VYVFKHRNQVQVVENNHAKEKESLVQKYESHEAERLHKEKELSLNEKYNKDTQLNKR 86
Auric_AQL56528 VKMFKANKQYKELQQARDREKLLTSDYEKRIETERVGGKKFSEQSQSYDAIVDDQSSQ 90
Abyss_RPF57660 VKMFKANKQYKELQQARDREKLLTSDYEKRIETERVGGKKFSEQSQSYDAIVDDQSSQ 90
Mepid_RAK44338 LALSCKKSIARKEEFKRAQKIRSDYHDESEKSRLOYKKEAEQKQETLQKTDIDEKSSH 88
Mcase_PKE19057 YALSSKRAKIRAKEALNKERSEMKNYEESEKSRITFKKELAEQKQDYEAQLSTQNAQ 120
Ssciu_WP_025905540 VSLKQKQKSNLKIQAHNKENETLSEHKEKLDHERVENKVVLTQKEETHQEAISQKRE 86
Sinte_PNZ51430 VALSKKKAKQTYATQYQTKQDKLTHEHQEELKVRIDKKKAETRHKEEYETMVSQKRE 86
Schro_KDP13111 FALRSKKAKETIYANQYQSRKLNNEHKEALEKARIEKKKSDTRHKEEYETMVSQKRE 86
Shyic_RTX86857 TALNSKKAQQAAEQYEAKEKSLKDNYEDELEKERVEHKVTYKQADFDATVDSKRE 83
Saur_NCTC8325 VALGSKKKVKRQTEEKYEQEQONIKKSHHEEALEKERIQNKKITKQEDYNHMVSTKRE 86
Ssimi_EHJ07687 VALGSKKKVKRQTEEKYEQEQONIKKTHEEQLEKERIENKKITKQEDYNEVMVSTKRE 86
Swarn_PTI58951 TALNSKKKIKQTEEEYQKQKSIKASHEEALEKERIENKKITKQEDYEAATVNSKRE 86
Scap_TPX81490 VANHSKKKIKNQTEAQYKEKEQHMKSHEEALEKERVENKAVTKQKEDFATVNSKRE 86
Mabsc_SLD57873 VANHSKKKVKRQTEAHYKEKEQHLKESHEEALEKERVENKVVTKQKEDFATVNSKRE 86
Sepid_KAB2218069 VANHSKKKVKRQTEAHYKEKEQHLKESHEEALEKERVENKVVTKQKEDFATVNSKRE 86
Sarle_EJY95024 VANHSKKKAQKAEHQAEHQKKEKQLQDSYAELEKERIENKKITKQKEDYHTVNSKRE 86
Ssapr_EHY92709 VALSKKKAQKVEAQYKREQLSDEHEEALEKERIENKKITKQKEDYEAATVNSKRE 86
Scarn_RTX88654 VTLKSNKNIKQNTKEEYSLKEKQMLEHEEALEKERIENKKITVTKQKEDFATISQKRE 86
Slugd_ADC87241 VALRNNKKIKRQTVDEYKLEKQMQESHDEEALEKERIENKKITVTKQKENEATVNSKRE 86

```

```

Nosoc_WP_068130731 LSSIQQFTVDKGEYLTDLALLNFKNKLVTERRIRESDMYILSNIVLPSRNYTNTRKIDHL 146
Aliic_SEV88016 LRSVSQFTSDKGEYLTDLALKDLKNQVLVDEKIRIDDLDMHLSNIVLPSRNYTNTRKVDHL 146
Salin_WP_020007446 LSSLRQFTVDKGEYLTDLSLIQLKRLVREDEKIRETDMHLSNVVLPVSRNYTNTRKIDHL 146
Jeotg_WP_026866661 LSSLKQFVSDKGEYLTDLALIQLKDLVREDEKIRESDMIILSNVLPVSRNYTNTRKIDHL 146
Auric_AQL56528 ISSLKQFTYKGSQYLTDTITLLSFRDKLIDQERIRPEDMHVLNVLIPSKNYKQTKQVDHV 150
Abyss_RPF57660 ISSLKQFTYKGSQYLTDTITLLSFRDKLIDQERIRPEDMHVLNVLIPSKNYKQTKQVDHV 150
Mepid_RAK44338 IESLKMFSKDKGEYLTDLTLIQLKEQFIREERIRPEDMHVLNIVIPGKRVKSTDRDLHV 148
Mcase_PKE19057 IDSLKLFSDKGEYLTDLTLINLKNLVAQERIRPEDMHVLNIVIPGKRVKSTDRDLHV 180
Ssciu_WP_025905540 IDSLLKFSKNSEYITDRHLLERLDQVLEERRIRPEDMHVMANIPLPKDPLGKVRIDHL 146
Sinte_PNZ51430 IDALKLFSKNHSEYITDMRLGIRERLVKEKRIRPEDMHVMANIPLPNDLEEDITRVSHL 146
Schro_KDP13111 IDALKLFSKNHSEYITDMRLGIRERLVKEKRIRPEDMHVMANIPLPNDLEEDITRVSHL 146
Shyic_RTX86857 IDALKLFSKNHSEYITDMRLGIRERLVKEKRIRPEDMHVMANIPLPKNDNIDIRVSHL 143
Saur_NCTC8325 IDALKLFSKNHSEYITDMRLGIRERLVKEKRIRPEDMHVMANIPLPKOCFNNTIRISHL 146
Ssimi_EHJ07687 IDALKLFSKNHSEYITDMRLGIRERLVKEKRIRPEDMHVMANIPLPSNKNFNDIRISHL 146
Swarn_PTI58951 IDALKLFSKNHSEYITDMRLGIRERLVKEKRIRPEDMHVMANIPLPNEFNNTIRISHL 146
Scap_TPX81490 IDALKLFSKNHSEYITDMRLGIRERLVKEKRIRPEDMHVMANIPLPNEFNNTIRISHL 146
Mabsc_SLD57873 IDALKLFSKNHSEYITDMRLGIRERLVKEKRIRPEDMHVMANIPLPNEFNNTIRISHL 146
Sepid_KAB2218069 IDALKLFSKNHSEYITDMRLGIRERLVKEKRIRPEDMHVMANIPLPNEFNNTIRISHL 146
Sarle_EJY95024 IDALKLFSKNHSEYITDMRLGIRERLVKEKRIRPEDMHVMANIPLPNEFNNTIRISHL 146
Ssapr_EHY92709 IDALKLFSKNHSEYITDMRLGIRERLVKEKRIRPEDMHVMANIPLPNEFNNTIRISHL 146
Scarn_RTX88654 IDALKLFSKNHSEYITDMRLGIRERLVKEKRIRPEDMHVMANIPLPNEFNNTIRISHL 146
Slugd_ADC87241 IDALKLFSKNHSEYITDMRLGIRERLVKEKRIRPEDMHVMANIPLPNEFNNTIRISHL 146

```

Nosoc_WP_068130731 VLTRTGIYLIDS~~SKYWSGHILHGVT~~EEQVDE IPYLEGIFQLLNLDPNKEQTLIFEKEND-- 204
 Aliic_SEV88016 VLTRTGIYLME~~S~~RFWKGHIHGVSE~~QNF~~EQLPVYVFNFFLEGLLNKKEQFIIEFKKDD-- 204
 Salin_WP_020007446 VLTRTGIYM~~IDS~~SKYWRGHILHGINEENFEE LPYTESFFDLELDKTKETLIFEKSDS-- 204
 Jeotg_WP_026866661 VLTRTGIYLIDS~~SKYWSGHILHG~~VNEAQFET VPVYVSEFFDLELDKDKKREQLTIFEKADQ-- 204
 Auric_AQL56528 LLTRTGIYIV~~DS~~SNYFSGHVYHG~~MNE~~QQFDDQ FPFLEGVYDALGYD~~H~~KDEYSFIVEPKDN-- 208
 Abyss_RPF57660 LLTRTGIYIV~~DS~~SNYFSGHVYHG~~MNE~~QQFDDQ FPFLEGVYDALGYD~~H~~KDEYSFIVEPKDN-- 208
 Mepid_RAK44338 VLTRTGIYLIDS~~SNYWTGHIYHG~~VSEM~~QF~~AG EPMLLEGVFNLELD~~P~~KLEQTIVLDKNKD-- 206
 Mcase_PKE19057 LLTRTGIYV~~IDS~~SNYWTGHIYHGISEM~~QF~~DDGEPIFETVFNILGLD~~P~~KSEQITICLDKAE-- 238
 Ssciu_WP_025905540 VLTRTGIYVID~~SNLVS~~GHIYHGITE~~Q~~QFSD FVFLGQVFTL~~DL~~DNPNKEQTLLEKQPN-N 206
 Sinte_PNZ51430 VLTRTGLYVID~~SELLK~~GHVYQGIS~~Q~~QFAD NPMMEQVFTKLNLS~~P~~QTPQTIVLDDQSEAAQ 205
 Schro_KDP13111 VLTRTGLYIIDS~~SELLK~~GHVYQGV~~S~~QNFRE NPMMEHVFTK~~TL~~LDGQTPQTIVLDDQKED-Q 205
 Shyic_RTX86857 VLTRTGLYIIDS~~QLL~~KGHVYNGIS~~G~~KQFAE LPTIEQVFNVLNLD~~Q~~RTPQTIVLDDENDD-Q 202
 Saur_NCTC8325 VLTRTGLYIIDS~~QLL~~KGHVYNGIS~~G~~QFQF LPPMEQVFTL~~DL~~DKSRPQTIVMDQND--K 205
 Ssimi_EHJ07687 VLTRTGLYIIDS~~QLL~~KGHVYNGIS~~G~~QFQF LPPMEQVFTL~~DL~~LDASRPQTIIMDQND-Q 205
 Swarn_PTI58951 VLTRTGLYIIDS~~QLL~~KGHVYNGIS~~G~~QFSE LPTMEQVFN~~TL~~LELDKGTPTIVLDDQNSD-E 205
 Scap_TPX81490 VLTRTGLYIIDS~~QLL~~KGHVYNGIS~~G~~QFKE LPTMSQVFTL~~DL~~DESTPQTIVLDDQNE--Q 205
 Mabsc_SLD57873 VLTRTGLYIIDS~~QLL~~KGHVYNGIS~~G~~QFKE LPTMSQVFTL~~DL~~DS~~S~~QFQPTIVLDDQNE--Q 205
 Sepid_KAB2218069 VLTRTGLYIIDS~~QLL~~KGHVYNGIS~~G~~QFKE LPTMSQVFTL~~DL~~DS~~S~~QFQPTIVLDDQNE--Q 205
 Sarle_EJY95024 VLTRTGLYIIDS~~QLL~~KGHVYNGIS~~G~~QFEE FPMMSQVFTL~~DL~~DKDPQVVLVDDQND--T 205
 Ssapr_EHY92709 VLTRTGLYIIDS~~QLL~~KGHVYNGV~~S~~AAQFKE QPMMEQVFN~~TL~~LDGQVFPQTIVLDDQNE--K 205
 Scarn_RTX88654 VLTRTGLYIIDS~~QLL~~KGHVYNGIS~~G~~NQFQE LPPMEQVFN~~TL~~LDL~~P~~KSPQTIVLDDQND--K 205
 Slugd_ADC87241 VLTRTGLYIIDS~~SKLL~~KGHVYNGIS~~G~~NQFNE LPMMQVFTL~~DL~~NAKAPH~~T~~IVLDDQND--Q 205

*****:***: ** :*: : * : : : *

Nosoc_WP_068130731 EKVAVNYNNTIEDTEMTAEKLRNVLKLQFDVVPVPIYFNPKN~~D~~GGHTIMNYATNSNAKVI 264
 Aliic_SEV88016 LNVTVSHFNHMIIEAKLTAEKLNKVLKLQFDVVPVVPVFNPE~~D~~NGNYSIANYSDNPSVKVL 264
 Salin_WP_020007446 KNVSVNHYNDTIDETKITAELKLRNVLKLQYD~~V~~PMIYFNPKN~~D~~GNYSITNYSADPSVKVL 264
 Jeotg_WP_026866661 KNVSVNHYNGVIDETKITAELKLNKVLKLQYD~~V~~PIYFNPKN~~D~~GNYSITNYSADPSVKVL 264
 Auric_AQL56528 GEVVMHPLD~~HQ~~IQDLKVTAEKIRN~~L~~KLQYPVKTI~~M~~FYNEQETKRNVSINYSTDKDVIVL 268
 Abyss_RPF57660 GEVVMHPLD~~HQ~~IQDLKVTAEKIRN~~L~~KLQYPVKTI~~M~~FYNEQETKRNVSINYSTDKDVIVL 268
 Mepid_RAK44338 GNAEFRTYNHSIEALKLKAERLEKVFELPYVPTPIAYYNAE~~G~~VGSEHITNYSRDNGVKVI 266
 Mcase_PKE19057 GSAQFKSYKHSIEELKKAERLEKVFELPYVPTPIAYYNAE~~G~~VGSEHITNYSRDNSVKVI 266
 Ssciu_WP_025905540 KTAAFHSYTDVEKVEDNTEELQRQLELKYTPPIYFNPKN~~E~~GVDTISNYASQDNPKVL 298
 Sinte_PNZ51430 NTL~~S~~VVDYTDRLAHVEALAVKLQKELDLKYTPPIYFNP~~R~~HEGDVTISNYASHGVTKVL 266
 Schro_KDP13111 QKLTVIDYTKHLDSVEKLATTLQQLN~~L~~KYAPTPIYFNP~~R~~HEGDVTISNYAQSGTKVL 262
 Shyic_RTX86857 QSATFVNYSKQLHYVEQLADALQRQLN~~L~~KYTPMALLYFNP~~K~~NEGAVTISNYAQNTNTKVL 262
 Saur_NCTC8325 RSL~~S~~FNYS~~DQ~~IEATKQ~~LA~~EDLQKELGAKYTPPTSILYFN~~L~~KNEGDVTISNYNQNSAVKVL 265
 Ssimi_EHJ07687 KSL~~S~~FNYS~~DK~~LESIKQ~~LA~~EDLQKELGTYTPPTSILYFN~~P~~KN~~D~~GVDTISNYNQNSAVKVL 265
 Swarn_PTI58951 KSL~~S~~FNYS~~DE~~IQQIQNVAGDLQSKLNTKYTPPTSILYFN~~P~~KN~~D~~GVDTISNYAQNSAVKVL 265
 Scap_TPX81490 QSL~~S~~FNYS~~EK~~IKHIQNL~~AG~~DLQSELNTKYTPPTSILYFN~~P~~KN~~D~~GVDTISNYNQNSAVKVL 265
 Mabsc_SLD57873 HSL~~S~~FNYS~~SD~~KIKHIEKLAGDLQNELNTKYTPPTSILYFN~~P~~KN~~D~~GVDTISHYTQSSNVKVL 265
 Sepid_KAB2218069 HSL~~S~~FNYS~~SD~~KIKHIEKLAGDLQNELNTKYTPPTSILYFN~~P~~KN~~D~~GVDTISNYAQSSNVKVL 265
 Sarle_EJY95024 QSL~~S~~VVNYSNHLEAVEKLAGDLQNELNTKYTPPTSILYFN~~P~~KN~~D~~GGVDTISNFAQTANSKVL 265
 Ssapr_EHY92709 DAL~~S~~FNYS~~Y~~THLNEIERLAGDIQTELNLKFTPTPIYFN~~P~~KN~~D~~GVDTISNYAQSSNVKVL 265
 Scarn_RTX88654 SLS~~S~~FNYS~~DQ~~LEALEK~~LA~~TDLQTLQGLTYTPPTSIMYFN~~P~~KN~~D~~GVDTISNYAQSSNVKVL 265
 Slugd_ADC87241 SLS~~S~~FLDYS~~QA~~LQIEK~~LA~~TDLQTLGLTYTPPTSILYFN~~P~~KN~~E~~GEVDTISNYAQTS~~S~~AKVL 265

: : : : : : : : : : : : : : *

Nosoc_WP_068130731 VGTEQLEDYFNKHFVQGRFQYTVKDLDEIAESLMRLNP 302
 Aliic_SEV88016 IGNEELDEYFKKYVFHGRFQYTVKDLTDIVDQLKALNP 302
 Salin_WP_020007446 VGEELEA~~F~~FLKYVFHGRFQYTVKDLDEIAEEIFNLNP 302
 Jeotg_WP_026866661 VGQEDLEA~~F~~FLKYVFHGRFQYTVKDLDEIADAILEQSL 302
 Auric_AQL56528 MGKPELEEYFEKHVFHGRFQYTVVEELEQIKQ~~L~~LEMNP 306
 Abyss_RPF57660 MGKPELEEYFEKHVFHGRFQYTVVEELEQIKQ~~L~~LEMNP 306
 Mepid_RAK44338 VGEEELQTFEKFVFHGRFQYVVEALENIMDQIEHLNP 304
 Mcase_PKE19057 VGEKELEHFFKVFHGRFQYVVEELEEVRAAIEHLNP 336
 Ssciu_WP_025905540 VGEKQLQ~~H~~FFNFVHGRFQYVSEDLERIMDEIEKFN 303
 Sinte_PNZ51430 VGPEQLNEFFNKFVHGRIQYVNDLQ~~N~~IMDEIESFN 303
 Schro_KDP13111 VGPAQLEDEFFNKFVHGRIQYVNDLQ~~A~~IMDEIEAFN 302
 Shyic_RTX86857 VGAEQLDEYFNKVFHGRIQYVNDLQ~~A~~IMDEIESFN 299
 Saur_NCTC8325 VGAEQLDEFFNKFVHGRIQYVNDLQ~~Q~~IMDKIESFN 302
 Ssimi_EHJ07687 VGKEQLDEFFNKFVHGRIQYVNDLQ~~N~~IMDKIESFN 302
 Swarn_PTI58951 VGPEQLDEFFNKFVHGRIQYVNDLQ~~Q~~IMEQIESFN 302
 Scap_TPX81490 VGPEQLDEFFNKFVHGRIQYVNDLQ~~T~~IMDKIESFN 302
 Mabsc_SLD57873 VGPEQLEE~~F~~FNKFVHGRIQYVNDLQ~~D~~IMDKIESFN 302
 Sepid_KAB2218069 VGPEQLDEFFNKFVHGRIQYVNDLQ~~D~~IMDKIESFN 302
 Sarle_EJY95024 VGPEQLDEYFNKVFHGRIQYVNDLQ~~Q~~IMDKIESFN 302
 Ssapr_EHY92709 VGPEQLDEFFNKFVHGRIQYVNDLQ~~R~~IMDEIESFN 302
 Scarn_RTX88654 VGPEQLDEFFNKFVHGRIQYVNDLQ~~S~~IMDKIETFN 302
 Slugd_ADC87241 VGPEQLNEFFNKFVHGRIQYVNDLQ~~E~~IMTKIESFN- 302

:* :*: :* :***:****: * * : : *

Fig. S4. Multiple sequence alignment of SmdA from different staphylococcal species. Protein sequences were aligned with Clustal Omega (Sievers et al., 2011). The blue shaded residues are predicted to be extracellularly, the transmembrane domain is shaded in grey, and the predicted NERD domain is shaded in yellow. *S. aureus* NCTC8325 is highlighted in bold, and residues that were mutated are marked in green. The accession number of the sequences are indicated, and the first five letter in the sequence tags indicate the genus or species corresponding the to the sequences (for example, Nosoc; *Nococomiicoccus*, Aliic; *Aliicoccus*, Salin; *Salinicoccus*, Jeotg; *Jeotgalicoccus*, Auric; *Auricoccus*, Abyss; *Abyssicoccus*, Mepid; *Macrococcus epidermidis*, Mcase; *Macrococcus caseolyticus*, Ssciu; *Staphylococcus sciuri*, Sinte; *Staphylococcus intermedius*).

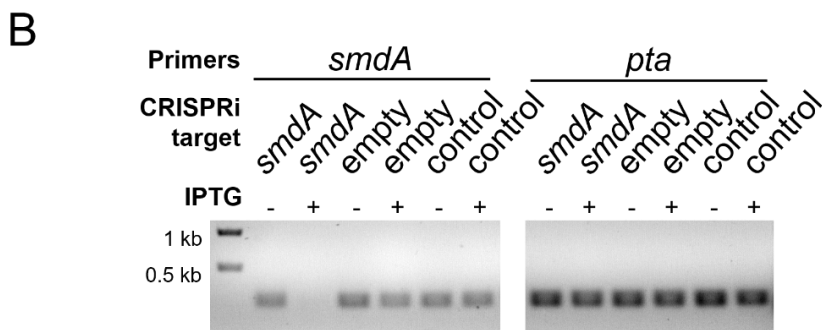
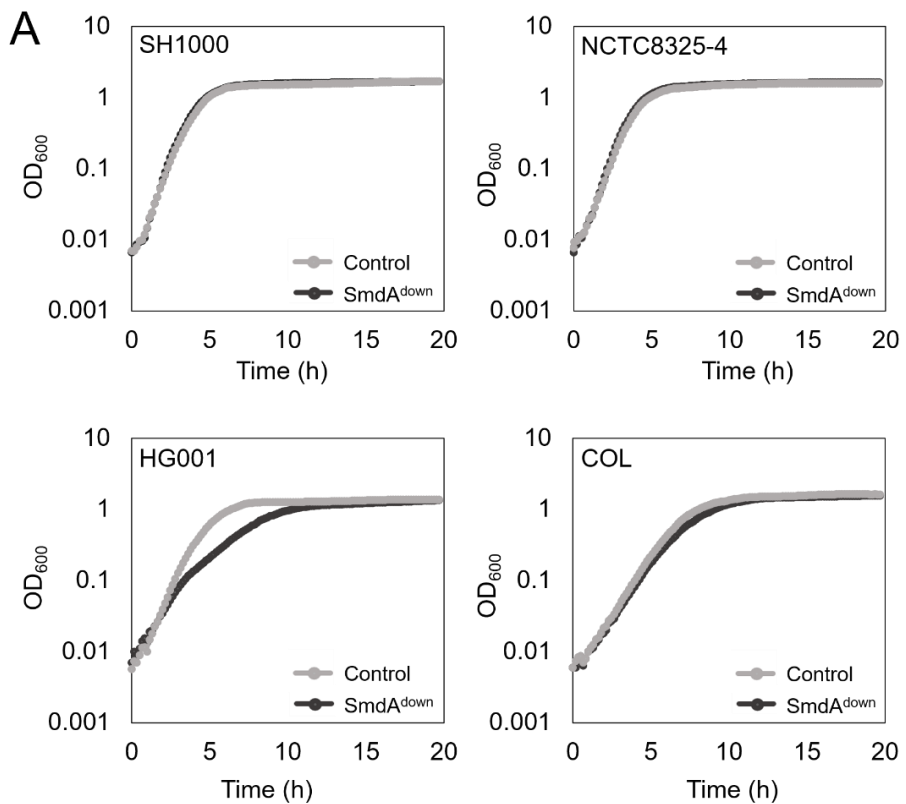


Fig. S5. Growth of *SmdA* knockdown strains in liquid cultures and verification of *smdA* silencing. (A) Growth of *SmdA*^{down} in *S. aureus* SH1000 (IM269), NCTC8325-4 (IM311), HG001 (IM312) and COL (IM294) were compared with their respective controls (IM284, IM307, IM313 and IM295) by measuring OD₆₀₀ in liquid cultures containing IPTG at 37°C. The control strains carries the CRISPRi system with a non-targeting sgRNA. (B) Verification of *smdA* silencing by PCR with RT-PCR. cDNA was synthesized from RNA isolated from induced and un-induced cultures of SH1000 *SmdA*^{down} (IM269) and the CRISPRi control strains (IM284; non-targeting sgRNA and IM165; empty plasmid without sgRNA). Primers targeting either *smdA* or the housekeeping gene *pta*.

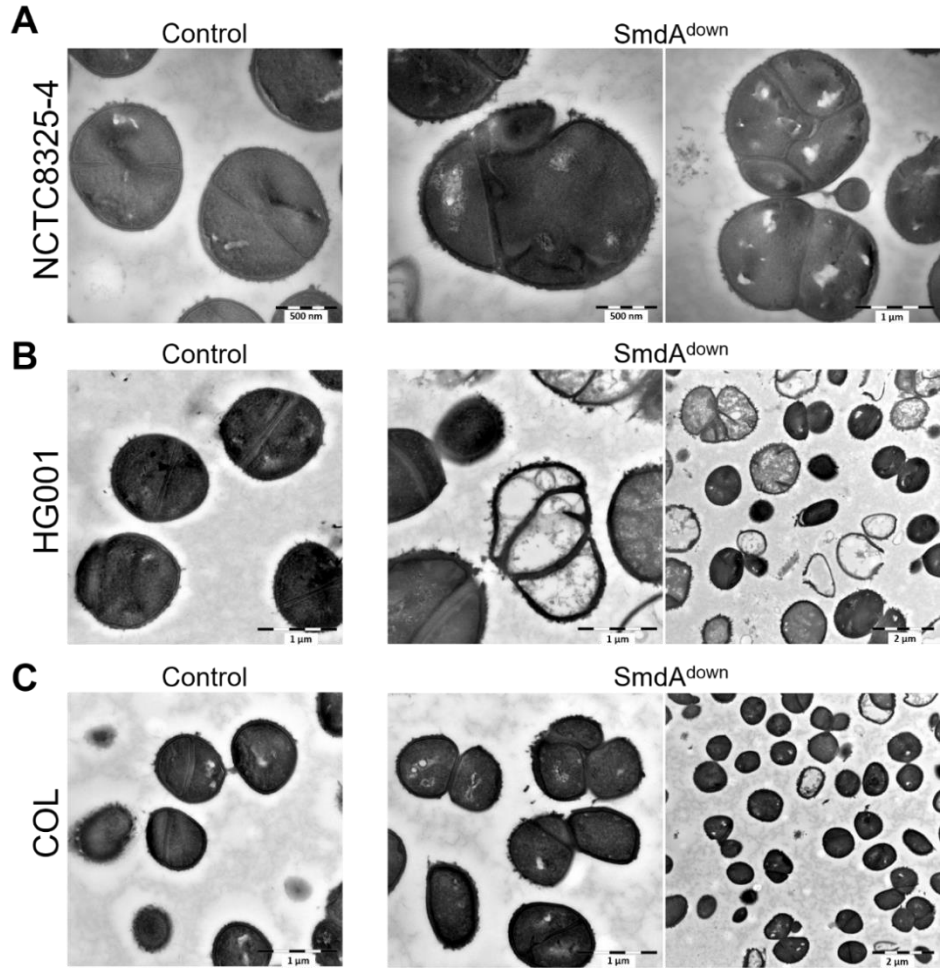


Fig. S6. Transmission electron microscopy (TEM) of different *S. aureus* strains with *SmdA* knockdown. *SmdA*^{down} and control cells analyzed with TEM in the *S. aureus* strains (A) NCTC8325-4 (IM311 and IM307), (B) HG001 (IM312 and IM313) and (C) COL (IM294 and IM295). The sizes of the scale bars are indicated in the images.

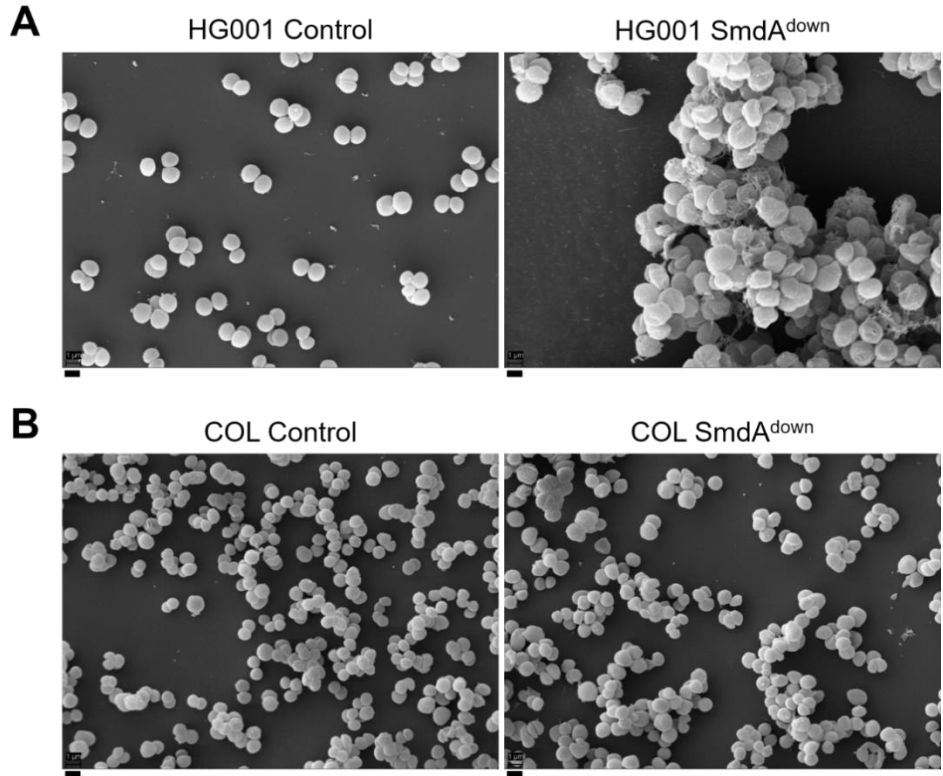


Fig. S7. Scanning electron microscopy (SEM) of cells depleted of SmdA. SEM micrographs of SmdA^{down} and control cells in *S. aureus* (**A**) HG001 (IM312 and IM313) and (**B**) COL (IM294 and IM295). All scale bars, 1 μ m.

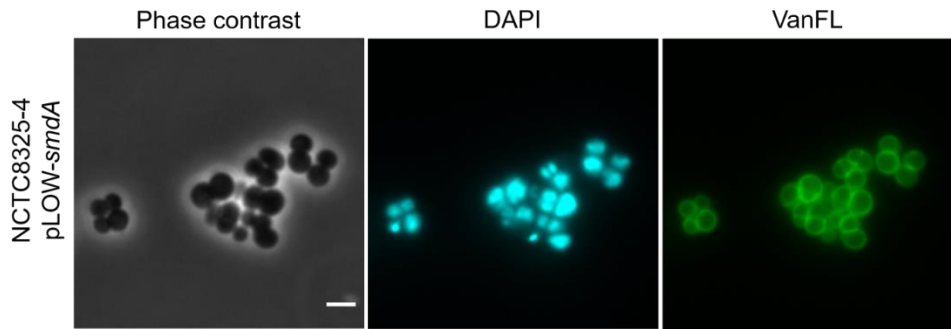


Fig. S8. Overexpression of SmdA. Induced expression of an ectopic copy of *smdA* in the plasmid pLOW in *S. aureus* NCTC8325-4 (MK1866). Cells were labelled with the DNA-marker DAPI and the cell wall marker fluorescent vancomycin (VanFL). Scale bar, 2 μ m.

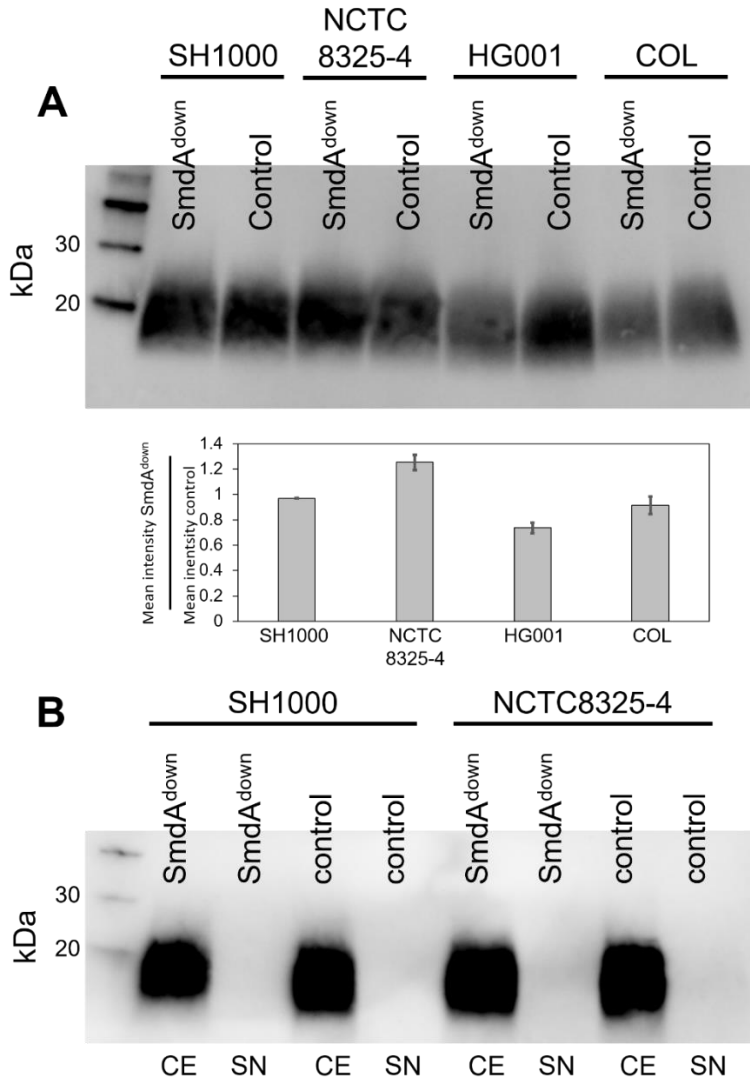


Fig. S9. Lipoteichoic acid (LTA) detection by immunoblotting. Immunoblotting with α -LTA antibody was performed with (A) cell extract samples from SmdA^{down} and CRISPRi control cells from *S. aureus* SH1000 (IM269 and IM284), NCTC8325-4 (IM311 and IM307), HG001 (IM312 and IM313) and COL (IM294 and IM295), and (B) cell extract (CE)- and supernatant (SN) samples from SmdA^{down} and CRISPRi control cells from *S. aureus* SH1000 and NCTC8325-4 (IM269, IM284, IM311 and IM307, respectively). In (A), the mean intensities in the bands (background subtracted) were determined using Fiji (Schindelin et al., 2012). The mean intensities of the LTA bands in the *smdA* depletions relative to their controls are plotted. All control strains express a non-targeting sgRNA.

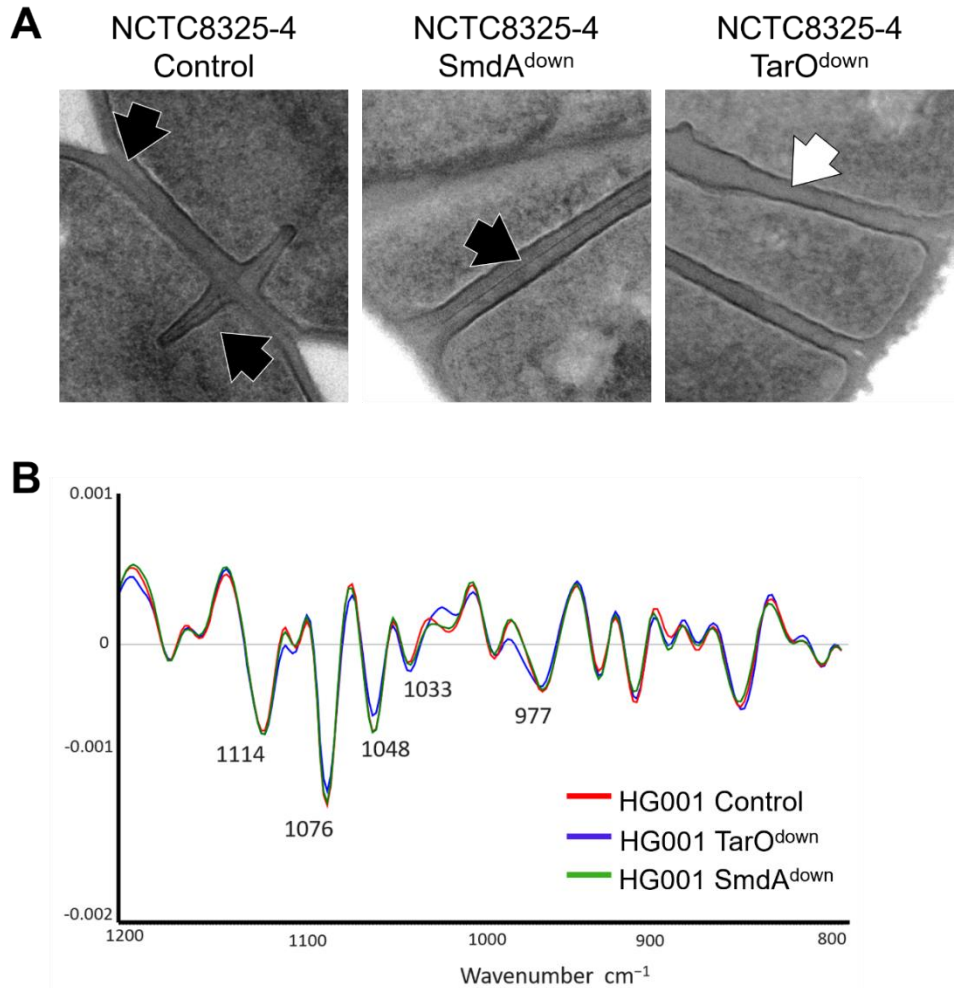


Fig. S10. SmdA does not have major impact on the synthesis of wall teichoic acids. (A) TEM micrographs of *S. aureus* NCTC8325-4 control strain (IM307) compared to SmdA and TarO knockdown strains IM311 and IM358, respectively. The black arrows indicate presence of a high-density layer in the septum, which is missing in the TarO depletion strain (white arrow). (B) Fourier transform infrared spectroscopy (FTIR) of *S. aureus* HG001 control strain (IM313) and knockdown strain of SmdA and TarO (IM312 and IM357, respectively). The polysaccharide region of the spectrum is shown, and the indicated peaks represents α - and β -glycosidic bonds.

Supplementary Tables

Table S1. Summary of results from subcellular localization- and gene knockdown screen.

Target gene (SAOUH SC ₁) ^a	CRISPRi strain	Growth ^b	Phenotypic Characteristics (microscopy) ^c	GFP-fusion strain	Predicted localization (C/M) ^d	Localization ^e
<i>00015-gdpP</i>	-	NT	NT	IM101	M	Membrane/septum
<i>00226-tarJ</i>	IM246	+	None	IM121 (00226)	C	Membrane
<i>00227-tarL</i> (00225)				IM123 (00227)	C or M	Membrane
<i>00345</i> (00344)	IM247	-	None	IM102	C	Cytoplasm
<i>00444</i>	IM248	+	Variable cell size Abnormal nucleoid staining	IM106	C	Cytoplasm
<i>00762-tarO</i>	IM249	(+)	None	IM105	M	Membrane/septum
<i>00892</i>	IM250	-	None	IM107	C	Cytoplasm
<i>00957</i>	IM251	(+)	None	IM162 ^f	M	Septum
<i>01244</i> (01242)	IM252	+	Clustering	IM124	C	Membrane
<i>01477</i>	IM253	+	Abnormal nucleoid staining	IM156	M	Cytoplasm
<i>01627</i>	IM254	-	Abnormal nucleoid staining	IM108	Unknown	Membrane
<i>01661-trmK</i> (01662)	IM255	+	Variable cell size Abnormal nucleoid staining	IM109	C	Cytoplasm
<i>01700</i> <i>01701</i> (1702)	IM256	+	Abnormal nucleoid staining	IM110 (01700)	C	Cytoplasm
				IM111 (01701)	C or M	Membrane
<i>01721</i> (01722)	IM257	+	Reduced cell size	IM112	C	Cytoplasm
<i>01756</i> (01757)	IM258	+	Increased cell size	IM103	C	Cytoplasm

			Abnormal nucleoid staining			
01770	IM259	-	None	IM113	C	Cytoplasm
01782	IM260	-	None	IM125	C	Membrane
01930	IM261	(+)	Reduced cell size Abnormal nucleoid staining	IM115	C	Membrane
02106- <i>gatD</i> (02107)	IM262	+	Increased cell size Abnormal nucleoid staining	IM116	C	No signal
02151- <i>pmtD</i> 02152-5	IM263	+	None	IM152 ^f	M	Septum
02279- <i>tsaB</i> 02280- <i>tsaE</i>	IM264	+	None	IM117 (02279)	C	Cytoplasm
				IM118 (02280)	C	No signal
02407- <i>dacA</i>	IM265	-	Clustering	IM119	M	Membrane/ septum
02720	-	NT	NT	IM120	C	Foci
01866- <i>ccrZ</i>	IM270	+	Clustering Variable cell size Abnormal nucleoid staining	IM182	C	Foci
01908	IM269	+	Clustering Variable cell size Abnormal nucleoid staining	IM104	M	Membrane /septum

^a Refers to locus tag of the gene targeted by the CRISPRi system. Additional genes target due to polar effects of the CRISPRi system (polycistronic genes) are given in parenthesis.

^b Strains where CRISPRi resulted in growth reduction is marked "+", slight growth reduction is marked "(+)" and no growth reduction is marked "-". See Fig. S1 for images of the growth assay. NT; not tested.

^c Phenotypic characteristics observed from micrographs of CRISPRi-strains labelled with fluorescent vancomycin and DAPI. Example images are shown in Fig. S2. NT; not tested.

^d Predicted localization according to PSORTb and LocateP (retrieved from <https://aureowiki.med.uni-greifswald.de/>).

^e Localization of GFP-fusion strains. Example images are shown in Fig. S3.

^f *S. aureus* RN4220 (SH1000 for all the others).

Table S2. Proteins pulled down with SmdA-GFP.

Protein	Description	Chromosomal <i>smdA-gfp</i> ^a		Plasmid-based <i>smdA-gfp</i>	
		Unique peptides	Ratio	Unique peptides	Ratio
SmdA	Uncharacterized protein	4	>4	35	8.8
Atl	Bifunctional autolysin	4	4	29	5.8
SAOUHSC_01193	Uncharacterized protein	3	>3	10	2.5
FtsH	ATP-dependent zinc metalloprotease	2	>2	22	11
PrsA	Foldase protein	2	>2	14	7
SpsB	Signal peptidase I	2	>2	12	>12
FhuD2	Heme ABC transporter	2	>2	12	>12
Pbp2	Penicillin-binding protein 2	1	>1	23	23
SAOUHSC_01676	UPF0365 protein	1	>1	14	14
SAOUHSC_00356	Uncharacterized protein	1	>1	14	>4
FruA	Fructose specific permease, putative	1	>1	12	>12
AtpA	ATP synthase subunit alpha	1	>1	12	>12
AlaS	Alanine--tRNA ligase	1	>1	12	12
GlpK	Glycerol kinase	1	>1	12	12
NrdE	Ribonucleoside-diphosphate reductase	1	>1	10	>10
RpoC	DNA-directed RNA polymerase subunit beta'	ND	NA	28	9.3
RpoB	DNA-directed RNA polymerase subunit beta	ND	NA	24	12
SAOUHSC_02525	Uncharacterized protein	ND	NA	18	>18
Pyk	Pyruvate kinase	ND	NA	17	5.7
AtpD	ATP synthase subunit beta	ND	NA	15	7.5
EzrA	Septation ring formation regulator	ND	NA	15	>15
GlpD	Aerobic glycerol-3-phosphate dehydrogenase	ND	NA	14	14
SAOUHSC_01895	Uncharacterized protein	ND	NA	14	>14
Pbp1	Penicillin-binding protein 1	ND	NA	14	>14
Pbp3	Penicillin-binding protein 3	ND	NA	14	>14
ClpB	Chaperone protein	ND	NA	14	>14
Mqo	Probable malate:quinone oxidoreductase	ND	NA	13	>13
SecD	Multifunctional fusion protein	ND	NA	13	>13
SAOUHSC_01974	Uncharacterized protein	ND	NA	13	>13
DltD	Protein DltD	ND	NA	12	>12

ClpC	ATP-dependent Clp protease ATP-binding subunit	ND	NA	12	>12
QoxA	Probable quinol oxidase subunit 2	ND	NA	11	11
GatB	Aspartyl/glutamyl-tRNA(Asn/Gln) amidotransferase	ND	NA	11	>11
SAOUHSC_00253	Uncharacterized protein	ND	NA	11	>11
SAOUHSC_00749	Uncharacterized protein	ND	NA	10	>10
Rny	Ribonuclease Y	ND	NA	10	>10
ArgG	Argininosuccinate synthase	ND	NA	10	>10
AccC	Biotin carboxylase	ND	NA	10	>10
HtrA1	Serine protease	ND	NA	10	>10
PfIB	Formate acetyltransferase	ND	NA	10	>10

^a ND; not detected, NA; not applicable.

Table S3. Strains used in this study.

Name	Genotype ^a	Source
<i>S. aureus</i>		
NCTC8325-4	MSSA strain, derivative of NCTC8325, cured of phages.	(Novick, 1967)
SH1000	<i>rbsU</i> ⁺ derivative of strain NCTC8325-4	(Horsburgh et al., 2002)
RN4220	Restriction deficient derivative of NCTC8325-4	(Kreiswirth et al., 1983)
HG001	MSSA-strain, derivative of NCTC8325	(Herbert et al., 2010)
COL	Hospital-associated MRSA strain	(Shafer & landolo, 1979)
Strains for the subcellular localization screen		
IM101	SH1000, pLOW-SAOUHSC_00015- <i>m(sf)gfp</i> , ery ^r	This study
IM121	SH1000, pLOW-SAOUHSC_00226- <i>m(sf)gfp</i> , ery ^r	This study
IM123	SH1000, pLOW-SAOUHSC_00227- <i>m(sf)gfp</i> , ery ^r	This study
IM102	SH1000, pLOW-SAOUHSC_00345- <i>m(sf)gfp</i> , ery ^r	This study
IM106	SH1000, pLOW-SAOUHSC_00444- <i>m(sf)gfp</i> , ery ^r	This study
IM105	SH1000, pLOW-SAOUHSC_00762- <i>m(sf)gfp</i> , ery ^r	This study
IM107	SH1000, pLOW-SAOUHSC_00892- <i>m(sf)gfp</i> , ery ^r	This study
IM162	RN4220, pLOW- <i>m(sf)gfp</i> -SAOUHSC_00957, ery ^r	This study
IM124	SH1000, pLOW-SAOUHSC_01244- <i>m(sf)gfp</i> , ery ^r	This study
IM156	SH1000, pLOW- <i>m(sf)gfp</i> -SAOUHSC_01477, ery ^r	This study
IM108	SH1000, pLOW-SAOUHSC_01627- <i>m(sf)gfp</i> , ery ^r	This study
IM109	SH1000, pLOW-SAOUHSC_01661- <i>m(sf)gfp</i> , ery ^r	This study
IM110	SH1000, pLOW-SAOUHSC_01700- <i>m(sf)gfp</i> , ery ^r	This study
IM111	SH1000, pLOW-SAOUHSC_01701- <i>m(sf)gfp</i> , ery ^r	This study
IM112	SH1000, pLOW-SAOUHSC_01721- <i>m(sf)gfp</i> , ery ^r	This study
IM103	SH1000, pLOW-SAOUHSC_01756- <i>m(sf)gfp</i> , ery ^r	This study
IM113	SH1000, pLOW-SAOUHSC_01770- <i>m(sf)gfp</i> , ery ^r	This study
IM125	SH1000, pLOW-SAOUHSC_01782- <i>m(sf)gfp</i> , ery ^r	This study
IM182	SH1000, pLOW-SAOUHSC_01866- <i>long-m(sf)gfp</i> , ery ^r	This study
IM104	SH1000, pLOW-SAOUHSC_01908- <i>m(sf)gfp</i> , ery ^r	This study
IM115	SH1000, pLOW-SAOUHSC_01930- <i>m(sf)gfp</i> , ery ^r	This study
IM116	SH1000, pLOW-SAOUHSC_02106- <i>m(sf)gfp</i> , ery ^r	This study
IM152	RN4220, pLOW- <i>m(sf)gfp</i> -SAOUHSC_02151, ery ^r	This study
IM117	SH1000, pLOW-SAOUHSC_02279- <i>m(sf)gfp</i> , ery ^r	This study
IM118	SH1000, pLOW-SAOUHSC_02280- <i>m(sf)gfp</i> , ery ^r	This study
IM119	SH1000, pLOW-SAOUHSC_02407- <i>m(sf)gfp</i> , ery ^r	This study
IM120	SH1000, pLOW-SAOUHSC_02720- <i>m(sf)gfp</i> , ery ^r	This study
Strains for the CRISPRi gene knockdown screen		
SAMK13	SH1000, pLOW- <i>dcas9</i>	(Stamsås et al., 2018)
IM246	SAMK13, pCG248-sgRNA(SAOUHSC_00225), ery ^r , cam ^r	This study
IM247	SAMK13, pCG248-sgRNA(SAOUHSC_00344), ery ^r , cam ^r	This study

IM248	SAMK13, pCG248-sgRNA(<i>SAOUHSC_00444</i>), ery ^r , cam ^r	This study
IM249	SAMK13, pCG248-sgRNA(<i>SAOUHSC_00762</i>), ery ^r , cam ^r	This study
IM250	SAMK13, pCG248-sgRNA(<i>SAOUHSC_00892</i>), ery ^r , cam ^r	This study
IM251	SAMK13, pCG248-sgRNA(<i>SAOUHSC_00957</i>), ery ^r , cam ^r	This study
IM252	SAMK13, pCG248-sgRNA(<i>SAOUHSC_01242</i>), ery ^r , cam ^r	This study
IM253	SAMK13, pCG248-sgRNA(<i>SAOUHSC_01477</i>), ery ^r , cam ^r	This study
IM254	SAMK13, pCG248-sgRNA(<i>SAOUHSC_01627</i>), ery ^r , cam ^r	This study
IM255	SAMK13, pCG248-sgRNA(<i>SAOUHSC_01662</i>), ery ^r , cam ^r	This study
IM256	SAMK13, pCG248-sgRNA(<i>SAOUHSC_01702</i>), ery ^r , cam ^r	This study
IM257	SAMK13, pCG248-sgRNA(<i>SAOUHSC_01722</i>), ery ^r , cam ^r	This study
IM258	SAMK13, pCG248-sgRNA(<i>SAOUHSC_01757</i>), ery ^r , cam ^r	This study
IM259	SAMK13, pCG248-sgRNA(<i>SAOUHSC_01770</i>), ery ^r , cam ^r	This study
IM260	SAMK13, pCG248-sgRNA(<i>SAOUHSC_01782</i>), ery ^r , cam ^r	This study
IM261	SAMK13, pCG248-sgRNA(<i>SAOUHSC_01930</i>), ery ^r , cam ^r	This study
IM262	SAMK13, pCG248-sgRNA(<i>SAOUHSC_02107</i>), ery ^r , cam ^r	This study
IM263	SAMK13, pCG248-sgRNA(<i>SAOUHSC_02155</i>), ery ^r , cam ^r	This study
IM264	SAMK13, pCG248-sgRNA(<i>SAOUHSC_02280</i>), ery ^r , cam ^r	This study
IM265	SAMK13, pCG248-sgRNA(<i>SAOUHSC_02407</i>), ery ^r , cam ^r	This study
IM269	SAMK13, pCG248-sgRNA(<i>SAOUHSC_01908_double</i>), ery ^r , cam ^r	This study
IM270	SAMK13, pCG248-sgRNA(<i>SAOUHSC_01866</i>), ery ^r , cam ^r	This study
Other CRISPRi depletion strains		
IM165	SH1000, pLOW- <i>dcas9</i> , pCG248(empty), ery ^r , cam ^r	This study
SAMK15/IM284	SAMK13, pCG248-sgRNA(control), ery ^r , cam ^r	(Stamsås et al., 2018)
IM307	NCTC8325-4, pLOW- <i>dcas9_extra_lacO</i> , pVL2336-sgRNA(control), ery ^r , cam ^r	This study
IM311	NCTC8325-4, pLOW- <i>dcas9</i> , pCG248-sgRNA(<i>smdA_double</i>), ery ^r , cam ^r	This study
IM313	HG001, pLOW- <i>dcas9</i> , pCG248-sgRNA(control), ery ^r , cam ^r	This study
IM312	HG001, pLOW- <i>dcas9</i> , pCG248-sgRNA(<i>smdA_double</i>), ery ^r , cam ^r	This study
IM294	COL, pLOW- <i>dcas9_aad9</i> , pCG248-sgRNA(<i>smdA_double</i>), spc ^r , cam ^r	This study
IM295	COL, pLOW- <i>dcas9_aad9</i> , pCG248-sgRNA(control), spc ^r , cam ^r	This study
IM358	NCTC8325-4, pLOW- <i>dcas9</i> , pCG248-sgRNA(<i>tarO</i>), ery ^r , cam ^r	This study
IM357	HG001, pLOW- <i>dcas9</i> , pCG248-sgRNA(<i>tarO</i>), ery ^r , cam ^r	This study
IM293	SH1000, pLOW- <i>dcas9_Patl-luc</i> , pVL2336-sgRNA(<i>walR</i>), ery ^r , cam ^r	This study
Strains for localization studies		
IM305	NCTC8325-4, pLOW- <i>smdA-m(sf)gfp</i> , ery ^r	This study
IM373	NCTC8325-4, pLOW- <i>smdAΔTMH-m(sf)gfp</i> , ery ^r	This study
IM308	SH1000 <i>smdA-m(sf)gfp_aad9</i> , spc ^r	This study
HC060	SH1000, pLOW- <i>smdA-mYFP</i> , pHc- <i>ftsZ-mKate2</i> , ery ^r , neo ^r	This study
SH4639	SH1000, <i>ezrA-gfp</i> , kan ^r	(Lund et al., 2018)

MK1952	SH4639, pLOW- <i>dcas9</i> , pCG248-sgRNA(<i>smdA</i>), ery ^r , cam ^r	This study
MK1953	SH4639, pLOW- <i>dcas9</i> , pCG248-sgRNA(control), ery ^r , cam ^r	This study
Strains used for overexpression and mutagenesis		
MK1866	NCTC8325-4, pLOW- <i>smdA</i> , ery ^r	This study
MK1911	NCTC8325-4, pLOW- <i>smdAΔTMH</i> , ery ^r	This study
IM377	NCTC8325-4, pLOW- <i>smdAΔTMH_mut1</i> (H145A), ery ^r	This study
IM378	NCTC8325-4, pLOW- <i>smdAΔTMH_mut2</i> (R150A, T151A), ery ^r	This study
IM379	NCTC8325-4, pLOW- <i>smdAΔTMH_mut3</i> (F280A, H281A), ery ^r	This study
Other strains		
IM164	SH1000, pLOW- <i>smdA-flag</i> , ery ^r	Lab coll.
<i>E. coli</i>		
IM08B	DH10B, Δdcm , P _{help} - <i>hsdMS</i> , P _{N25} - <i>hdsS</i> (expressing the <i>S. aureus</i> CC8 specific methylation genes)	(Monk et al., 2015)
BTH101	Used for BACTH analysis	Euromedex
XL1-Blue	Host strain	Agilent
Strains harboring plasmids used to facilitate cloning		
IM6	IM08B, pLOW- <i>ftsZ-m(sf)gfp</i> , amp ^r	This study
IM98	IM08B, pLOW- <i>ftsZ-m(sf)gfp_KpnI</i> , amp ^r	This study
IM33	IM08B, pLOW- <i>lacA-m(sf)gfp</i> , amp ^r	This study
IM7	IM08B, pLOW- <i>ftsZ-mYFP</i> , amp ^r	This study
IM8	IM08B, pLOW- <i>ftsZ-mKate2</i> , amp ^r	This study
IM187	IM08B, pMAD- <i>smdA-flag_aad9</i> , amp ^r	This study
Strains used for BACTH assays		
GS1225	XL1-Blue, pKNT25- <i>smdA</i> , kan ^r	This study
GS1226	XL1-Blue, pUT18- <i>smdA</i> , amp ^r	This study
GS1302	XL1-Blue, pKNT25- <i>smdAΔTMH</i> , kan ^r	This study
GS1303	XL1-Blue, pUT18- <i>smdAΔTMH</i> , amp ^r	This study
GS1134	XL1-Blue, pKT25- <i>pbp1</i> , kan ^r	(Stamsås et al., 2018)
GS1135	XL1-Blue, pUT18C- <i>pbp1</i> , amp ^r	(Stamsås et al., 2018)
GS1136	XL1-Blue, pKT25- <i>pbp2</i> , kan ^r	(Stamsås et al., 2018)
GS1137	XL1-Blue, pUT18C- <i>pbp2</i> , amp ^r	(Stamsås et al., 2018)
GS1138	XL1-Blue, pKT25- <i>pbp3</i> , kan ^r	(Stamsås et al., 2018)
GS1139	XL1-Blue, pUT18C- <i>pbp3</i> , amp ^r	(Stamsås et al., 2018)
GS1187	XL1-Blue, pKNT25- <i>ezrA</i> , kan ^r	(Stamsås et al., 2018)
GS1188	XL1-Blue, pUT18- <i>ezrA</i> , amp ^r	(Stamsås et al., 2018)

Table S4. Primers used in this study.

Primer	Sequence (5'-3') ^a
Primers used for construction of plasmids used in subcellular screening	
im1_linker-FP_F_BamHI	ACTGGATCCCCGGATCTGGTGGAGAAGCTGCA
im2_m(sf)gfp_R_NotI_EcoRI	AGTGAATTCGGGGCCGCCTTACTTATAAAAGCTCATCCATGCC
im14_lacA_F_XhoI_Sall_RBS_NcoI	ATCCTCGAGGTCGACCAATAAAACTAGGAGGAAATTTCCATG GCGATTATTATTGGTTCAG
im15_lacA_R_BamHI	TCCGGGGATCCAGCACATTTTATTAAGCATATCTAC
im35_SA0015_F_NcoI	ATCCCATGGATCGGCAGTCCACTAAG
im36_SA0015_R_BamHI	TCCGGGGATCCATGCATCTTCACCTACTTAAAT
im37_SA0226_F_NcoI	ATCCCATGGTTAATCAAGTATATCAATTAG
im38_SA0226_R_BamHI	TCCGGGGATCCACATAATCCATTTTAATACTGTTTTA
im39_SA0227_F_NcoI	ATCCCATGGTTAAAAGTAAGATATATATAG
im40_SA0227_R_BamHI	TCCGGGGATCCAGCTACCAAATAAATTTCTGACTA
im41_SA0345_F_NcoI	ATCCCATGGCGTCAAAATATGGAATAAA
im42_SA0345_R_BamHI	TCCGGGGATCCATCTTTGTGTATCATCATGAGATT
im43_SA0444_F_NcoI	ATCCCATGGGCGGTGGCGGAAAC
im44_SA0444_R_BamHI	TCCGGGGATCCACATTCAGGGATGTTTTAAGCC
im45_SA0762_F_NcoI	ATCCCATGGTTACATTATTACTAGTTGC
im46_SA0762_R_BamHI	TCCGGGGATCCATTCCCTCTTTATGAGATGACTTAC
im47_SA0892_F_NcoI	ATCCCATGGGTGTAACCTGGTATTCAAC
im48_SA0892_R_BamHI	TCCGGGGATCCAGTCGTTTCGAATTGCTCGCT
im49_SA1627_F_NcoI	ATCCCATGGAAAAATTTGGTTTCAATTGTTG
im50_SA1627_R_BamHI	TCCGGGGATCCATGATTTTGCATTTAAGTTAATTTTG
im51_SA1661_F_NcoI	ATCCCATGGTTTCGTTAAATAACCGATTA
im52_SA1661_R_BamHI	TCCGGGGATCCATAACACCCTTTCAATTACAGCA
im53_SA1700_F_NcoI	ATCCCATGGCTGACATTTTAAAATGTATC
im54_SA1700_R_BamHI	TCCGGGGATCCATAAAATAGAATTTCTTAATACAACAT
im55_SA1701_F_NcoI	ATCCCATGGGTTTAGTTTCGCAAGTTTT
im56_SA1701_R_BamHI	TCCGGGGATCCAATTTTCTCCCATGTGATATAAC
im57_SA1721_F_NcoI	ATCCCATGGAAAACCTTGATAAAACAATG
im58_SA1721_R_BamHI	TCCGGGGATCCATTTATTTGCTCTTTTAAATAGTAAG
im59_SA1770_F_NcoI	ATCCCATGGGCGGCGACTTGATAG
im60_SA1770_R_BamHI	TCCGGGGATCCAAATTTGCTGTGAGTTTCACG
mk353_SA1866_F_long_NcoI	GATCCCATGGAGCAGTTTATCAATTAGG
im62_SA1866_R_BamHI	TCCGGGGATCCAAATAAACATGTTACTATTCATAACT
im63_SA1930_F_NcoI	ATCCCATGGTTGTAATTATAATTTTAATATTG
im64_SA1930_R_BamHI	TCCGGGGATCCATTTATTTGACGATTTTGTCTTT
im65_SA2106_F_NcoI	ATCCCATGGATGAATTGACTATTTATCAT
im66_SA2106_R_BamHI	TCCGGGGATCCAACGAGATTTCTTCTGTCTATTTG
im67_SA2279_F_NcoI	ATCCCATGGATTCGCTGCTCATTGATA
im68_SA2279_R_BamHI	TCCGGGGATCCAATTTCTTTTACTGTTGATCC
im69_SA2280_F_NcoI	ATCCCATGGATCAATTTGCTATATTTTTAG
im70_SA2280_R_BamHI	TCCGGGGATCCAATGAGCAGCGAATTCATGGAT
im71_SA2407_F_NcoI	ATCCCATGGATTTTCCAACCTTTTTCFAA
im72_SA2407_R_BamHI	TCCGGGGATCCATTTACACCTTTCTTTTGAAGC
im73_SA2720_F_NcoI	ATCCCATGGCAGTAGTAGGGGAT
im74_SA2720_R_BamHI	TCCGGGGATCCATTGTAATATTGCAAAAATACATTGC
im75_SA1756_F_Sall_RBS	ATCGTCGACCAATAAAACTAGGAGGAAATTTAAATGATTACT GTTGATATTACAGTT

im76_SA1756_R_BamHI	TCCGGGGATCCACTTATAATTTAATCTAATATTCTCAT
im77_SA1908_F_Sall_RBS	ATCGTCCGACCAATAAAACTAGGAGGAAATTTAAATGGATTTA TCTTCACCGATAG
im78_SA1908_R_BamHI	TCCGGGGATCCAATTGAATGATTCAATTTTATCCATC
im79_linker- FP_F_KpnI_BamHI	ACTGGATCCGGTACC CCGGATCTGGTGGAGAAGCTGCA
im80_SA1244_F_Sall_RBS	ATCGTCCGACCAATAAAACTAGGAGGAAATTTAAATGAAAAAG AAAAAAATTCCGATG
im81_SA1244_R_KpnI	TCCGGGGTACCATTTTGGGATCTCTTCTCTATAAAA
im82_SA1782_F_Sall_RBS	ATCGTCCGACCAATAAAACTAGGAGGAAATTTAAATGTCTAAA TTTGATGAACAAATC
im83_SA1782_R_KpnI	TCCGGGGTACCATAAATCTTGAAGGATTAATGCAC
im95_m(sf)gfp_F_Sall_RBS	ATCCAGTCCGACCAATAAAACTAGGAGGAAATTTAAATGTCAA AAGGAGAAGAGCTGTTC
im96_m(sf)gfp_R_linker- overlap	CTTTAGCTGCAGCTTCTCCACCAGATCCCTTATAAAGCTCATC CATGCC
im97_SA1477_F_BamHI_link er-overlap	TGGAGAAGCTGCAGCTAAAGCTGGAGGATCCATGATAATTTA TTTCGTAATATTAATG
im98_SA1477_R_EcoRI_NotI	TGGATGCGGCCGCGAATTC T TAAATCACTTGAACGCGCAATC
im99_SA2151_F_BamHI	ATCCAGGATCCATGAGAAATTTAAATTTAGTTAAGTA
im100_SA2151_R_EcoRI_Not I	TGGATGCGGCCGCGAATTC T TAAATGTCTTTTTTTAGCGACA TA
im101_SA0957_F_BglII	ATCCAAGATCTATGTTAATGGATCCAAGTTTGAT
im102_SA0957_R_EcoRI_Not I	TGGATGCGGCCGCGAATTC T TATTTATGCGATTTTTTTATTT TTAAC

Primers used for making pLOW-dcas9 compatible in MRSA

im183_pLOW_F	TACTGCAATCGGATGCGATTA
im184_pLOW_R	GTTAAGGGATGCATAAACTGC
im185_aad9_F_ol-im183	TAATCGCATCCGATTGCAGTAATTGGGCCACCTAGGATC
im186_aad9_R_ol-im184	GCAGTTTATGCATCCCTTAACGCCGGTAATAAACTATCAA

Primers used for construction of sgRNA plasmids used in depletion strains

SAOUHSC_02225_for	TATAACTGTTACGTTTAAATATG
SAOUHSC_02225_rev	AAACCATATTTTAAACGTAACAGT
SAOUHSC_00344_for	TATACAGTATTTTAAATAACTATGA
SAOUHSC_00344_rev	AAACTCATAGTTATTTAAATACTG
SAOUHSC_00444_for	TATAGTAGCATTTCAATATCGTCT
SAOUHSC_00444_rev	AAACAGACGATATTGAAATGCTAC
SAOUHSC_00762_for	TATATTCGATATTGCAATAACAAT
SAOUHSC_00762_rev	AAACATTGTTATTGCAATATCGAA
SAOUHSC_00892_for	TATAGTCTCAACAAACGCACCGTA
SAOUHSC_00892_rev	AAACTACGGTGCCTTTGTTGAGAC
SAOUHSC_00957_for	TATAAAATAAGGTAAGATCAAACCT
SAOUHSC_00957_rev	AAACAGTTTGATCTTACCTTATTT
SAOUHSC_01242_for	TATAAAATTCAGTCTTCCATAAT
SAOUHSC_01242_rev	AAACATTATGGAAGACTTGAATTT
SAOUHSC_01477_for	TATAACTTTGTGTTGTGCCATAA
SAOUHSC_01477_rev	AAACTTATGGGCACAACACAAAGT
SAOUHSC_01627_for	TATATCTGTTGTTTTTCTTCTAA
SAOUHSC_01627_rev	AAACTTAGAAGAAAAACAACAGA

SAOUHSC_01662_for	TATAACATCTTCTAATGTTAATGT
SAOUHSC_01662_rev	AAACACATTAACATTAGAAGATGT
SAOUHSC_01702_for	TATATATTGTTACTTCTTCTTCCA
SAOUHSC_01702_rev	AAACTGGAAGAAGAAGTAACAATA
SAOUHSC_01722_for	TATAATTGGCACTAATGGTGCAGA
SAOUHSC_01722_rev	AAACTCTGCACCATTAGTGCCAAT
SAOUHSC_01757_for	TATAACTGTTGCACCTTCAACTGT
SAOUHSC_01757_rev	AAACACAGTTGAAGGTGCAACAGT
SAOUHSC_01770_for	TATATTTTGACTACAAAGCATATA
SAOUHSC_01770_rev	AAACTATATGCTTTGTAGTCAAAA
SAOUHSC_01782_for	TATATCAAAAATATTTTGACCTTC
SAOUHSC_01782_rev	AAACGAAGGTCAAAAATATTTTGA
SAOUHSC_01866_for	TATAGCTGATAATGCCGCAATAAA
SAOUHSC_01866_rev	AAACTTTATTGCGGCATTATCAGC
mk299_sgRNA_1908	TACCTAAGGCAACTAAAAAA GTTTAAGAGCTATGCTGGAAACAG
mk323_sgRNA_01908_V2	ATAATGAGTCCAATGACTAT GTTTAAGAGCTATGCTGGAAACAG
SAOUHSC_01930_for	TATATAATAGAATAACCATCCATT
SAOUHSC_01930_rev	AAACAATGGATGGTTATTCTATTA
SAOUHSC_02107_for	TATATACGCGCCAATTTGCTAGA
SAOUHSC_02107_rev	AAACTCTAGCGAAATTTGGCGGTA
SAOUHSC_02155_for	TATATGCTTAATCTGTTTATAAAT
SAOUHSC_02155_rev	AAACATTTATGAACAGATTAAGCA
SAOUHSC_02280_for	TATATTTAATGATGTTAAATGTGCG
SAOUHSC_02280_rev	AAACCGACATTTAACATCATTAAA
SAOUHSC_02407_for	TATATTACAATTTTTAACGTACTG
SAOUHSC_02407_rev	AAACCAGTACGTTAAAAATTGTAA
Primers used for chromosomal fusions and plasmids for localization studies	
im147_SA1908_up_F_MluI	ACCTACGCGTGATTTTCGGTATATAAAATGATAA
im148_SA1908_R_NotI_flag-overlap	TCTTTATAATCAATATCATGATCTTTATAATCACCATCATGAT CTTTATAATCCGCGGCCGCTTGAATGATTCAATTTTATCCA
im149_aad9_up_F_SpeI_flag-overlap	GATCATGATATTGATTATAAAGATGATGATGATAAATAAACT AGTATTGGGCCACCTAGGAT
im150_aad9_down_R_1908 down-overlap	TCATCACTTCAGCCTAACATCTCGAGGCCGCGGTAAT
im151_SA1908_down_F	ATGTTAGGCTGAAAGTGATGA
im152_SA1908_down_R_BamHI	AGTCGGATCCTGATTTAAACCATCAATTTCGC
im153_linker-FP_F_NotI	ACTGCGGCCGCGGATCTGGTGGAGAAGCTG
im154_m(sf)gfp_R_SpeI	AGTACTAGTTTACTTATAAAGCTCATCCATG
im5_mKate_R_NotI_EcoRI	AGTGAATTCGCGGCCGCTTAAACGGTGTCCCAATTTACTAGG
USHC109	GCGACGCGTTTAAACGGTGTCCCAATTTACTAGG
USHC148	CGCGTCGACAGGAGGATAATTTATTTAGTGAATTTGAAC AAGG
im3_cfp_myfp_R_NotI_EcoRI	AGTGAATTCGCGGCCGCTTATTTATAAAGTTCGTCCATACC
Primers used for verifying <i>smdA</i> silencing	

im126_RT-q_pta_F	ATCATTGATGGCGAATTCCAAT
im127_RT-q_pta_R	GGACCAACTGCATCATATCC
im137_RT-q_SA1908_F	TATGTAACGGACATGAGATTAAT
im138_RT-q_SA1908_R	CTAATACCATTATAAACATGACC
Primers used for construction of plasmids for overexpression	
mk517_1908_R_NotI	ACGAGCGGCCGCATATAGTCATCACTTCAGCCT
mk518_1908_F_RBS_Sall	ATCCAGT <u>CGACCAATAAAAACTAGGAGGAAATTTAAATG</u> AGTAAGAAAAAAGTTAAGCGACAAAC
mk519_1908_H145A_F	GAACGAATTAGT GCTTT AGTATTAACAAG
mk520_1908_H145A_R	CTTGTTAATACTAAAGCACTAATTCGTTC
mk521_1908_RT_AA_F	TTAGTATTAACAG CAGCT GGTCTTTATATT
mk522_1908_RT_AA_R	AATATAAGACCAG CTGCT GTTAATACTAA
mk529_1908_FH_AA_F	CTTTAACAAATTTGTAG CCGCT GGTCGTATTCAAT
mk530_1908_FH_AA_R	ATTGAATACGACCAG CGGCT TACAAATTTGTTAAAG
Primers used for construction of plasmids to BACTH assays	
gs718_SA1908_F_BamHI	GATCGGAT <u>CCCGATTTATCTTCACCGATAGTCATTG</u>
gs719_SA1908_R_KpnI	GATCGG <u>TACCGATTGAATGATTCAATTTTATCCATC</u>
gs735_SA1908 Δ TMH_F_BamHI	GATCGGAT <u>CCCGGTAGTAAGAAAAAAGTTAAGCGAC</u> HI
Primers used for sequencing and to check constructs	
im16_protein- msfgfp_check_R	AGTGTGTCACCTTCAAACCTTC
im110_seq-pLOW_up ermC	TTGGTTGATAATGAACTGTGCT
im94_m(sf)gfp- protein_check_F	GCAAACCTCAAAATCCGTCATA
im134_pLOW_down_check_R	TGTGCTGCAAGCGGATTAAG
mk25_pCG248_r_check	AAATCTCGAAAATAATAGAGGGA
mk26_pCG248_f_up_check	GGATAACCGTATTACCGCCT
im156_pMAD_check_F	AATCTAGCTAATGTTACGTTACA
mk177_pMAD_check_R	GATGCCCGCGAAGCGAG
im198_aad9-pLOW_check_R	CTCATATCTTTTATTCAATAATCG
im244_up1908_F_check	GACGTATTAGCCTTCTCTC
im245_down1908_R_check	CATACCGTAATGATAGATATGG

^aRestriction sites are underlined, sequences included as overhang in italic and inserted mutations in bold.

References

- Chatterjee, S. S., Joo, H.-S., Duong, A. C., Dieringer, T. D., Tan, V. Y., Song, Y., Fischer, E. R., Cheung, G. Y., Li, M. & Otto, M. (2013). Essential *Staphylococcus aureus* toxin export system. *Nature medicine*, 19 (3): 364-367. doi: 10.1038/nm.3047.
- Chaudhuri, R. R., Allen, A. G., Owen, P. J., Shalom, G., Stone, K., Harrison, M., Burgis, T. A., Lockyer, M., Garcia-Lara, J., Foster, S. J., et al. (2009). Comprehensive identification of essential *Staphylococcus aureus* genes using Transposon-Mediated Differential Hybridisation (TMDH). *BMC genomics*, 10 (1): 291. doi: 10.1186/1471-2164-10-291.
- Corrigan, R. M., Abbott, J. C., Burhenne, H., Kaefer, V. & Gründling, A. (2011). c-di-AMP is a new second messenger in *Staphylococcus aureus* with a role in controlling cell size and envelope stress. *PLoS pathogens*, 7 (9): e1002217. doi: 10.1371/journal.ppat.1002217.
- Deutsch, C., El Yacoubi, B., de Crécy-Lagard, V. & Iwata-Reuyl, D. (2012). Biosynthesis of threonylcarbamoyl adenosine (t6A), a universal tRNA nucleoside. *Journal of biological chemistry*, 287 (17): 13666-13673. doi: 10.1074/jbc.M112.344028.
- Gallay, C., Sanselicio, S., Anderson, M. E., Soh, Y. M., Liu, X., Stamsås, G. A., Pelliciani, S., van Raaphorst, R., Dénéréaz, J., Kjos, M., et al. (2021). CcrZ is a pneumococcal spatiotemporal cell cycle regulator that interacts with FtsZ and controls DNA replication by modulating the activity of DnaA. *Nature microbiology*, 6 (9): 1175-1187. doi: 10.1038/s41564-021-00949-1.
- Herbert, S., Ziebandt, A.-K., Ohlsen, K., Schäfer, T., Hecker, M., Albrecht, D., Novick, R. & Götz, F. (2010). Repair of global regulators in *Staphylococcus aureus* 8325 and comparative analysis with other clinical isolates. *Infection and immunity*, 78 (6): 2877-2889. doi: 10.1128/IAI.00088-10.
- Horsburgh, M. J., Aish, J. L., White, I. J., Shaw, L., Lithgow, J. K. & Foster, S. J. (2002). σ^B modulates virulence determinant expression and stress resistance: characterization of a functional *rsbU* strain derived from *Staphylococcus aureus* 8325-4. *Journal of bacteriology*, 184 (19): 5457-5467. doi: 10.1128/JB.184.19.5457-5467.2002.
- Kreiswirth, B. N., Löfdahl, S., Betley, M. J., O'reilly, M., Schlievert, P. M., Bergdoll, M. S. & Novick, R. P. (1983). The toxic shock syndrome exotoxin structural gene is not detectably transmitted by a prophage. *Nature*, 305 (5936): 709-712. doi: 10.1038/305709a0.
- Lund, V. A., Wacnik, K., Turner, R. D., Cotterell, B. E., Walther, C. G., Fenn, S. J., Grein, F., Wollman, A. J., Leake, M. C., Olivier, N., et al. (2018). Molecular coordination of *Staphylococcus aureus* cell division. *eLife*, 7: e32057. doi: 10.7554/eLife.32057.
- Monk, I. R., Tree, J. J., Howden, B. P., Stinear, T. P. & Foster, T. J. (2015). Complete bypass of restriction systems for major *Staphylococcus aureus* lineages. *mBio*, 6 (3): e00308-15. doi: 10.1128/mBio.00308-15.
- Münch, D., Roemer, T., Lee, S. H., Engeser, M., Sahl, H. G. & Schneider, T. (2012). Identification and in vitro analysis of the GatD/MurT enzyme-complex

- catalyzing lipid II amidation in *Staphylococcus aureus*. *PLoS pathogens*, 8 (1): e1002509. doi: 10.1371/journal.ppat.1002509.
- Novick, R. (1967). Properties of a cryptic high-frequency transducing phage in *Staphylococcus aureus*. *Virology*, 33 (1): 155-166. doi: 10.1016/0042-6822(67)90105-5.
- Qian, Z., Yin, Y., Zhang, Y., Lu, L., Li, Y. & Jiang, Y. (2006). Genomic characterization of ribitol teichoic acid synthesis in *Staphylococcus aureus*: genes, genomic organization and gene duplication. *BMC genomics*, 7 (1): 1-12. doi: 10.1186/1471-2164-7-74.
- Santiago, M., Matano, L. M., Moussa, S. H., Gilmore, M. S., Walker, S. & Meredith, T. C. (2015). A new platform for ultra-high density *Staphylococcus aureus* transposon libraries. *BMC genomics*, 16 (1): 1-18. doi: 10.1186/s12864-015-1361-3.
- Schindelin, J., Arganda-Carreras, I., Frise, E., Kaynig, V., Longair, M., Pietzsch, T., Preibisch, S., Rueden, C., Saalfeld, S. & Schmid, B. (2012). Fiji: an open-source platform for biological-image analysis. *Nature methods*, 9 (7): 676-682. doi: 10.1038/nmeth.2019.
- Sewell, E. W. & Brown, E. D. (2014). Taking aim at wall teichoic acid synthesis: new biology and new leads for antibiotics. *The journal of antibiotics*, 67 (1): 43-51. doi: 10.1038/ja.2013.100.
- Shafer, W. M. & Iandolo, J. J. (1979). Genetics of staphylococcal enterotoxin B in methicillin-resistant isolates of *Staphylococcus aureus*. *Infection and immunity*, 25 (3): 902-911. doi: 10.1128/iai.25.3.902-911.1979.
- Sievers, F., Wilm, A., Dineen, D., Gibson, T. J., Karplus, K., Li, W., Lopez, R., McWilliam, H., Remmert, M., Söding, J., et al. (2011). Fast, scalable generation of high-quality protein multiple sequence alignments using Clustal Omega. *Molecular systems biology*, 7: 539. doi: 10.1038/msb.2011.75.
- Stamsås, G. A., Myrbråten, I. S., Straume, D., Salehian, Z., Veening, J. W., Håvarstein, L. S. & Kjos, M. (2018). CozEa and CozEb play overlapping and essential roles in controlling cell division in *Staphylococcus aureus*. *Molecular microbiology*, 109 (5): 615-632. doi: 10.1111/mmi.13999.
- Valentino, M. D., Foulston, L., Sadaka, A., Kos, V. N., Villet, R. A., Santa Maria, J., Lazinski, D. W., Camilli, A., Walker, S. & Hooper, D. C. (2014). Genes contributing to *Staphylococcus aureus* fitness in abscess-and infection-related ecologies. *mBio*, 5 (5): e01729-14. doi: 10.1128/mBio.01729-14.

PAPER IV



CRISPR Interference for Rapid Knockdown of Essential Cell Cycle Genes in *Lactobacillus plantarum*

Ine Storaker Myrbråten,^a Kamilla Wiull,^a Zhian Salehian,^a Leiv Sigve Håvarstein,^a Daniel Straume,^a Geir Mathiesen,^a Morten Kjos^a

^aFaculty of Chemistry, Biotechnology and Food Science, Norwegian University of Life Sciences, Ås, Norway

ABSTRACT Studies of essential genes in bacteria are often hampered by the lack of accessible genetic tools. This is also the case for *Lactobacillus plantarum*, a key species in food and health applications. Here, we develop a clustered regularly interspaced short palindromic repeat interference (CRISPRi) system for knockdown of gene expression in *L. plantarum*. The two-plasmid CRISPRi system, in which a nuclease-inactivated Cas9 (dCas9) and a gene-specific single guide RNA (sgRNA) are expressed on separate plasmids, allows efficient knockdown of expression of any gene of interest. We utilized the CRISPRi system to gain initial insights into the functions of key cell cycle genes in *L. plantarum*. As a proof of concept, we investigated the phenotypes resulting from knockdowns of the cell wall hydrolase-encoding *acm2* gene and of the DNA replication initiator gene *dnaA* and of *ezrA*, which encodes an early cell division protein. Furthermore, we studied the phenotypes of three cell division genes which have recently been functionally characterized in ovococcal bacteria but whose functions have not yet been investigated in rod-shaped bacteria. We show that the transmembrane CozE proteins do not seem to play any major role in cell division in *L. plantarum*. On the other hand, RNA-binding proteins KhpA and EloR are critical for proper cell elongation in this bacterium.

IMPORTANCE *L. plantarum* is an important bacterium for applications in food and health. Deep insights into the biology and physiology of this species are therefore necessary for further strain optimization and exploitation; however, the functions of essential genes in the bacterium are mainly unknown due to the lack of accessible genetic tools. The CRISPRi system developed here is ideal to quickly screen for phenotypes of both essential and nonessential genes. Our initial insights into the function of some key cell cycle genes represent the first step toward understanding the cell cycle in this bacterium.

KEYWORDS CRISPRi, *Lactobacillus plantarum*, *acm2*, bacterial cell cycle, *cozE*, *dnaA*, *eloR*, *ezrA*, *khpA*, knockdown

The lactic acid bacterium (LAB) *Lactobacillus plantarum* is an important species for food and health applications. *L. plantarum* is naturally found in a variety of habitats, including meat and dairy products and fermented vegetables and in the oral cavity and gastrointestinal tract of humans (1–3). It has been documented that *L. plantarum* strains have probiotic effects on humans (4–6), and at least some strains have been shown to modulate the immune system (7). Furthermore, extensive research has been performed in recent decades in investigations of LAB, including *L. plantarum*, as live delivery vehicles for therapeutic molecules such as antigens, cytokines, and antibodies (8–11). Given the importance and the potential new applications of *L. plantarum*, there is a need to develop strains with improved growth, robustness, and protein secretion capacities.


Such strain development heavily relies on further insights into the biology of these

Citation Myrbråten IS, Wiull K, Salehian Z, Håvarstein LS, Straume D, Mathiesen G, Kjos M. 2019. CRISPR interference for rapid knockdown of essential cell cycle genes in *Lactobacillus plantarum*. *mSphere* 4:e00007-19. <https://doi.org/10.1128/mSphere.00007-19>.

Editor Maria L. Marco, University of California, Davis

Copyright © 2019 Myrbråten et al. This is an open-access article distributed under the terms of the [Creative Commons Attribution 4.0 International license](https://creativecommons.org/licenses/by/4.0/).

Address correspondence to Geir Mathiesen, geir.mathiesen@nmbu.no, or Morten Kjos, morten.kjos@nmbu.no.

 Phenotyping of key cell cycle genes in *Lactobacillus plantarum* using CRISPRi. @Morten3891 @MathiesenG @DanStream

Received 5 January 2019

Accepted 2 March 2019

Published 20 March 2019

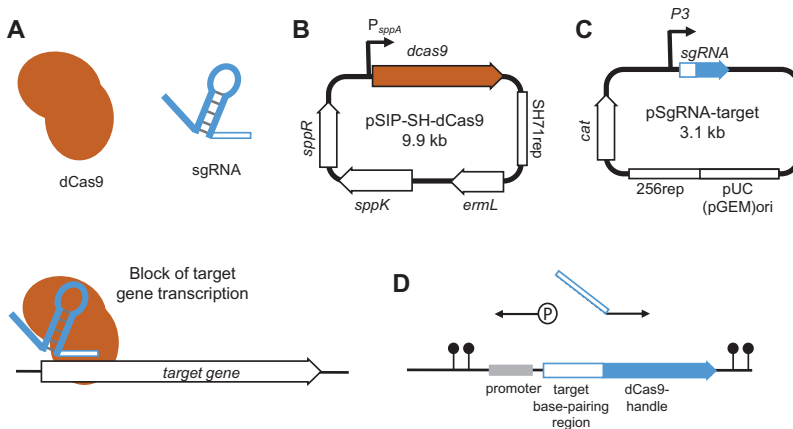


FIG 1 The two-plasmid CRISPRi-system. (A) Schematic presentation of transcriptional knockdown by CRISPRi. Block of RNA polymerase and transcription occurs when dCas9 (orange) and the sgRNA (blue) bind specific sites in the 5' end of the target gene, guided by the 20-nucleotide (nt) sgRNA sequence. (B) Overview of pSIP-SH-dCas9 plasmid. The *dcas9* gene is located downstream of the inducible *sppA* promoter (P_{sppA}). The two-component regulatory genes, *sppK* and *sppR*, are located on the same plasmid. "*ermL*" and "*SH71_{rep}*" indicate the erythromycin resistance gene and the replicon determinant, respectively. (C) Overview of the prototype expression vector of sgRNA. The sgRNA is constitutively expressed from promoter P3. "*cat*" and "*256_{rep}/pUC(pGEM)ori*" indicate the chloramphenicol resistance gene and the replicon determinant, respectively. Both plasmids (see panels B and C) were transformed into *L. plantarum* to achieve transcriptional knockdown of the target gene. (D) A detailed view of the sgRNA-region in pSgRNA-target. The gene-specific target region (white) and dCas9-handle region (blue) of the sgRNA are shown downstream of the cognate promoter (gray). Terminator sequences are indicated by lollipops. New sgRNA plasmids were constructed by inverse-PCR using two primers as indicated by arrows in the figure, with one phosphorylated (P) reverse primer annealing immediately upstream of the targeting-region and one nonphosphorylated forward primer annealing to the dCas9-handle region, containing a 20-nt overhang which is specific to a target gene.

cells. Most studies on *L. plantarum* have been performed in the model strain WCFS1 (12), which was the first *Lactobacillus* strain whose genome was sequenced. This strain is easily transformable by electroporation, and tools for plasmid-based expression platforms are available, including inducible expression systems based on bacteriocin regulatory systems (pSIP, pNICE) (13–16). The high transformation efficiency has also allowed the construction of a number of isogenic mutants in genes involved in different pathways and functions. In particular, the *Cre-lox* system, which is based on double-crossover gene replacement, has been important in this field (17), although mutants have also been made using suicide vectors (18). Mutant construction in *L. plantarum* is, however, a laborious and time-consuming process, and novel methods for phenotyping are highly desirable.

Here we have developed a gene knockdown method known as clustered regularly interspaced short palindromic repeat interference (CRISPRi) in *L. plantarum* WCFS1 that permits easy downregulation of any gene of interest (19, 20), and, most importantly, it allows studies of essential genes. CRISPRi exploits the CRISPR/Cas9 system by utilizing a catalytically inactive Cas9 protein (dCas9) together with a single guide RNA (sgRNA) that harbors an easily replaceable 20-nucleotide (nt) base-pairing region and a Cas9-handle region. The 20-nt base-pairing region is selected to target the gene of interest, and the sgRNA can easily be redesigned to target any gene of interest. The dCas9 will have lost its ability to cleave DNA, but the DNA-binding property of this protein remains intact. Expression of *dcas9* together with sgRNA thus causes a transcriptional blocking of the RNA polymerase, leading to knockdown of gene expression of the target gene (19, 20) (Fig. 1A). CRISPRi has been successfully established in bacterial species such as *Escherichia coli* (20), *Bacillus subtilis* (21), *Streptococcus pneumoniae* (22), *Staphylococcus aureus* (23–26), and *Lactococcus lactis* (27). Note that CRISPR-based tools have been used in lactobacilli previously. In *Lactobacillus casei*, a nickase Cas9 was used for

genome editing (28), while in *L. plantarum*, genome editing was performed by recombineering double-stranded DNA templates into target sites using cleavage by Cas9 (29). Notably, the latter work demonstrated that the outcomes of the CRISPR experiments could vary between different *L. plantarum* strains.

While *L. plantarum* has been extensively studied with respect to host cell interaction, immune cell modulation, protein secretion, biofilm formation, interaction with food components, and production of bacteriocins (30), much less is known about essential processes of the bacterial cell cycle in these rod-shaped bacteria. Most of our knowledge on the cell cycle of Gram-positive, rod-shaped bacteria comes from *B. subtilis*, where DNA replication, chromosome segregation, cell wall synthesis, and cell division, as well as the coordination of these processes, have been investigated in detail (31–33). Although *L. plantarum* is related to *B. subtilis*, there are also key differences between the cell cycles of these species, for example, with regard to sporulation. Specific knowledge about the functions of proteins and factors affecting cell cycle processes in *L. plantarum* is therefore important, since such knowledge may pave the way for development of strains with improvements with respect to protein secretion or interactions with host cells (18).

In this study, we utilized the CRISPRi system to get initial insights into the functions of putative cell cycle proteins in *L. plantarum*. As a proof of principle, we studied proteins hypothesized to affect different stages of the bacterial cell cycle. These included (i) Acn2, a cell wall hydrolase previously shown to play a major role in daughter cell separation in *L. plantarum* (34, 35); (ii) the bacterial DNA replication initiator protein DnaA (36); and (iii) the early cell division protein EzrA. EzrA is a membrane-associated protein involved in coordination of cell division and cell wall synthesis in Gram-positive bacteria (37). The CRISPRi system was also used to study the functions of proteins putatively involved in bacterial cell elongation but whose functions have not previously been studied in rod-shaped bacteria. These proteins, named CozE (38), EloR (39), and KhpA (40), have all been identified as essential for proper cell elongation in the oval-shaped bacterium *S. pneumoniae*. CozE (coordinator of zonal elongation) has been shown to control cell elongation by directing the activity of cell wall synthesizing proteins (38, 41). Homologs of CozE (CozEa and CozEb) are also essential for proper cell division in *S. aureus* (23). EloR (elongation regulator) and KhpA (KH-containing protein A) are two cytoplasmic, RNA-binding proteins which form a midcell-localized heterocomplex (39, 40, 42).

RESULTS AND DISCUSSION

Construction of a two-plasmid system for CRISPR interference in *L. plantarum*.

Given the lack of tools for fast and easy depletion of genes in *L. plantarum*, we developed a two-plasmid CRISPRi system for this purpose (Fig. 1). The system is based on the CRISPRi systems developed for *S. pneumoniae* (22) and *S. aureus* (23). This CRISPR/Cas9-based system can be utilized in *L. plantarum* WCFS1, since this strain does not encode any native CRISPR/Cas9 (12). For expression of nuclease-inactive Cas9 (dCas), *dcas9* was cloned under the control of the inducible promoter *sppA* in the plasmid pSIP403 (15), harboring an erythromycin resistance gene, *ermL*, as well as *sppK* and *sppR*, encoding a histidine protein kinase and a response regulator, respectively. By external addition of the inducer peptide SppIP, expression from promoter *sppA* is induced via this two-component regulatory system (15). The replicon 256_{rep} in pSIP403 was exchanged with the lactococcal SH71_{rep} replicon (Fig. 1B) to make it compatible with the sgRNA-target plasmid, which also is a derivative of pSIP403.

The sgRNA plasmids contain a chloramphenicol resistance gene (*cat*) and an sgRNA cassette under the control of a synthetic, constitutively expressed promoter, P3 (22) (Fig. 1C). The sgRNA cassette includes a 20-nt base-pairing region and a dCas9-handle region (Fig. 1D). The sgRNA-target sequence can easily be exchanged using inverse-PCR with a forward primer containing the gene-specific 20-nt base-pairing region as an overhang (Fig. 1D). The sgRNA has the capability of binding target DNA by complementary base pairing and dCas9 through the secondary structure of the Cas9-handle.

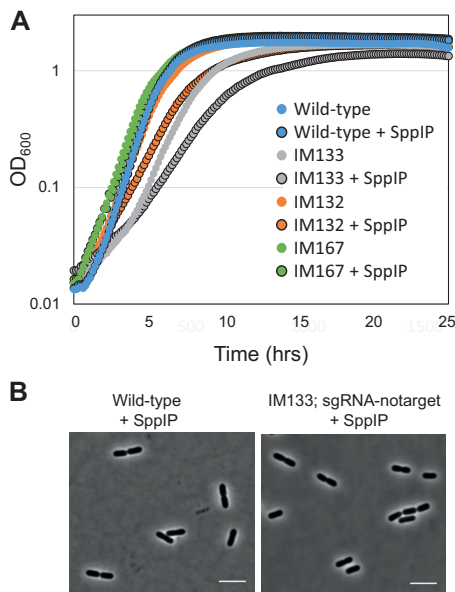


FIG 2 Analysis of dCas9 expression. (A) Growth analysis of wild-type *L. plantarum* WCFS1 (blue), IM133 (WCFS1 carrying pSIP-SH-dCas9 and pSgRNA-notarget; gray), IM132 (WCFS1 carrying only pSIP-SH-dCas9; orange), and IM167 (WCFS1 carrying pEV and pSgRNA-notarget; green). Levels of growth of noninduced cultures and induced cultures (25 ng/ml inducer pheromone SppIP; black outline) are shown. (B) Phase-contrast micrographs of wild-type *L. plantarum* WCFS1 cells and IM133. The scale bars represent 5 μ m.

Induced expression of dCas9 leads to formation of a sgRNA-dCas9-DNA complex that acts as a physical blockage for RNA polymerase (Fig. 1A). In all cases, the sgRNAs were designed to target a location close to the 5' end of the gene of interest. The replicon of the sgRNA plasmids (256_{rep}) has a narrow host range which has been shown to work in only a few *Lactobacillus* species, namely, *L. plantarum*, *Lactobacillus sakei*, and *Lactobacillus curvatus* (43).

High production levels of heterologous proteins using the pSIP expression system have been shown previously to cause growth retardation in *L. plantarum* WCFS1 (13). Expression of the CRISPRi system with a nontargeting sgRNA (IM133; pSIP-SH-dCas9 and pSgRNA-notarget) indeed resulted in growth reduction (Fig. 2A). In fact, induction of dCas9 expression alone (IM132; pSIP-SH-dCas9) caused a growth defect, while the combination of an empty pSIP vector (pEV) with a nontargeting sgRNA plasmid (IM167; pEV and pSgRNA-notarget) did not. This clearly indicates that overproduction of dCas9 results in impaired growth of *L. plantarum*. The morphologies of IM133 cells were not affected compared to those of the wild-type cells (Fig. 2B, see below); however, we cannot exclude the possibility that other cellular processes are affected upon dCas9 production in these cells.

Characterizing the CRISPRi system by targeting *acm2*. We tested the CRISPRi system by targeting a cell division gene with a known knockout phenotype. Previous work had shown that deletion of the gene coding for the major autolysin *Acm2* (*lp_2645*), a cell wall hydrolase (N-acetylglucosaminidase) important for daughter cell separation, results in cell chaining and sedimentation of cultures (34, 44). We constructed a strain targeting *acm2* (IM134, pSIP-SH-dCas9 and pSgRNA-*acm2*) and analyzed the knockdown effects using the wild-type strain and a nontargeting CRISPRi strain as controls (IM133; pSIP-SH-dCas9 and pSgRNA-notarget).

First, to test the efficiency of the transcriptional knockdown, we performed droplet digital PCR (ddPCR). Knockdown of *acm2* was achieved in strain IM134, and the results

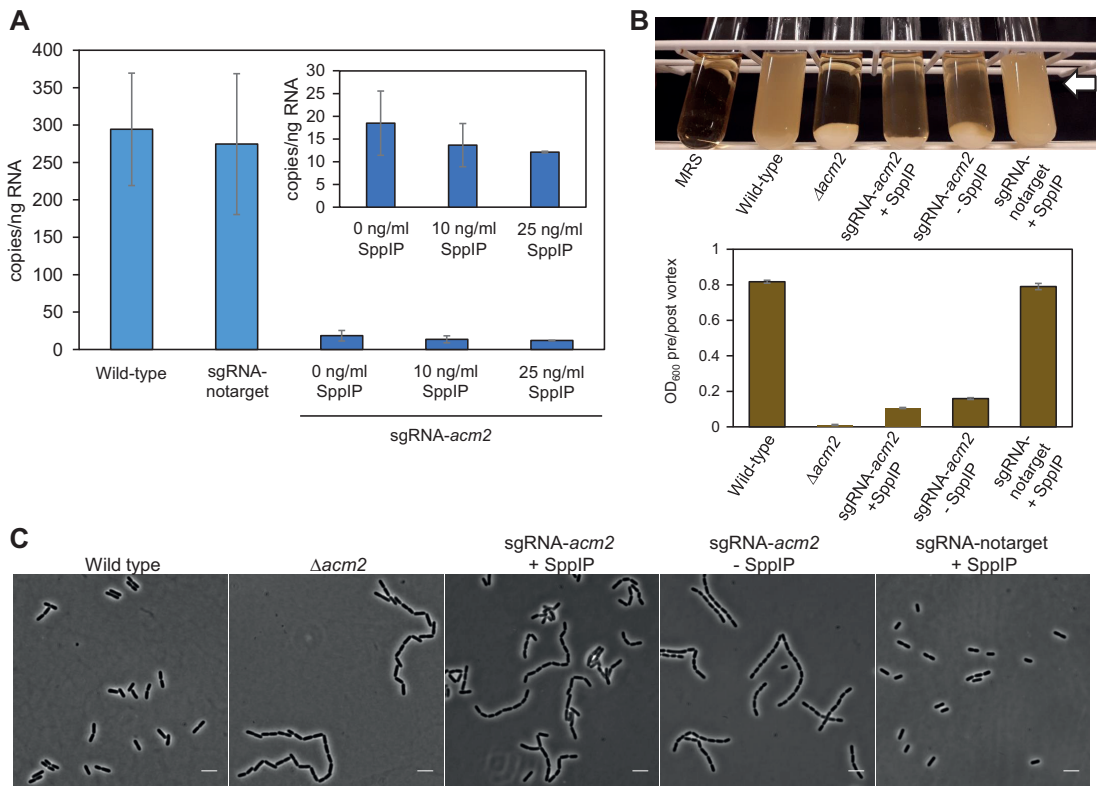


FIG 3 Using CRISPRi to knock down *acm2* expression in *L. plantarum* WCFS1. (A) Quantifying the expression of *acm2* using droplet digital PCR. The transcriptional levels of *acm2* in wild-type *L. plantarum* WCFS1, in control cells with nontargeting sgRNA (IM133), and in CRISPRi strain cells with sgRNA targeting *acm2* (IM134) are indicated. For the latter, cultures with SppIP inducer concentrations of 10 and 25 ng/ml were compared to uninduced culture, and those results are also shown (inset). The error bars represent standard deviations of results from at least two biological replicates, each of which was analyzed with three technical replicates. (B) Growth of *L. plantarum* with various expression levels of *acm2*. (Top panel) Culture tubes of *L. plantarum* grown for 16 h. Sedimentation of cells was clearly observed when *acm2* was deleted ($\Delta acm2$ [34]) or knocked down (IM134 with or without added SppIP) but not in the wild-type or control cells (IM133). (Bottom panel) Quantification of cell sedimentation by measuring *OD*₆₀₀ in the upper layer of the medium (see arrow in top panel) before and after vortex mixing. The ratios are plotted in the bar plot. The error bars represent standard deviations of data from three parallel measurements. (C) Phase-contrast images of the corresponding strains. The CRISPRi strains were imaged at the exponential-growth phase. The scale bar is 5 μ m.

were compared to the control strains (Fig. 3A). Notably, the knockdown was highly effective even without induction, showing that leakage from the *sppA* promoter was sufficient to efficiently drive the CRISPRi system. Only a slight additional decrease in transcription was observed upon induction (10 or 25 ng/ml SppIP) (Fig. 3A, inset).

We next monitored cell sedimentation by growing strains in standing cultures at 37°C for 16 h (Fig. 3B). To quantify the sedimentation, the optical density at 600 nm (*OD*₆₀₀) was measured in the upper part of the culture volume before and after vortex mixing. In a homogenous culture, the ratio should be close to 1, which was the case for the wild-type WCFS1 and IM133 control cells. In contrast, deletion strain $\Delta acm2$ showed full sedimentation of cells and a ratio close to zero. Similarly to the results seen with mutant $\Delta acm2$, depletion of *acm2* in strain IM134 exhibited a high degree of sedimentation with a ratio at 0.1, reflecting that this is a knockdown and not a knockout of *acm2*. Notably, the noninduced cultures and the induced cultures of IM134 displayed similar sedimentation phenotypes. Furthermore, microscopy analyses of the same strains revealed that knockdown of *acm2* by CRISPRi resulted in a chaining phenotype similar to that seen with knockout mutant $\Delta acm2$; since daughter cell separation was

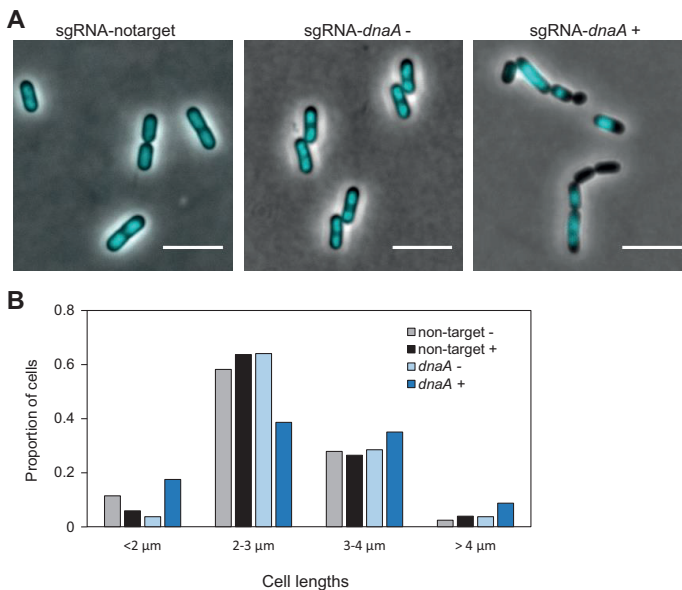


FIG 4 Effect of depleting replication initiation factor *dnaA* in *L. plantarum*. (A) Micrographs (overlay of phase-contrast and DAPI images) of control cells (strain IM133) and *dnaA*-depleted cells (strain IM137) grown without or with inducer. Cells were grown in the presence of 25 ng/ml SppIP. The scale bar is 5 μm. (B) Cell length analysis of *dnaA* knockdown cells ($n = 194$) compared to control cells ($n = 204$) and noninduced cells ($n = 320$). Cell lengths were measured using MicrobeJ (59). Cell populations were split in four groups based on lengths (<2 μm, 2 to 3 μm, 3 to 4 μm, and >4 μm), and the proportion of cells in each group is plotted. Plus signs (+) and minus signs (-) indicate that cells were grown in the presence and absence of 25 ng/ml SppIP, respectively.

inhibited, the cells formed long chains compared to the control (Fig. 3C). Also here, similar phenotypes were observed in induced and noninduced cultures.

Together, these results show that the CRISPRi system functions efficiently and that low basal expression from the *sppA* promoter (16, 45) is sufficient for transcriptional knockdown in *L. plantarum* WCFS1. Only a small additional knockdown effect was observed after external addition of inducer SppIP, which indicates that the basal promoter activity resulted in production of sufficient numbers of dCas9 proteins for efficient knockdown.

Knockdown of *dnaA* and *ezrA*. The results described above show that the CRISPRi system is suitable for transcriptional knockdown of genes in *L. plantarum* and that the system can be used to study phenotypes of cells when a key cell division gene is depleted. However, *acm2* is a nonessential gene in *L. plantarum*, since a deletion mutant could be constructed (34). In addition to its easy introduction into *L. plantarum*, the main strength of a CRISPRi knockdown system is that it allows studies of phenotypes of essential genes in this bacterium. As a further proof of concept, and to gain further insights into the suitability of the CRISPRi system to study essential processes in *L. plantarum*, we designed sgRNA plasmids to target well-studied bacterial cell cycle proteins, namely, the DNA replication initiator DnaA and the early cell division protein EzrA.

DnaA (*p_0001*) is essential for initiation of DNA replication from *oriC* in bacteria and has been studied in a number of different bacterial species, including *B. subtilis* (31). We investigated the CRISPRi knockdown phenotype of *dnaA* by microscopy of cells stained with the nucleoid marker DAPI (4',6-diamidino-2-phenylindole). As expected, DnaA seems to be essential for proper DNA replication in *L. plantarum* (Fig. 4A). Upon induction with SppIP, the growth rate was reduced and we observed a large fraction of

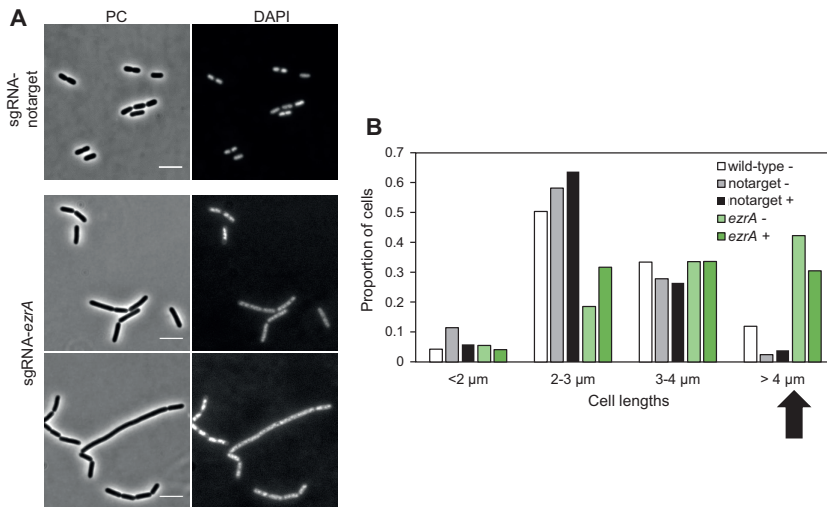


FIG 5 Effect of depleting the cell division protein EzrA in *L. plantarum*. (A) Phase-contrast (PC) micrographs of cells depleted of *ezrA* (IM188) compared to control cells (IM133). DAPI staining of nucleoids is also shown. The scale bar is 5 μm . (B) Cell length analysis of *ezrA* knockdown cells compared to control cells (IM133) and wild-type cells. Cell lengths were measured using MicrobeJ (59). Cell populations were split into four groups based on lengths, and the proportion of cells in each group is plotted. The black arrow points to the large-cell group (cells $\geq 4 \mu\text{m}$), where *ezrA*-depleted cells are clearly overrepresented compared to the control cells. Plus signs (+) and minus signs (-) indicate SppIP-induced and uninduced cells, respectively. Numbers of cells analyzed were as follows: $n = 377$ for wild-type cells, $n = 122$ for notarget control cells (strain IM133) (uninduced), $n = 204$ for notarget control cells (strain IM133) (induced), $n = 506$ for sgRNA-*ezrA* cells (strain IM188) (uninduced), and $n = 413$ for sgRNA-*ezrA* cells (strain IM188) (induced).

cells (59.7%, $n = 139$) that were anucleate or displayed abnormal nucleoid morphologies. Such a phenotype was observed neither in the IM133 control cells (0.2% abnormal nucleoids, $n = 250$) nor in the uninduced cells (5.9% abnormal nucleoids, $n = 320$). The latter demonstrates that in the case of *dnaA* knockdown, the induction of dCas9 by SppIP is necessary to observe the full depletion phenotype. Interestingly, the cell morphologies of the *DnaA*-depleted cells were also severely perturbed. Cell lengths were measured based on the phase-contrast micrographs. This showed that the majority of control cells were between 2 μm and 4 μm in length; however, in the *dnaA* knockdown strain after induction, the fractions of both short (<2- μm) cells and long (>4- μm) cells were larger (Fig. 4B). This supports the notion that proper DNA replication and chromosome segregation are essential for proper cell division, since all cell cycle processes are interlinked (32).

Next, we made a CRISPRi knockdown strain targeting *ezrA* (*lp_2328*). EzrA is known to interact with a number of different proteins, including FtsZ and penicillin binding proteins, for coordination of cell division and cell wall synthesis in Gram-positive bacteria (46, 47). The growth rate of the *ezrA* knockdown strain was not significantly reduced compared to the control. Cell lengths of the knockdown strain were then analyzed using phase-contrast microscopy. While more than 90% of control cells were between 2 μm and 4 μm in length, up to 40% of the cells were longer than 4 μm in the *ezrA* depletion strain (Fig. 5). The elongated cells were found both with and without induction with SppIP. A similar phenotype was previously reported in *B. subtilis* (37, 48); *B. subtilis* cells lacking *ezrA* had delayed cell division and were thus longer than wild-type cells (37, 48). On the other hand, this was not observed in a conditional *ezrA* knockdown in *Listeria monocytogenes* (49), another rod-shaped Gram-positive species. Together, the data suggest that the role of EzrA in cell division may vary between different rod-shaped bacterial species.

Depletion of CozE homologs does not perturb division in *L. plantarum*. Using CRISPRi to knock down transcription of *acm2*, *dnaA*, and *ezrA* demonstrated the

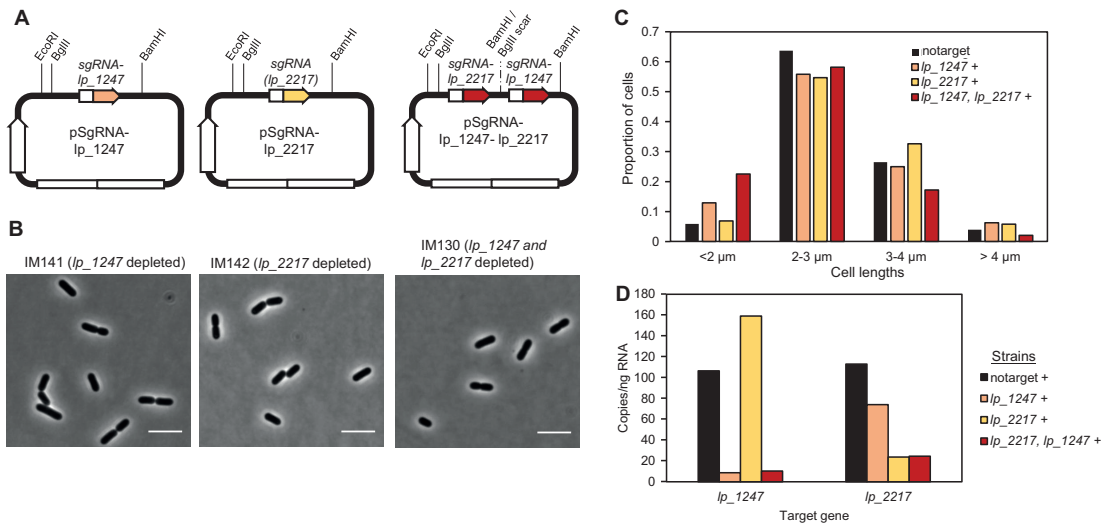


FIG 6 CozE homologs do not dramatically affect cell division in *L. plantarum*. (A) Schematic overview of plasmids harboring sgRNA to knock down expression of *cozE* homologs *lp_1247* (strain IM141) and *lp_2217* (strain IM142) and double knockdown of *lp_1247* and *lp_2217* (strain IM130). The restriction sites utilized for construction of the double-sgRNA plasmids are indicated (see Materials and Methods for details). (B) Phase-contrast micrographs of cells depleted of *lp_1247* or *lp_2217* or both. Cells were grown in the presence of 25 ng/ml SppIP. The scale bar is 5 μ m. (C) Cell length analysis of the corresponding strains compared to control cells (strain IM133). Cell lengths were measured using MicrobeJ (59). Cells were split in four groups based on lengths, and the proportion of cells in each group is plotted. Numbers of cells analyzed were as follows: $n = 204$ for control cells (strain IM133), $n = 256$ for sgRNA-*lp_1247* (strain IM141), $n = 190$ for sgRNA-*lp_2217* (strain IM142), and $n = 244$ for sgRNA-*lp_1247*-*lp_2217* (strain IM130). Plus signs (+) indicate that cells were grown in the presence of 25 ng/ml SppIP. (D) The transcription levels of genes *lp_1247* and *lp_2217* in different strains as analyzed by droplet digital PCR. In addition to *lp_2217* cells (strain IM142), *lp_1247* cells (strain IM141), and the double-knockdown cells (strain IM130), control cells with nontargeting sgRNA (strain IM133) were included in the analysis.

suitability of this system to phenotype key cell cycle genes. We therefore used this system to screen the phenotypes of genes which have as-yet-unknown functions in rod-shaped bacterial cells. CozE proteins have been shown to be essential for proper cell division both in oval-shaped *S. pneumoniae* and coccus-shaped *S. aureus*, but despite its conservation across the bacterial kingdom (38), their involvement in cell division has hitherto not been studied in rod-shaped bacteria. Homology searches revealed that *L. plantarum* WCFS1 encodes two CozE homologs; Lp_1247 (35% identity and 60% similarity to CozE from *S. pneumoniae*) and Lp_2217 (29% identity and 52% similarity to CozE from *S. pneumoniae*). We constructed CRISPRi strains targeting each of these and analyzed the morphologies of the knockdown strains by microscopy. However, no differing phenotype was observed; the cells appeared similar to wild-type cells (Fig. 6B). We then constructed a double-sgRNA vector to target both *cozE* homologs at the same time (see Materials and Methods). Note that the sgRNA vectors are designed in a way that allows multiple sgRNAs to be cloned into the vector in parallel using BglI/Brick cloning, thus making simultaneous knockdown of several genes possible (Fig. 6A; see also Materials and Methods). Cell length analysis of the resulting double-knockdown strain did not reveal any drastic shift in cell lengths compared to control cells, although slightly increased numbers of short (<2- μ m) cells were observed (Fig. 6C).

Since we did not observe any phenotype upon depletion of the CozE homologs, we analyzed the transcriptional knockdown using ddPCR. This showed that the CRISPRi system had indeed worked as expected and that knockdown of *lp_1247* or *lp_2217* or both was achieved in the respective CRISPRi strains (Fig. 6D). From this assay, we therefore conclude that CozE homologs *lp_1247* and *lp_2217* do not seem to play any prominent role in cell division in *L. plantarum*.

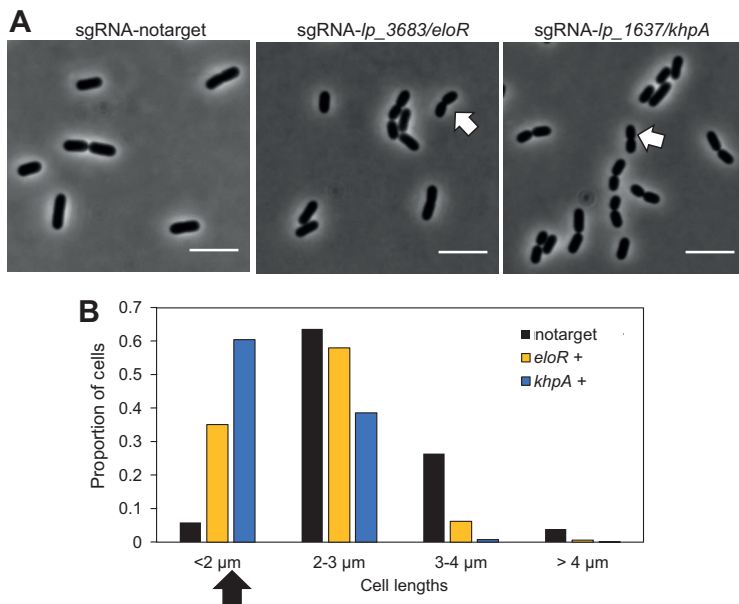


FIG 7 Cells depleted of *lp_3683* (*eloR* homolog) and *lp_1637* (*khpA* homolog) display reduced elongation. (A) Phase-contrast micrographs of control cells with nontargeting sgRNA (strain IM133) and of cells depleted of *lp_3683/eloR* (strain IM138) and *lp_1637/khpA* (strain IM139). Cells were grown in the presence of 25 ng/ml SppIP. Examples of short cells are indicated with white arrows. The scale bar is 5 μm. (B) Cell length analysis of corresponding strains. Cell lengths were measured using MicrobeJ (59). Cells were split in four groups based on lengths, and the proportion of cells in each group is plotted. Numbers of cells analyzed were as follows: $n = 204$ for notarget control cells (strain IM133), $n = 689$ for sgRNA-*eloR* cells (strain IM138), and $n = 1025$ for sgRNA-*khpA* cells (strain IM139). The black arrow points to the short-cell group, where cells depleted of *lp_3683/eloR* and *lp_1637/khpA* were overrepresented. Plus signs (+) indicate that cells were grown in the presence of 25 ng/ml SppIP.

EloR and KhpA are necessary for proper cell elongation. EloR and KhpA are two cytoplasmic, RNA-binding proteins which have been identified in *S. pneumoniae* as important for proper cell elongation (39, 40, 42, 50). The two proteins form a hetero-complex, and the absence of either of them results in shorter and smaller cells. By knocking down expression of either the *eloR* homolog *lp_3683* (29% identity to the *S. pneumoniae* EloR protein) or the *khpA* homolog *lp_1637* (47% identity to the *S. pneumoniae* KhpA protein), we also observed that *L. plantarum* cell lengths were reduced in both cases and that the reduction was most drastic in the experiments performed with *lp_1637* (*khpA*) (Fig. 7). To our knowledge, this is the first time that these RNA-binding proteins have been investigated with respect to cell biology in rod-shaped bacteria, and the results suggest that they are important for cell elongation also in these cells. The modes of cell elongation are radically different between oval-shaped *S. pneumoniae* and rod-shaped cells, such as *L. plantarum*. While both septal cell wall synthesis and peripheral cell wall synthesis occur in the mid-cell area of ovococcal cells, elongation in rod-shaped bacteria is directed by the actin homologue MreB and occurs over most of the cell length (51). It will therefore be of great interest for future studies to unravel in detail how these proteins affect cell elongation in cells with different shapes.

Concluding remarks. The CRISPRi system developed in the present study is a significant addition to the genetic toolbox of *L. plantarum*. It allows quick and easy generation of transcriptional knockdowns, which can be used to study functions of essential genes or as part of a simple method to screen for phenotypes prior to performing time-consuming construction of knockouts or deletions. We decided to use

a two-plasmid system to allow easy replacement of sgRNA sequences by inverse PCR. The design of the plasmids also allows double or multiple knockdowns to be performed simultaneously. Given the host range of the plasmids used, we also expect that the two-plasmid CRISPRi system can be directly transferred to at least two other species; *L. sakei* and *L. curvatus*.

While the CRISPRi system was shown to function well, it should also be noted that studies in *E. coli* have shown that CRISPRi can be toxic to the cells under certain conditions. It was shown that some sgRNA sequences were toxic and showed off-target effects when combined with high levels of dCas9 expression (52). We cannot exclude the possibility that similar issues may occur in *L. plantarum*, and the current CRISPRi system could be further improved with more strictly regulated promoters. Furthermore, the fact that the CRISPRi system is active even without induction could potentially result in problems in studies generating strains targeting essential genes whose reduced transcription has a detrimental effect on growth. Our results also show that the inducer concentrations needed for knockdown differ between different genes. Nevertheless, we have shown the suitability of the transcriptional knockdown system for screening for phenotypes by targeting different cell cycle genes. The initial insights into essential cell cycle processes in *L. plantarum* presented here form a basis for further studies of DNA replication, chromosome segregation, cell division, and cell wall synthesis in this species.

MATERIALS AND METHODS

Bacterial strains and growth conditions. *E. coli* TOP10 or DH5 α cells were grown in brain heart infusion medium (Oxoid Ltd., Carlsbad, CA) or lysogeny broth at 37°C with shaking. *L. plantarum* cells were grown in de Man, Rogosa, and Sharpe (MRS) broth (Oxoid) at 37°C without shaking. Solid media were prepared by addition of 1.5% (wt/vol) agar to the broth. *L. lactis* was used as subcloning host for plasmids containing the SH71_{rep} replicon and were transformed as previously described (53). All other plasmids were subcloned in *E. coli*. The final plasmids were electrotransformed into *L. plantarum* (54). When required, antibiotic concentrations were added as follows: for *L. plantarum* and *L. lactis*, 10 μ g/ml erythromycin and 10 μ g/ml chloramphenicol; for *E. coli*, 200 μ g/ml erythromycin and 10 μ g/ml chloramphenicol.

Construction of plasmids. To develop the CRISPR interference system, we constructed a two-plasmid system in which both plasmids are derivatives of pSIP403 (15). Plasmids were purified using a NucleoSpin plasmid miniprep kit (Macherey-Nagel GmbH & Co., Düren, Germany). All plasmids used in the study are listed in Table 1. All PCRs were performed using Q5 High-Fidelity DNA polymerase (New England Biolabs [NEB], Ipswich, MA), and the primers used for PCR amplification are listed in Table 2. Constructs were verified by DNA sequencing.

Construction of plasmid pSIP-SH-dCas9 for expression of dCas9. To construct the plasmid containing the *dcas9* gene under the control of the inducible *sppA* promoter, the *dcas9* sequence was amplified from pLOW-dCas9 (23) using primer pair Cas9NcoF/Cas9XhoR. The amplicon was cloned into NcoI/XhoI-digested pSIP403 (15) using an In-Fusion HD cloning kit (Clontech Laboratories, Mountain View, CA), resulting in plasmid pSIP-dCas9. Then, to exchange the 256_{rep} replicon with the SH71_{rep} replicon, the SH71_{rep} replicon was excised from plasmid pSIP411 (16) using BamHI and XhoI and was ligated into the same sites of pSIP-dCas9, resulting in plasmid pSIP-SH-dCas9.

Construction of plasmids for expression of sgRNAs. We initially constructed a plasmid containing sgRNA-notarget under the control of a constitutive promoter. The sgRNA-notarget cassette was amplified from plasmid pPEPX-P3-sgRNALuc (22) with primer pair SgRNA_F/SgRNA_R, and the chloramphenicol resistance gene with the cognate promoter was amplified from plasmid pValac (55) using primer pair 403BamCmF/403SalCmR. The two fragments (with 36 overlapping base pairs) were fused by PCR, using the outer primers SgRNA_F and 403SalCmR. The 1.4-kb amplicon was subsequently cloned into BamHI/Acc65I-digested pSIP403 (15), using an In-Fusion HD cloning kit (Clontech Laboratories, Mountain View, CA), resulting in plasmid pSgRNA-notarget. This plasmid was used as a starting point for the insertion of gene-specific sgRNAs.

Gene-specific base-pairing regions for the sgRNAs were selected according to criteria previously used for other bacteria (22, 56). Shortly, we used CRISPR Primer Designer (57) to find potential protospacer-adjacent motif (PAM) sites (5'-NGG-3') and adjacent base-pairing regions close to the 5' end of the gene of interest. Base-pairing sequences binding to the nontemplate DNA strand were selected. BLAST searches (using the PAM-proximal 12 bp of the sgRNA as the query) against the WCFS1 genome were performed to ensure that there were no secondary target site on the genome. To verify that the base-pairing region does not interfere with the secondary structure of the dCas9 handle region, RNAfold from the ViennaRNA package was used to predict the sgRNA secondary structure.

New sgRNA plasmids were then constructed using inverse PCR. The base-pairing regions were introduced as overhangs in the forward primer, while the reverse primer was 5'-phosphorylated. Following inverse PCR, the template plasmid was digested using DpnI at 37°C for 2 h. The amplified PCR fragment were self-ligated using T4 DNA ligase (NEB) following the manufacturer's protocol and trans-

TABLE 1 Strains and plasmids used in this study

Strain or plasmid	Relevant characteristic(s) ^a	Reference or source
Strains		
<i>E. coli</i> TOP10	Cloning host	Thermo Fisher
<i>E. coli</i> DH5 α	Cloning host	Laboratory stock
<i>L. lactis</i> Il1403	Cloning host	60
<i>L. plantarum</i> WCFS1	Host strain	12
<i>L. plantarum</i> NZ3557	WCFS1, Δ acm2::cat	34
<i>L. plantarum</i> IM167	WCFS1, pEV, pSgRNA-notarget	This study
<i>L. plantarum</i> IM132	WCFS1, pSIP-SH-dCas9	This study
<i>L. plantarum</i> IM133	WCFS1, pSIP-SH-dCas9, pSgRNA-notarget	This study
<i>L. plantarum</i> IM134	WCFS1, pSIP-SH-dCas9, pSgRNA-acm2	This study
<i>L. plantarum</i> IM137	WCFS1, pSIP-SH-dCas9, pSgRNA-dnaA	This study
<i>L. plantarum</i> IM188	WCFS1, pSIP-SH-dCas9, pSgRNA-ezrA	This study
<i>L. plantarum</i> IM141	WCFS1, pSIP-SH-dCas9, pSgRNA-lp_1247 (<i>cozE</i> homolog)	This study
<i>L. plantarum</i> IM142	WCFS1, pSIP-SH-dCas9, pSgRNA-lp_2217 (<i>cozE</i> homolog)	This study
<i>L. plantarum</i> IM130	WCFS1, pSIP-SH-dCas9, pSgRNA-lp_1247-lp_2217 (<i>cozE</i> homologs)	This study
<i>L. plantarum</i> IM138	WCFS1, pSIP-SH-dCas9, pSgRNA-lp_3683 (<i>eloR</i> homolog)	This study
<i>L. plantarum</i> IM139	WCFS1, pSIP-SH-dCas9, pSgRNA-lp_1637 (<i>khpA</i> homolog)	This study
Plasmids		
pSIP403	<i>spp</i> -based expression vector; Em ^r ; 256 _{rep} pUCori; P _{sppA} :: <i>gusA</i>	15
pSIP411	<i>spp</i> -based expression vector; Em ^r ; SH71 _{rep} ; P _{sppQ} :: <i>gusA</i>	16
pSIPdCas9	Em ^r ; 256 _{rep} pUCori; P _{sppA} ::dCas9	This study
pSIP-SH-dCas9	Em ^r ; SH71 _{rep} ; P _{sppA} ::dCas9	This study
pPEPX-P3-sgRNA _{lac}		22
pValac	Template for chloramphenicol resistance gene (Cm ^r)	55
pEV	Em ^r ; control plasmid, empty vector	61
pSgRNA-notarget	Cm ^r ; 256 _{rep} pUCori P3::sgRNA-notarget	This study
pSgRNA-acm2	Cm ^r 256 _{rep} pUCori P3::sgRNA-lp_2645	This study
pSgRNA-dnaA	Cm ^r 256 _{rep} pUCori P3::sgRNA-lp_0001	This study
pSgRNA-ezrA	Cm ^r 256 _{rep} pUCori P3::sgRNA-lp_2328	This study
pSgRNA-lp_1247	Cm ^r 256 _{rep} pUCori P3::sgRNA-lp_1247	This study
pSgRNA-lp_2217	Cm ^r 256 _{rep} pUCori P3::sgRNA-lp_2217	This study
pSgRNA-lp_1247-lp_2217	Cm ^r 256 _{rep} pUCori P3::sgRNA-lp_1247-lp_2217	This study
pSgRNA-lp_3683/ <i>eloR</i>	Cm ^r 256 _{rep} pUCori P3::sgRNA-lp_3683	This study
pSgRNA-lp_1637/ <i>khpA</i>	Cm ^r 256 _{rep} pUCori P3::sgRNA-lp_1637	This study

^aEm, erythromycin; Cm, chloramphenicol.

formed into *E. coli*. Purified sgRNA plasmids were verified by sequencing and transformed into electro-competent *L. plantarum* harboring pSIP-SH-dCas9.

Construction of double-sgRNA plasmid. A plasmid for simultaneous depletion of *lp_1247* and *lp_2217* (pSgRNA-lp_1247-lp_2217) was made using BglBrick cloning (58). Plasmid pSgRNA-lp_1247 was digested using EcoRI and BglII, while the sgRNA-lp_2217 fragment was digested from plasmid pSgRNA-lp_2217 using EcoRI and BamHI and was ligated into the EcoRI/BglII sites of plasmid pSgRNA-lp_1247 to generate the double-sgRNA plasmid (see also Fig. 6A).

Total RNA extraction and cDNA synthesis. Overnight cultures of *L. plantarum* harboring pSIP-SH-dCas9 and sgRNA plasmids were diluted in fresh MRS medium with appropriate antibiotics to an OD₆₀₀ of 0.01 and induced with 25 ng/ml IP-67 (SpplP) (45) (Caslo, Lyngby, Denmark). In dose-response experiments, the inducer concentration range from 0 to 25 ng/ml. When cultures reached an OD₆₀₀ of 0.4, 5 ml of culture was added to an equal volume of Bacteria Protect (Qiagen, Hilden, Germany) and the culture was subsequently harvested by centrifugation for 10 min at 5000 \times g and 22°C. Total RNA was extracted using an RNeasy minikit (Qiagen). Cell pellets were resuspended in 700 μ l RLT buffer (Qiagen) with 1.5% β -mercaptoethanol. For lysis by mechanical disruption, the suspensions were transferred to 2 ml lysing matrix B tubes (MP Biomedicals) and placed in a FastPrep-24 instrument (MP Biomedicals) at 6.5 m/s for 30 s. The agitation was repeated three times with a 1-min pause between agitations. Further steps were carried out according to the protocol provided by the manufacturer (Qiagen). After extraction, a Heat&Run genomic DNA (gDNA) removal kit (ArcticZymes, Tromsø, Norway) was used according to the manufacturer's instructions to remove residual gDNA. The concentrations of the RNA samples were determined using a NanoDrop spectrophotometer (Thermo Fisher Scientific Inc, Waltham, MA). cDNA was synthesized by the use of iScript Reverse Transcription Supermix (Bio-Rad, Hercules, CA, USA), where 100 ng RNA was used as the template. Negative controls (not containing reverse transcriptase) were prepared for each sample to check that all gDNA had been removed. Reactions were set up as described by the manufacturer. To prevent saturation of template in droplet digital PCR reactions, all cDNA samples were diluted 100 \times .

Droplet digital PCR (ddPCR). ddPCR was performed by mixing 11 μ l of 2 \times EvaGreen Supermix (Bio-Rad), 1 μ l of 2 μ M stocks for each primer (see Table 2), and distilled water (dH₂O) to reach a total volume of 20 μ l for each reaction. The mix was dispersed into PCR strips, and then 2 μ l of the template

TABLE 2 Primers used in this study

Primer and category	Sequence (5'–3') ^a
Cloning	
403BamCmF	TATGCGTGCGGGATCCTTATTTGCTGAAAATGAGGAATTAATAAAAAAGA
403SalCmR	GTGCTTTGCCGATGCGTGCACCTTATAAAAAGCCAGTCATTAGGCCT
SgRNA_F	GACTGGCTTTTATAAGTCGACGCATGCGGCAAGCACTCAAAGT
SgRNA_R	TCGAACCCGGGGTACCACTTAAAAAAAACCGCGCCCT
Cas9NcoF	AGTATGATCCCATGGATAAGAAATACTCAATAGGCCT
Cas9XhoR	TACCGAATTCCTCGAGGTCGACTTAGTCACCTCT
sgRNA	
Phospho-sgRNA_promoter_R	Phosphp-5'-TATAGTTATTATACCAAGGGGACAGTGC
ezrA_lp_2328SgRNA	<u>GTTGCCGTTCCGTC</u> CAATTGAGTTTAAGAGCTATGCTGGAACAG
lp_p2645F	<u>TTTCCCTTAGTCGCAGCTGCGTTT</u> AAGAGCTATGCTGGAACAG
mk277_sg_lp0001_dnaA	<u>TCGAGTTGGAGTGGTTTTTGGCGTTT</u> AAGAGCTATGCTGGAACAG
mk281_sg_lp1247	<u>ACACTTAAAAACGTGCCGATGTTT</u> AAGAGCTATGCTGGAACAG
mk282_sg_lp2217	<u>CACCGTTGTTCTGTGAATCGTTT</u> AAGAGCTATGCTGGAACAG
mk276_sg_lp2189_divIVA	<u>CCAAGAACGGTTGGACTCGAGTTT</u> AAGAGCTATGCTGGAACAG
mk278_sg_lp3683 (eloR)	<u>ACCGTTAGCCGTA</u> CTTGGCGTTTAAAGAGCTATGCTGGAACAG
mk279_sg_lp1637 (spr0683)	<u>AACTAACGGGGTGACAA</u> CCGGTTTAAAGAGCTATGCTGGAACAG
ddPCR	
Lp_1247_F	CACGATTACGAGTGTGACGA
Lp_1247_R	CTAGAAATCGTGCGCCAT
Lp_2217_F	CCATGGATGTTGGTCCAAGT
Lp_2217_R	CAAGATCGCATAGCCTGGAA
Lp_2645_F	ATTCTGGAAGTGGTTGGGG
Lp_2645_R	ACTTCGAAAAGCGCTTTGA

^aRestriction sites are indicated in italics; base-pairing regions in the sgRNA primers are underlined.

was added. The reaction mixtures were loaded into a QX200 system (Bio-Rad) for droplet generation. Droplet generation required 20 μ l of sample and 70 μ l of droplet generation oil for EvaGreen (Bio-Rad). Droplets were created in a volume of 40 μ l and were transferred to a High-Profile 96-well PCR plate (Bio-Rad). The plate was sealed using a PX1 PCR plate sealer (Bio-Rad) and put into a thermocycler with a ramp rate of 2°C/s. The cycling program was 95°C for 10 min, 40 cycles of 95°C for 30 s and 60°C for 1 min, and then 4°C for 5 min and 90°C for 5 min, followed by an optional infinite hold at 4°C. After amplification, droplet signals were analyzed using a QX200 reader (Bio-Rad). Data were analyzed using QuantaSoft Analysis Pro with the default setup. Only results from wells where RNA samples were partitioned in >10,000 droplets were included in further calculations.

Phase-contrast and fluorescence microscopy analysis. To prepare samples for microscopy analysis, overnight cultures of *L. plantarum* were diluted in fresh MRS medium with appropriate antibiotics to an OD₆₀₀ of 0.01 and induced with 25 ng/ml SppIP (Caslo). When the OD₆₀₀ reached 0.4, 80- μ l samples were collected and subsequently mixed with 31.25 μ g/ml DAPI for staining of DNA. A Zeiss AxioObserver and ZEN blue software were used for microscopy, and images were taken with an Orca-Flash4.0 V2 Digital complementary metal-oxide semiconductor (CMOS) camera (Hamamatsu Photonics) through a 100 \times PC objective. An HPX 120 Illuminator was used as a light source for fluorescence microscopy analysis.

Growth assays. Growth assays were conducted in a Synergy H1 hybrid reader (BioTek). Overnight cultures of *L. plantarum* were diluted to an OD₆₀₀ of 0.01 in fresh MRS medium containing appropriate antibiotics. Cell suspensions were dispersed in a 96-well microtiter plate with 270 μ l culture in each well. Cultures were induced with 25 ng/ml SppIP (Caslo). OD₆₀₀ was measured every 10 min at 37°C during growth.

ACKNOWLEDGMENTS

We thank Linda Bergaust, Norwegian University of Life Sciences, for help with ddPCR.

This work was supported by a grant from the Research Council of Norway (project number 250976).

L.S.H., D.S., G.M., and M.K. conceived and designed the study. I.S.M., K.W., Z.S., and G.M. performed experiments. I.S.M., K.W., G.M., and M.K. analyzed data. I.S.M., K.W., G.M., and M.K. wrote the paper and designed the figures, with input from all of us.

REFERENCES

- Ahme S, Nobaek S, Jeppsson B, Adlerberth I, Wold A, Molin G. 1998. The normal *Lactobacillus* flora of healthy human rectal and oral mucosa. *J Appl Microbiol* 85:88–94. <https://doi.org/10.1046/j.1365-2672.1998.00480.x>.
- Ross RP, Morgan S, Hill C. 2002. Preservation and fermentation: past, present and future. *Int J Food Microbiol* 79:3–16. [https://doi.org/10.1016/S0168-1605\(02\)00174-5](https://doi.org/10.1016/S0168-1605(02)00174-5).

3. Cleveland J, Montville TJ, Nes IF, Chikindas ML. 2001. Bacteriocins: safe, natural antimicrobials for food preservation. *Int J Food Microbiol* 71: 1–20. [https://doi.org/10.1016/S0168-1605\(01\)00560-8](https://doi.org/10.1016/S0168-1605(01)00560-8).
4. Alander M, De Smet I, Nolle L, Verstraete W, Von Wright A, Mattila-Sandholm T. 1999. The effect of probiotic strains on the microbiota of the simulator of the human intestinal microbial ecosystem (SHIME). *Int J Food Microbiol* 46:71–79. [https://doi.org/10.1016/S0168-1605\(98\)00182-2](https://doi.org/10.1016/S0168-1605(98)00182-2).
5. de Vries MC, Vaughan EE, Kleerebezem M, de Vos WM. 2006. *Lactobacillus plantarum*—survival, functional and potential probiotic properties in the human intestinal tract. *Int Dairy J* 16:1018–1028. <https://doi.org/10.1016/j.idairy.2005.09.003>.
6. Niedzielin K, Kordecki H, Birkenfeld B. 2001. A controlled, double-blind, randomized study on the efficacy of *Lactobacillus plantarum* 299V in patients with irritable bowel syndrome. *Eur J Gastroenterol Hepatol* 13:1143–1147. <https://doi.org/10.1097/00042737-200110000-00004>.
7. Mohamadzadeh M, Olson S, Kalina WV, Ruthel G, Demmin GL, Warfield KL, Bavari S, Kleenhammer TR. 2005. Lactobacilli activate human dendritic cells that skew T cells toward T helper 1 polarization. *Proc Natl Acad Sci U S A* 102:2880–2885. <https://doi.org/10.1073/pnas.0500098102>.
8. Kuczkowska K, Myrbråten I, Øverland L, Eijsink VG, Follmann F, Mathiesen G, Dietrich J. 2017. *Lactobacillus plantarum* producing a *Chlamydia trachomatis* antigen induces a specific IgA response after mucosal booster immunization. *PLoS One* 12:e0176401. <https://doi.org/10.1371/journal.pone.0176401>.
9. Kuczkowska K, Kleiveland CR, Minic R, Moen LF, Øverland L, Tjåland R, Carlsen H, Lea T, Mathiesen G, Eijsink VG. 2016. Immunogenic properties of *Lactobacillus plantarum* producing surface-displayed *Mycobacterium tuberculosis* antigens. *Appl Environ Microbiol* 83:e02782-16. <https://doi.org/10.1128/AEM.02782-16>.
10. Wells JM, Mercenier A. 2008. Mucosal delivery of therapeutic and prophylactic molecules using lactic acid bacteria. *Nat Rev Microbiol* 6:349–362. <https://doi.org/10.1038/nrmicro1840>.
11. Bermudez-Humaran LG, Kharrat P, Chatel JM, Langella P. 2011. Lactococci and lactobacilli as mucosal delivery vectors for therapeutic proteins and DNA vaccines. *Microb Cell Fact* 10:54. <https://doi.org/10.1186/1475-2859-10-51-54>.
12. Kleerebezem M, Boekhorst J, van Kranenburg R, Molenaar D, Kuipers OP, Leer R, Turchini R, Peters SA, Sandbrink HM, Fiers MWEJ, Stiekema W, Lankhorst RMK, Bron PA, Hoffer SM, Groot MNN, Kerkhoven R, de Vries M, Ursing B, de Vos WM, Siezen RJ. 2003. Complete genome sequence of *Lactobacillus plantarum* WCFS1. *Proc Natl Acad Sci U S A* 100:1990–1995. <https://doi.org/10.1073/pnas.0337704100>.
13. Mathiesen G, Sørvig E, Blatny J, Naterstad K, Axelsson L, Eijsink V. 2004. High-level gene expression in *Lactobacillus plantarum* using a pheromone-regulated bacteriocin promoter. *Letts Appl Microbiol* 39: 137–143. <https://doi.org/10.1111/1472-765X.2004.01551.x>.
14. Pavan S, Hols P, Delcour J, Geoffroy M-C, Grangette C, Kleerebezem M, Mercenier A. 2000. Adaptation of the nisin-controlled expression system in *Lactobacillus plantarum*: a tool to study in vivo biological effects. *Appl Environ Microbiol* 66:4427–4432. <https://doi.org/10.1128/AEM.66.10.4427-4432.2000>.
15. Sørvig E, Grönqvist S, Naterstad K, Mathiesen G, Eijsink VG, Axelsson L. 2003. Construction of vectors for inducible gene expression in *Lactobacillus sakei* and *L. plantarum*. *FEMS Microbiol Lett* 229:119–126. [https://doi.org/10.1016/S0378-1097\(03\)00798-5](https://doi.org/10.1016/S0378-1097(03)00798-5).
16. Sørvig E, Mathiesen G, Naterstad K, Eijsink VG, Axelsson L. 2005. High-level, inducible gene expression in *Lactobacillus sakei* and *Lactobacillus plantarum* using versatile expression vectors. *Microbiology* 151: 2439–2449. <https://doi.org/10.1099/mic.0.28084-0>.
17. Lambert JM, Bongers RS, Kleerebezem M. 2007. Cre-lox-based system for multiple gene deletions and selectable-marker removal in *Lactobacillus plantarum*. *Appl Environ Microbiol* 73:1126–1135. <https://doi.org/10.1128/AEM.01473-06>.
18. Grangette C, Nutten S, Palumbo E, Morath S, Hermann C, Dewulf J, Pot B, Hartung T, Hols P, Mercenier A. 2005. Enhanced antiinflammatory capacity of a *Lactobacillus plantarum* mutant synthesizing modified teichoic acids. *Proc Natl Acad Sci U S A* 102:10321–10326. <https://doi.org/10.1073/pnas.0504084102>.
19. Bikard D, Jiang W, Samai P, Hochschild A, Zhang F, Marraffini LA. 2013. Programmable repression and activation of bacterial gene expression using an engineered CRISPR-Cas system. *Nucleic Acids Res* 41: 7429–7437. <https://doi.org/10.1093/nar/gkt520>.
20. Qi LS, Larson MH, Gilbert LA, Doudna JA, Weissman JS, Arkin AP, Lim WA. 2013. Repurposing CRISPR as an RNA-guided platform for sequence-specific control of gene expression. *Cell* 152:1173–1183. <https://doi.org/10.1016/j.cell.2013.02.022>.
21. Peters JM, Colavin A, Shi H, Czarny TL, Larson MH, Wong S, Hawkins JS, Lu CHS, Koo B-M, Marta E, Shiver AL, Whitehead EH, Weissman JS, Brown ED, Qi LS, Huang KC, Gross CA. 2016. A comprehensive, CRISPR-based functional analysis of essential genes in bacteria. *Cell* 165:1493–1506. <https://doi.org/10.1016/j.cell.2016.05.003>.
22. Liu X, Gallyat C, Kjos M, Domenech A, Slager J, van Kessel SP, Knoops K, Sorg RA, Zhang JR, Veening JW. 2017. High-throughput CRISPRi phenotyping identifies new essential genes in *Streptococcus pneumoniae*. *Mol Syst Biol* 13:931. <https://doi.org/10.15252/msb.20167449>.
23. Stamsås GA, Myrbråten IS, Straume D, Salehian Z, Veening JW, Håvarstein LS, Kjos M. 2018. CozEa and CozEb play overlapping and essential roles in controlling cell division in *Staphylococcus aureus*. *Mol Microbiol* 109:615–632. <https://doi.org/10.1111/mmi.13999>.
24. Zhao C, Shu X, Sun B. 2017. Construction of a gene knockdown system based on catalytically inactive (“dead”) Cas9 (dCas9) in *Staphylococcus aureus*. *Appl Environ Microbiol* 83:e00291-17. <https://doi.org/10.1128/AEM.00291-17>.
25. Dong X, Jin Y, Ming D, Li B, Dong H, Wang L, Wang T, Wang D. 2017. CRISPR/dCas9-mediated inhibition of gene expression in *Staphylococcus aureus*. *J Microbiol Methods* 139:79–86. <https://doi.org/10.1016/j.mimet.2017.05.008>.
26. Wang K, Nicholou M. 2017. Suppression of antimicrobial resistance in MRSA using CRISPR-dCas9. *Clin Lab Sci* 30:207–213. <https://doi.org/10.29074/ascls.30.4.207>.
27. Berlec A, Škrlec K, Kocjan J, Olenic M, Štrukelj B. 2018. Single plasmid systems for inducible dual protein expression and for CRISPR-Cas9/CRISPRi gene regulation in lactic acid bacterium *Lactococcus lactis*. *Sci Rep* 8:1009. <https://doi.org/10.1038/s41598-018-19402-1>.
28. Song X, Huang H, Xiong Z, Ai L, Yang S. 2017. CRISPR-Cas9(D10A) nickase-assisted genome editing in *Lactobacillus casei*. *Appl Environ Microbiol* 83:e01259-17. <https://doi.org/10.1128/AEM.01259-17>.
29. Leenay RT, Vento JM, Shah M, Martino ME, Leulier F, Beisel CL. 2018. Genome editing with CRISPR-Cas9 in *Lactobacillus plantarum* revealed that editing outcomes can vary across strains and between methods. *Biotechnol J* 29:e1700583. <https://doi.org/10.1002/biot.201700583>.
30. van den Nieuwboer M, van Hemert S, Claassen E, de Vos WM. 2016. *Lactobacillus plantarum* WCFS1 and its host interaction: a dozen years after the genome. *Microb Biotechnol* 9:452–465. <https://doi.org/10.1111/1751-7915.12368>.
31. Jameson KH, Wilkinson AJ. 2017. Control of initiation of DNA replication in *Bacillus subtilis* and *Escherichia coli*. *Genes* 8:22. <https://doi.org/10.3390/genes8010022>.
32. Hajduk IV, Rodrigues CD, Harry EJ. 2016. Connecting the dots of the bacterial cell cycle: coordinating chromosome replication and segregation with cell division. *Semin Cell Dev Biol* 53:2–9. <https://doi.org/10.1016/j.semcdb.2015.11.012>.
33. Bisson-Filho AW, Hsu YP, Squyres GR, Kuru E, Wu F, Jukes C, Sun Y, Dekker C, Holden S, VanNieuwenhze MS, Brun YV, Garner EC. 2017. Treadmilling by FtsZ filaments drives peptidoglycan synthesis and bacterial cell division. *Science* 355:739–743. <https://doi.org/10.1126/science.aak9973>.
34. Fredriksen L, Mathiesen G, Moen A, Bron PA, Kleerebezem M, Eijsink VG, Egge-Jacobsen W. 2012. The major autolysin Acm2 from *Lactobacillus plantarum* undergoes cytoplasmic O-glycosylation. *J Bacteriol* 194: 325–333. <https://doi.org/10.1128/JB.06314-11>.
35. Rolain T, Bernard E, Courtin P, Bron PA, Kleerebezem M, Chapot-Chartier MP, Hols P. 2012. Identification of key peptidoglycan hydrolases for morphogenesis, autolysis, and peptidoglycan composition of *Lactobacillus plantarum* WCFS1. *Microb Cell Fact* 11:137. <https://doi.org/10.1186/1475-2859-11-137>.
36. Skarstad K, Katayama T. 2013. Regulating DNA replication in bacteria. *Cold Spring Harb Perspect Biol* 5:a012922. <https://doi.org/10.1101/cshperspect.a012922>.
37. Levin PA, Kurtser IG, Grossman AD. 1999. Identification and characterization of a negative regulator of FtsZ ring formation in *Bacillus subtilis*. *Proc Natl Acad Sci U S A* 96:9642–9647. <https://doi.org/10.1073/pnas.96.17.9642>.
38. Fenton AK, El Mortaji L, Lau DT, Rudner DZ, Bernhardt TG. 2017. CozE is a member of the MreCD complex that directs cell elongation in *Streptococcus pneumoniae*. *Nat Microbiol* 2:17001.
39. Stamsås GA, Straume D, Ruud Winther A, Kjos M, Frantzen CA, Hå-

- varstein LS. 2017. Identification of EloR (Spr1851) as a regulator of cell elongation in *Streptococcus pneumoniae*. *Mol Microbiol* 105:954–967. <https://doi.org/10.1111/mmi.13748>.
40. Zheng JJ, Perez AJ, Tsui HCT, Massidda O, Winkler ME. 2017. Absence of the KhpA and KhpB (JAG/EloR) RNA-binding proteins suppresses the requirement for PBP2b by overproduction of FtsA in *Streptococcus pneumoniae* D39. *Mol Microbiol* 106:793–814. <https://doi.org/10.1111/mmi.13847>.
 41. Straume D, Stamsås GA, Berg KH, Salehian Z, Håvarstein LS. 2017. Identification of pneumococcal proteins that are functionally linked to penicillin-binding protein 2b (PBP2b). *Mol Microbiol* 103:99–116. <https://doi.org/10.1111/mmi.13543>.
 42. Winther AR, Kjos M, Stamsås GA, Håvarstein LS, Straume D. 2019. Prevention of EloR/KhpA heterodimerization by introduction of site-specific amino acid substitutions renders the essential elongasome protein PBP2b redundant in *Streptococcus pneumoniae*. *Sci Rep* 9:3681. <https://doi.org/10.1038/s41598-018-38386-6>.
 43. Sørvig E, Skaugen M, Naterstad K, Eijsink VG, Axelsson L. 2005. Plasmid p256 from *Lactobacillus plantarum* represents a new type of replicon in lactic acid bacteria, and contains a toxin-antitoxin-like plasmid maintenance system. *Microbiology* 151:421–431. <https://doi.org/10.1099/mic.0.27389-0>.
 44. Palumbo E, Deghorain M, Cocconcelli PS, Kleerebezem M, Geyer A, Hartung T, Morath S, Hols P. 2006. D-Alanyl ester depletion of teichoic acids in *Lactobacillus plantarum* results in a major modification of lipoteichoic acid composition and cell wall perforations at the septum mediated by the Acm2 autolysin. *J Bacteriol* 188:3709–3715. <https://doi.org/10.1128/JB.188.10.3709-3715.2006>.
 45. Brurberg MB, Nes IF, Eijsink VG. 1997. Pheromone-induced production of antimicrobial peptides in *Lactobacillus*. *Mol Microbiol* 26:347–360. <https://doi.org/10.1046/j.1365-2958.1997.5821951.x>.
 46. Claessen D, Emmins R, Hamoen LW, Daniel RA, Errington J, Edwards DH. 2008. Control of the cell elongation-division cycle by shuttling of PBP1 protein in *Bacillus subtilis*. *Mol Microbiol* 68:1029–1046. <https://doi.org/10.1111/j.1365-2958.2008.06210.x>.
 47. Haeusser DP, Schwartz RL, Smith AM, Oates ME, Levin PA. 2004. EzrA prevents aberrant cell division by modulating assembly of the cytoskeletal protein FtsZ. *Mol Microbiol* 52:801–814. <https://doi.org/10.1111/j.1365-2958.2004.04016.x>.
 48. Kawai Y, Ogasawara N. 2006. *Bacillus subtilis* EzrA and FtsL synergistically regulate FtsZ ring dynamics during cell division. *Microbiology* 152:1129–1141. <https://doi.org/10.1099/mic.0.28497-0>.
 49. Considine KM, Sleator RD, Kelly AL, Fitzgerald GF, Hill C. 2011. Identification and characterization of an essential gene in *Listeria monocytogenes* using an inducible gene expression system. *Bioeng Bugs* 2:150–159. <https://doi.org/10.4161/bbug.2.3.15476>.
 50. Ulrych A, Holečková N, Goldová J, Doubravová L, Benada O, Kofroňová O, Halada P, Branny P. 2016. Characterization of pneumococcal Ser/Thr protein phosphatase phpP mutant and identification of a novel PhpP substrate, putative RNA binding protein Jag. *BMC Microbiol* 16:247. <https://doi.org/10.1186/s12866-016-0865-6>.
 51. Scheffers DJ, Pinho MG. 2005. Bacterial cell wall synthesis: new insights from localization studies. *Microbiol Mol Biol Rev* 69:585–607. <https://doi.org/10.1128/MMBR.69.4.585-607.2005>.
 52. Cui L, Vigouroux A, Rousset F, Varet H, Khanna V, Bikard D. 2018. A CRISPRi screen in *E. coli* reveals sequence-specific toxicity of dCas9. *Nat Commun* 9:1912. <https://doi.org/10.1038/s41467-018-04209-5>.
 53. Holo H, Nes IF. 1989. High-frequency transformation, by electroporation, of *Lactococcus lactis* subsp. *cremoris* grown with glycine in osmotically stabilized media. *Appl Environ Microbiol* 55:3119–3123.
 54. Aukrust T, Blom H. 1992. Transformation of *Lactobacillus* strains used in meat and vegetable fermentations. *Food Res Int* 25:253–261. [https://doi.org/10.1016/0963-9969\(92\)90121-K](https://doi.org/10.1016/0963-9969(92)90121-K).
 55. Guimaraes V, Innocentin S, Chatel JM, Lefevre F, Langella P, Azevedo V, Miyoshi A. 2009. A new plasmid vector for DNA delivery using lactococci. *Genet Vaccines Ther* 7:4. <https://doi.org/10.1186/1479-0556-7-4>.
 56. Larson MH, Gilbert LA, Wang X, Lim WA, Weissman JS, Qi LS. 2013. CRISPR interference (CRISPRi) for sequence-specific control of gene expression. *Nat Protoc* 8:2180–2196. <https://doi.org/10.1038/nprot.2013.132>.
 57. Yan M, Zhou SR, Xue HW. 2015. CRISPR Primer Designer: design primers for knockout and chromosome imaging CRISPR-Cas system. *J Integr Plant Biol* 57:613–617. <https://doi.org/10.1111/jipb.12295>.
 58. Anderson J, Dueber JE, Leguia M, Wu GC, Goler JA, Arkin AP, Keasling JD. 2010. BglBricks: a flexible standard for biological part assembly. *J Biol Eng* 4:1. <https://doi.org/10.1186/1754-1611-4-1>.
 59. Ducret A, Qardokus EM, Brun YV. 2016. MicrobeJ, a tool for high throughput bacterial cell detection and quantitative analysis. *Nat Microbiol* 1:16077. <https://doi.org/10.1038/nmicrobiol.2016.77>.
 60. Bolotin A, Wincker P, Mauger S, Jaillon O, Malarme K, Weissenbach J, Ehrlich SD, Sorokin A. 2001. The complete genome sequence of the lactic acid bacterium *Lactococcus lactis* ssp. *lactis* IL1403. *Genome Res* 11:731–753. <https://doi.org/10.1101/gr.169701>.
 61. Fredriksen L, Kleiveland CR, Hult LTO, Lea T, Nygaard CS, Eijsink VG, Mathiesen G. 2012. Surface display of N-terminally anchored invasins by *Lactobacillus plantarum* activates NF- κ B in monocytes. *Appl Environ Microbiol* 78:5864–5871. <https://doi.org/10.1128/AEM.01227-12>.

ISBN: 978-82-575-1868-4

ISSN: 1894-6402



Norwegian University
of Life Sciences

Postboks 5003
NO-1432 Ås, Norway
+47 67 23 00 00
www.nmbu.no